PROGRESS IN OPTICS

VOLUME II

FROM THE SERIES IN PHYSICS

General Editors:

J. DE BOER, Professor of Physics, University of Amsterdam
H. BRINKMAN, Professor of Physics, University of Groningen
H. B. G. CASIMIR, Director of the Philips' Laboratories, Eindhoven

Monographs:

B. BAK, Elementary Introduction to Molecular Spectra
V. L. BONCH-BRUEVICH and S. V. TYABLIKOV, The Green Function Method in Statistical Mechanics
H. G. VAN BUEREN, Imperfections in Crystals
V. L. GINZBURG, Propagation of Electromagnetic Waves in Plasma
S. R. DE GROOT and P. MAZUR, Non-Equilibrium Thermodynamics
E. A. GUGGENHEIM, Thermodynamics
J. HILGEVOORD, Dispersion Relations and Causal Description (An Introduction to Dispersion Relations in Field Theory)
R. HOSEMANN and S. N. BAGCHI, Direct Analysis of Diffraction by Matter
H. JONES, The Theory of Brillouin Zones and Electronic States in Crystals
K. KUMAR, Perturbation Theory and the Nuclear Many Body Problem
J. G. LINHART, Plasma Physics
H. J. LIPKIN, Beta Decay for Pedestrians
J. P. MARCHAND, Distributions
J. MCCONNELL, Quantum Particle Dynamics
A. MESSIAH, Quantum Mechanics
P. H. E. MEIJER and E. BAUER, Group Theory, the Application to Quantum Mechanics
E. J. POST, Formal Structure of Electromagnetics
S. RAIMES, The Wave Mechanics of Electrons in Metals
P. ROMAN, Theory of Elementary Particles
J. L. SYNGE, Relativity: The Special Theory
J. L. SYNGE, Relativity: The General Theory
J. L. SYNGE, The Relativistic Gas
D. TER HAAR, Elements of Hamiltonian Mechanics
S. TOMONAGA, Quantum Mechanics
A. VAŠÍČEK, Optics of Thin Films

Edited Volumes:

J. DE BOER and G. E. UHLENBECK (editors), Studies in Statistical Mechanics. Vol. I
P. M. ENDT and M. DEMEUR (editors), Nuclear Reactions, Vol. I
P. M. ENDT and PH. B. SMITH (editors), Nuclear Reactions, Vol. II
FUNDAMENTAL PROBLEMS IN STATISTICAL MECHANICS. Proceedings of the NUFFIC International Summer Course in Science (Nijenrode, 1961)
C. J. GORTER (editor), Progress in Low Temperature Physics, Vols. I-III
H. MAECKER (editor), Proceedings of the 5th International Conference on Ionization Phenomena in Gases (München, 1961)
K. SIEGBAHN (editor), Beta- and Gamma-Ray Spectroscopy
S. F. SINGER (editor), Progress in the Astronautical Sciences, Vol. I
J. G. WILSON and S. A. WOUTHUYSEN (editors), Progress in Elementary Particle and Cosmic Ray Physics, Vols. I-VI
E. WOLF (editor), Progress in Optics, Vols. I and II

B. VAN DER POL, Selected Scientific Papers
P. EHRENFEST, Collected Scientific Papers

CONTENTS OF VOLUME I (1961)

PROGRESS IN OPTICS

VOLUME II

EDITED BY

E. WOLF
University of Rochester, N.Y., U.S.A.

Contributors

G. W. STROKE, J. M. BURCH,
R. G. GIOVANELLI, J. TSUJIUCHI,
L. MANDEL, F. ABELÈS

1963

PUBLISHERS:
NORTH-HOLLAND PUBLISHING CO. – AMSTERDAM
SOLE DISTRIBUTORS FOR U.S.A.:
INTERSCIENCE PUBLISHERS, a division of
JOHN WILEY & SONS, INC. – NEW YORK

PREFACE

The aim of this series of books has been outlined in the preface to Volume I, which was published in 1961. It will therefore, suffice to say here that in the present volume, six review articles are being presented to our readers which cover progress in the following subjects: optical gratings for high resolution spectroscopy, metrological applications of diffraction gratings, diffusion through non-uniform media, modern methods for image correction of optical systems, fluctuations of light beams and methods for determining optical parameters of thin films.

EMIL WOLF

Department of Physics and Astronomy
University of Rochester
Rochester 20, New York

March, 1963

CONTENTS

III. DIFFUSION THROUGH NON-UNIFORM MEDIA

by R. G. GIOVANELLI (Chippendale, N.S.W.)

IV. CORRECTION OF OPTICAL IMAGES BY COMPENSATION OF ABERRATIONS AND BY SPATIAL FREQUENCY FILTERING

by JUMPEI TSUJIUCHI (Tokyo)

V. FLUCTUATIONS OF LIGHT BEAMS

by L. MANDEL (London)

VI. METHODS FOR DETERMINING OPTICAL PARAMETERS OF THIN FILMS

by F. ABELÈS (Paris)

I

RULING, TESTING AND USE OF OPTICAL GRATINGS FOR HIGH-RESOLUTION SPECTROSCOPY

BY

GEORGE W. STROKE

Department of Electrical Engineering and Research Laboratory of Electronics,

Massachusetts Institute of Technology, Cambridge 39, Massachusetts

CONTENTS

§ 1. Introduction

One of the most significant developments in optical spectroscopy that has occurred since interferometric devices were developed at the beginning of this century by Charles Fabry and A. A. Michelson is the attainment of luminous diffraction gratings usable for high-resolution spectroscopic studies in the one million resolving power range. Resolutions in the 1 million range in the visible and even higher in the ultraviolet are indeed now being obtained with the help of the large grating recently produced by ruling under interferometric control on the M.I.T. ruling engine (STROKE [1961]; HARRISON and STROKE [1960, 1955]). Gratings of very high spectroscopic quality for somewhat smaller resolutions had already been produced for several years on engines at the Johns Hopkins University (STRONG [1951, 1960]) and at the Mt. Wilson and Palomar Observatory Laboratory (BABCOCK and BABCOCK [1951]). Interferometric control is now also being applied to the Mt. Wilson Laboratory engine (BABCOCK [1962]) as well as to several engines in industrial laboratories (Bausch and Lomb Co., Jarrell-Ash Co.), and gratings of increasingly good quality have been produced on these engines, by purely mechanical means, for several years (STRONG [1960]; A. K. PIERCE [1957]).

In this article we propose to deal more particularly with the developments in the *ruling, testing and use of high resolution gratings*, on which we have worked in the last ten years, for a part with G. R. Harrison, since they represent in several aspects significant departures from past approach to the production, evaluation and use of optical diffraction gratings (STROKE [1961]; HARRISON and STROKE [1960]; STROKE [1955]). Rowland and later Michelson when writing on the subject of diffraction gratings both dealt more particularly with their own problems and with their contributions both to the theory of image formation by imperfect gratings, as well as to the improvement of the diffraction gratings which they were ruling. A better understanding

of the effects of ruling imperfections on the distribution of light in the spectral images formed by imperfect gratings was also then at the root of grating improvements (ROWLAND [1902]; MICHELSON [1927]).

It is known that over 90 per cent of the spectroscopic studies in the classification of energy levels in atomic spectra have been carried out with the help of diffraction gratings (SHENSTONE [1960]), but it had generally been considered for many years that the resolving powers on the order of 100 000, that were sufficient for the study of these spectra, were also the best resolving powers that could be easily attained with diffraction gratings. This was in fact true for gratings ruled on the very fine mechanical engines developed after H. A. Rowland constructed the first of his engines in 1882 at the Johns Hopkins University. New demands on spectroscopic resolution have been made in optical studies of Zeeman effects in complex spectra, and, more recently, in the study of solar line shapes, as well as in the study of the structure of the atomic nucleus which manifests itself in the optical domain. The study of line shapes in optical masers is presenting further challenging demands on the quality of gratings.

Several ingenious mechanical designs have therefore been carried out in an attempt to improve the regularity and quality of the gratings ruled on mechanical engines by one or even two orders of magnitude, as required in modern high resolution spectroscopic studies. The work of John Anderson, R. W. Wood and John Strong at the Johns Hopkins University, that of A. A. Michelson at the University of Chicago and the work of Horace D. Babcock and Horace W. Babcock at the Mt. Wilson and Palomar Observatory Laboratory is particularly well known for its import on the development of the mechanical ruling art in the United States of America.

Significant contributions to the improvement of grating ruling engines have also been made by M. Siegbahn in Sweden, as well as by T. R. Merton in Great Britain. New mechanical designs are still being developed in several countries, Germany, Russia, France, Japan, Great Britain and in the U.S.A. in particular, in a tradition that has been growing ever since Rittenhouse and Fraunhofer ruled what are believed to be the first optical diffraction gratings in 1785 and 1823 respectively. (STROKE [1961]; STRONG [1960]; HARRISON [1949, 1950]; JARRELL [1960]; HANSEN [1961]; GERASIMOV [1954, 1958]; INGALLS [1952]; SAYCE [1953]).

Unlike what appeared necessary in the past, however, it became clear very early in our attempt to improve the quality of diffraction

gratings by ruling under interferometric control, that a quantitative method of measurement of the position of the grooves ruled on the grating had to be developed to permit a satisfactory control of grating ruling. The experimental attainment of an actual graph of the distribution of errors in groove positioning across the entire grating width thus appeared very desirable. At first it seemed that a measurement of the groove location on the grating with respect to the origin might present a problem of a complexity comparable to that of placing any particular groove or portion of groove in a high resolution grating within better than $\frac{1}{10}\lambda$ in the visible, that is within better than 0.05 microns or 2 microinches from the beginning of the grating. However, after several unsuccessful attempts, we succeeded in developing an interferometric wave front measuring method (STROKE [1955]) which does in fact provide such a graph directly in an experiment, after only a few seconds of exposure time on photographic film.

The interferometric grating testing method did in fact provide the key to the successful solution of the control of the M.I.T. ruling engine by interferometric photoelectric servo-mechanisms. But there remained the problem which has plagued every grating ruling engine designer and that is the fact that no engine has yet been made to operate as perfectly as would have been desirable at the time of its construction. Of the various improvements to the ruling engine which appear possible at such instances, one needs to be able to select to work on these improvements which are most likely to significantly improve the spectral quality of the gratings. Thus, for example, at the time when Rowland was ruling his gratings, the gratings were being used for spectroscopic work in domains far removed from their theoretical resolving power. In other words the spectral lines produced by the gratings were to have good quality in a region rather distant from the line centers. The spectral lines, it is well known, are images of the entrance slit of the spectrograph. The grating errors which would most disturbingly affect these regions happened to be periodic errors in the positioning of the grooves on the gratings. Periodic ruling errors found in imperfect gratings generally extend over significant portions of the grating, for example, with periods of the order of $\frac{1}{30}$ inch, or so. They correspond to the pitch of the engine screw, and result in the appearance of what has since been called Rowland ghosts. Periodic ghosts generally appear in symmetric position with respect to the line centers, as if they had their origin in a 'ghost' grating having precisely the period of the screw. In his theoretical work,

Rowland attached particular significance to the study of the effect of periodic ruling errors of very small amplitude, with a view of reducing their appearance in the gratings ruled on his engines.

The effect of *macroscopic* errors on the distribution of light in the spectral images, in high-resolution gratings is however considerably more damaging than the effect of local or microscopic errors. The 'macroscopic' errors may extend over $\frac{1}{4}$ inch or more of the grating width. As recently shown by STROKE [1960, 1961], HARRISON and STROKE [1960], the macroscopic errors, with comparatively small amplitudes, predominantly affect the immediate neighborhood of the line centers by the production of generally asymmetric 'satellite' lines. The more 'local' or 'microscopic' ruling and groove errors are primarily at the origin of 'scattered light' and 'ghosts' which appear in regions much more distant from the line centers, and are thus less harmful in high-resolution spectroscopy. Before the general theory of the effects of grating ruling errors was given by Stroke in 1960, MICHELSON [1912, 1927] had examined several cases related to errors occurring in his engines, and the problem had received a great deal of attention by many authors, among them Lord RAYLEIGH [1874], ROWLAND [1893, 1902], MASCART [1889], ALLEN [1902], SPARROW [1919], J. A. ANDERSON [1922], R. W. WOOD [1924], DITCHBURN [1930], GALE [1937], J. STRONG [1951], BABCOCK and BABCOCK [1951], INGELSTAM and DJURLE [1952, 1953, 1954], LOHMANN [1959]. It is also interesting to note in this connection that it is quite clear in his book 'Studies in Optics' that Michelson was not only aware of the formulation of scalar diffraction theory in terms of Fourier transformations, but actually used it in his work. Oddly enough, however, for the creator of modern interferometers, Michelson was not given the privilege of seeing a measure of the quality of his gratings in one of his interferometers, even though he had of course conceived of the possibility of examining the diffracted wave fronts in this way (MICHELSON [1902, 1927]). It is indeed remembered that there was no collimator in Michelson's interferometer, unlike in that used by Stroke which is the Michelson interferometer as modified by Twyman and Green (STROKE [1955]). In Michelson's interferometer a perfect wave front reflected from a perfect mirror, or diffracted by a perfect grating, would result in the appearance of a system of rings somewhat similar to Newton's rings rather than to a straight-line fringe system as is the case in the Michelson–Twyman–Green interferometer. Grating imperfections would thus have been very difficult to interpret in this way, even if examination of gratings

at high angles had been possible at Michelson's times. In fact, the spectroscopic light sources available at those times did not make such a high angle examination of gratings possible as it is today with the help of the sharp lines from single isotope sources, such as the Hg 198 source for example (STROKE [1955, 1960, 1961]). Light from optical masers should also be helpful in interferometry.

The development of the ruling art, which has preceded the modern methods of controlled grating ruling was described in a comprehensive study by G. R. HARRISON in 1949. More recently John Strong has reviewed the ruling of gratings at the Johns Hopkins University to which he himself has made such a significant contribution (STRONG [1960]). From these studies, as well as from the experience of G. W. Stroke in developing with G. R. Harrison, the new method of ruling diffraction gratings under interferometric control of the ruling engine, one significant feature may be singled out. There is no simple prescription for building a ruling engine in such a way that it will perform successfully immediately after completion, or, for that matter, during any great length of time after its first successful ruling without the close attention of the instrument maker, physicist or engineer who has made it operate successfully in the first place. This has been proven to be true even on the servo-controlled M.I.T. ruling engine of which the principle of interferometric control was first described by G. R. HARRISON and G. W. STROKE in 1955.

As a corollary, one may also state that the description of the various ingenious mechanical (and now also of the optical and electronic) features that may have been incorporated into the building of any particular ruling engine is truly only interesting for an engine that has been made to work successfully. And even then the design features should be considered as materializing basic principles rather than an optimum achievement of an idea.

Even though there are no simple statements about the 'best method' of constructing a successful ruling engine it may be noted that the spectroscopic quality of the best gratings ruled on the M.I.T. ruling engine now exceeds by a factor of almost 100 the quality of the already very famous gratings ruled on Rowland's engines around 1915. At the same time the large 10×5 inch high-resolution gratings ruled on the M.I.T. ruling engine also exceed by a factor of probably at least 10 the quality of the very fine gratings being ruled on a number of other mechanical engines in several laboratories in the U.S.A. in particular. There may therefore be some merit in describing

the control features of the interferometrically controlled M.I.T. ruling engine in some detail, since we believe that the control principles developed for use on that engine will help in improving by at least one order of magnitude, the quality of gratings ruled on any other of the good mechanical engines, which exist or are being built. One may also note here that, in addition to the Johns Hopkins University and the Mt. Wilson Observatory Laboratory, and to the University of Michigan (which has long been a primary source of infrared gratings) (RANDALL [1939, 1954]), the Bausch-Lomb Company of Rochester, New York and the Jarrell-Ash Company of Newtonville, Mass. have in the recent years supplied the scientific and industrial community with several hundreds of very fine diffraction gratings ranging in size from 2×2 inches to 8×4 inches ruled on mechanical engines developed in their own laboratories. These firms have also developed successful grating replication processes and have been able to duplicate the quality of a given master ruling in a great number of replicas, in a manner which bears some resemblance to that used in the reproduction of high-fidelity records (STROKE [1961]).

Replicas of the high-resolution gratings ruled on the M.I.T. ruling engine are becoming generally available through the replication methods developed by industrial firms. We have reached a period where the simplicity of the spectroscopic use of optical diffraction gratings has become more widely available to the scientific community and laboratories than would have been considered possible only then years ago. The resolution in the 1 to 2 million resolving range that can now be easily obtained with modern gratings has made possible the use of high-resolution grating spectrographs and spectrometers for applications in which the use of interferometers was conceived as the only solution heretofore. Even much greater resolutions are obtainable when two gratings are used in series (STROKE and STROKE [1958]; HARRISON and STROKE [1960]; STROKE [1961]), or when a grating is used in immersion (HULTHÈN and NEUHAUS [1954]; BJÖRKLUND [1958]), or in a multi-pass arrangement (JENKINS and ALVAREZ [1952]; FASTIE and SINTON [1952]; RANK and WIGGINS [1952]; SHEARER *et al.* [1956]; RANK *et al.* [1957]).

The spectroscopic information about the intensity distribution in a light source as a function of wavelength (or frequency) which is sought in spectroscopic studies is generally obtained with a grating considerably more simply than with an interferometer. Moreover, the diffraction grating, as an optical element, has the significant advantage

of having its optical quality and resolving power built into it, as it were once and for all (in the form of the ruling of grooves on an aluminized mirror or in a replica), while an interferometer in order to perform with an equivalent quality, must be brought into adjustment, general at the time of use, with the help of additional optical and mechanical devices. This is of course also the case for the control interferometers that are used to introduce the precision into the high-resolution gratings in the first place.

§ 2. Quality of Gratings Required for High-Resolution Spectroscopy

Here we wish to deal more particularly with the new use of gratings to obtain resolutions up to the order of 2 million or so in the visible and near ultraviolet domains. This is the domain of high-resolution spectroscopy which has been discussed by several authors and, in particular, by S. Tolansky in his now classical treatise on High-Resolution Spectroscopy, first published in 1947.

More recently P. JACQUINOT [1960], whose significant contributions to interferometric spectroscopy are well known, discusses the new developments in interference spectroscopy, and in particular the use of interferometers in spectrometers with photoelectric detection. R. J. HULL and H. H. STROKE [1960, 1961] have used high-resolution gratings for the study of charge distribution and magnetism in radioactive nuclei with as little as 10^{12} atoms in the source. It is significant to note that even in 1960 when P. Jacquinot published his article in *Reports on Progress in Physics*, the spectroscopic resolution capabilities of the new high-resolution gratings were not yet sufficiently well known to affect what may well be called the classical impression that the domain of the high-resolution studies in the 10^6 resolving power range was only accessible to interferometric devices.

The significant advantages of convenience, broad spectral coverage, simplicity of wavelength reduction, speed and efficiency of order separation that can be obtained with a grating spectrograph (or spectrometer) have been foreseen theoretically ever since the first gratings were ruled at the end of the 18th and beginning of the 19th centuries. However, as is frequently the case in technological developments, the ruling of sufficiently good high-resolution gratings has lagged so much behind the definition of the theoretical capabilities that the basic advantages of built-in-precision and simplicity, characteristic of gratings, have somehow been forgotten.

In section 4 we shall compare the use of gratings with the use of interferometers in modern high-resolution applications. Optical instruments can in general not be built to be perfect in terms of their optimum theoretical capabilities. This is of course equally true for interferometers and gratings. It is good therefore to discuss separately on one hand the optimum theoretical capabilities of the instrument, and, on the other hand, various limitations in actual performance that may arise from residual manufacturing imperfections, from the restrictions imposed by the available intensities in the light sources that are being studied, and from the threshold and signal-to-noise characteristics of the receptors. R. Chabbal has carried out a comprehensive study of the effects of various Fabry–Perot etalon manufacturing imperfections on its spectrometric applications (cf. CHABBAL [1957, 1958]). More recent contributions to the evaluation and photoelectric use of Fabry–Perot interferometers have also been made by KOPPELMANN and KREBS, in particular [1961]. Chabbal's and Jacquinot's conclusions are also discussed by P. Jacquinot in his 1960 *Reports on Progress in Physics* paper. Here we discuss comparable theoretical capabilities and experimental limitations of plane diffraction gratings. It should be borne in mind, both for Fabry–Perot etalon and for high-resolution grating limitations, that the departures from perfection of spectroscopic elements, as they are obtainable today, are measured in very small fractions of a wavelength in the optical domain, typically $\frac{1}{20}\lambda$ (0.05 microns or 10^{-6} inches) for high-resolution gratings, and $\frac{1}{100}\lambda$ (0.01 microns of 2×10^{-7} inches) for Fabry–Perot etalon plates of comparable quality. High-resolution gratings can indeed stand departures from perfection which are five times as great as those acceptable in Fabry–Perot etalon plates for comparable spectroscopic quality. Moreover, the spectroscopic quality is built into the grating, as it were, once and for all, while the spectroscopic quality of the Fabry–Perot etalon can be attained only by correspondingly good mechanical adjustment of the parallelism of the plates (an adjustment which usually needs to be carried out at or just prior to the use of the etalon). Difficulties in mechanical adjustments of spectroscopic interferometers should not be overemphasized, we know. Interferometers are, after all, being used in the ruling of the high-resolution gratings which we are describing here. We therefore know that interferometers can be set and maintained in stable adjustment for great lengths of time (of the order of many days) if appropriate precautions are taken in the control of the temperature and mechanical suspension

of the mirrors. However, interferometer adjustments require expert handling which is frequently outside of the immediate interest of the spectroscopist using the instrument.

2.1. THEORETICAL PERFORMANCE CHARACTERISTICS OF PERFECT DIFFRACTION GRATINGS

2.1.1. *Wave fronts, diffraction patterns and grating equation*

The optimum theoretical characteristics of a plane diffraction grating can be stated in very simple terms (Fig. 1 and Fig. 2). When a plane wave front is incident on a plane diffraction grating so as to form an angle i with the grating surface, a perfect grating of width W produces a set of plane diffracted wave fronts of width $A = W \cos i'$ to which correspond diffraction patterns with first minima at λ/A radians from the line centers. The line centers themselves correspond to the direction i' of the diffracted wave fronts which is related to the direction i of the incident wave front by the equation (1),

$$\sin i + \sin i' = \frac{m\lambda}{a}, \tag{1}$$

where m is an integer, λ the wavelength and a the grating spacing constant. The diffracted wave fronts are surfaces of constant phase and have a physical reality with measurable parameters. The interferograms, by which STROKE [1955, 1960, 1961] compares the diffracted wave fronts to a plane wave front reflected from a perfect mirror, display the wave front topography in a most spectacular manner. The interferometer used to obtain the wave front interferograms is schematically shown in Fig. 3a and an experimental arrangement in Fig. 3b. Wave front interferograms permit to evaluate a grating immediately after the ruling, if necessary, to assess any departures from perfection. A typical interferogram is shown in Fig. 4.

The theoretical description of the diffraction of light and of the formation of spectral images by gratings is extremely straightforward, as far as the diffraction patterns and their imperfections are concerned (STROKE [1960, 1961]).

Consider indeed a plane reflecting surface infinitely extended in the x direction and periodically deformed in the y direction as a function of x (the surface deformation of the grating is considered to be independent of z). Let plane wave fronts $\sum_i$ (such as a wave front

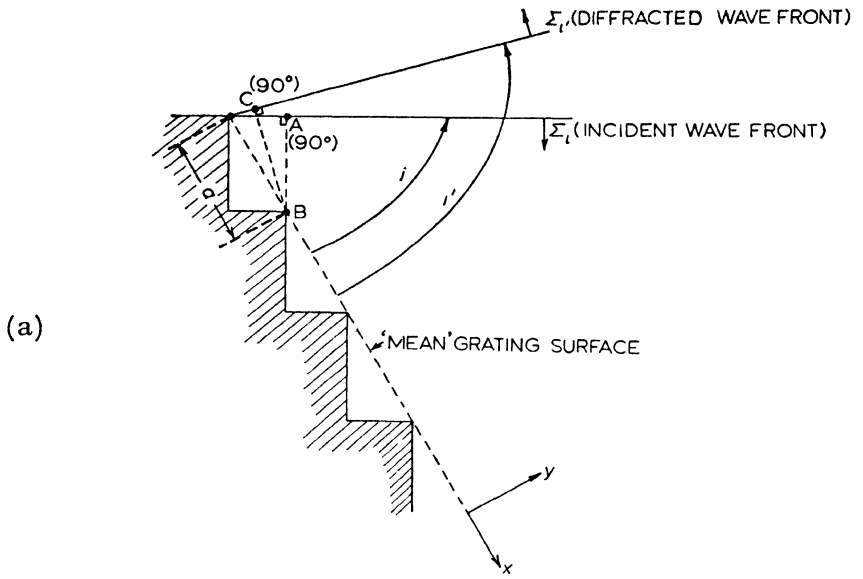

(a)

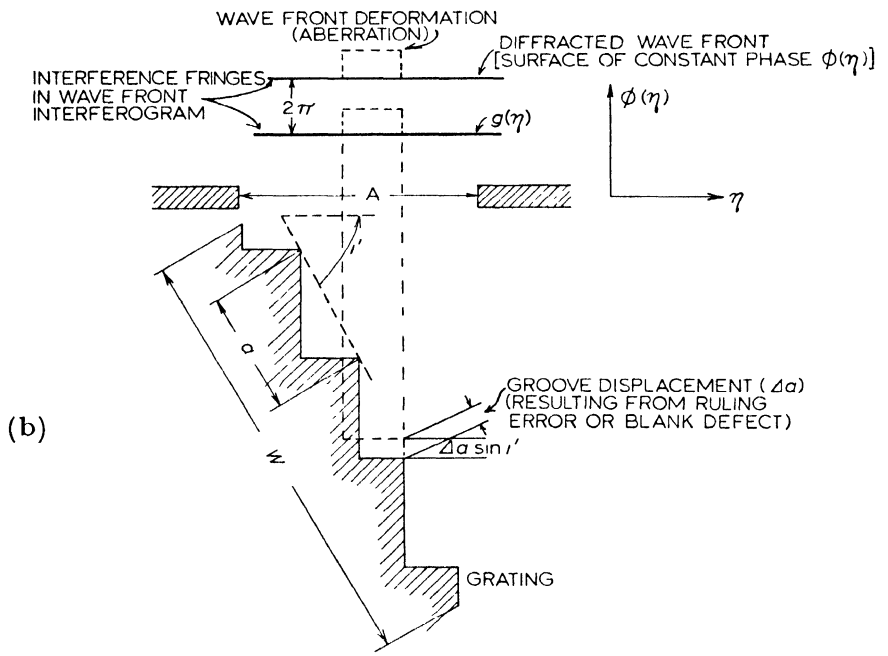

(b)

Fig. 1a. Diffraction of plane waves by a plane reflection grating. a = grating spacing constant. i = angle of incidence. i' = angle of diffraction.

Fig. 1b. Effect of ruling errors on diffracted wave fronts. Errors in the positioning of the grooves result in deformations of the diffracted wave fronts. The wave-front deformations (aberrations) appear as deviations from straightness in the experimental wave-front interferograms (see Fig. 4). One fringe ($\frac{1}{2}\lambda$) of groove displacement (Δa) results in ($\Delta a \sin i'$) fringes of deviation in the wave-front interferogram. The errors in positioning of the grooves may result from errors in the ruling or servo-control, from curvature of the grating blanks or from defects in flatness of the metallic coatings in which gratings are being generally ruled.

reflected by a mirror and produced from light originating at a point source in the focal plane of the mirror) be incident on the grating so as to form an angle i with the mean surface of the grating. As a result, simply, of the periodic nature of the surface deformation, a spectrum of 'diffracted' plane waves will leave the grating under the angles i' corresponding to equation (1) (U. FANO [1938]; STROKE [1960]).

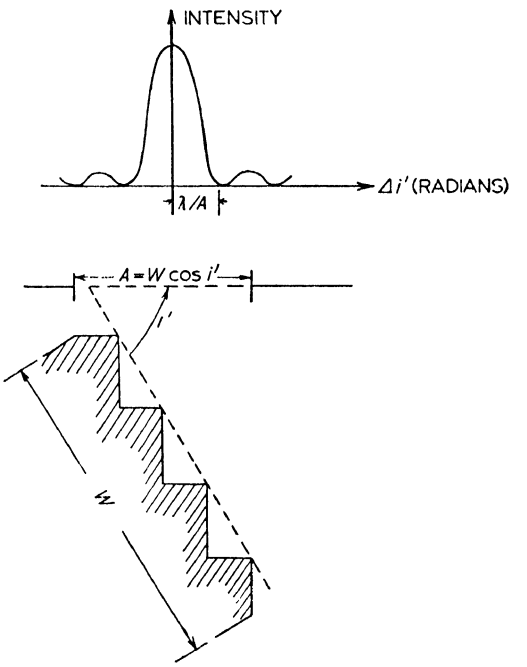

Fig. 2. Grating diffraction parameters. Grating of width W in autocollimation ($i = i'$). Diffracted wave front of aperture $A = W \cos i'$. Diffraction pattern with first minimum at (λ/A) radians. It is clear that the width of the diffraction pattern, in a given wavelength λ, depends only on the grating width W and the angle i'. It is independent of the grating spacing constant a. The 'resolving power' of a perfect grating in any wavelength is determined by the grating width and angle only.

Equation (1) can be simply derived as shown in Fig. 1. If the diffracted wave front is to be a surface of constant phase, just like the incident wave front, then the distance $\overline{AB} + \overline{BC}$ must be equal to an integral number of half wavelengths. When the grating has a finite rectangular width W, as is the case in practice, then each of the diffracted wave fronts is bounded to have a width $A = W \cos i'$. Similarly to any other plane wave front of finite width (such as a wave front transmitted by a lens or a wave front reflected by a mirror), the bounded diffracted wave front produces in the focal plane

of a lens or mirror a diffraction pattern of which the first minimum is at $(\lambda/A)f$ from the center, as shown in Fig. 2. Here F is the focal length (or projection distance) of the lens (or mirror). In fact, it is helpful to consider the angular domain as seen from the diffraction grating rather than the corresponding linear domain in the focal plane

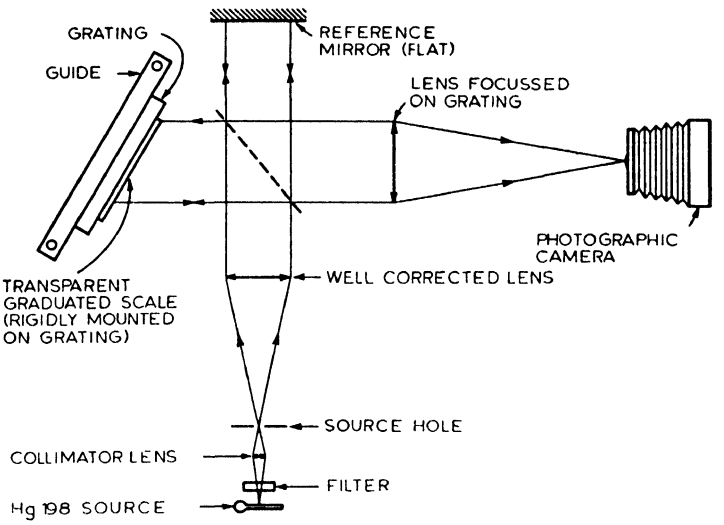

Fig. 3a. Grating testing interferometer. The gratings should be examined at the highest angle permitted by the blaze. For good fringe contrast, the reference mirror needs to be carefully autocollimated on the source hole. The grating is so adjusted, with the help of leveling screws, that the fringes of the mean wave front appear at right angles to the groove length (STROKE [1955, 1960, 1961]).

of the mirror. It is seen that the first minimum of the diffraction pattern which corresponds to a diffracted wave front of width A is at λ/A radians from the line center, and we remember that the line centers themselves are found at the angles i' given by equation (1).

2.1.2. *Fourier transform description of grating diffraction problem*

We next express the diffraction of light by a grating in the scalar approximation. Let us define the angular coordinate β in the Fraunhofer domain by

$$\beta = \pi \frac{x}{(\lambda/A)f} = \pi \frac{x}{x_0}, \tag{2a}$$

$$\beta = 0 \quad \text{for} \quad i' = \sin^{-1}[(m\lambda/a) - \sin i] \tag{2b}$$

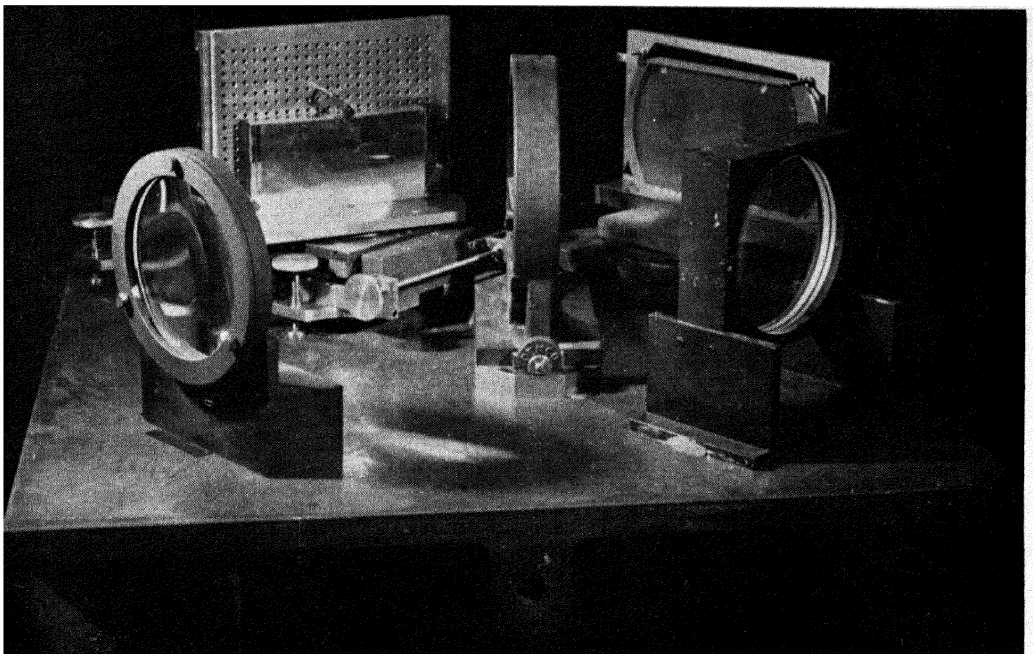

Fig. 3b. Grating testing interferometer. From left to right: camera lens, 8-inch grating (shown here at low angle for clarity), beam splitter, reference mirror, collimator. As shown, this interferometer permits testing of gratings up to approximately 12 inches in width at the highest angles (76°) in autocollimation. Mechanical vibrations in such interferometers are easily avoided if the mechanical mounts are fairly heavy, if possible made out of 'meehanite', and have well-machined, flat supporting surfaces.

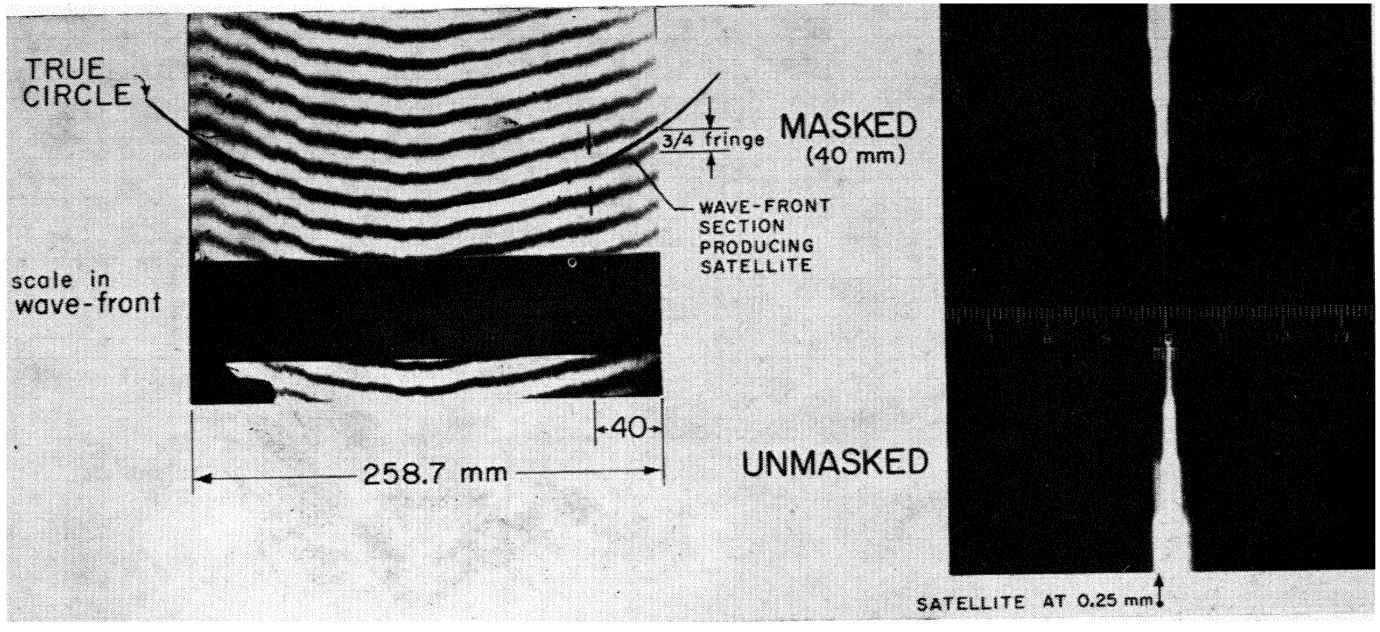

Fig. 4. Wave-front interferogram and corresponding spectrogram of Hg 198 green line (5461 Å). The wave-front interferogram displays the topography of the diffracted wave front. A perfect wave front produces straight (horizontal) fringes. (The grooves project vertically on the interferogram.) Other than a plane wave front (to which correspond straight fringes), a parabolically curved wave front of small curvature will also result in 'perfect' diffraction patterns. Aberrations from either a plane or a parabolically (in practice spherically) curved wave front result in the appearance of spurious spectral lines (satellites, grass, ghosts). When the 40 mm wave-front section (on right of interferogram) is masked off, the satellite at 0.25 mm is seen to disappear (in spectrogram). For the calculation of the position of satellite see text, section 2.2.7.

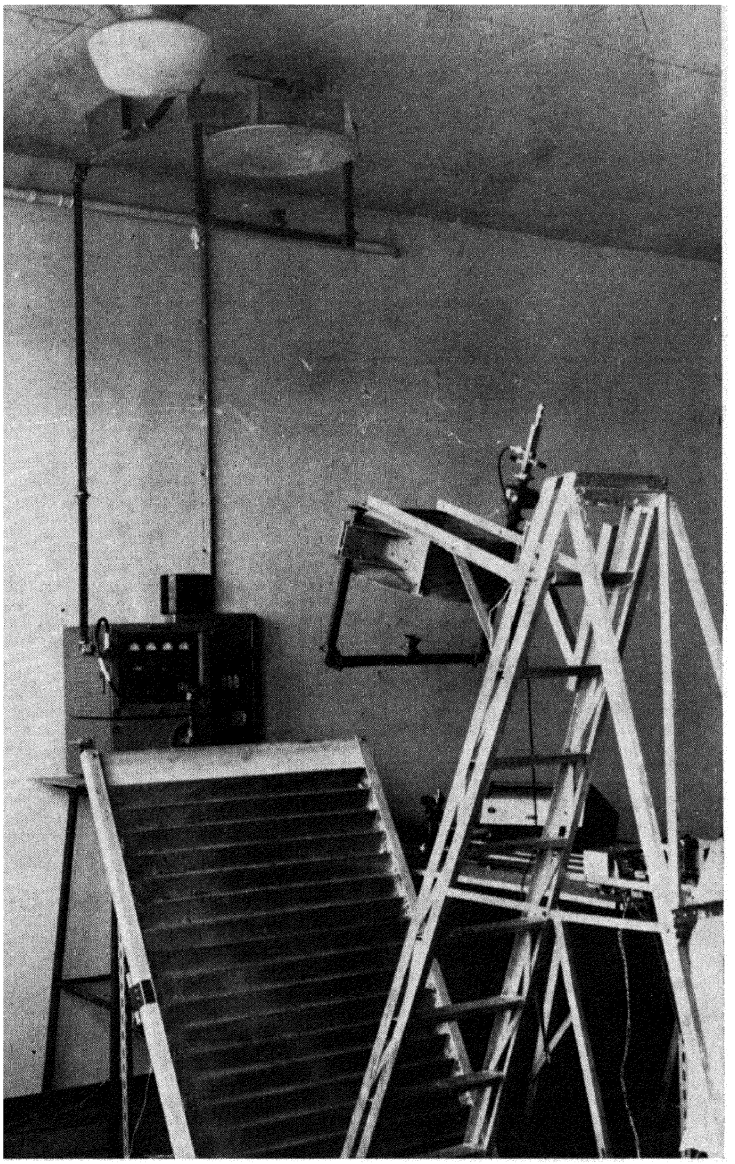

Fig. 5. Study of the diffraction of light by gratings with the help of measurements in the microwave domain. A grating with rectangular groove steps 2λ deep and 1λ wide in normal incidence on the 1λ groove side is shown here, with the E field in the incident wave normal to the 2λ side. This is the case of the 'anomaly' described by MARÉCHAL and STROKE [1959] (see also STROKE [1960]): no energy is 'diffracted' into the 3rd order, at some 37° from the vertical, while some 20 per cent of the incident energy would be expected there if the diffraction of light could be described by a scalar approximation when calculating the distribution of light energy with angle and order in general. To measure the phase across the wave front in the 3rd order, as obtained in Fig. 6, the other polarization with the E field in the incident wave front is parallel to the 2λ sides. Also, rather than the receiving antenna shown here, only a small directive horn was used for detection by scanning across the diffracted wave front, in a microwave analogue to a two-beam interferometer.

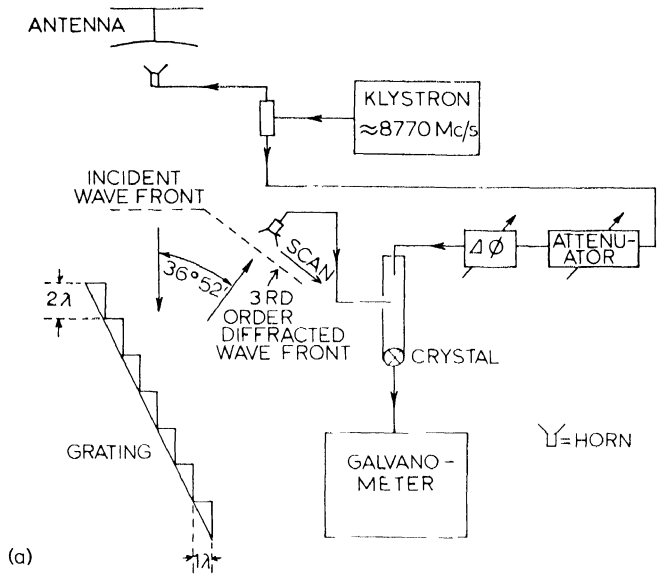

Fig. 6a. Measurement of phase across the diffracted wave front (schematic). The question may be asked whether the 'plane' wave fronts produced by diffraction on a plane grating are truly continuous, as can be expected on the basis of rigorous theory, or whether they keep some 'memory' of any individual 'diffraction' by the grooves of the grating, as might be concluded from a scalar description of diffraction using Huygens' principle. The arrangement used for the measurement is essentially the microwave analogue of a two-beam interferometer. The receiving horn was made to scan across a 3rd order diffracted wave front, at about 45 wavelengths from the grating surface, and the result of the measurement is shown in Fig. 6b (STROKE [1960]).

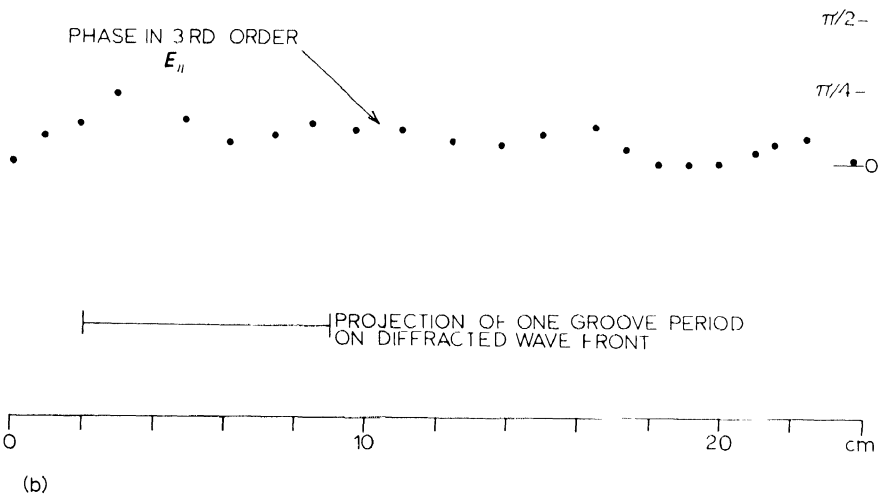

Fig. 6b. Continuity of the wave fronts diffracted by a grating. Unlike classical descriptions of the diffracted wave fronts as being 'envelopes' of little Huygens 'wavelets', it is seen that the phase across the wave fronts diffracted by a grating is perfectly *continuous* already in the immediate neighborhood (some 40 to 50 wavelengths) from the grating surface (STROKE [1960]).

where x is a length in the focal plane of the spectrograph and $x_0 = (\lambda_0 A)f$ is the so-called 'diffraction unit' (distance of the first minimum from the center of the diffraction pattern). β is measured from the centers of the spectral lines. Let

$$\eta = u/\tfrac{1}{2}A \tag{3}$$

be a normalized length in the diffracted wave front itself.

The distribution of complex amplitude of the light in the diffraction pattern $\mathscr{A}(\beta)$ is given by the Fourier transform of the complex amplitude distribution across the wave front:

$$\mathscr{A}(\beta) = \int_{-1}^{+1} g(\eta) \exp[i\beta\eta]\, d\eta, \tag{4}$$

where

$$g(\eta) = \mathscr{A}(\eta) \exp[i\Phi(\eta)] \tag{5}$$

is the distribution of complex amplitude of the light in the diffracted wave front (STROKE [1960]). The distribution of light intensity $I(\beta)$ in the diffraction pattern is proportional to the product of $\mathscr{A}(\beta)$ with its complex conjugate $\mathscr{A}(\beta)^*$, and we have with the above normalization

$$I(\beta) = \tfrac{1}{4}\mathscr{A}(\beta)\,\mathscr{A}(\beta)^*. \tag{6}$$

We know, of course, that only the intensity distribution $I(\beta)$ can be recorded by any detector, such as a photoelectric receiver or photographic plate.

2.1.3. *Physical basis for description of grating diffraction in terms of wave fronts and diffraction patterns*

Equations (4), (5) and (6) result from the scalar description of diffraction and apply to the description of diffraction patterns formed by wave fronts which are extended when compared to the wavelength. This is the case of diffraction gratings. Equation (4) can be considered as expressing a form of Huygens' principle. It is important to note that the relation between the diffracted wave front and the corresponding diffraction pattern does not in any way distinguish the origin of the wave front in the 'diffraction' by individual grooves of the grating. This is in agreement with experiment.

In order to establish this fact and to verify that a diffracted wave front does not keep a memory, as it were, of its origin in the diffraction by individual grooves, G. W. STROKE [1960] measured the phase across the wave front produced by a grating in the 3.4 cm microwave

domain. With microwave analogue gratings a detailed measurement within regions that are small when compared both to the groove spacing and the wavelength is possible. Fig. 5 shows the experimental arrangement and Fig. 6 the result of the measurement. Unlike what is generally assumed in textbooks, it is seen that the diffracted wave fronts produced by a grating are truly continuous wave fronts with no memory of the local shape of the groove profile. What gives rise to the phenomenon of diffraction by a grating and the resulting production of plane diffracted wave fronts is the periodic spacing of the 'grooves' on its surface. The diffracted wave fronts produced by a perfect grating cannot be otherwise distinguished from a wave front produced by reflection or refraction. It is clear, therefore, that the Fourier transform description of the diffraction of light by optical systems developed by MICHELSON [1927], DUFFIEUX [1946], MARÉCHAL [1947, 1948, 1960], ELIAS [1952, 1953], O'NEILL [1957], INGELSTAM [1953], WOLF [1951, 1953, 1955, 1959], and others (see BARAKAT [1961], applies to gratings without reservations as shown above. In fact, considerable simplification results in the practical application of the Fourier transform description of optical processes to the case of grating, as a result of the one-dimensional description of the grating and of its diffracted wave fronts. In other optical instruments the aberrations generally vary with two dimensions across the wave front. For uniformly blazed gratings, with a constant amplitude $\mathscr{A}(\eta)$ across their width, as is generally the case in practice, equation (5) takes on a particularly simple form

$$g(\eta) = \exp[\mathrm{i}\Phi(\eta)]. \tag{5a}$$

Equation (5) is remarkable by the fact that the phase $\Phi(\eta)$ is the very function which appears already in graphical form in the experimental wave-front interferograms (STROKE [1955, 1960, 1961]). The reader should also consult STROKE [1964].

2.1.4. *The problem of spectral resolution. Incoherence of 'spectral lines'*

In section 2.2 we shall consider the effect of grating imperfections on the spectral quality of gratings. We shall show that grating imperfections simply result in corresponding diffraction-pattern imperfections. But first we need to complete the theory of the formation of spectral images by optical gratings.

As an optical instrument, a grating is used to produce a spectrum of the light that is incident on the entrance slit of the spectrometer

or spectrograph (Fig. 7). As a dispersive instrument, a grating spreads out the light of various wavelengths as a function of angle according to equation (1). For every monochromatic (single frequency) wavelength each point of the entrance slit results in the production of a diffraction pattern according to equations (4) and (5), and a slit of finite width and height gives rise to a slit image of finite width and height, just as if the grating were a mirror. This is true since the grating does not disperse the light of a single frequency by definition. When the collimator and camera mirrors have the same focal length, the mono-

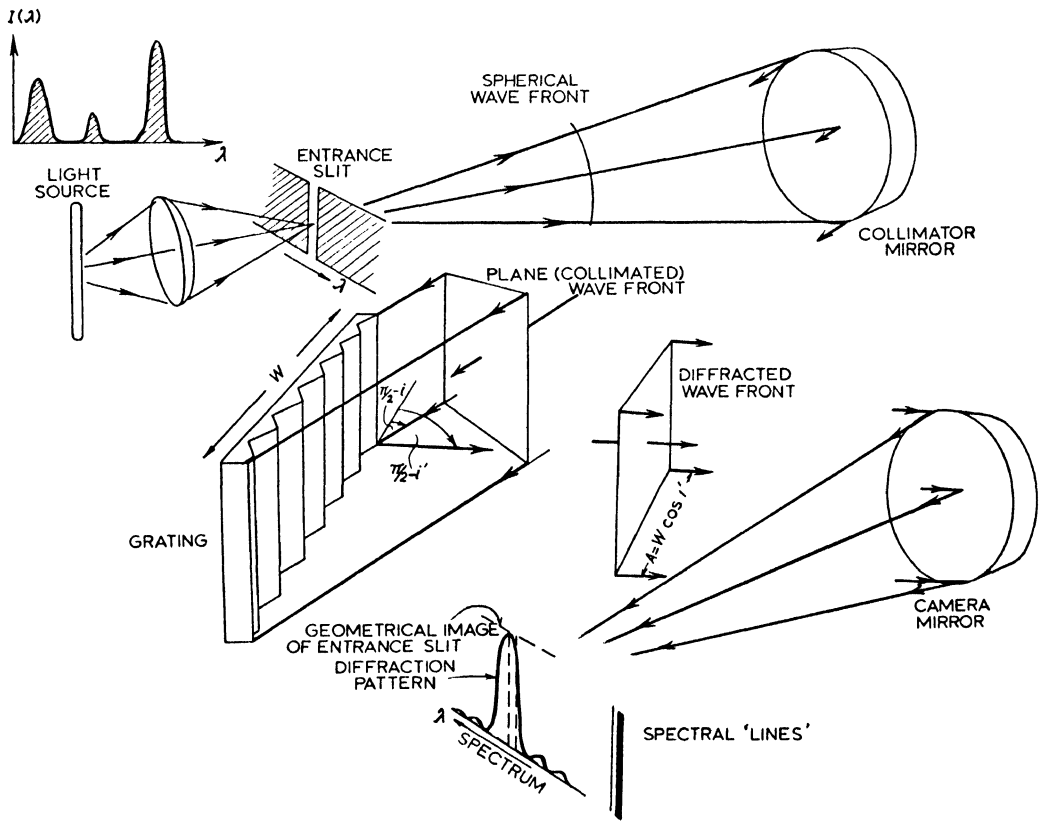

Fig. 7. Grating spectrograph or spectrometer. Schematic diagram showing parameters discussed in text.

chromatic images of the entrance slit produced by the grating are thus 'images' in the usual sense in optics.

We next note that in usual light sources, there is no coherence between photons of different energies. Light of different 'monochromatic' wavelengths is usually completely incoherent. It becomes clear that the formation of slit images in different wavelengths is not related by interference, but rather that the light intensity detected at a given point in the focal plane of the camera mirror is the sum of

the light intensities produced there by each wavelength separately of all others.

Now in the ideal case if both the entrance slit and the diffraction patterns were infinitely narrow, only one wavelength would produce a detectable intensity at each point in the focal plane of the spectrograph. The neighboring point would be illuminated by light from a different wavelength, and one would obtain infinite *spectral resolution.* In reality, both the entrance slit and the diffraction patterns have finite spread. Moreover, there is frequently also an exit slit in the instrument. The effect of finite entrance and exit slits is simple to understand (JACQUINOT and DUFOUR [1948], JACQUINOT [1954]), and to take into account. In practice, we shall see, one can generally use slits that are very narrow when compared to the width of the diffraction patterns, even in the ideal case of perfect grating. No loss of generality therefore results from the use of an infinitely narrow slit in the following analysis. We can indeed always replace the use of the diffraction patterns $I(\beta)$ of equation (5), corresponding to an infinitely narrow slit, by a pattern $I(\beta)'$, taking into account the effect of the slight broadening by the slit. [The broadening of $I(\beta)$ to give $I(\beta)'$ can be rigorously calculated, graphically or analytically, as a convolution of $I(\beta)$ with a rectangular slit function $s(\beta)$.]

2.1.5. *The formation of the spectrum in terms of image-formation theory*

We are now in a position to formally describe the formation of the spectrum in a grating of light intensity in the spectrum of a light source and produced by a grating, as shown in Fig. 8. The angle β is measured from the direction i' as given in equation (1). As a result of the incoherence between the diffraction patterns of different wavelengths, the intensity of the spectrum recorded at a point β (in the angular domain) is simply given by the sum of intensities produced at that point by all other spectral intensities at the various points β', each of the spectral intensities being weighted by the value at β of the diffraction intensity corresponding to the intensity of the spectrum at the point β'. If the detector at β has a finite width $\Delta\beta$, we can express the intensity $I(\beta)_{\text{spectrometer}}$ recorded at β as

$$I(\beta)_{\text{spectrometer}} = \sum I(\beta')_{\text{spectrum}}\, I(\beta - \beta')\, \Delta\beta, \tag{7}$$

or more exactly as

$$I(\beta)_{\text{spectrometer}} = \int_{-\infty}^{+\infty} I(\beta')_{\text{spectrum}}\, I(\beta - \beta')\, \mathrm{d}\beta, \tag{8}$$

where $I(\beta - \beta')$ is the value at β of the diffraction pattern $I(\beta)$ centered at β'. Equation (8) is usually described as a *convolution integral.* One says that the *spectral intensity, as recorded in the spectrometer, is the convolution of the 'true' intensity distribution in the spectrum with the intensity distribution in the diffraction patterns.* Equation (8) is sometimes written as

$$I(\beta)_{\text{spectrometer}} = I(\beta)_{\text{spectrum}} \otimes I(\beta), \tag{9}$$

where it is understood that

$$I(\beta) \equiv I(\beta)_{\text{diffraction pattern}} \tag{10}$$

and $\otimes$ stands for the convolution operation.

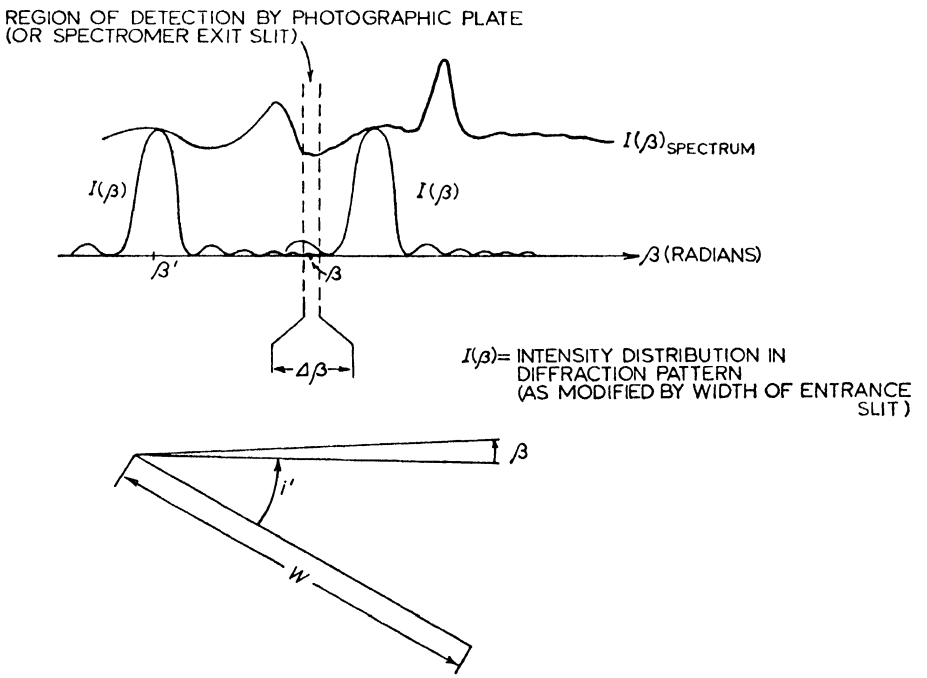

Fig. 8. Formation of spectral images by grating. The intensity distribution recorded by the receiver is seen to be a convolution of the 'true' intensity distribution in the spectrum with the intensity distribution in the diffraction pattern.

2.1.6. *The 'true' distribution of intensity in the spectrum of a light source*

We know, of course, that the aim of spectroscopic analysis is to obtain the 'true' distribution of light intensity, $I(\beta)_{\text{spectrum}}$, in the spectrum of the source that is being studied. We note, however, that any spectrometer or spectrograph will only provide the spectral

intensity distribution as modified by several convolutions involving the parameters which limit the ideal performance of the spectroscopic element. In the case of Fabry–Perot etalons, for instance, three functions have been singled out as being important in the convolution: 1) the well-known 'Airy' function (which corresponds to the perfect diffraction pattern in a grating); 2) a function involving the effect of surface imperfections in the etalon plates; and 3) the function resulting from the use of a finite range of angles of incidence (CHABBAL [1957, 1958], JACQUINOT [1960]). As it happens, the three functions involved in the spectroscopic use of Fabry–Perot etalons have comparable importance, and their exact description needs to be obtained when an attempt is made to retrieve the 'true' distribution of light intensity in the spectrum. For high-resolution gratings the situation is fortunately simple: the 'square' shaped functions resulting from the use of finite slit apertures have been shown to be negligible in practice when compared to the diffraction patterns. Thus, only the convolution with the diffraction pattern is involved in the use of high-resolution gratings. This is true, moreover, not only in the case of perfect diffraction patterns, but also in the case of imperfect patterns, since the above analysis makes no special assumptions about the distribution of light in the diffraction pattern. We have only assumed the existence of an extended diffraction pattern, as a result of the finite width of the grating. It is clear that if it were possible to obtain experimentally the distribution of light $I(\beta)$ in the diffraction patterns of a given grating (as can now be done), then it would be possible to obtain unlimited information about the spectrum of the source in an ideal noiseless case. Direct measurement of the distribution of intensity $I(\beta)$ in diffraction patterns has been attempted for many years for this purpose (DITCHBURN [1930], STRONG [1951], BABCOCK and BABCOCK [1951], HULTHÈN and UHLER [1952], RANK *et al.* [1955], A. KEITH PIERCE [1957], HARRISON *et al.* [1957], RANK *et al.* [1957], HARRISON *et al.* [1959]), but is fraught with unsurmountable practical difficulties as we shall see in section 3. Fortunately, as shown by STROKE [1955, 1960] the distribution of phase $\Phi(\eta)$ in the diffracted wave fronts can be measured without difficulty by placing the grating at its angle of use into one of the arms of a Michelson–Twyman–Green interferometer. Moreover, the distribution of intensity in the 'monochromatic' diffraction patterns, namely $I(\beta)$, can be rapidly and simply calculated from the wave front interferograms by Fourier transformation according to equation (4) with the help of a digital computer

(STROKE [1958, 1960, 1961]). With these methods, the problem of theoretical characterization of a grating for use in spectroscopic analysis can be considered as solved and we may summarize the solution as follows.

The spectroscopic behaviour of a diffraction grating is characterized by $I(\beta)$, the distribution of light in the *diffraction pattern* formed by the diffracted wave fronts in various wavelengths. $I(\beta)$ can be computed by Fourier transformation with all the required accuracy and very simply from the light distribution $g(\eta)$ in the diffracted wave fronts. And, finally, the distribution of light in the diffracted wave fronts can be found in readily usable graphical form in the experimental wave front interferograms.

To retrieve the 'true' distribution of light intensity in the spectrum from the measurement in the spectrometer, one only needs to solve equation (8) or (9) or its equivalent Fourier transform representation, namely

$$T[I(\beta)_{\text{spectrometer}}] = T[I(\beta)_{\text{spectrum}}] \cdot T[I(\beta)], \tag{9a}$$

where T [ ] indicates the Fourier transform of the function in brackets. The numerical solution of equation (9a) with the help of digital computers should be fairly straightforward, and work towards this goal is proceeding (STROKE [1959, 1960]). Similar problems also arise in radio astronomy (ARSAC [1959], BRACEWELL [1961]) and in the use of optical systems as computers in some radar work (CUTRONA *et al.* [1959, 1960]).

2.1.7. *'Resolving power' and 'dispersion' of gratings in terms of wave front and diffraction pattern formulation*

We shall next show how the description of diffraction gratings by wave fronts and diffraction patterns permits to simply derive and interpret the classical resolving power equation. Consider equation (1)

$$\sin i + \sin i' = \frac{m}{a}\lambda,$$

which gives the angles i' at which one finds the centers of the diffraction pattern of different wavelengths λ. By differentiation, we have

$$\cos i \, \mathrm{d}i + \cos i' \, \mathrm{d}i' = \frac{m}{a} \mathrm{d}\lambda. \tag{11}$$

For a constant angle of incidence, $di = 0$, and

$$\cos i' \, di' = \frac{m}{a} d\lambda. \tag{12}$$

High-resolution gratings are generally used in the neighbourhood of autocollimation when

$$i' \simeq i. \tag{13}$$

Equation (1) then becomes

$$2 \sin i' = \frac{m}{a} \lambda \quad \text{(autocollimation)}.$$

By dividing equation (12) into equation (1′) we get

$$\delta = \frac{di'}{d\lambda} = \frac{2 \tan i'}{\lambda} \quad \text{(autocollimation)}. \tag{14}$$

Equation (14) gives the so-called 'angular dispersion' $\delta = di'/d\lambda$ of the grating. It is to be noted that the *angular dispersion is independent of the grating constant 'a'*. The angular dispersion gives the local value of the *change* of angle i' with wavelength, about the angle i', as determined by equation (1). It is clear that if a given angle of incidence i, and a given angle of diffraction i' are both postulated, one can always find a ratio of (m/a) to produce a wave front in the wavelength λ provided only that m is at least equal to unity. For example, for $i = i' \simeq \frac{1}{2}\pi$, the condition $m \geqq 1$ gives $a \geqq \frac{1}{2}\lambda$. With this remark in mind, we note that the angular dispersions at a given wavelength and at given angles of incidence and diffraction is the same for all gratings, regardless of the grating constant. This is, of course, also true where $i \neq i'$, when the dispersion is

$$\frac{di'}{d\lambda} = \frac{(\sin i / \cos i') + \tan i'}{\lambda}. \tag{15}$$

According to Lord RAYLEIGH [1888] two neighbouring spectral lines of different wavelength are called 'resolved' if the diffraction maximum of one of the lines coincides with the first diffraction minimum of the other. Now the diffraction patterns of two closely neighbouring lines have practically the same shape. We have seen that the first diffraction minimum for a grating of rectangular width W is found at

$$u = \Delta i' = \frac{\lambda}{A} = \frac{\lambda}{W \cos i'}. \tag{16}$$

The minimum wavelength difference $\Delta\lambda$ which will be resolvable in terms of Rayleigh's 'criterion' is found from equations (14) and (16) by rewriting equation (14) as

$$\Delta i' = \frac{2 \tan i'}{\lambda} \Delta\lambda \tag{14a}$$

and by equating (14a) and (16). We get

$$\Delta\lambda = \frac{\lambda^2}{2W \sin i'}$$

and, in the more usual form

$$\boxed{\text{R.P.} = \frac{\lambda}{\Delta\lambda} = \frac{2W \sin i'}{\lambda}.} \tag{17}$$

The expression R.P. $= \lambda/\Delta\lambda$ is usually called 'resolving power' in spectroscopy. Here again we note that the 'resolving power' of a grating depends only on the grating width W and angle of use, as well as on the wavelength, but that it is independent of the number of grooves or grating constant. In fact, this result is not surprising.

The dispersion of a grating does not depend on its grating constant, and the diffraction pattern width (between its first minima) is also independent of the grating constant. Most fundamentally, the resolving power is, of course, simply determined by the width A of the diffracted wave front and the dispersion δ. In fact, since

$$A = W \cos i',$$

$$\delta = \frac{\Delta i'}{\Delta\lambda} = \frac{2 \tan i'}{\lambda},$$

$$\text{and R.P.} = \frac{2W \sin i'}{\lambda} = \frac{\lambda}{\Delta\lambda}$$

we see immediately that

$$\boxed{\text{Resolving power} = (\text{Aperture}) \times (\text{Angular Dispersion})}$$

or

$$\text{R.P.} = A\delta. \tag{18}$$

Equation (18) conveniently summarizes the physical origin of the resolving power, and equation (17) relates the resolving power to the relevant parameters. It is important to note that A and δ are in general not independent variables since they both depend on i'.

It is remembered that the resolving power is sometimes given in textbooks as R.P. $= Nm$ where N is the total number of grooves on the gratings and m the order of diffraction. This relation might tend to be misleading by singling out the total number of grooves and the order as contributing to high resolving powers. The equation is, of course, correct, and in agreement with equation (17). Since $W = Na$, and $\sin i' = m\lambda/2a$ in autocollimation, we can instead write equation (17) as

$$\text{R.P.} = \frac{2Nam\lambda}{2a\lambda} = Nm.$$

But while N, like W, is an independent variable, m depends on a and is equal to $(2a \sin i'/\lambda)$ in autocollimation. Since we know that R.P. is independent of a at a given angle, we need to write $Na = W$ and thus retrieve equation (17) which was derived from first principles above.

We conclude by noting that *high resolving powers are obtained by using large gratings at high angles of incidence and diffraction, in the neighbourhood of autocollimation.*

High angular dispersion is also obtained by using the gratings at high angles.

It is clear, though, that the aperture A of the grating will decrease with increasing angle, and therefore it might at first appear that a less efficient use of the light will be made when using gratings at high angles. Just the contrary is true, however, as we shall show in section 6, and also in section 5, when dealing simultaneously with the problem of *luminosity and resolution.*

2.1.8. *Dispersion, resolving power, aperture and luminosity of gratings*

Let us merely recall here that what matters in the use of gratings in spectrographs and spectrometers is not the angular dispersion δ, but rather the linear dispersion $D = f\delta$ which gives the linear distance of two neighbouring lines in the focal plane of the instrument. Limitations in resolution are ultimately set by granularity and noise in detectors, as well as by threshold sensitivities to observable light flux. Noise limitations are always less serious when the spectral lines are widely

spread out in comparison to the grain of the photographic plates, or when one can use rather large exit slits (provided, of course here, that the slits have a small width when compared to the diffraction pattern width). Moreover, the linear dispersion is to be sufficiently great to provide 'resolving power'. Now, it is clear that a given linear dispersion D can be maintained within a wide range of variation of the angular dispersion δ and of the focal length f, provided only that their product $f\delta = D$ remains constant. How this variation has a bearing on our problem appears when the criterion of 'luminosity' is introduced, as in section 5. Luminosity has to do with the light flux reaching the detector, and we know that the flux F is proportional to HA/f^2, where $A = W\cos i'$ as before and H is the length of the grooves (or height of grating). We can write $F = k_f A/f^2$, where the constant k_f is given by $k_f = shHB_\lambda \Delta\lambda T_G$. Here s = entrance slit width, h = entrance slit height parallel to H, B_λ = brightness of spectrum as a function of λ, $\Delta\lambda$ = wavelength bandwidth admitted through slit and T_G = transmittivity of grating. It is clear that if D is given, s and $\Delta\lambda$ do not vary with f. (h can in practice be maintained constant with f, or even increased with shorter f.) We therefore find that we can make $k_f = k$, a constant, in the important practical case of high-resolution grating spectrometers and spectrographs. A very useful set of equations which permits the evaluation of the performance of gratings in spectrometers and spectrographs can now be given as follows:

$$\textit{Aperture width}: \quad A = W\cos i' \tag{19a}$$

$$\textit{Linear dispersion}: \quad D = \frac{2f\tan i'}{\lambda} \tag{19b}$$

$$\textit{Resolving power}: \quad \text{R.P.} = \frac{2W\sin i'}{\lambda} = \frac{AD}{f} \tag{19c}$$

$$\textit{Flux}: \quad F = \frac{k_f A}{f^2} = k_f \frac{1}{f}\frac{\text{R.P.}}{D} = k_f \frac{1}{f}\frac{1}{D}\frac{2W\sin i'}{\lambda} \tag{19d}$$

(grating ruled width = W, angle of incidence and diffraction = i', focal length = f).

It is immediately apparent from these equations that while the flux F decreases with i' as $\cos i'$, this decrease may be more than compensated by the increase in flux with decreasing f, as $1/f^2$. In

fact, when the flux is written as

$$F = k_t \frac{1}{f} \frac{1}{D} \frac{2W \sin i'}{\lambda} \tag{20}$$

and if $D = (2f \tan i')/\lambda =$ constant is taken as a criterion, it becomes clear that an increase in i' will both increase $\sin i'$ and permit a reduction in f, both of which result in an increase of flux. The flux for resolving power at constant dispersion also increases with *angle* for the same reason, as can be seen from

$$\frac{F}{\text{R.P.}} = k_t \frac{1}{f} \frac{1}{D}. \tag{21}$$

Numerical examples for high-resolution gratings are given in section 6.

2.2. THE EFFECT OF GRATING IMPERFECTIONS ON THE SPECTRAL QUALITY OF GRATINGS

2.2.1. *Criteria for the spectral quality of gratings and some orders of magnitude*

It is clear that a perfect diffraction pattern of width λ/A (at the first minima) is the best possible image that can be formed by a grating of aperture $A = W \cos i'$. For a plane reflection grating, plane diffracted wave fronts are therefore the best wave fronts that one generally wishes to attain. (We do not here discuss the special cases where 'apodization' of the wave fronts may be of significant advantage as shown by JACQUINOT [1950], DOSSIER [1953, 1954, 1956] and others. The recent availability of large gratings has made it desirable to establish criteria for the performance of gratings which produce wave fronts that have only small aberrations from planeness, even when used at the highest angle of incidence and diffraction. Many rather artificial criteria (such as 'resolving power') have been sought for many years, but their use has been unsuccessful. Resolving power criteria are indeed not only arbitrary, but they have been found to be unreliable and insufficiently sensitive. High-resolution gratings performance, even when using not quite perfect gratings, is truly limited by diffraction. STROKE [1960, 1961] has recently shown that gratings are best characterized by the amplitude and extent of the wave front aberrations, as they are easily measurable in the wave front interferograms (STROKE [1955, 1960, 1961]). Unique relations exist between the diffracted wave fronts, and the corresponding

diffraction patterns. In fact, STROKE [1960, 1961] shows further that the various spurious spectral lines that appear in the spectrum are nothing but *diffraction pattern imperfections.*

It is clear that a thorough understanding of the origins of the various spectral line imperfections should be of singular help in the improvement of ruling engine performance and the ruling of perfect high-resolution gratings. This has indeed been the case as we show in section 4.

Experience in the use of even the best gratings shows that false spectral lines generally appear more or less closely to the 'true' lines corresponding to a given frequency or wavelength in the spectrum. The appearance of symmetric 'Rowland Ghosts' was referred to above as resulting from a ghost grating having a period of the ruling engine screw. Spurious lines appearing more closely to the line centers have been variously referred to as 'satellites' or 'grass' (WOOD [1934], HARRISON and STROKE [1960]). High-resolution gratings are primarily used in the neighbourhood of their limits of resolution. 'Satellite' lines, therefore, take on a predominant importance in high-resolution gratings since they affect the very region around the centers of the diffraction patterns.

In order to evaluate the quality of high-resolution gratings, we first note a number of relevant orders of magnitude. As recently reported by STROKE [1961], even when used at the highest angles (around 64° or 76°) in autocollimation, the good M.I.T. gratings show residual satellites only in the immediate vicinity of the line centers, in regions some 100 times closer to the line centers than the region of the now completely negligible Rowland ghosts. The best of the new M.I.T. gratings have no satellites stronger than $\frac{1}{100}$ of the main-line intensity in this region in the visible, and the Rowland ghosts are weaker than $\frac{1}{2000}$ at these angles. This corresponds to only 1.5×10^{-5} in the first order of a 15 000 lines/inch grating in the usual description of Rowland ghost intensities. The central region in which any satellites stronger than $\frac{1}{1000}$ are found extends typically to only some 20–30 diffraction units on either side of the line centers even in the ultraviolet. One diffraction unit (u) corresponds to the distance from the center of the first diffraction minimum for a rectangular aperture $A = W \cos i'$. The first diffraction minimum is at $u = (\lambda/A)f$, where f is the focal length of the camera mirror in the spectrograph. For a 10-inch grating used at 64° the first minimum is at about 1 sec of arc from the center in the visible. Figure 9a shows the wave-front interferogram, Fig. 9b

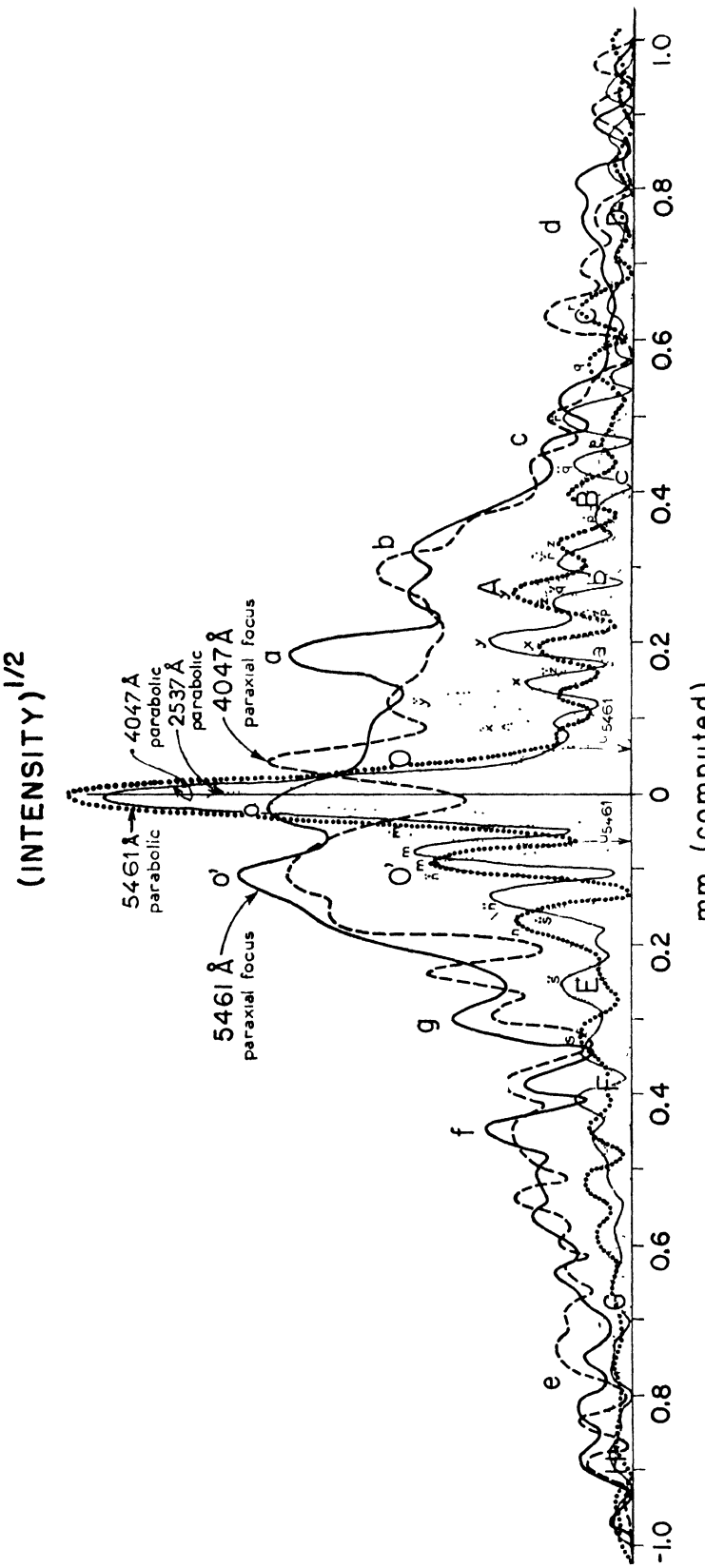

Computed by Fourier transformation of experimental wave front (IBM 704 computer)

Fig. 9c. Computed intensity distributions in diffraction patterns produced by wave front of Fig. 9a. The corresponding spectra are shown in Fig. 9b. (See text under Fig. 9a.)

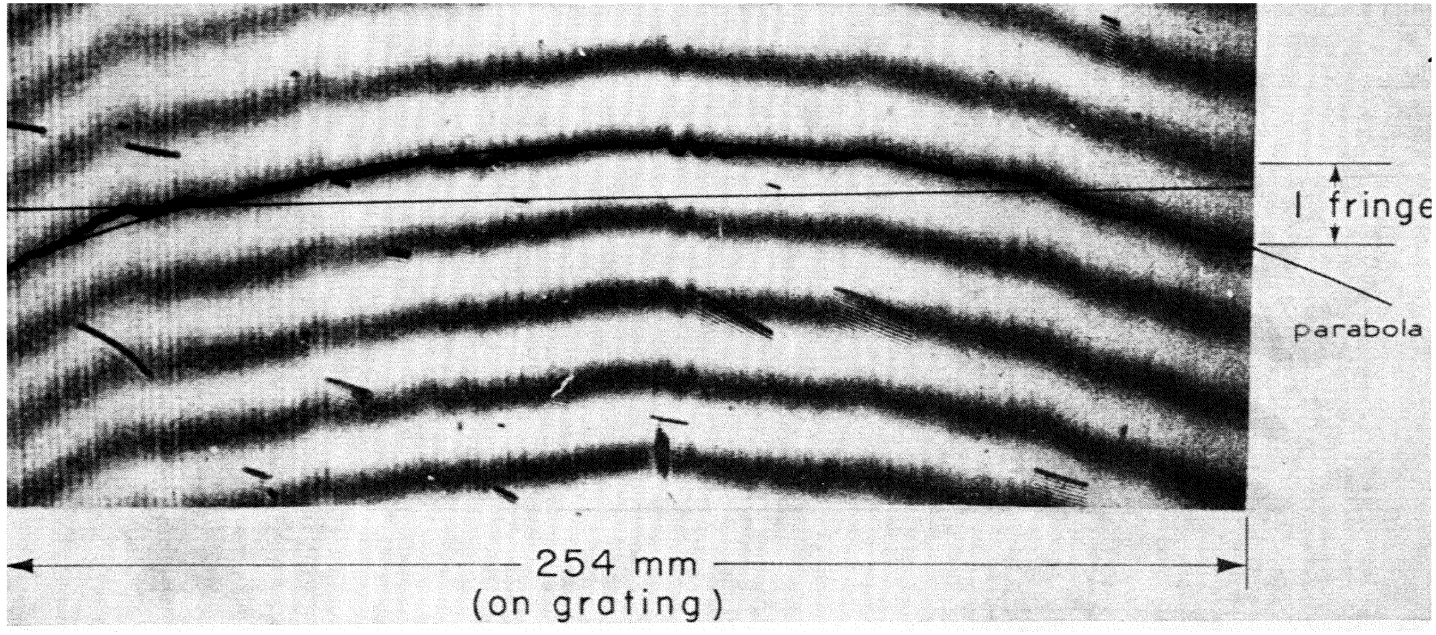

Fig. 9a. Wave-front interferogram in 5461 Å for a 10-inch high-resolution grating at 64° (M.I.T., No. 97). Enlarged Hg 198 spectrograms produced by this grating are shown in Fig. 9b, and computed intensity distributions in the corresponding diffraction patterns in Fig. 9c. The computations were carried out by Fourier transformation of the phase distribution as it appears in graphical form in the experimental wave-front interferogram. It is seen that perfect agreement exists between the computed and experimental intensity distributions in the spectra wherever comparison is possible. Of course, the computed distributions give the diffraction-pattern intensity also within the central region where most of the intensity is concentrated, but where no experimental all the Hg 198 spectrograms should be single lines under any exposure (the exposure was doubled from step to step in Fig. 9b). It is clear that the various *spurious spectral lines* are nothing but *diffraction-pattern imperfections* as caused by the diffracted wave-front aberrations (which, in turn, result from the grating imperfections). The grating shown is so good that it was necessary to plot the *square root* of the intensity for clarity in Fig. 9c (the relative intensity of the satellite peaks on an intensity plot is smaller, of course). The mean wave-front curvature happens to be almost parabolic along the grating width, in this case, and results principally in a shift of the best focus. The aberrations used in the computing were measured from the parabola shown.

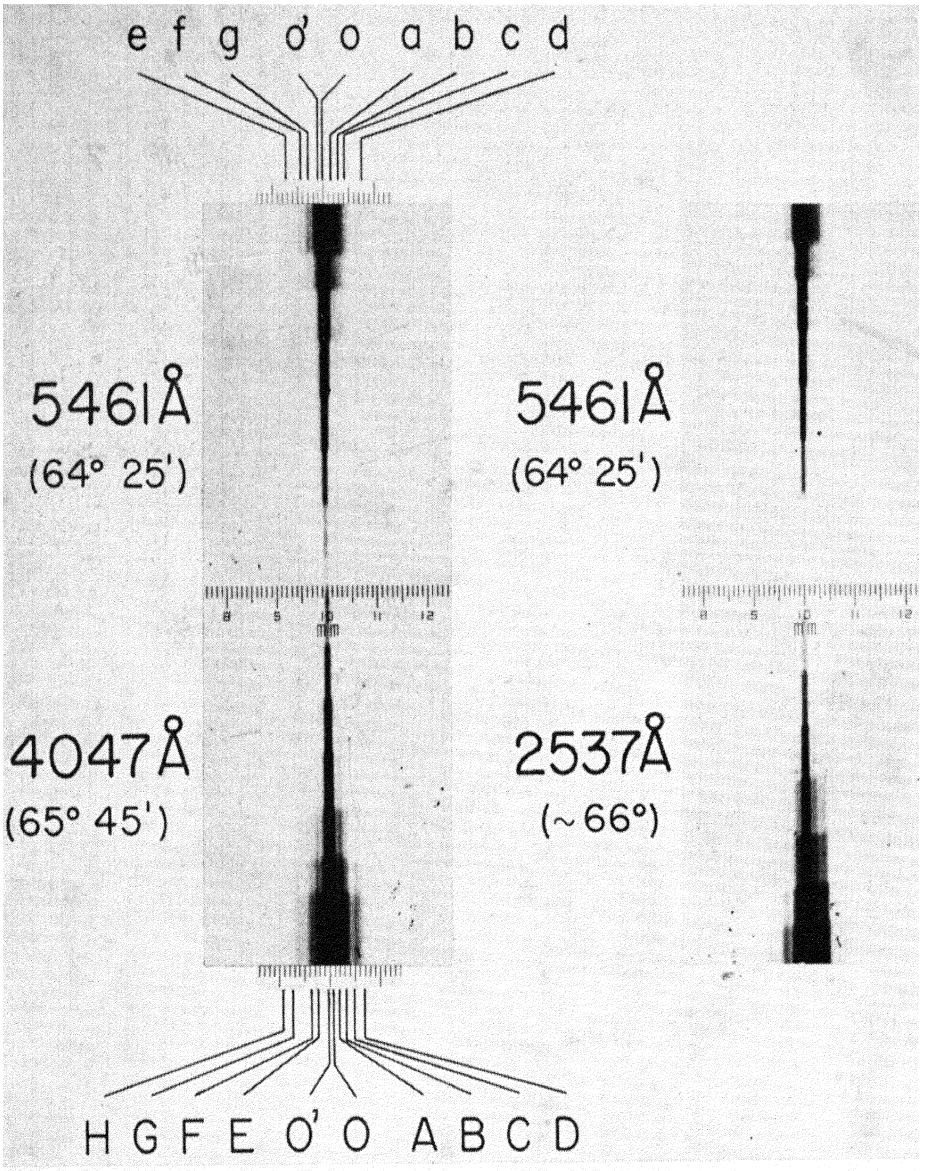

Fig. 9b. Enlarged Hg 198 spectrograms in three wavelengths from grating 97 of Fig. 9a. The scale shown has 0.1 mm divisions and is placed on the photographs obtained in the focal plane of a 12.2 meter spectrograph. The first minimum of the diffraction pattern at 5461 Å is at about 1 second of arc from the line center (about 0.06 mm here), and the diffraction-pattern width is of the same order as the Doppler width of the line. It is clear that the wavelength-dependent shift of the center of gravity which appears in the computed curves of Fig. 9c could have resulted in systematic errors (errors of 'coincidence' in the use of this grating for accurate wavelength measurements, if the computed curves were not available (HARRISON and STROKE [1960], STROKE [1960]).

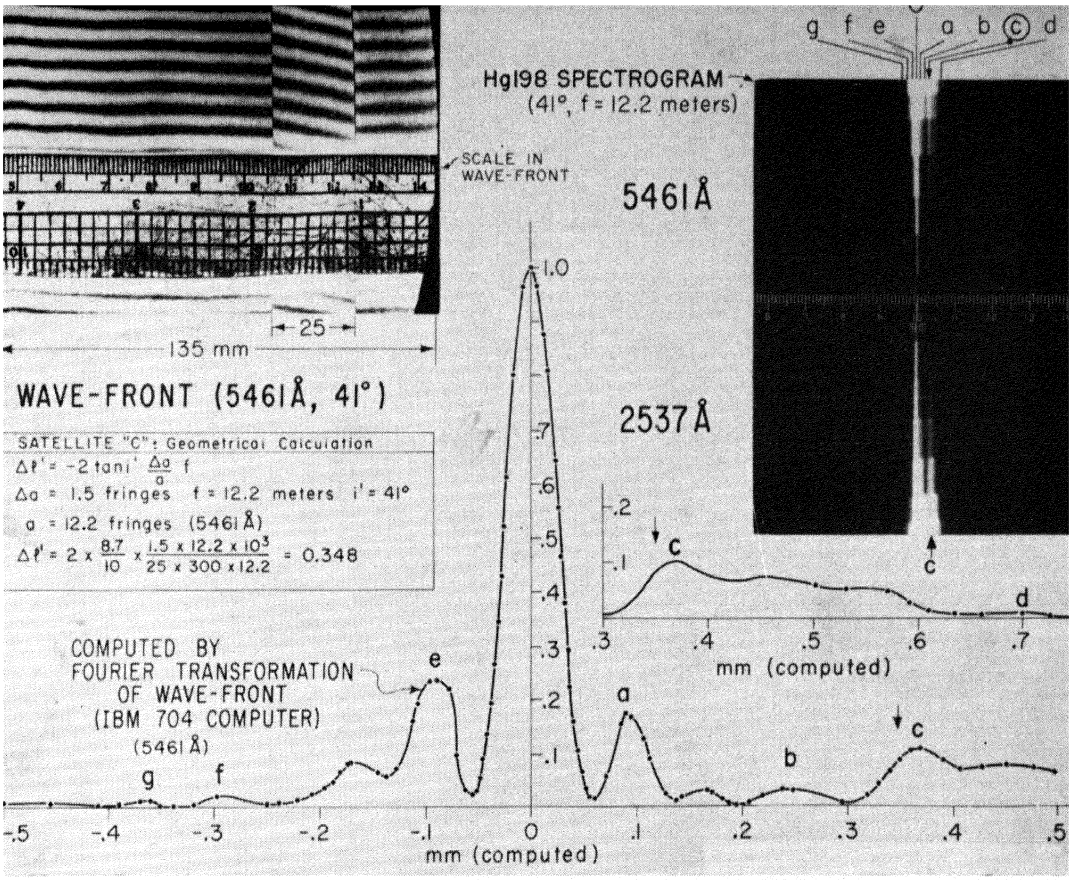

Fig. 10. 'Controlled-error' grating, ruled under interferometric control on the M.I.T. ruling engine so as to obtain a 'linear' wave-front aberration in almost pure form in an otherwise perfect grating (STROKE [1960, 1961]). The wave-front interferogram in 5461 Å, spectrograms in two wavelengths (5461 Å and 2537 Å) and computed diffraction pattern in 5461 Å are shown. Even an apparently simple aberration, as that shown, results in fairly complex diffraction-pattern defects. For this special case of an extended small-amplitude 'linear' aberration, the centers of gravity of the principal satellite 'C' are seen to be at a wavelength-independent distance from the line centers at a given grating angle. The same is true for the relative intensity. The detail of the diffraction-pattern intensity distribution is wavelength-dependent, of course (see text).

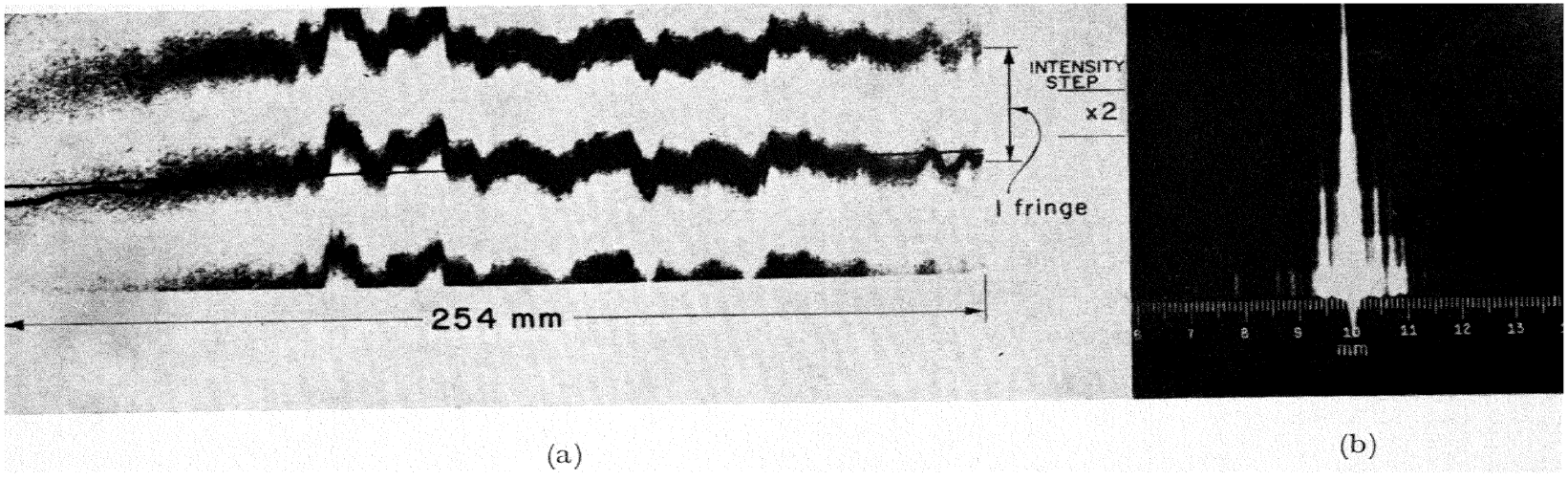

Fig. 11a. Wave-front interferogram (at 75.6° in autocollimation) and Fig. 11b, Hg 198 spectrogram (at 53.8°, $f = 12.2$ m) produced by a 10-inch wide grating having numerous small-amplitude departures from wave-front flatness at these angles. The corresponding computed diffraction pattern is shown in Fig. 11c for comparsion with the spectrogram. (The exposures are doubled from step to step in the spectrogram.)

the Hg 198 spectrograms of the satellite distributions in three wavelengths produced by the first-generation 10-inch grating 97 and Fig. 9c the computed intensity distributions in the diffraction patterns. For the ruling of high-resolution gratings, STROKE [1961] also shows that while the 'resolving power' of a grating of a given width increases in theory with the sine of the angle of use in autocollimation (the 'resolving power' being some 10 times greater at high-resolution angles of 64° than at low-resolution angles of 5° corresponding to 'first-order' work), the *quality* of the grating needs to increase with the *square of the sine of the angle* in order to permit the actual attainment of the resolution corresponding to the increased available 'resolving power'. In the visible a ruling quality some 100 times greater than that required at low angles needs therefore to be achieved in order to attain a satisfactorily high-resolution grating. Moreover, at shorter wavelengths, the image quality of a given grating deteriorates still further with the inverse square of the wavelength, and the grating quality needs to increase further with the square of the visible wavelength/ultraviolet wavelength ratio in order to maintain the performance achieved in the visible.

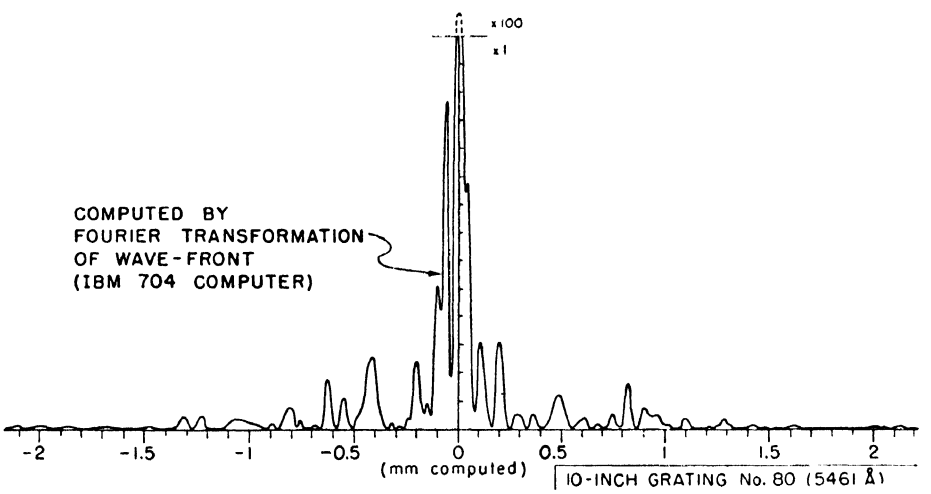

Fig. 11c. Computed diffraction pattern for a 10-inch wide grating having numerous small-amplitude departures from wave-front flatness. The corresponding wave-front interferograms and Hg 198 spectrogram are shown in Fig. 11a and 11b. It is clear that no simple relationship exists between any given satellite and a particular region in the wave front. The entire intensity distribution in the spectral line, with all the spurious imperfections (satellites, ghosts, grass) is simply the diffraction pattern as formed by the entire wave front with all its aberrations.

Finally, $\frac{1}{10}\lambda$ in the wavelength of interest (and in particular in the shortest wavelength) may be considered as an upper limit of a tolerable 'extended' wave front aberration in a grating, and also as the limit of tolerable macroscopic ruling errors (such as cumulative errors and blank and coating defects), which will not noticeably affect its spectroscopic high-resolution performance under usual conditions. The reason why good high-resolution gratings might in a sense be considered as more perfect optical elements in the visible than the best of the available FP etalons may be that with a finesse of 25 (which multiplies the etalon flatness deviations by factors up to 25) an etalon good to $\frac{1}{50}$ wavelength over its surface results in path-difference variations, between extreme beams, of up to $\frac{1}{2}\lambda$. Tolerances for 'local' errors such as for random positioning of the grooves or portions of the grooves, as well as for irregularities resulting from diamond bounce, chattering and other causes of unevenness in the groove sides, which all result in scattered light, and for the periodic spacing variations leading to Rowland ghosts, are some 50 to 100 times smaller, but are also generally correspondingly easier to achieve. A study of the scattered light produced by local 'microscopic' errors has been recently carried out by MARÉCHAL [1958].

2.2.2. *The origin of spurious spectral lines*

Many attempts have been made in the past to trace the origins of particular spurious spectral lines produced by imperfect gratings back to particular error regions in the grating or the wave fronts (E. MASCART [1889], ALLEN [1902], WOOD [1924], GALE [1937], HARRISON [1949], STRONG [1951], INGELSTAM and DJURLE [1952, 1953], STROKE [1952], DJURLE [1952, 1954], RANK *et al.* [1955]). It is important to note that except for the 'linear' wave front aberrations (and the periodic errors which used to affect the more distant image regions) it is in general not possible to single out given grating regions as having errors at the origin of a particular spurious satellite: this is no more possible that it is possible to single out an 'error' region in a perfect wave front as being at the origin of what should then be called the 'spurious' secondary maxima in a perfect diffraction pattern. It is known, of course, that the first secondary maximum corresponding to the rectangular aperture presented by a grating has an intensity of the order of 4 percent and that the peak appears at a distance of about two diffraction units from the line center. These are precisely the orders of magnitude of the spurious satellites of a few percent in-

tensity with which we are dealing here. In fact, as stated before, STROKE [1960, 1961] shows that all spurious spectral lines are nothing but *diffraction-pattern imperfections* caused by the entire diffracted wave front. The simplest relation between the complex amplitude of the electromagnetic disturbance in the diffracted wave front and the complex amplitude in any of the spectral image-points takes on the form of the Fourier transformation given in equations (4), (5) and (6). Only in the important special case of the 'linear' wave front aberrations, which we will discuss in section 2.2.7, and in the case of periodic errors can diffraction-pattern imperfections be predicted in detail by mere inspection of the wave-front interferograms. In general, the distribution of light in the diffraction patterns of a given grating can now be obtained by simply carrying out the Fourier transformation of the phase distribution in the diffracted wave fronts as it appears in readily usable graphical form in the wave-front interferograms. The numerical computation can be easily carried out with the help of a digital computer (STROKE [1960, 1961]).

Figure 10 shows the distribution of light in the diffraction pattern computed by Fourier transformation of the phase distribution in the wave front for a grating which we have ruled under interferometric control by deliberately introducing a controlled, pure 'linear' wave-front aberration into an otherwise perfect grating. Figure 10 shows the typical complexity of the diffraction-pattern imperfections that result from even an apparently simple aberration. Perfect agreement between the spectrogram and the computation is seen to exist throughout the entire region where comparisons are possible: and the computation has of course the significant advantage of providing the intensity distribution in the immediate vicinity and within the central part of the diffraction pattern where most of the energy is concentrated, but where no such information was heretofore available from more classical tests, such as resolution photographs for example. Computed diffraction patterns such as the one in Fig. 10 (which corresponds to an infinitely narrow perfectly monochromatic slit) have permitted correction of 'errors of coincidence' resulting from systematic, center-of-gravity displacements of spectral lines. They should prove invaluable in spectral-line-shape studies, since the intensity distribution recorded in the spectrometer is simply equal to the convolution of the 'true' intensity distribution in the spectrum (which is sought) with these (computed) diffraction-pattern intensity distributions (when the slit width has been taken into account, which presents no problem).

The complexity of the satellite distribution that results from a grating wave front having numerous departures from flatness is shown in Fig. 11. It is quite clear that no simple relationship exists between any individual satellite and a special wave-front region. Here again excellent agreement is found between the satellite pattern and the light distribution predicted by Fourier-transform computation from the experimental wave-front interferogram.

While no problem in carrying out such Fourier transformations has appeared, STROKE [1960, 1961] has nevertheless found it desirable to derive two general laws in order to help in predicting the effects of wave-front and grating imperfections on the quality of the spectral lines without actually carrying out the Fourier transformations. With the help of these laws, which we shall now discuss, it is in general possible to immediately characterize a grating by merely inspecting the wave-front interferograms.

2.2.3. *Effect of diffracted wave-front imperfections on the spectral images and variations of spectral quality with wavelength and angle*

We first give our results in the form of the principal conclusions established by STROKE [1960]. According to the first law it is possible to separate formally the macroscopic or *extended* errors in the grating (and wave fronts) from the *local* or microscopic errors which correspond to displacements of individual grooves or small-groove regions, and to irregularities in the groove faces themselves. It is the *extended* errors, which may for example extend over $\frac{1}{2}$ inch to 2- or 3-inch regions in a 10-inch grating, which are responsible for the appearance of the harmful spurious satellites in the neighbourhood of the line centers. On the other hand, the *local* errors, covering regions of say less than $\frac{1}{2}$ inch on the grating, are at the origin of more distant satellites and scattered light which can be as harmful to certain other spectroscopic applications as is the presence of satellites in high-resolution spectroscopy: this is particularly true in infrared and Raman spectroscopy, for example.

The *second law*, which has emerged from Stroke's study of spectral-image imperfections is that the knowledge of the imperfections of a spectral line in only one wavelength and, in general at only one angle, is sufficient to predict the imperfections for the particular grating in all other wavelengths and at all other angles of interest. We find that the intensities of corresponding spurious satellites and grass in im-

perfect diffraction patterns increase as $\sin^2 i'/\lambda^2$ for a given high-resolution grating in which the worst aberration in the shortest wavelength of interest is of the order of $\frac{1}{4}$ fringe ($\frac{1}{8}\lambda$). We further find that imperfect diffraction patterns in the various wavelengths and at various angles are similar to each other in the ratio $\lambda/\cos i'$. With these two satellite-variation laws we have established a simple means of predicting the satellite position and intensity distribution in all wavelengths and at all angles provided only that, in addition to the wave-front interferograms, one of these patterns has been obtained (for example, in the light of a single line from the Hg 198 source, or with the help of the 'C' component in the hyperfine structure of the green 5461-Å line of natural mercury, or else by Fourier transformation – in one wavelength – from the wave-front interferogram). The only important exception to the general satellite-variation laws is a *special law* which we have determined *for the 'linear' wave-front aberrations* which will be discussed below: for this case we find that the distances from the line centers as well as the relative intensities of the principal satellites are wavelength independent at a given grating angle (see Fig. 10). In practice satellite patterns obtained in two wavelengths immediately permit to distinguish this important special case.

Finally, we have also shown that the *wave-front aberration corresponding to a given ruling error increases with the sine of the angle* of use of the grating in autocollimation, while the *aberrations corresponding to blank or coating defects decrease with the cosine* of the same angle, but both also increase with decreasing wavelength. In fact, when measured in fringes ($\frac{1}{2}\lambda$) of the same wavelength, the wave-front aberration as it appears in the interferogram is simply $\sin i$ times the ruling error and $\cos i$ times the blank defect. More generally, the wave-front aberration in a wavelength λ is $(\sin i)(\lambda_0/\lambda)$ times the ruling error measured in the wavelength λ_0, and $(\cos i)(\lambda_0/\lambda)$ times the blank or coating defect measured in λ_0. Even though blank defects and ruling errors may result in similar wave-front aberrations and corresponding image imperfections, the sensitivity of the wave fronts to ruling errors is seen to increase with grating angle, while the sensitivity to blank defects fortunately decreases with angle. The spectral diffraction-pattern imperfections, that is the spurious satellite lines, ghosts, and grass in which we are interested in the final analysis have of course been found to increase with the *squares* of the ratios given above, that is as $(\sin i)^2(\lambda_0/\lambda)^2$ for image imperfections caused by ruling

errors, and as $(\cos i)^2(\lambda_0/\lambda)^2$ for image imperfections caused by blank and coating defects. It is this *square-law dependence of the image quality on ruling perfection and blank quality* which makes any improvement in grating quality so significant, but also makes the attainment of a really good high-resolution grating so difficult. All these conclusions have been fully borne out by experiment (STROKE [1960], HARRISON and STROKE [1960], STROKE [1961]).

We may close this section by again stressing the role of the interferometric method of measuring the diffracted wave-front aberrations. This method has been found to be the single most important tool not only in the immediate assessment of the grating quality and the prediction of the distribution of light in the spectral images, but also in the improvement of grating ruling engines and of the ruling process itself.

Next we give the principal steps in the mathematical development of these conclusions.

2.2.4. *Mathematical description of relation between diffracted wave fronts and spectral diffraction patterns*

Equations (4) and (5) give, in normalized form, the distribution of complex amplitude $\mathscr{A}(\beta)$ in the diffraction patterns produced by wave fronts in which the complex amplitude distribution is $g(\eta)$ as a function of coordinate η oriented along the width A of the wave front (of square aperture AH). The wave front width A is normalized to be equal to 2 and $\eta = u/\frac{1}{2}A)$, where u is the true coordinate in the aperture. We recall that the angular coordinate $\beta = \pi x/(\lambda/A)f$ is measured from the center of the diffraction patterns that correspond to the grating equation (1), viz.

$$\sin i + \sin i' = m\lambda/a.$$

We have the formulae (4) and (5)

$$\mathscr{A}(\beta) = \int_{-1}^{+1} g(\eta) \exp\,[\mathrm{i}\beta\eta]\,\mathrm{d}\eta$$

and

$$g(\eta) = \mathscr{A}(\eta) \exp\,[\mathrm{i}\Phi(\eta)],$$

where $\Phi(\eta)$ appears in graphical form in the wave-front interferograms. For a grating of uniform 'blaze' and polarization we have $\mathscr{A}(\eta) \equiv 1$ and we may write

$$g(\eta) = \exp\,[\mathrm{i}\Phi(\eta)]. \tag{5a}$$

It is frequently useful to write the Fourier transform relation between the wave front and the diffraction patterns, as given in equation (5), in operational form

$$\mathscr{A}(\beta) = T[g(\eta)]. \tag{4a}$$

For the case of uniform blaze and polarization, we have

$$\mathscr{A}(\beta) = T[\mathrm{i}\Phi(\eta)]. \tag{4b}$$

It is clear that the description of the distribution of light in the diffraction patterns does not call for any formal distinction between perfect or imperfect wave fronts.

We may take the distribution of light in the diffraction pattern formed by a perfectly plane wave front as a criterion of perfection. We can then consider any departures from planeness in the wave front and any departures for the light intensity distribution in the 'perfect' diffraction pattern as imperfections. The departures from perfection in the wave fronts are called 'aberrations' and the spurious peaks in the grating diffraction patterns are variously called 'satellites', 'grass' or 'ghosts'. It is only as a result of the work by STROKE [1960] that the *spurious spectral lines* have been formally recognized as *diffraction-pattern imperfections*. For a perfectly plane diffracted wave front, $\Phi(\eta)$ is a constant and

$$\mathscr{A}(\beta) = \int_{-1}^{+1} \exp\,[\mathrm{i}\beta\eta]\mathrm{d}\eta = 2\,\frac{\sin\beta}{\beta}. \tag{22}$$

The corresponding intensity $I(\beta)$, in the form normalized according to equation (6),

$$I(\beta) = \tfrac{1}{4}\mathscr{A}(\beta)\,\mathscr{A}(\beta)^*$$

is given, for a perfect diffraction pattern, by

$$I(\beta) = \left(\frac{\sin\beta}{\beta}\right)^2. \tag{23}$$

A perfect diffraction pattern is thus seen to have a $[\sin\beta/\beta]^2$ intensity distribution, with a first zero at $\beta = \pi$ or

$$x = x_0 = \left(\frac{\lambda}{A}\right) f$$

in the focal plane of the mirror (with a focal length equal to f). This

is the same diffraction pattern as would be obtained by any plane wave front in a square aperture of width A. The normalization given here is immediately applicable to computer use (STROKE [1960]).

When a wave front is imperfectly plane, $\Phi(\eta)$ is not a constant. One can write

$$\Phi(\eta) = k\Delta(\eta), \tag{24}$$

where

$$k = \frac{2\pi}{\lambda}. \tag{25}$$

The importance of equation (24) resides also in the fact that the 'aberration' $\Delta(\eta)$ in the wave front can be simply related to grating imperfections. In fact, two general types of grating imperfections need to be distinguished:

a) ruling imperfection

b) grating-blank imperfections.

We shall next investigate how $\Delta(\eta)$ varies with these imperfections as a function of angle and wavelength. Let us first summarize the relation between wave fronts and diffraction patterns by the equation

$$\mathscr{A}(\beta) = T[\mathrm{i}\Phi(\eta)] = T[\mathrm{i}k\Delta(\eta)] \tag{4c}$$

where $T[\ ]$ stands for Fourier transform of $[\ ]$ as before, for the case of $\mathscr{A}(\eta) = 1$.

2.2.5. *Relation between ruling errors and wave-front aberrations as a function of grating angle and wavelength*

It is clear that a perfectly ruled plane grating will produce perfectly plane diffracted wave fronts. In autocollimation, a grating may be thought of as an inclined staircase viewed by an observer standing in the vertical diffracted wave front. The diffracted wave front is parallel to the vertical groove (or step) sides and inclined by an angle $i' = i$ with respect to the mean grating surface. Should a step be displaced along the mean surface of the grating, by an amount Δa, then its component normal to the wave front is given by $\Delta a \sin i'$. In this case of autocollimation the aberration path difference is clearly $2\Delta a \sin i'$. Except for the normalization, the wave-front aberration is thus given by

$$\Delta(\eta) = 2\Delta a \sin i' \tag{26}$$

and the phase aberration by

$$\Delta\Phi(\eta) = \frac{2\pi}{\lambda} 2\Delta a \sin i'. \tag{27}$$

It is very useful to express the groove errors in terms of $\frac{1}{2}\lambda$, where $\frac{1}{2}\lambda = 1$ fringe. If the aberrations are measured in terms of the same wavelength λ as the ruling errors, then an aberration $\Delta a = \frac{1}{2}\lambda$ will result in

$$\left.\begin{aligned} \Delta(\eta) &= \lambda \sin i' && (28) \\ \text{and} \qquad & && (\text{per } \Delta a = \tfrac{1}{2}\lambda). \\ \Phi(\eta) &= 2\pi \sin i' && (29) \end{aligned}\right\}$$

But an aberration $\Phi(\eta) = 2\pi$ corresponds to precisely *one* fringe of deviation in the wave-front interferograms. We thus have the important conclusion that *when the ruling errors are measured in fringes* ($\frac{1}{2}\lambda$) *of the same wavelength as that used in the interferometric measurement of the diffracted wave-front aberrations, then one fringe of ruling error will result in* $\sin i'$ *fringes of wave-front aberration when the grating is used in autocollimation at the angle* i'.

The effect of ruling errors on the diffracted wave fronts is thus seen to increase with the sine of the grating angle. It also clearly increases with decreasing wavelength (eq. (27)). Of course, the diffracted wave-front aberrations result in corresponding spectral diffraction-pattern imperfections.

2.2.6. *Relation between blank imperfections and wave-front aberration as a function of grating angle and wavelength*

It is perfectly possible to space the grooves regularly in a plane, yet to obtain an imperfect grating when the surface of the blank on which the grooves are being ruled is itself not plane. Gratings are most frequently being ruled in comparatively thick films of aluminum deposited by evaporation on optical blanks. Aluminum thicknesses from 3 to 30 microns are used for ruling purposes. Experience has shown that it seems to be as difficult to evaporate sufficiently flat films on large gratings as it is to rule with corresponding regularity. Deviations from flatness may of course also result from imperfection in the blanks themselves, from stresses in the mountings of the grating during ruling or in use, as well as from deformations in replication.

Unlike the effect of ruling errors, which has been shown to increase

with grating angle as $\sin i'$, the effect of blank imperfections can be shown to decrease with grating angle as $\cos i'$ (both effects increase with decreasing wavelength, of course). Consider indeed the grating spacing 'a' as it appears from an angle $i \pm \Delta i$ when compared to the angle i. We have

$$a \sin (i \pm \Delta i) \simeq a(\sin i \pm \Delta i \cos i) \tag{30a}$$

and we immediately see that the groove which is properly positioned by ruling, but happens to be ruled on the portion of the blank inclined by Δi with respect to the rest of blank, will appear displaced by the quantity $\Delta a = \pm a \Delta i \cos i$, (30b), when viewed from the diffracted wave front at the angle i. If the blank error extends linearly over N grooves (distance on grating $= Na$ fringes) then we find a fringe displacement reaching

$$\delta_I = Na\Delta i \cos i \text{ fringes} \tag{31}$$

in the wave-front interferogram. The fringe displacement caused by a 'linear' blank imperfection is of course a linear departure of the fringes from straightness. A 'linear' blank imperfection is an inclination of a flat portion of a grating blank with respect to the remainder of an otherwise perfectly flat blank. It is essential to observe that linear fringe deviations in the wave front will result not only from grating blank imperfection, but also from ruling imperfections. In fact, since both rulings and blank imperfections of small amplitude, when extending over a significant portion of the grating, may frequently be first approximated by a 'linear' departure from perfection, we find that the case of 'linear' wave-front aberrations take on a particularly significant importance in high-resolution gratings, both in theory and in practice.

2.2.7. *The important special case of 'linear' wave-front aberrations*

Linear diffracted wave-front aberrations may be considered without regard to their origin in ruling or blank errors, even though reference to the grating is helpful for a qualitative understanding. In fact, one can always consider that a linear wave-front aberration has resulted either

a) from a portion of a perfect grating ruled on a part of the blank inclined with respect to the main part of the grating (case of 'blank imperfections') or

b) from a portion of a grating ruled on perfectly flat blank, but

with a spacing constant that increases linearly over the imperfect portion (case of 'cumulative ruling errors').

Both cases have, of course, physical significance and can be used to compute the diffraction pattern imperfections in detail if properly interpreted.

In fact, the diffraction pattern of Fig. 10 for the 'controlled-error' grating can be calculated with these interpretations. We have, of course, also calculated the diffraction pattern by digital Fourier transformation on the M.I.T. IBM 704 computer, and found it to be in perfect agreement with the experimental spectrogram.

To calculate the effect of the inclined portion of the wave front on the diffraction pattern, according to the interpretation (a), we remember that what is being summed are complex amplitudes. To simplify the calculation, let us assume that the linear aberration extends over a fraction $1/M$ of the wave front, at the center of the grating. Let the linear phase aberration be

$$\Phi(\eta) = \pm\, km\eta, \tag{32}$$

where m is a constant and $k = 2\pi/\lambda$ as before.

Since

$$\mathscr{A}(\beta) = \int_{-1}^{+1} \exp\,[\mathrm{i}\Phi(\eta)] \exp\,[\mathrm{i}\beta\eta]\mathrm{d}\eta,$$

we have here

$$\mathscr{A}(\beta) = \int_{-1}^{1/M} \exp\,[\mathrm{i}\beta\eta]\mathrm{d}\eta + \int_{-1/M}^{+1/M} \exp\,[\pm\, \mathrm{i}km\eta] \exp\,[\mathrm{i}\beta\eta]\mathrm{d}\eta + \int_{+1/M}^{+1} \exp\,[\mathrm{i}\beta\eta]\mathrm{d}\eta, \tag{33}$$

which gives

$$\mathscr{A}(\beta) = 2\frac{\sin\beta}{\beta} - \frac{2}{M}\frac{\sin\,(\beta/M)}{(\beta/M)} + \frac{2}{M}\frac{\sin\,[(\beta \mp km)/M]}{(\beta \mp km)/M} \tag{34}$$

a result which can be very simply interpreted in the following terms. The complex amplitude in the diffraction pattern is formed of the sum of

1) the perfect diffraction pattern (amplitude) corresponding to a perfect grating wave front of width A;
2) minus a diffraction pattern (amplitude) corresponding to a perfect wave front of width A/M;
3) plus a diffraction pattern (amplitude) corresponding to a wave front width A/M, but having its center displaced by $\Delta\beta = \pm\, km$ in the β domain.

A graphical plot of these patterns and their summation does indeed give the computed pattern of Fig. 10.

More generally, we have shown (STROKE [1960]) that if

$$\mathscr{A}(\beta) = T[g(\eta)_0] \tag{36}$$

then

$$\mathscr{A}(\beta \mp kn) = T[g(\eta)_0 \exp(\pm ikn\eta)]. \tag{37}$$

The interpretation of a linear wave-front aberration as resulting from a linear spacing variation may also be used for this calculation although it does not immediately give the detail of the diffraction-pattern imperfections, but rather only the maximum of the principal spurious satellite which one would expect to find when a sizable portion of the grating is inclined with respect to the main grating. Qualitatively, when a grating is formed of two perfectly ruled portions inclined with respect to each other, one would expect to find two spectral lines in each wavelength, slightly displaced with respect to each other and with intensities in the ratio of the widths of the two portions of the grating.

Consider indeed a portion of the grating on which the spacing varies linearly according to the equation $\Delta a/a$, such that

$$\frac{\Delta a}{a} = \pm \frac{a \Delta i \cos i'}{a \sin i'} = \pm \frac{\Delta i}{\tan i'} \tag{38}$$

according to equations (30a) and (30b).

We also have, by differentiating the grating equation (1) with respect to a

$$\Delta i' = -2 \frac{\Delta a}{a} \tan i'. \tag{39a}$$

We therefore have

$$\Delta i' = -2\Delta i, \tag{40}$$

which is indeed the effect that one would expect to obtain by making the grating by an angle Δi with respect to the incident wave front at any angle in autocollimation. With the focal distance f of the mirror, we get in the focal plane

$$\Delta l' = -2f \frac{\Delta a}{a} \tan i'. \tag{39b}$$

We need to recall that the ruling error Δa which enters these equations is $(\sin i')^{-1}$ the maximum fringe error as it appears in the wave-front interferogram. For the grating of Fig. 10 we have

$$\Delta a = \frac{1}{\sin 41^\circ} \text{ fringes} = \frac{1}{0.6561} \text{ fringes} \simeq 1.5 \text{ fringes}$$

and since this error appears in 25 mm of the grating ruled at 300 grooves per millimeter, each groove having a spacing of 12.2 fringes we have

$$\frac{\Delta a}{a} = \frac{1.5}{25 \times 300 \times 12.2}$$

and finally

$$\Delta l' = -2f \frac{\Delta a}{a} \tan i' = -0.348 \text{ mm}$$

in perfect agreement with the experimental spectrogram.

In fact, a notable characteristic of linear wave-front aberrations is that the distance from the line centers of the centers of gravity of the principal satellites which they produce is wavelength-independent at a given grating angle, in agreement with equations (39a), (34) and (37), as well as with experiment (Fig. 10). Moreover, the relative intensity of these satellites, when compared to the principal lines, is also seen to be wavelength independent for extended 'linear' aberrations.

Linear aberrations have been found to be the single most important origin of spectral line imperfection in high-resolution gratings since they can result from a number of different causes, such as cumulative ruling errors, blank and coating imperfections, and imperfections in the mounting and replication of gratings. The cumulative ruling errors themselves may result from different origins, of which variable friction, diamond motion, temperature distortions of the ruling engine, are particularly well known. Elimination of such errors from modern gratings is at the root of the attainment of high-resolution gratings. These gratings are, however, also characterized by notable reduction in more local, but still extended aberrations of a general type. The effect of such aberrations is discussed in the next section.

2.2.8. *The effect of grating imperfections on the spectral lines in the general case and variation of spectral-line imperfections with angle and wavelength*

Only gratings with comparatively small extended aberrations, on the order of up to a wavelength or so, are considered as gratings good enough for general spectroscopic work. Except for the special defect of parabolically curved wave fronts (which may exceed several wavelengths and to which correspond perfect but out-of-focus diffrac-

tion patterns) wave-front aberrations tolerable in high-resolution gratings should generally remain smaller than $\frac{1}{5}\lambda$, since any extended aberration exceeding $\frac{1}{10}\lambda$ produces noticeable spurious spectral diffraction-pattern imperfections. (Tolerances for periodic ruling errors are 10 to 50 times smaller.) We have already stated that the distribution of light in the diffraction patterns produced by grating with imperfections of any general amplitude and nature can be fully calculated with the help of a digital computer, by carrying out the Fourier transformation of the phase distribution as it appears in a readily usable form in the diffracted wave-front interferograms. Details are given by STROKE in his 1960 thesis. It is of considerable theoretical and practical interest to predict the variation of spectral line imperfections with grating angle and wavelength. STROKE [1960] also shows that the general relation between aberrated diffracted wave fronts and the corresponding diffraction patterns can indeed be expressed in a form which permits to predict this variation. We get

$$\mathscr{A}(\beta) = \int_{-1}^{+1} \exp\left[\mathrm{i}\alpha\Phi(\eta)_0\right] \exp\left[\mathrm{i}\frac{\lambda}{\lambda_0}\frac{\cos i_0}{\cos i}\beta_0\eta\right] \mathrm{d}\eta, \tag{41}$$

where

$$\beta = \frac{\lambda}{\lambda_0}\frac{\cos i_0}{\cos i}\beta_0 \tag{42}$$

and

$$\alpha \equiv \alpha_{\mathrm{R}} = \frac{\lambda_0}{\lambda}\frac{\sin i}{\sin i_0} \quad \text{(grating } \textit{ruling} \text{ errors)}, \tag{43}$$

and

$$\alpha \equiv \alpha_{\mathrm{B}} = \frac{\lambda_0}{\lambda}\frac{\cos i}{\cos i_0} \quad \text{(grating } \textit{blank} \text{ errors)}. \tag{44}$$

With the help of these equations, a *diffraction pattern similarity law* and a *diffraction pattern imperfection variation law* can be rather simply established.

a) Diffraction pattern similarity law

It can be seen by inspection of equation (41), that imperfect diffraction patterns will, in general, be similar to each other in the ratio $(\lambda/\lambda_0)(\cos i_0/\cos i)$, just like perfect diffraction patterns. This has been verified experimentally. (The case of 'linear' aberrations discussed above is an exception which can be singled out experimentally with the help of interferograms taken at two angles.)

b) Diffraction pattern imperfection variation law

By noting that $g(\eta)$ can be written as

$$g(\eta) = \exp[i\Phi(\eta)] = 1 - \tfrac{1}{2}\Phi(\eta)^2 + i\Phi(\eta) + \operatorname{Res}\Phi(\eta) \quad [\text{for } |\Phi(\eta)| < \tfrac{1}{2}\pi] \tag{45}$$

that is for the case of small aberrations, and by observing that

$$T[\Phi(\eta)_0^2] = T[\Phi(\eta)_0] \otimes T[\Phi(\eta)_0] \tag{46}$$

and that $T[\Phi(\eta)_0^2] \to 0$ outside of the diffraction-pattern centers, that is precisely in the region of interest where the spurious spectral lines (satellites and grass) appear, STROKE [1960] shows that the diffraction-pattern intensities at the wavelength λ_0 and angle i_0, on one hand, and at the wavelength λ and angle i, on the other hand, can be written as

$$I(\beta_0) \simeq \left(\frac{\sin\beta_0}{\beta_0}\right)^2 + \tfrac{1}{4}\{T[\Phi(\eta)_0]\}^2 \tag{47}$$

and

$$I(\beta) \simeq \left(\frac{\sin\beta}{\beta}\right)^2 + \tfrac{1}{4}\alpha^2\{T[\Phi(\eta)_0]\}^2 \tag{48}$$

respectively, and that therefore *the contribution $\Delta I(\beta)$ to the diffraction-pattern imperfections* (satellites and grass) *vary as*

$$\Delta I(\beta) \simeq \alpha^2 \Delta I(\beta_0) \tag{49}$$

that is as α^2, where

$$\alpha^2 \equiv \alpha_R^2 = \left(\frac{\lambda_0}{\lambda}\right)^2 \left(\frac{\sin i}{\sin i_0}\right)^2 \quad \text{(grating } \textit{ruling} \text{ errors)} \tag{50a}$$

$$\alpha^2 \equiv \alpha_B^2 = \left(\frac{\lambda_0}{\lambda}\right)^2 \left(\frac{\cos i}{\cos i_0}\right)^2 \quad \text{(grating } \textit{blank} \text{ errors).} \tag{50b}$$

In words, for aberrations smaller than $\frac{1}{2}\pi$ or $\frac{1}{4}\lambda$, the *diffraction-pattern imperfections that appear outside of the line centers increase with the square of the decrease in wavelength; for ruling errors they further increase with the square of the sine of the grating angle. But for blank errors, the diffraction-pattern imperfections fortunately decrease with the square of the cosine of the grating angle.*

2.2.9. *Periodic errors*

This is the case first examined by ROWLAND [1902] and before that by PIERCE [1879]. Strangely enough, STROKE [1960] shows this case to

appear, formally, as an application of his treatment of the 'linear' wave-front aberrations. Here, just like in the case of the 'linear' aberrations, both the position and intensity of the diffraction-pattern imperfections can be predicted in detail.

For a simple-harmonic error of amplitude ε and period P on a grating used at the angle i' in autocollimation, symmetric ghosts of orders n (n = integer) are found at a distance

$$(\Delta x)_n = n \frac{\lambda}{P \cos i'} f \tag{51}$$

in a spectrograph of focal length f. The relative intensities of the first-order ($n = 1$) and second order ($n = 2$) ghosts are found to be

$$G_1 = [J_1(\Phi_M)^2] = \frac{4\pi^2 \varepsilon^2 \sin^2 i}{\lambda^2} \tag{52}$$

and

$$G_2 = [J_2(\Phi_M)^2] = \frac{4\pi^4 \varepsilon^4 \sin^4 i}{\lambda^4}, \tag{53}$$

where

$$\Phi_M = \frac{2\pi}{\lambda} 2\varepsilon \sin i$$

and $J_1[\ ]$ and $J_2[\ ]$ are Bessel functions. It is clear that the first-order ghost predominates, and also that the variation of its position and intensity, with grating angle and wavelength, is in agreement with the general laws given in the preceding section. It is also important to note that Rowland ghosts result from only the simple harmonic components in the ruling errors and the corresponding wave-front aberrations, and not from the maximum aberration-amplitude, which is in general considerably greater.

It is also important to observe that attempts to analyze imperfect wave fronts in terms of Fourier-series contributions and summations of ghost-amplitudes fail, because of the practical difficulty resulting from the need of including a sufficiently great number of terms and from the fact that the summation needs to be carried out over the complex amplitudes of the ghosts, and not over their intensities. When a sufficiently great number of terms is included, one simply gets back to the Fourier-transform representation which we have used in the first place, on more general grounds.

§ 3. The Attainment of High-Resolution Gratings by Ruling under Interferometric Control

3.1. INTERFEROMETRIC CONTROL OF GRATING RULING

The principle of interferometric control of a continuously moving carriage, used successfully to rule 10-inch diffraction gratings on the M.I.T. ruling engine, was first described by HARRISON and STROKE [1955], and is deceptively simple. To rule a perfect grating, it is sufficient to make the instantaneous distance of the grating carriage from the start of the ruling be rigorously proportional to the accumulated 'position' which the diamond tip has reached since the start of the first groove as it rules the grooves, always in the same 'ruling plane', in a cyclic motion across the grating. The position of the diamond tip is measured by the accumulated angular position of the motor shaft that drives the diamond carriage and is taken as a reference. (Departures from linearity in the diamond velocity across the grating, along the groove length, can be simply corrected by mechanical means if necessary.) The instantaneous position of the grating carriage with respect to the start of the ruling is measured interferometrically with the help of an interferometer mirror rigidly attached to the grating carriage and moving with it, and the start of the ruling is materialized by another mirror and beam splitter which are maintained in a fixed position with respect to the 'ruling plane'. The grating carriage is made to advance at approximately the correct rate with the help of the ruling engine screw and an electromechanical gear system, connecting the diamond shaft to the screw through a differential. A grating-position control motor is also connected to this differential. If, as a result of mechanical imperfections in the engine and the screw, the grating carriage is incorrectly positioned by the direct drive, then the grating position error appears as an electrical signal. The error signal is produced by comparison of the instantaneous amplitude of the interferometric fringe signal (obtained from a photo-multiplier tube) and the instantaneous amplitude of the diamond-position reference signal (obtained from a signal-generator which is also geared into the diamond shaft). The grating position-error signal is made to rotate the servo-control motor in such a direction as to continuously and constantly maintain the grating in its correct position with respect to the start of the ruling and the diamond position by appropriately adding or subtracting to the carriage motion determined by the

rotation of the engine screw, which is itself driven by the diamond shaft. A schematic diagram of the servo-control loop used in the control of the carriage translation on the M.I.T. ruling engine is shown in Fig. 12. Interferometric wave-front studies of gratings ruled on the M.I.T. ruling engine with this control scheme have demonstrated that grating imperfections could arise even on an interferometrically controlled engine, unless one also controlled any rotation, about a vertical axis passing through the translation-control mirror if necessary (that is when rotations result from any curvature of the grating-carriage ways). Moreover, ruling errors will arise in an interferometrical-

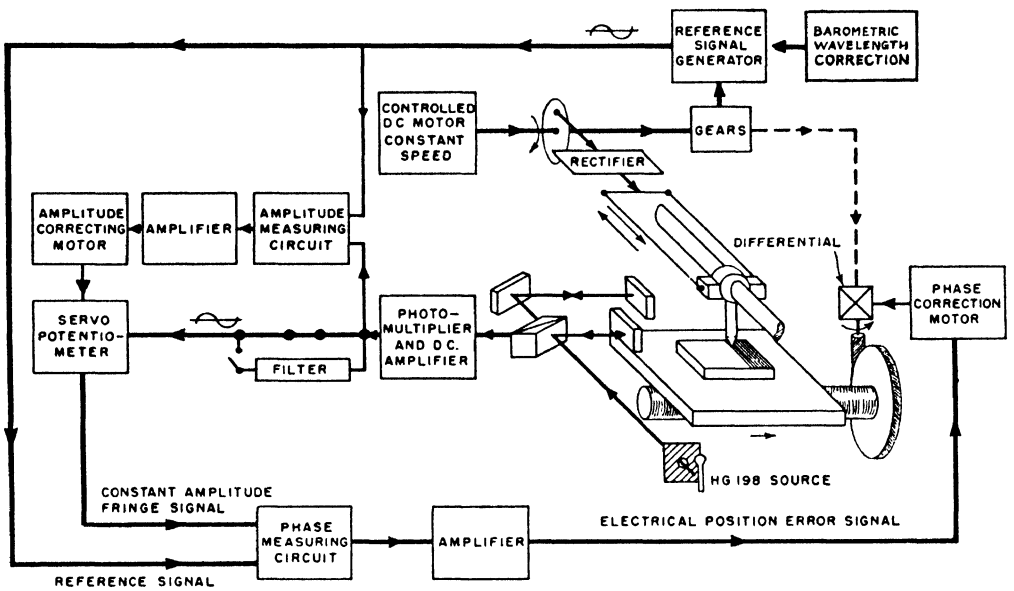

Fig. 12. Servo-control loop for interferometric control of grating ruling, as first described by G. R. HARRISON and G. W. STROKE [1955] for the control of the M.I.T. ruling engine. Similar loops are used for both the translation and the rotation control (see Fig. 20).

ly controlled engine if the grating plane (diamond tip) does not coincide with the center of gravity of the control-interferometer mirrors, in case of rotations (or 'tips') about horizontal axis normal to the ruling direction. Finally, second-order ruling errors can also result, if unchecked, from a combination of interferometric and servo-control effects, as we show below. Moreover, since the groove spacing, under interferometric control, is determined by the wavelength of a light source in air, it is also necessary to *either* maintain constant atmospheric conditions during the course of the ruling, *or* to measure any atmospheric variations, to compute their effect on the ruling and to

correct for them if they have occurred. Harrison and Stroke have found it preferable to use a simple analogue computer to correct for the effect of atmospheric variations, and in particular for the effect of pressure variations which have, by far, the largest effect.

The idea of controlling the ruling of gratings with the help of interferometers can certainly be traced all the way back to MICHELSON [1927] who used interferometers and visual fringe settings to improve the quality of his ruling-engine screws. HARRISON [1949] refers to W. W. Hansen of Stanford University as having undertaken work on interferometric control before his untimely death. More recently H. W. BABCOCK [1962] has adopted interferometric control to the stop-and-go motion of the Mt. Wilson Laboratory engine in Passadena, with pressure-correction similar to that used on the M.I.T. engine. However, rather than continuously correcting for errors as they occur (as is done on the M.I.T. engine), Babcock corrects for the error actually introduced into the grating on the nth groove by shifting the following $(n + 1)$th groove in an attempt of minimizing cumulative and local errors. Since extended errors are more harmful to high-resolution gratings than residual local and periodic errors, it is probable that outstanding gratings will result with this method, even though it does not aim at as complete a ruling control as that achieved in the method originated by HARRISON and STROKE [1955] and subsequently expanded by HARRISON *et al.* [1957], STROKE [1957, 1958], HARRISON [1958], HARRISON *et al.* [1959], STROKE [1961].

It is known that both the Bausch and Lomb Company of Rochester, N.Y. and the Jarrell-Ash Company of Newtonville, Mass. have adopted the Harrison and Stroke scheme of interferometric control to engines in their ruling laboratories (STROKE and JARRELL [1963]), and that other laboratories are preparing similar control.

3.2. QUALITY OF GRATINGS RULED UNDER INTERFEROMETRIC CONTROL

Figure 13 shows the wave-front interferograms and corresponding hyperfine structure and isotope shift patterns produced by two outstanding 10-inch gratings (No. 97 and No. 143) ruled one before and the other after new improvements of the M.I.T. engine had been recently carried out by STROKE [1961]. These patterns will be simply described as hfs patterns in the remainder of this paper. As a general order of magnitude, the good gratings now ruled on the M.I.T. engine

are found to be superior by factors of 100 to the famous gratings ruled by Rowland and Anderson at the beginning of this century, and in the early 1920's. Figure 14 reproduces for comparison two low-angle (45°) wave-front interferograms, one of a plane grating ruled by J. A. Anderson in 1914 on speculum metal on Rowland's engine, and considered as very good at that time, and the other of an early grating ruled under interferometric control on the M.I.T. ruling engine. It is apparent from the discussion in section 2 that Rowland's gratings were considered to be so good at their time because they were meant to be used only at very low angles, up to 10° or so in autocollimation, where the wave fronts were some 4 times better and the spectral quality of the gratings some 16 times better than here at 45°.

How much care needs to be exerted in comparing grating performance, with only the help of resolution photographs or his patterns similar to Fig. 13, as has been a practice in the past, becomes clear when the hfs of Fig. 15 is compared to the structures of Fig. 13. Unlike the patterns of Fig. 13, which were photographed with gratings 143 and 97 on a fast spectrographic plate 103aF in only 30 sec, the hfs of Fig. 15 was obtained with the same first-generation grating 97 of Fig. 13, but now on a low-contrast, rather slow and considerably finer Panatomic-X film. An exposure of $1\frac{1}{2}$ min was required in Fig. 15 to attain a density comparable to the hfs of Fig. 13b. A considerably better appearance of the hfs results under the conditions of Fig. 15, which, it is known, tend to conceal the existence of spurious satellites and weak ghosts and are usually impractical for spectrographic purposes: the hfs of grating 97 taken on the fine-grain film of Fig. 15 would in fact erroneously tend to favor this grating when compared to the hfs of grating 143 taken on the coarse-grain plate in Fig. 13(a). For the purpose of working comparison, the hfs patterns of Fig. 13 were obtained with both gratings under normal spectrographic conditions: in fact the hfs of the two gratings were actually photographed on the same plate and with the same exposure, in an attempt to bring out the component 'a' with the most similar density possible (which was almost achieved on the plate). It is quite apparent from Fig. 13 that a group of satellite lines described by 's' appears in the use of grating 97 with a density very similar to the density of component 'a': the satellites 's' result in a broadening of the lines from grating 97 when compared to the new grating 143 (where no such satellites appear and where the resolution is noticeably better under identical conditions). The wave-front interferograms of Fig. 13 are

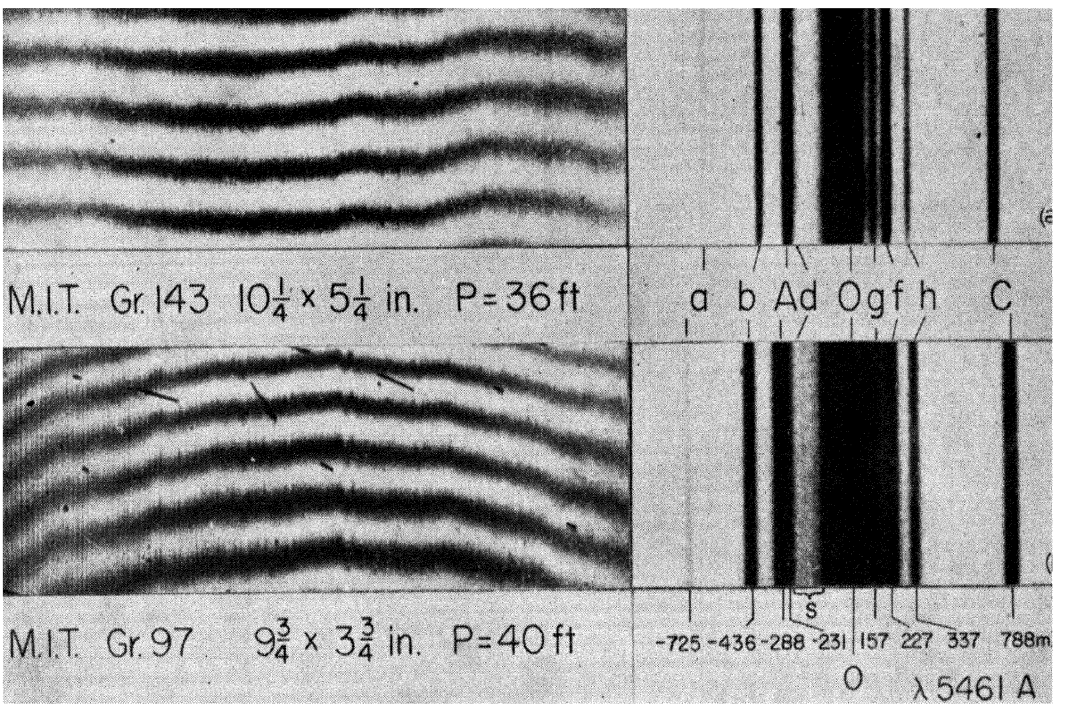

Fig. 13. Wave-front interferogram and mercury green line (5461 Å) spectrograms for two outstanding 10-inch high-resolution gratings produced on the M.I.T. ruling engine. As a result of improvements described in the text (and by G. W. STROKE [1961]), it is seen that no satellites appear in the use of Gr. 143, while such satellites, as described by 's' appear in the use of Gr. 97 with an intensity comparable to the component 'a'. Both spectrograms were obtained on the same fast 103aF spectrographic plate. Wave-front interferograms and spectrograms were both obtained at 64° in autocollimation.

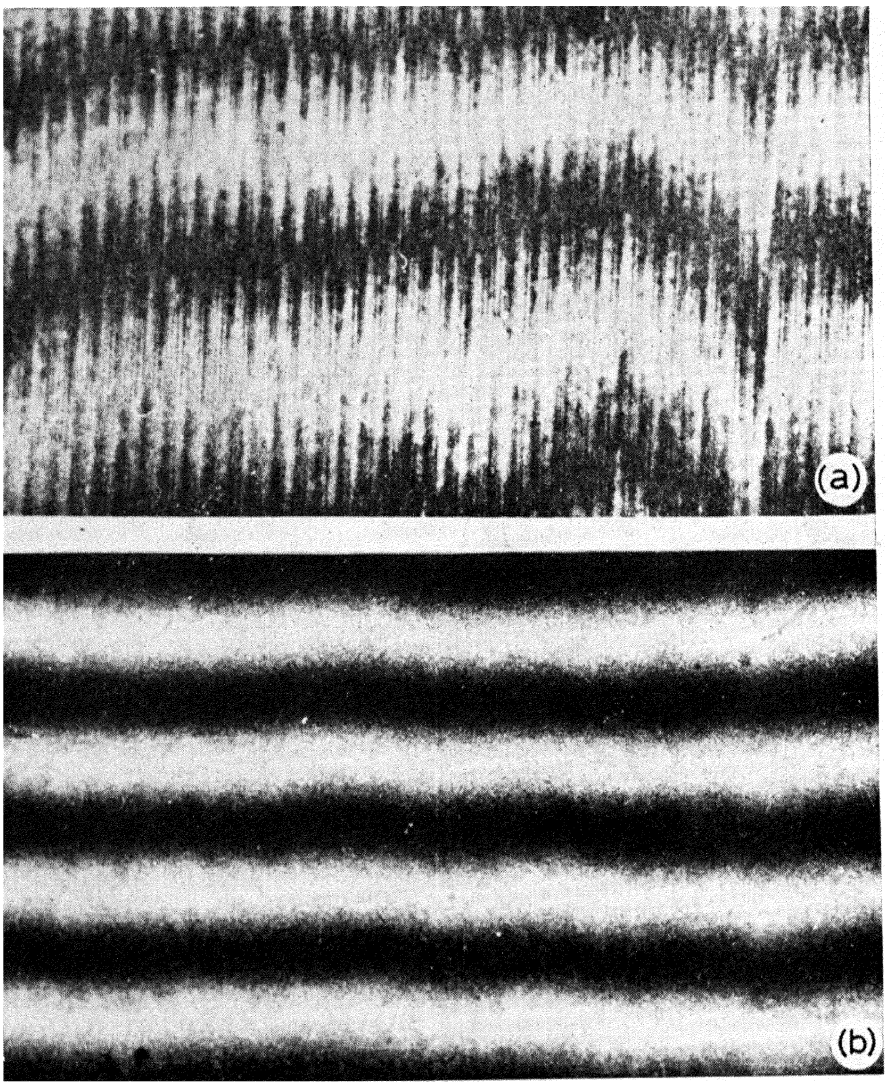

Fig. 14. Comparison of modern high-resolution grating with good grating of Rowland's period: (a) wave-front section of a grating ruled by J. A. Anderson on a Rowland engine in 1914 and considered very good at that time; (b) wave-front interferogram of similar section of an early M.I.T. grating ruled under interferometric control. Both interferograms were taken at 5461 Å at 45° in autocollimation.

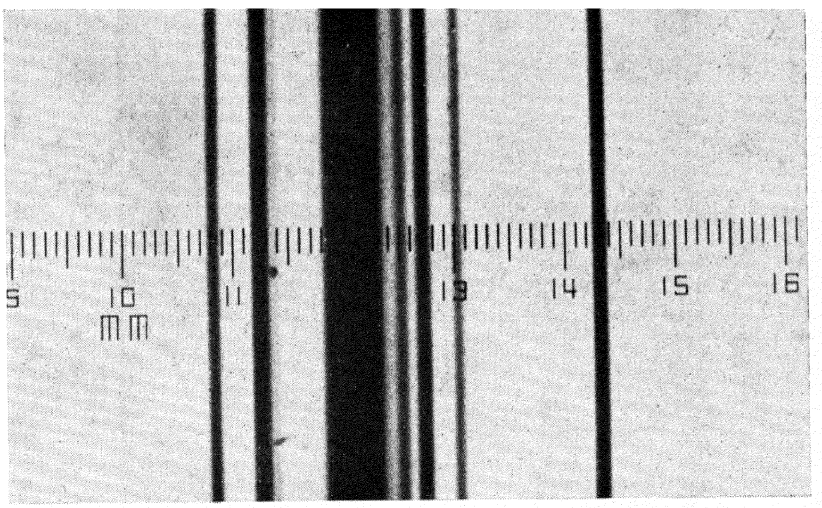

Fig. 15. Mercury green line (5461 Å) hyperfine structure (hfs) pattern obtained with grating 97 in same spectrograph as that used to obtain the spectrogram of Fig. 13b, but now on slow, fine-grain Panatomic X film. The photographic conditions shown here tend to conceal residual spectral line imperfections and permit to obtain such beautiful spectrograms under favorable conditions. But it is clear that hfs spectrograms shown alone, without wave-front interferograms and Hg 198 spectrograms may provide little useful information about the spectroscopic quality of a grating. The spectrogram shown here was obtained at 64° in autocollimation in the same 12-meter spectrograph as that used to obtain the spectrograms of Fig. 13.

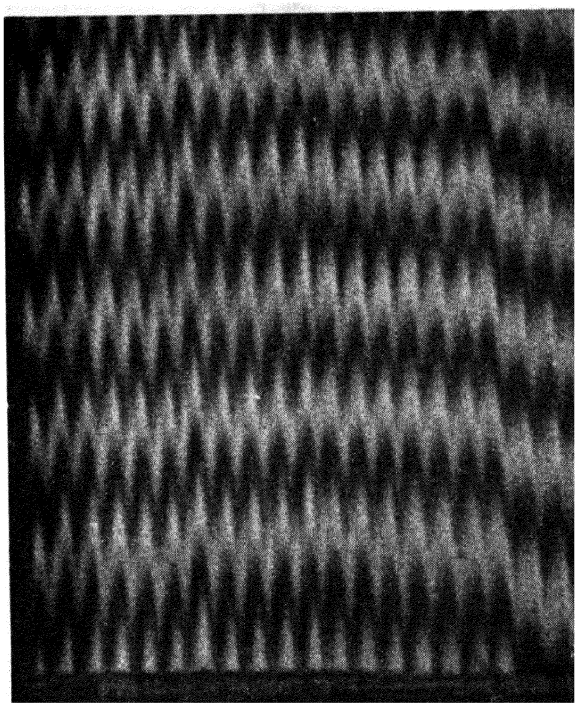

Fig. 16. Low angle (16°) wave-front interferogram of grating ruled on the M.I.T. ruling engine without servo-control. When compared with Anderson's grating (of which the 45° interferogram is shown in Fig. 14a) it is seen that, without control, the M.I.T. ruling engine cannot produce an acceptable grating even for low angle use, while the controlled engine can effectively remove the major part of the mechanical errors and produce outstanding high-resolution gratings of the quality shown in Fig. 13.

not subject to any such photographic effects: their power in grating assessment and engine improvements has now been established and clearly appears from these comparisons.

That the quality of the M.I.T. gratings is indeed being attained as a result of interferometric control is illustrated by the low angle (16°) interferogram of Fig. 16: when compared with Anderson's grating of Fig. 14a, it is seen that without control the M.I.T. engine does not produce an acceptable grating even for use at the lowest possible angles around 5°, while the controlled engine is capable of producing the outstanding grating of Fig. 13a.

The engine control-conditions which have resulted in the ruling of high-resolution gratings of the quality of grating 143 will now be briefly described. Experience has shown that their systematic use will indeed combine to result in the attainment of outstanding, flat, high-resolution gratings when ruled under interferometric control.

3.3. ADJUSTMENTS OF INTERFEROMETERS FOR GRATING-RULING CONTROL

Uncalled-for corrections might be introduced by the photoelectric servo-mechanism into the ruling engine if the interferometer-mirror motion results in an instantaneous flux distribution across the mirror aperture which does not properly represent the grating position. Errors can result in particular from improper location of the center of gravity of the interferometer-mirrors with respect to the grating plane.

An equal-inclination ring fringe-system obtained from flat mirrors is used for the interferometric control of the moving grating-blank carriage on the M.I.T. ruling engine as shown in Fig. 17. The green 5461-Å line is obtained from a Meggers Hg198 tube excited in an electrodeless discharge at about 200 Mc/sec and cooled by a moderately strong air current at about 70° F (MEGGERS and WESTFALL [1950]). Only a small portion of the central part of the ring system is isolated by a circular diaphragm (source hole) placed in the focal plane of the collimator lens. The flux transmitted through the interferometer, and modulated as a result of the motion of the moving mirror, at the rate of 1 fringe cycle for every $\frac{1}{2}\lambda$ of carriage advance, is focused onto a 931-Å photomultiplier tube. It is important that the source hole be accurately centered on the common normal to the moving and reference mirrors, which is also the center of the ring system in the focal plane

of the collimator. The diameter of the rings decreases with the mirror separation according to well-known laws, and a source-hole aperture of 1-mm diameter (in the focal plane of the 1 m collimator) is chosen so as to correspond to only a small fraction of the central fringe at the maximum mirror separation of 5 inch used in the ruling of 10-inch gratings. It is essential not only to center the hole by autocollimation on the mirrors, but to center it actually on the ring system. Although this was pointed out in the original paper by HARRISON and STROKE [1955] dealing with the principle of the interferometric control used

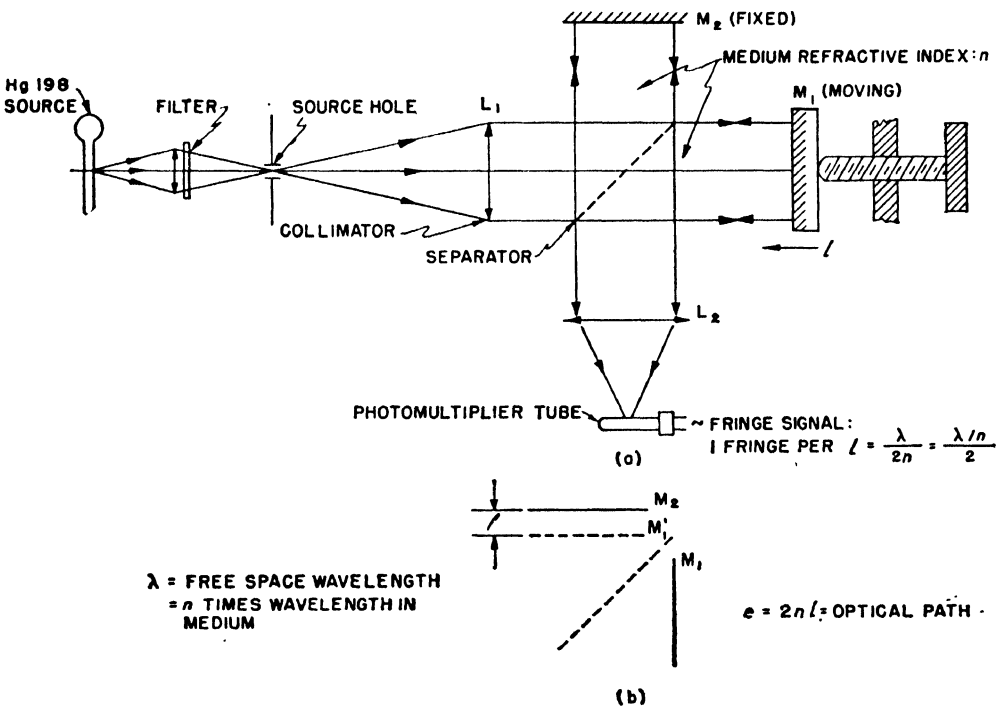

Fig. 17. Photoelectric interferometer used in servo-control of ruling engine (schematic).

on the M.I.T. engine, experience has shown that some additional clarification to what is meant by 'interferometric' centering may be desirable (STROKE [1961]). An eccentricity of only 1 mm in the focal plane of the 1 m collimator will indeed result in the additional count of an entire fringe on either extreme of a 10-inch grating, which may be sufficient to account for the curvature of some of the 10-inch gratings previously described.

The source hole can be easily centered by first setting the interferometer to some small mirror separation of, say, 20 to 40 mm. After bringing the two source-hole images into coincidence in the usual

manner, the straight-line fringe system located in the vicinity of the mirrors can be observed with the help of a low-power telescope. When the interferometer mirrors have been made as parallel as possible by spreading out the fringes, a very clearly visible ring fringe-system will be observable in the plane of the extended Hg198 tube if the telescope has been refocused on the source hole, and the source hole then removed. If the telescope cross hair is brought to coincide with the center of the ring system, and the source hole is replaced into its position in front of the Hg198 tube, it can be easily moved until its image coincides with the cross hair of the undisturbed telescope. An adjustment within 0.1 mm in the source plane (corresponding to about $\frac{1}{10}$ fringe of grating flatness) is easily achieved.

Any local change in fringe-signal amplitude will be interpreted by the servo-control as a translation error of the control-mirror involved. If the amplitude change is caused by a local mirror-parallelism variation, an uncalled-for correction may result and an error might be introduced into a grating at a place where it was properly positioned by the fringe field. The rotation control about an axis normal to the grating plane and to the direction of grating advance helps in suppressing effects resulting from rotations about vertical axes. But rotations about a horizontal axis parallel to the gratings plane and normal to the direction of grating advance will result in both a simple geometrical ruling error (when the interferometer mirror aperture is not centered on the grating plane) and in a more subtle error caused by a combination of interferometric and servo-mechanical origins. The geometrical error can be simply taken care of by centering the interferometer mirror aperture on the ruling plane within the tolerances of the order of 1 mm, as appears from Fig. 18. The fringe-signal amplitude variations across the mirror aperture which result from rotations about the horizontal axes – and which attend the use of plane mirrors – may, however, still lead to ruling errors unless their effect is also rendered negligible. The fringe-single amplitude referred to here is that by which one usually describes the amplitude of the periodic signal: it is not the instantaneous value of the fringe-signal (which does, however, depend on the amplitude, or course). Local errors up to $\frac{1}{2}$ fringe would result in the gratings ruled on the M.I.T. ruling engine before the new corrections were recently carried out by STROKE [1961] (Fig. 19). The effect discussed here had also been predicted on theoretical grounds (STROKE [1957]), and it was shown that it increases with the number (or fractional number) of fringes

in the interferometer aperture (for imperfectly parallel mirrors), or alternately with the size of the aperture in presence of the number of fringes in the aperture. The new improvement consisted simply in masking down the vertical height of the interferometer aperture to about 10 mm or less. It remains, of course, essential to locate the center of gravity of the interferometer aperture slit on the plane of the ruling.

We might note, in conclusion, that the mirror location problem is somewhat different in interferometric spectrometers (MICHELSON [1927], FELLGETT [1951, 1958], JACQUINOT [1954, 1958, 1960], CONNES [1960, 1961]): there the motion of interest is that of the mirror or the

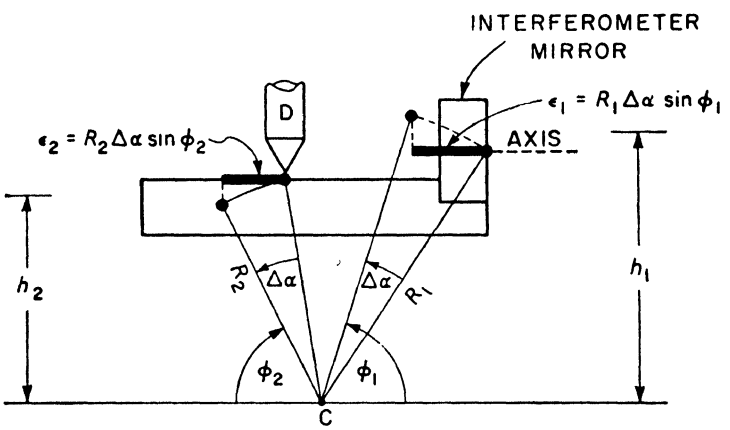

Fig. 18. Ruling error ($\varepsilon_2 - \varepsilon_1$) which would result from incorrect centering ($h_2 - h_1$) of interferometer mirror axis on ruling plane (at tip of diamond) in the presence of a pitchlike rotation ($\Delta\alpha$) occurring during the course of the grating advance.

corner cube itself, and it is sufficient that its own position be correctly measured and controlled. In the controlled ruling of gratings, the interferometric element is generally placed at some considerable distance from the groove that is being ruled: it is the difference in translational components between the grating and the interferometers which tends to result in ruling errors if permitted to remain uncorrected. It is in fact the problem of correctly positioning the grating over its entire traverse when moving over rather imperfect ways which has made it so difficult to attain high-resolution gratings.

3.4. ROTATION CONTROL

Translation control alone, in the direction of blank advance, has been found to be insufficient on the M.I.T. ruling engine, as a result of the various rotations caused by the balls on which the blank-

carriage rolls in the course of its advance, and as a result of the curvature of the cylindrical ways which guide the balls (HARRISON, STURGIS, BAKER and STROKE [1957]). More classical ruling engine ways, such as the 'doublevee' ways already used by Rowland, may also cause rotation problems, in particular as a result of lubrication irregularities.

With the help of an alignment interferometer, the ways can be easily and rapidly adjusted to an average straightness of ± 1 fringe (measured across a 10-inch interferometer arm) over the 10-inch traverse in a horizontal plane (STROKE [1961]). The local parallelism of the grating advance continues to be maintained with the help of an interferometric servo-mechanism identical to the one used in the translation-control loop (Fig. 12) by comparing the fringe signals obtained from two regions of the same mirror placed some 4 inch apart, as illustrated in Fig. 20. One of these mirror regions is located exactly above a preloaded

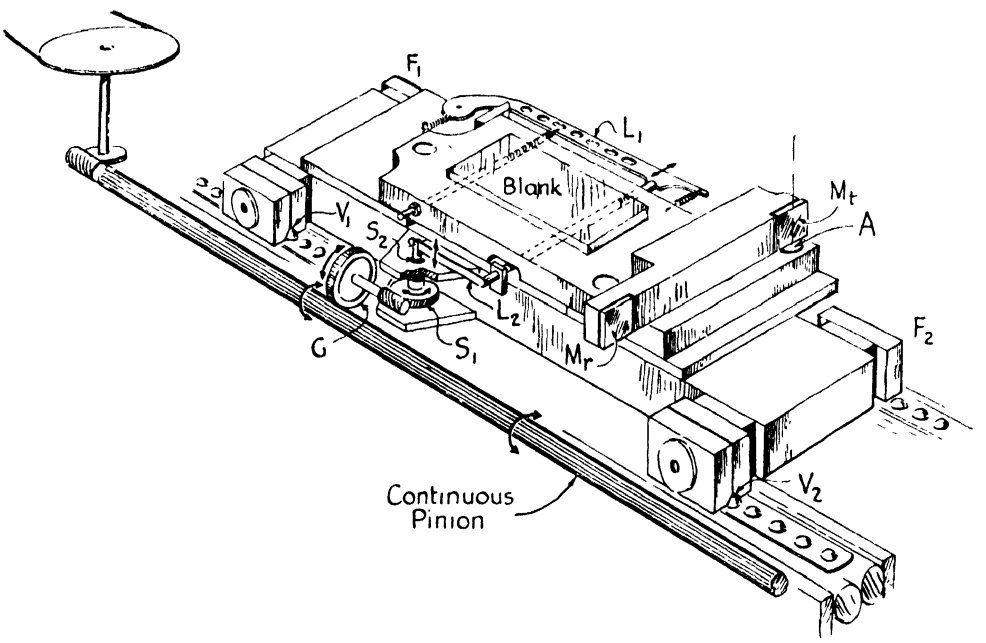

Fig. 20. Rotation control of grating carriage used on M.I.T. ruling engine (HARRISON, STURGIS, BAKER and STROKE [1957]). Rotations about the vertical axis through the center of the translation-control mirror M_t will result in translation components and errors in the grating (blank) if left uncorrected. The two interferometric fringe signals from M_t and M_r are compared and maintained in phase with the help of a servo-control loop similar to that of Fig. 12. As a result of lubrication irregularities, rotation errors may appear even in ruling engines using the more classical 'double-vee' carriage ways, rather than balls and cylindrical ways. Besides their apparent disadvantage in sensitivity to dust and other material particles, balls have the advantage of resulting in macroscopically reproducible traverses, requiring only local corrections.

ball-bearing pivot and the entire grating table is rotated by the interferometric rotation-control servomechanism about a vertical axis defined by the ball bearing and passing through the front of the translation mirror. The translation control results in accurate positioning of the grating-carriage within about $\pm\frac{1}{100}$ fringe (about $\pm 0.003\,\mu$ or $\pm 10^{-7}$ inch) over the 10-inch traverse, and in maintaining the parallelism to $\pm\frac{1}{200}$ sec of arc.

A general view of the M.I.T. ruling engine is shown in Fig. 21 and a close-up of the control-interferometers in Fig. 22. A view of the control room is shown in Fig. 23.

3.5. CORRECTION FOR THE EFFECTS ON THE INTERFEROMETRIC CONTROL SYSTEM OF BAROMETRIC CHANGES OF WAVELENGTH

Under interferometric control, the groove position and spacing are determined by the wavelength of the green Hg198 radiation in air. The wavelength in air changes with variation barometric pressure, temperature, water vapor and CO_2 partial pressure as well as with the introduction of any foreign gases or vapors (BARRELL and SEARS [1939]). In practice, when the temperature is controlled to the tolerances of $\frac{1}{100}$° C or better as required by the mechanical elements of the ruling engine, variations in barometric pressure produce the major change of wavelength, according to an equation

$$\Delta m = 3.31\,\Delta P \Delta L,$$

where Δm is the fringe shift in $\frac{1}{100}$ fringe ($\frac{1}{2}\lambda$), ΔP is the pressure variation in inches of mercury, ΔL is the mirror separation from zero path difference in mm. For example, if a pressure change of $\Delta P = \frac{1}{3.3}$ inches should occur when the grating is at $\Delta L = 100$ mm from zero path difference, then the grating would be shifted by $\Delta m \simeq 100$ hundredths of a fringe, or approximately by one fringe by the controlling servo-mechanisms, a very large error indeed, if it remained uncorrected. In reality the pressure change does not only result in a shift of the grating at the time when a pressure change occurs, but it also produces further errors as a result of a spacing in the now incorrect wavelength (as compared to the wavelength at the pressure P_0 at the start of ruling). Finally, the sign of the grating shift changes when the grating interferometer mirror passes through zero path difference. When the grating moves towards zero path difference, a pressure increase (which decreases the wavelength and tends to pull the grating towards zero path difference) moves the grating 'forward'

in the direction of its motion. However, the pull towards zero path difference will move the grating backwards from its direction of motion when the grating moves away from zero path difference. The grating shifts, both 'instantaneous' (at the time of the pressure change) and 'cumulative' (as a result of the changed wavelength) result from the operation of the servo-control phase detecting system, which is designed to continuously synchronize the interferometric fringe signal with the diamond-position reference signal. The phase detecting system only knows about fringes and their position relative to the reference, but it ignores the differences in the origin of fringe shifts (real position error or change of wavelength). It is the function of the analogue computing cam shown in Fig. 23, to calculate the instantaneous *uncalled-for* grating shifts, and to accordingly shift the reference signal generator, relatively to the diamond-shaft, in order to maintain the correct grating position relative to the start of ruling and the diamond. The height of the two-dimensional hyperbolic cam materializes, with the help of appropriate linear slopes, the variations of fringe-shift as a function of path difference and pressure change in the range of operation. The pointer which rides on the cam is directly geared into a differential placed between the diamond-shaft and the diamond-position reference signal generator. The computing can also be carried out with the help of an electronic multiplication circuit using 'helipot' resistors and a servo-motor to feed the differential.

3.6. ENGINE TEMPERATURE CONTROL

Simple control priciples have been established for the temperature control of the oil-bath in which the M.I.T. engine is immersed. The temperature stability of the order of $\pm 0.001°$ C which has been achieved is indeed necessary for the ruling of high-resolution gratings, since the control system assumes that the distance between the beam-splitting tower and the reference mirror some 500 mm away remains constant during the course of the $4\frac{1}{2}$ to 5 days required for ruling a 10-inch grating at 300 grooves/mm. With a temperature coefficient of 10^{-5}/deg C of the steel casting on which both the tower and the reference mirror are placed, an increase of 0.001° C will tend to shift the reference mirror by approximately 0.02 fringes with respect to the tower. Since the control mirror carried by the grating carriage moves with respect to the reference mirror in the course of its advance during the ruling, a shift in the grooves of this order of magnitude

would occur if no other effects were involved. In fact, some compensation may appear possible, but it is found that differential expansions finally combine to call for a temperature stability of the order of $\pm 0.002°$ C, especially at the part of the ruling where the control mirror is closest to the tower.

Of course, it is not possible to maintain the 300 gallons of oil in the bath and the entire engine at the same temperature in the presence of the heat sources used in the control and the various radiative and conduction losses around the engine. One attempts rather to maintain all the local temperature fluctuations within the $\pm 0.001°$ C, while at the same time establishing small gradients from the control point to the outside of the vat. Dimensional equilibrium is thus achieved under dynamical rather than semistatic conditions. It is in fact the magnitude of the gradients, or rather the temperature level at the control point (located in the center of the engine, halfway between the reference-mirror and the beam-splitting tower) which has been found to be crucial in the success of the control. A temperature level some $0.05°$ to $0.1°$ C above the level of the unheated oil at the control point has been found to be the best operating temperature level about which the $\pm 0.001°$ C is then achieved under optimun conditions. A period of 12 to 18 hr is usually required to raise the engine and oil to the operating temperature. At the 78° F at which the engine room is normally controlled to about $\pm 0.02°$ C on the average, a heat input of about 20 W is used to bring the engine and oil to the operating level, and input variations of the order of ± 1 to 3 W in the course of 1.5-hr periods are observed during the control. A proportional control operating from a Wheatstone bridge is used to change the voltage across the heater with the help of a Variac transformer, and care is taken to deflect the oil stream from the heater to the sensing element with the help of stirrers and appropriate shields to avoid lag in the sensing and to suppress temperature oscillations. Of course, the stirrers need to be carefully isolated from the floor and the engine to avoid vibrations in the control interferometers and the ruling diamond.

3.7. DIAMOND-CARRIAGE CONTROL

The interferometric control of the grating-carriage advance implies that the diamond carriage moves in the ruling plane parallel to the fixed reference mirror within a few hundredths of a fringe (some 0.01 μ) during the course of some 15 miles of equivalent traverse,

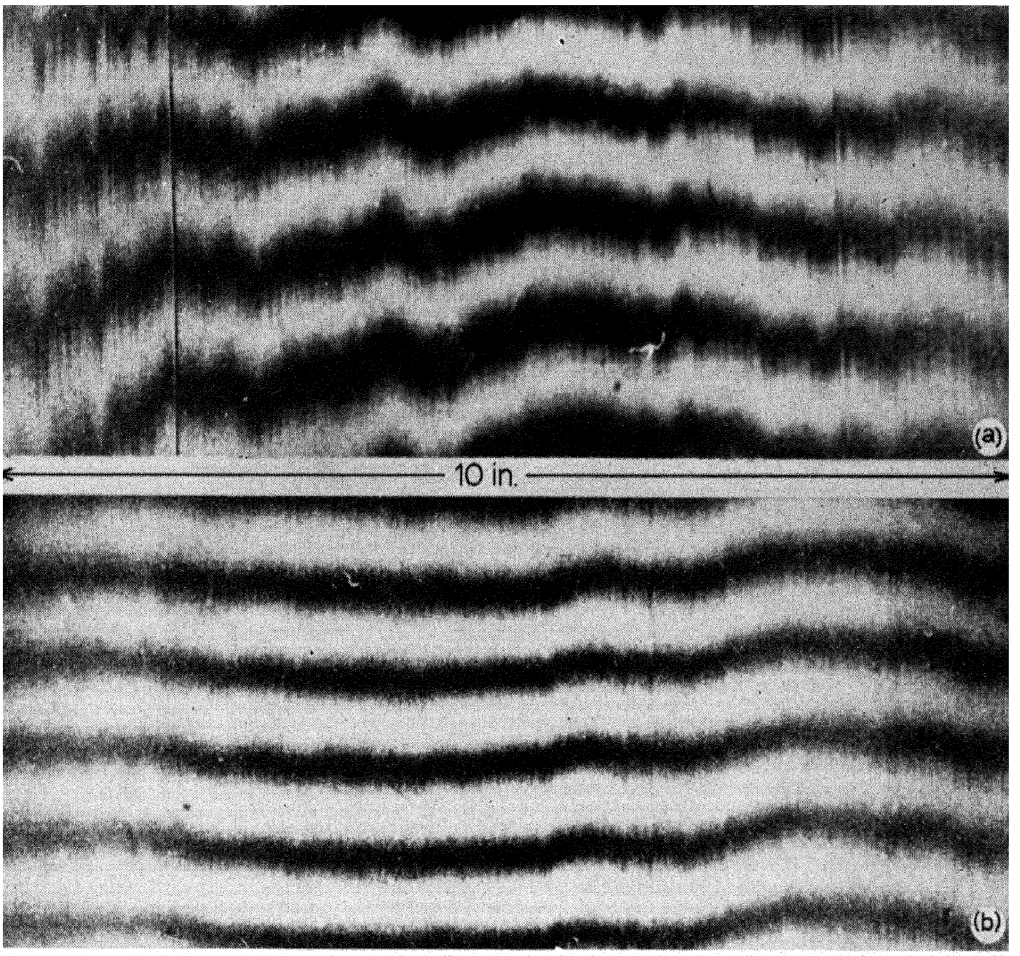

Fig. 19. Wave-front interferograms in 5461 Å at 64° of two 10-inch gratings ruled on the M.I.T. engine and illustrating the effect of what might seem, at first sight, to be comparatively minor improvements of the ruling engine and interferometric control system. Grating (a) is unusable as a good grating, while grating (b), even when completely unmasked, has proven to have the most outstanding spectral quality of any 10-inch grating ruled so far. The improvements (discussed in the text and also by STROKE [1961]) have demonstrated that a correct application of the control principles and engine adjustments will indeed permit to obtain outstanding gratings of the quality of (b). About six months of work were involved in systematically isolating the origins of the errors appearing in grating (a) and in improving the engine and control adjustments to obtain grating (b), without involving any extensive changes in the engine elements or control systems.

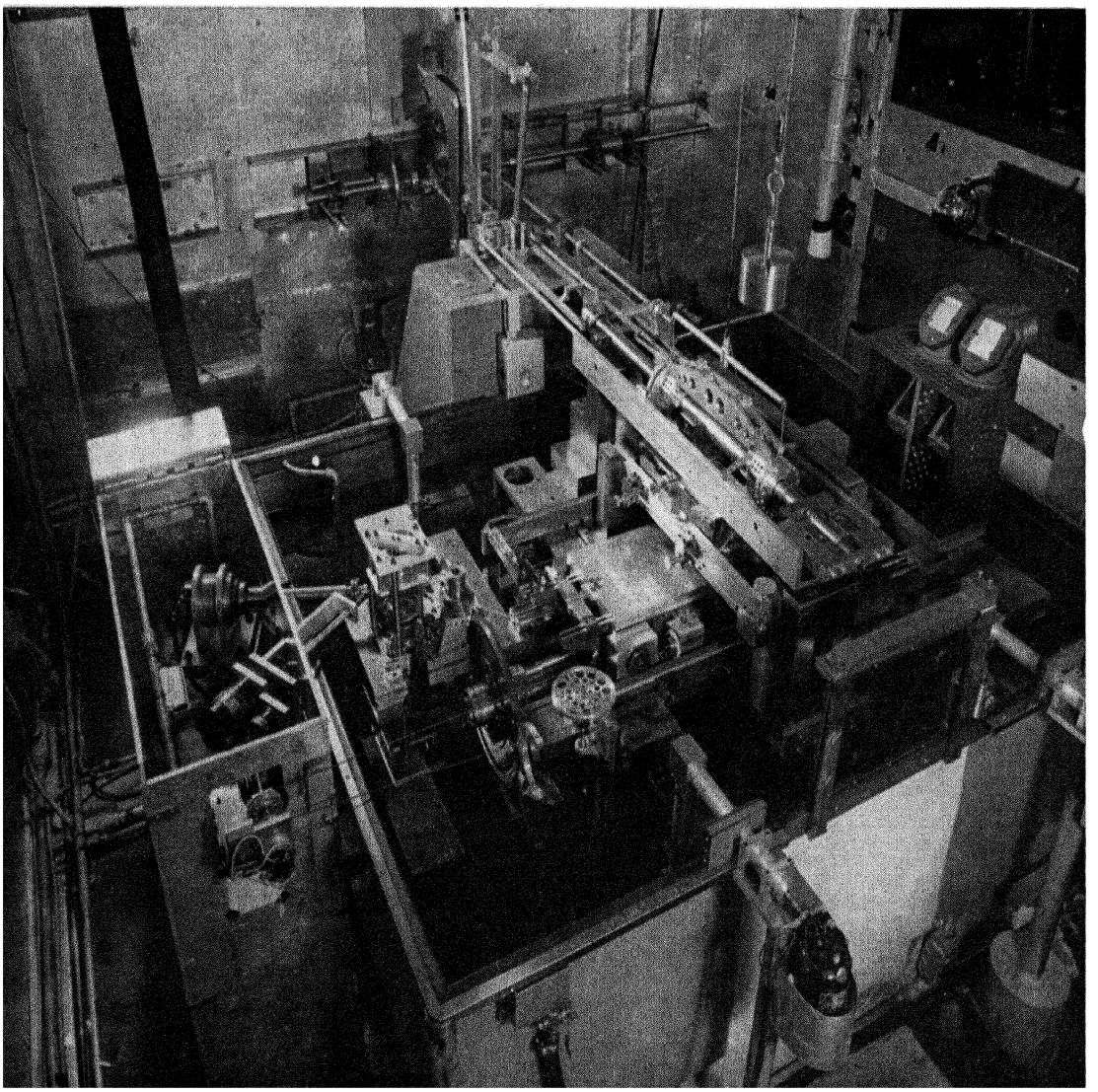

Fig. 21. General view of M.I.T. ruling engine

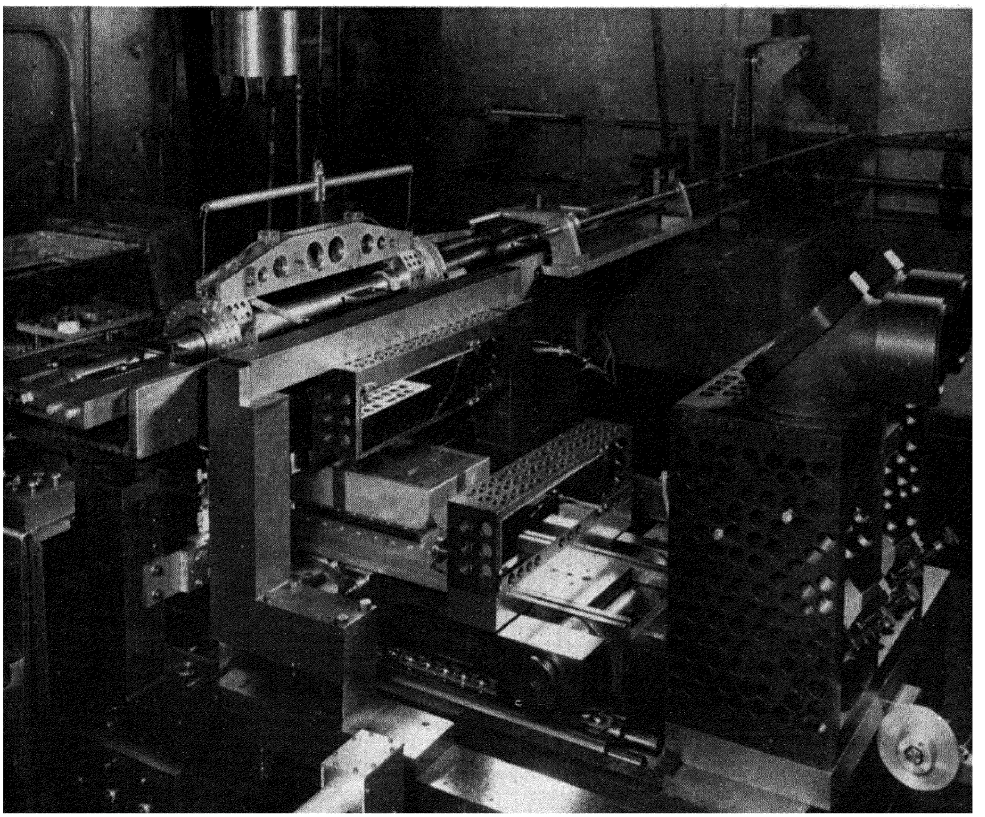

Fig. 22. Close-up view of control-interferometer side of M.I.T. ruling engine. A ruled 10-inch grating is shown on the grating-carriage. This carriage also carries the long mirror used for translation and rotation control. The beam splitting tower is shown in the right foreground, and the large reference mirror on the left, above the grating, near the cylindrical monorail which supports the diamond carriage.

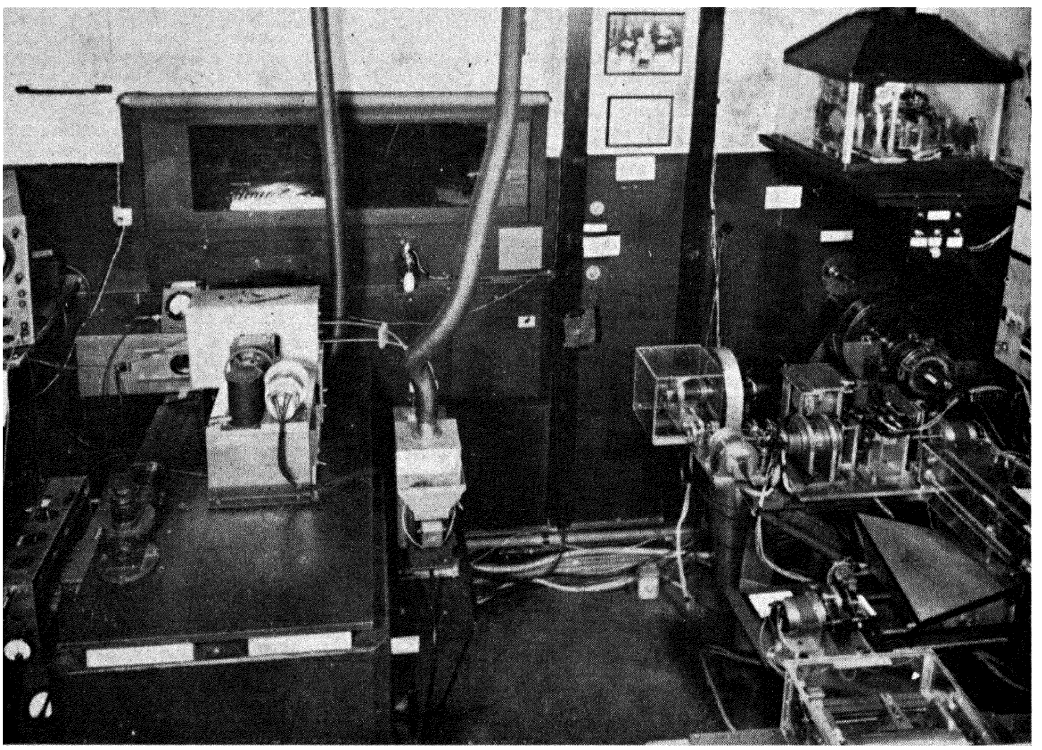

Fig. 23. Control room of M.I.T. ruling engine. The Hg 198 light source and reference-signal rotating-polaroid generator are shown in the left center. On the right is the gear system connecting the main diamond shaft to the engine screw and the reference signal generator. In the lower right, one can see the saddle-shaped cam used in computing the corrections for the effects of atmospheric pressure variations on the interferometric control system (HARRISON and STROKE [1955], HARRISON *et al.* [1957], STROKE [1961]).

which correspond to the ruling of a 10-inch grating at 300 grooves/mm. The design of the grating carriage used on the M.I.T. ruling engine was described by HARRISON and STROKE [1955], and it has successfully withstood the test of time in maintaining the diamond in the ruling plane within better than $\frac{1}{15}$ fringe. This result is of course not achieved without careful adjustment of the mechanical elements involved. The diamond carriage is suspended from two bearings riding on a monorail, which is fixed on the engine, and rests with a plastic (Rulon) shoe on a long optical flat, which is also fixed on the engine in a position at right angles to the grating motion. It is the long flat which determines the ruling plane. So far it has not been found necessary to use interferometric control of the diamond with respect to its reference mirror, but further improvements in grating quality may result from the use of a servo-system for that purpose, as well as from possible interferometric monitoring of the reference-mirror position itself with respect to the beam-splitting tower and other fixed interferometer components, in particular: the use of the extremely sharp spectral lines produced by optical masers (SCHAWLOW and TOWNES [1958], JAVAN [1960], JAVAN *et al.* [1961]) should prove invaluable in interferometric control.

§ 4. High-Resolution Gratings in Comparison with Fabry-Perot Etalons in Spectrometers and Spectrographs

It may not yet be generally appreciated that the well-blazed and extremely luminous, large high-angle gratings have opened to spectroscopy the field of high-resolution studies in the 10^6 resolving-power range, which was previously considered accessible only to rather more complicated interferometric devices. The advantages of simplicity and broad spectral coverage associated with the use of gratings and echelles for high-resolution spectrographic studies were recently emphasized by HARRISON and STROKE [1960]. Considerable further advantages of luminosity and compactness result from the use of high-resolution gratings in scanning monochromators and spectrometers.

These advantages are particularly significant in the light of an exhaustive general study of Fabry–Perot spectrometers carried out by Chabbal and published in his 1957 thesis (CHABBAL [1957, 1958]). More recently, JACQUINOT [1960] has reviewed the new developments in interference spectroscopy, a field which he has so much stimulated by his now well recognized significant contributions. Chabbal shows

that in order to filter out all the unwanted overlapping flux, which marks the high-order use of interference spectrometers, and make out of a FP etalon a high-resolution single bandpass 'integral' FP spectrometer comparable to a high-resolution grating-spectrometer, one needs to use as a premonochromator not only the large grating with which comparison is being made, but also another FP etalon. As a result, the very considerable inherent superiority of FP luminosity per resolution first pointed out by Jacquinot in 1954 (which could attain the order of 200 per unit area in the aperture if the FP etalon could be used alone as a spectrometer) may be reduced to an order only slightly exceeding unity, and rarely attaining ten, when the FP etalon is associated to its premonochromator. As pointed out by Jacquinot, the remaining gain in flux in a single bandpass FP spectrometer may indeed be found to be widely variable and in unfavorable cases comparatively small, except in special applications when considerably less thorough filtering can be tolerated and when possibly confusing 'ghosts' next to significant spectral lines can be ignored as a result of separate study (CHABBAL and JACQUINOT [1961]).

A similar conclusion is obtained by GREENLER [1955] in a study of infrared spectrometers. When comparison is made in energy-limited infrared spectrometers of the now available 10×18 inch infrared gratings (BARKER and RANDALL [1961]) with a 3-inch FP etalon according to Greenler's calculation, the gain in resolving limit at a given flux (under the stated assumptions of low angle 20° to 30° blazed gratings and an interferometer transmittance of 60 %) has in fact now become slightly tipped in favor of the grating. In the visible, where sufficiently good FP etalon plates have so far rarely had a useful diameter exceeding 60 mm (JACQUINOT [1960], CHABBAL [1958], KOPPELMAN and KREBS [1961]), the gain of the FP interferometer which existed according to Greenler's calculation only a few years ago has now been reduced to the order of unity as a result of the availability of the new high-resolution gratings described here. One is led to the conclusion that the use of FP etalons for spectroscopic studies which can be more simply carried out with gratings and echelles is, in general, not warranted. The use of gratings in high-resolution infrared spectrometers has also been described by LORD and MCCUBBIN [1955]. It is clear, of course, that for studies in the resolving power domains of 3 to 4×10^6 in the visible and ultraviolet which are not yet accessible to single gratings, and where a loss of light resulting from the association of an FP etalon with a

low-resolution monochromator is acceptable, the etalon is the high-resolution device to be used. More generally, one can use a FP etalon in conjunction with an existing grating or prism low-resolution monochromator in order to increase its resolution (even though this may result in a more complicated scanning arrangement than that which could be used to obtain the same high resolution with a large grating monochromator). For ultimate resolutions, Conne's spherical FP etalon (CONNES [1956, 1958]) does in fact yield considerably more flux per bandwidth than a plane FP etalon with otherwise comparable limitations in free spectral range.

It is the very large free spectral-range characteristic of the small groove depth in gratings and echelles which is one of the great assets of diffraction gratings in high-resolutions spectroscopic studies. It is indeed the independence of free spectral range from both resolving power and dispersion which is at the heart of the advantages of diffraction gratings over FP etalons in high-resolution studies that fall within their domain. Unlike that in gratings, the free spectral range of an FP etalon varies inversely with its resolution and falls to extremely small values even at resolving powers which are very moderate in terms of its capabilities. Even a 1 cm FP etalon, of RP $= 10^6$ at 5000 Å (with a finesse of 25), has a free spectral range of only $\frac{1}{2}$ cm^{-1}, which is insufficient to study the hfs of either the blue or green mercury lines without a premonochromator. On the other hand, the same resolving power of 10^6 can be obtained with a 300 groove/mm, 10-inch grating or a 10-groove/mm 10-inch echelle in autocollimation at 76°, with the very large free spectral ranges of 3×10^3 and 100 cm^{-1}, respectively. One recalls that the free spectral range is the wave number range that can be obtained without overlapping. It is given by $\Delta\sigma = 1/(2t)$, where t is both the thickness of the FP etalon and the apparent groove depth of the grating, of which the spacing constant is a. (Thus $t = a \sin i$ for a grating in autocollimation at an angle i.) For the FP, the resolving power RP $= \sigma/\delta\sigma$, where $\delta\sigma = \Delta\sigma/N$; the wave number $\sigma = 1/\lambda$ ($N = 25$ for plates flat to $\frac{1}{50}\lambda$, and in general $N = \frac{1}{2}m$ for plates flat to λ/m). For a grating of ruled width W, the resolving power is RP $= 2W \sin i/\lambda$, and the dispersion

$$\mathrm{d}i'/\mathrm{d}\lambda = 2 \tan i'/\lambda;$$

both are seen to be independent of the spacing constant a.

The attainment with gratings of resolving powers in the 10^6 range has indeed greatly altered the classical concept of the need of an

FP spectrograph or spectrometer as the only practical tool for high-resolution spectroscopic studies. In fact, in the case of 'high' resolutions between 10^5 and 10^6, for which the use of gratings was considered impossible only a few years ago because of imperfections, HULL and H. H. STROKE [1961] have recently found that even spectroscopic light sources containing as few as 10^{12} to 10^{13} atoms (about 1 mμg of matter at the atomic weights around 200 of the radioactive elements involved) can be studied to advantage with the help of the new, well-blazed, very luminous gratings now available.

Two examples of the extreme resolutions and luminosity that can be obtained with modern high-resolution gratings are shown in Figs. 24 and 25.

Fig. 24 shows the central five components of the green 5461-Å mercury line comfortably resolved on a 103aF fast spectrographic plate at a dispersion of about 24 mm/Å in a 40-ft (12-m) spectrograph with a resolving power of 1.25×10^6 obtained by using two 7.5-inch gratings in series as described by G. W. STROKE and H. H. STROKE [1958, 1963]. The resolution of these components has long been considered a test of performance for high-resolution interferometers.

Fig. 25 shows a photoelectric recording of the hyperfine structure of the blue 4358-Å mercury line obtained by direct scanning in a very luminous Jarrell–Ash spectrometer of only 1-m focal length (BREHM [1961]), using a $7\frac{1}{4}$ inch wide replica of one of the new M.I.T. gratings (No. 140) described in the present work. The 44-mm cathode diameter of the 13-stage EMI 6255B tube used in the spectrometer permits exploitation of the full advantage of the 2-inch long curved Fastie slits (FASTIE [1952], CROSSWHITE and FASTIE [1956]) open here to only 2μ.

These results demonstrate the versatility and adequate luminosity of diffraction gratings when used to obtain resolving powers up to the order of 2×10^6 in spectrometers and spectrographs. Possibilities of even further improvements are presented in the next section.

§ 5. High-Resolution Grating Spectrometers and Spectrographs

The two examples in Figs. 24 and 25 serve to illustrate the respective advantages of photographic spectrographs and photoelectric spectrometers, which both conserve the remarkable simplicity associated with the use of gratings in high-resolution studies. They also bring out certain important differences between spectrographs and spectro-

meters, as well as the possibilities of further gains and improvements in luminosity, compactness and resolution.

5.1. SPECTROGRAPHS

In photographic grating-spectrographs we have quite generally found that the limitations of practically attainable resolution are set by the granularity of the best spectroscopic plates which are available when short exposures of, the order of a few seconds to the order of a few minutes, are desired. This is the case in usual high-resolution studies. An exception is found in the study of the radioactive isotopes with only millimicrograms of matter in the source, where exposures of 2 to 4 hr have been reported (HULL and STROKE [1961]) as well as in some astronomical work (KEITH PIERCE [1957], EVANS [1961], FEHRENBACH [1960]).

The use of fast spectrographic plates is thus generally appropriate in spectroscopic studies. When weak components on the wings of strong components are to be clearly separated, as in Fig. 24, their separation on a Kodak 103 plate needs to be of the order of at least 0.1 mm in practice for beautiful resolution. Hence the projection distances of the spectrographs have to be correspondingly long, of the order of 6 to 12 m when gratings are used at 64° in autocollimation as has been the practice in recent years. Even longer projection distances of the order of 50ft have been described in astronomical applications (KEITH PIERCE [1957]). It is clear, of course, that microdensitometer recording of the spectrograms permits some reduction of the long projection distances, but the orders of magnitude of 6 to 12 m are representative of the lengths necessary for comfortable work with a single high-resolution grating used around 64°.

A very significant gain in the compactness and luminosity of grating spectrographs and spectrometers should be achievable if the gratings (and echelles) were used in autocollimation around 76° rather than at 64° as has been customary. In this paper we do not distinguish between gratings or echelles except when necessary. While the limiting resolution will be only slightly improved by increasing the angle to 76° (since $\mathrm{RP} = 2W \sin i/\lambda$), the angular dispersion will double and therefore permit a reduction by a factor of 2 of the projection distance required for a given comfortable photographic resolution at an unchanged linear dispersion. At the same time an increase of luminosity of the order of 2 is also achieved since the reduction in apparent grating

aperture by a factor of 1.83 is more than compensated by the reduction of projection distance by a factor of 2, to which would correspond a luminosity gain by a factor of 4 with an unchanged aperture. The use of high-resolution gratings blazed at 76° should thus provide the simplest, most practical means of increasing considerably, the luminosity and compactness of high-resolution grating spectrographs and spectrometers. We have, however, also explored other methods of efficiently extracting the spectroscopic information contained in the diffracted wave fronts.

By using two high-resolution gratings in series so as to add their dispersions, as described by G. W. STROKE and H. H. STROKE [1958, 1963], and shown in Fig. 26, it is possible to increase still further the luminosity obtainable from a single grating by another factor of the order of 2 to 3 (with a grating efficiency of 50 to 75 %), since the doubled angular dispersion permits another reduction by a factor of 2 of the projection

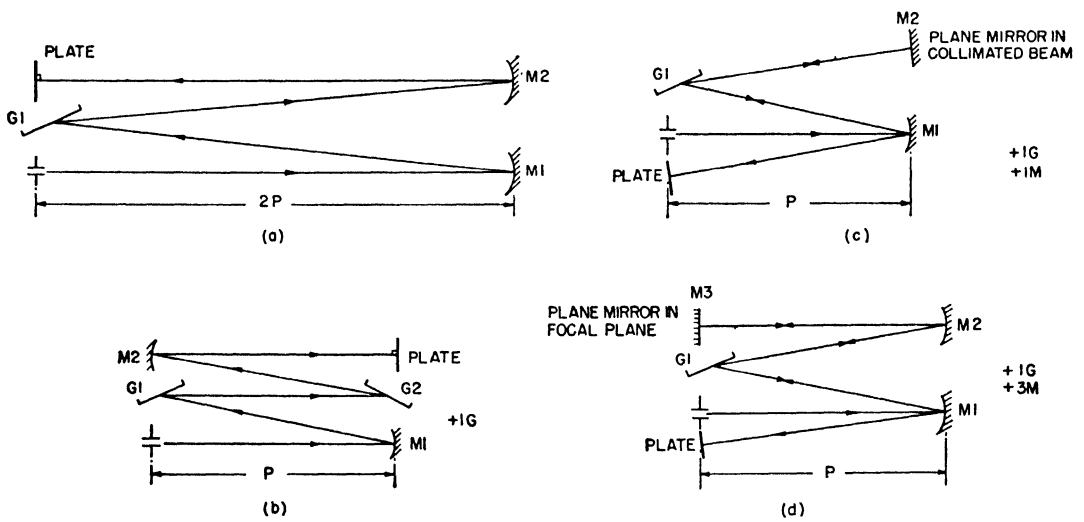

Fig. 26. Use of multiple diffractions to increase resolving power, dispersion, luminosity and compactness of grating spectrographs and spectrometers. Two gratings in series, (b), or a grating with a mirror, (c and d), can be used with a projection distance of only P to double the resolving power, at constant linear dispersion, obtainable with a single grating in a projection distance $2P$, (a). The arrangements in (b), (c), and (d) may have the further paradoxical advantage of resulting in greater luminosity than the basic single-diffraction arrangement of (a) (see text). The arrangement (b) (STROKE and STROKE [1958, 1963], STROKE [1960]) has the advantage of being the most luminous, since it requires no additional mirror reflexion (in addition to the +1G additional grating dispersion common to all these arrangements), while (c) and (d) require respectively one (+1M) and three (+3M) additional mirror reflexions. Moreover, the arrangement of (b) is also applicable to broad spectral coverage echelle spectrographs as shown in Fig. 27.

distance required to achieve a given linear dispersion on the plate. Unlike what is needed in grating 'mosaics', no accurate adjustment other than good alignment is required. The 'two-in-series' grating arrangement has also of course, the further advantage of doubling the resolving power of the single grating, since the doubled angular dispersion is attained with unchanged grating aperture in this case. The central components of Fig. 24 were photographed with such an arrangement. Comparable 'double-pass' arrangements used with a single grating are also shown in Fig. 26 and had been previously described: they are less luminous as a result of the required use of at least one more mirror reflexion in addition to the two grating dispersions which are common to all these arrangements (JENKINS and ALVAREZ [1952], FASTIE and SINTON [1952], RANK and WIGGINS [1956], SHEARER and WIGGINS [1956], RANK *et al.* [1957]). Prism double-pass arrangements had been previously used (COUDERC [1937]). Grating-immersion arrangements to increase the grating dispersion and resolving power have also been described (HULTHÈN and NEUHAUS [1954] and BJÖRKLUND [1958]). The 'two-in-series' arrangement also has the advantage of being applicable to echelle spectrographs, as described by HARRISON and STROKE [1960], as shown in Fig. 27a, b. 'Echelleograms' such as that shown in Fig. 27b for a two-echelle arrangement were first obtained by WOOD [1947] in an arrangement suggested by Shane, using a single echelette crossed with a prism, and later by HARRISON *et al.* [1949, 1950, 1952] in an arrangement using a single echelle crossed with a grating. There exists no basic difference between an 'echelette' and an 'echelle', both of which are blazed 'high-order gratings' (STROKE and STROKE [1963]).

5.2. SPECTROMETERS

Finally, very considerable advantages in both luminosity and compactness, with respect to any given spectrographic monochromator using gratings, can be obtained by using directly-scanning, grating monochromators with photoelectric or other physical receivers. These advantages have been achieved without any sacrifice of the simplicity, wave-length stability and large free spectral range at high resolutions that are inherent in the use of gratings. In fact, the scanning monochromator of only 1-m focal length (BREHM [1961]) which was used to record the hfs of Fig. 25 has a luminosity for a given resolution which is more than 10 times as great as that which can be obtained with the same grating when a photoelectric detector is used in the 10-m spectro-

graph appropriate for photographic use (STROKE[1961]). The important gain in luminosity in the 1-m spectrometer results from the fact that the 2μ-wide slit is not only small enough in terms of the 10.8 width of the diffraction pattern (between the first diffraction minima on both sides of the center) in the 1-m spectrometer, but also still large when compared to the 4358 Å wavelength. If a photoelectric receiver were used for scanning in a 10-m spectrograph, there would be no advantage in using a slit narrower than 20μ. Because of the gain of 100 in luminosity resulting from the reduction of the focal length from 10 m to 1 m, the 1-m spectrometer is therefore seen to be 10 times as luminous as a 10-m spectrometer using the same grating. The hfs of the mercury 4358-Å line shown in Fig. 25 was obtained in only 1 min by scanning a 7-inch grating in the 1-m monochromator. For comparison, we also show the spectrogram of the same hfs obtained in a 15-sec exposure on a 103aF plate in an 11-m spectrograph with the new M.I.T. 10-inch grating No. 143 of the same quality and used at the same angle of 64°.

The important gain in luminosity and compactness of about a factor of 2 which should be achieved in spectrographs by blazing the gratings at 76° rather than at 64° will also result in a similar gain in spectrometers, although for different reasons. While the limiting resolution in spectrographs is in practice set by the grain of the plate, in spectrometers it is similarly set by the smallest practical slit width. A further limitation in all spectrometers is set by the minimum energy in a given spectral bandwidth (or the smallest number of photons of a given energy) which will result in a response of the detector.

When an increase of slit width in the spectrometer is of interest, the change of blaze angle from 64° to 76° will permit doubling the slit width in an instrument of given focal length without loss in flux, flux per bandwidth, or resolution, which all remain unchanged.

On the other hand, when an increase in total flux in the spectrometer is desired, and the reduction of slit width and focal length are both possible, the change of blaze angle from 64° to 76° permits doubling this flux in an instrument with half the focal length and half the slit width, and this is again accomplished without any loss in either resolution or flux per bandwidth, which remain unchanged.

We may conclude by noting that very great further advantages of luminosity per resolution have been obtained with the help of large gratings, in particular, at lower resolutions and in the infrared, by using gratings in somewhat less conventional spectrometric arrange-

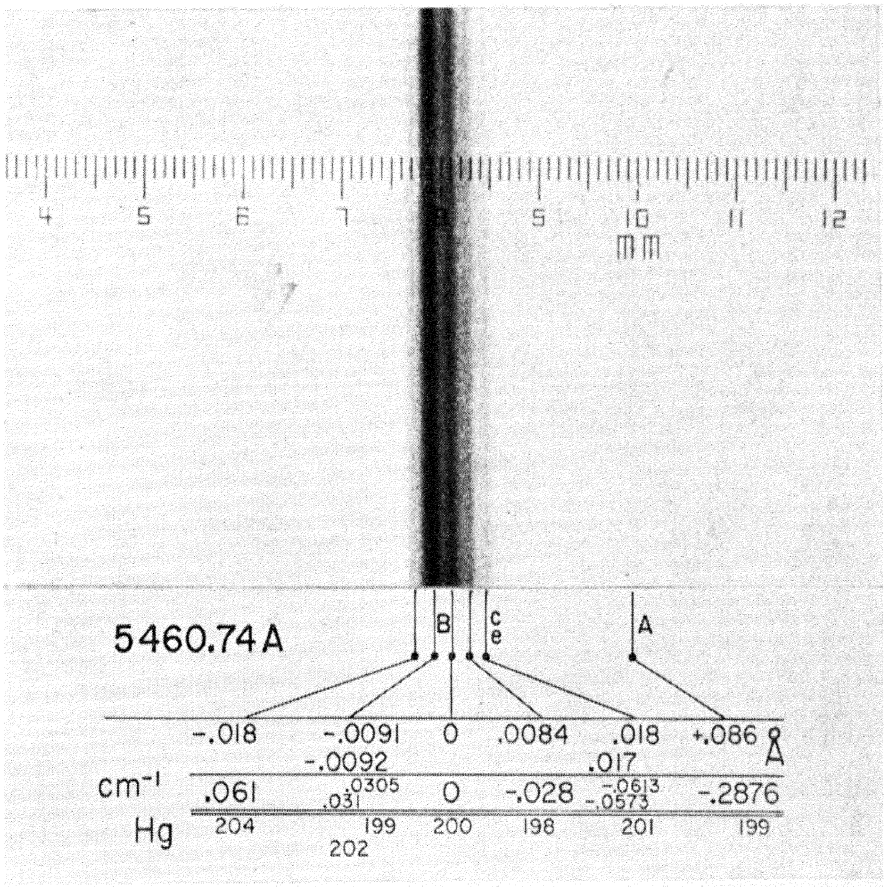

Fig. 24. Resolution of central components of mercury green line (5461 Å) hyperfine structure pattern, showing resolving power in excess of 1.2 million. The entire pattern shown here corresponds to component 0 in Fig. 13a. (The wave-number scale is reversed here with respect to Fig. 13, as seen from the position of component 'A'.) The dispersion is twice that of Figs. 13 and 15, and is obtained by using two 7.5-inch gratings in series as described by G. W. STROKE and H. H. STROKE [1958, 1963]. The exposure was about 10 minutes on a 103aF plate with an electrodeless discharge tube excited by an RF oscillator at about 100 Mc/sec and cooled to 0° C.

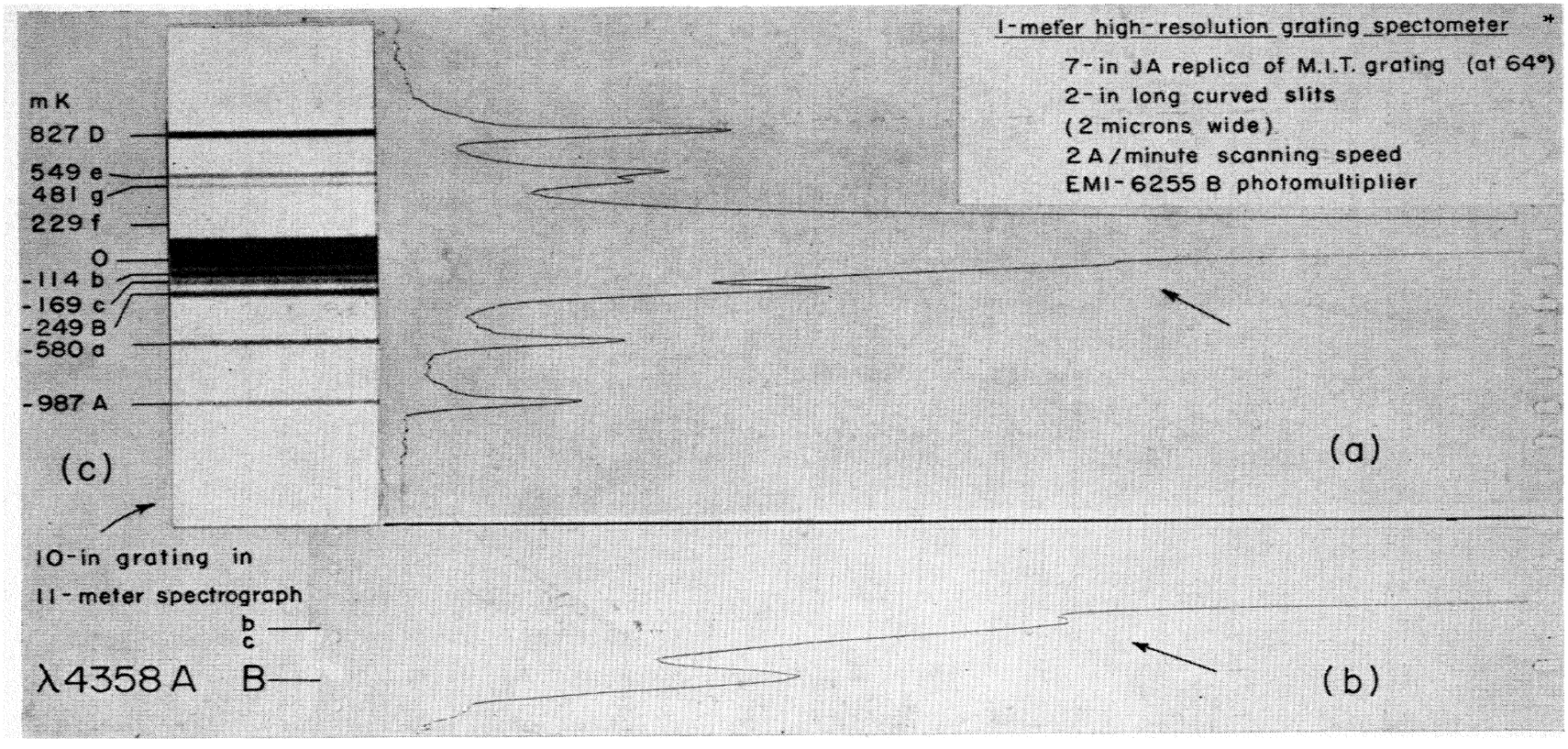

Fig. 25. Photoelectric recording of 4358 Å hyperfine structure pattern obtained by a direct scanning of a $7\frac{1}{4}$-inch wide replica of an M.I.T. grating (No. 140) in a 1-meter high-resolution $f/10$ Jarrell-Ash spectrometer, and showing resolution in excess of 500 000 at the scanning speed of 2 Å/min. (a) It is of interest to note the smoothness of the scanning obtained by rotation of the grating, even at the slower speed (b), used to exploit more closely the theoretical resolving power of 760 000. The photographic spectrogram shown on the left was obtained with the 10-inch grating (No. 143) of Fig. 13a on a 103aF plate in a 15-sec exposure with a different source, at a resolution in excess of 1 million.

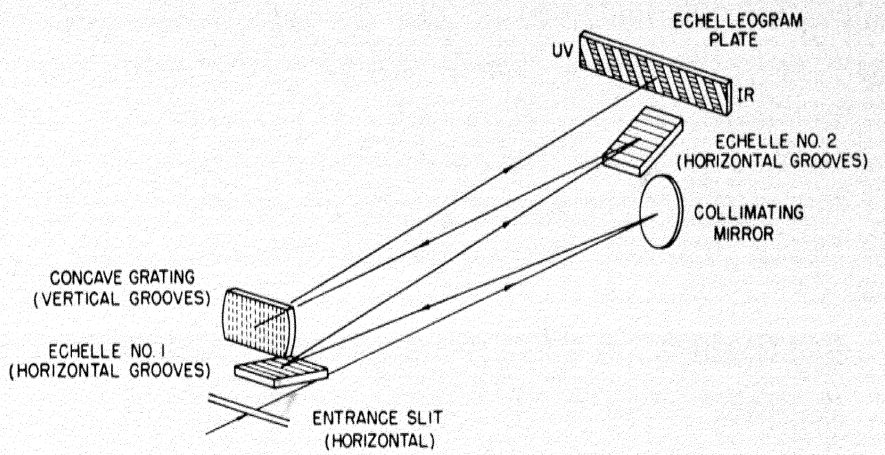

Fig. 27a.

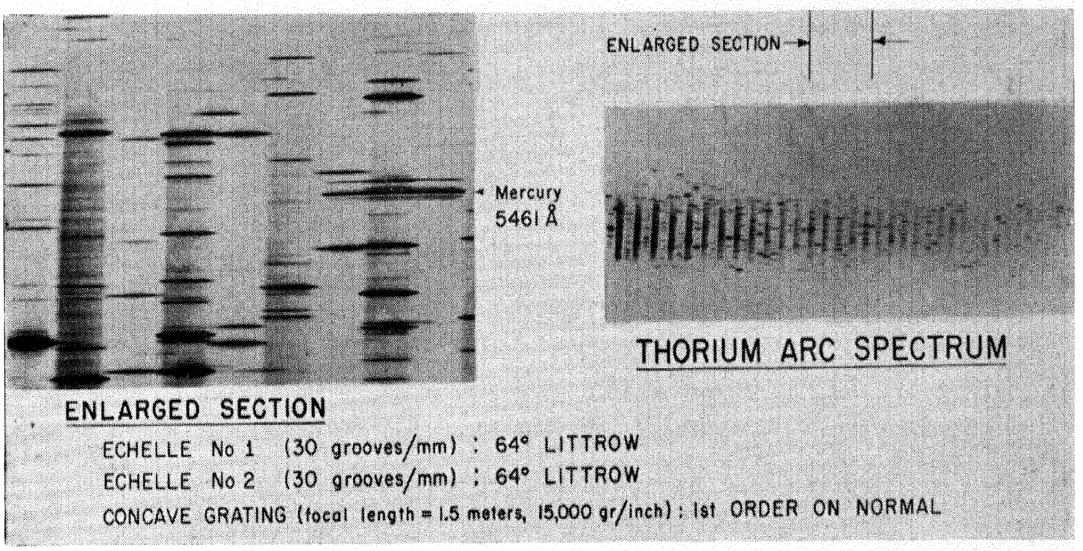

Fig. 27b.

Fig. 27. Two echelle-gratings used in series in broad spectral coverage high-resolution spectrograph as described by HARRISON and STROKE [1960]. An early plate obtained with a thorium arc shows some residual astigmatism from the concave grating which disappears when the plate is taken more closely to the normal of the concave grating (which was not the case here). The remarkable resolving power obtained with only a 1.5 meter projection distance and two 4-inch wide experimental echelles is demonstrated by the mercury green line hfs resolution.

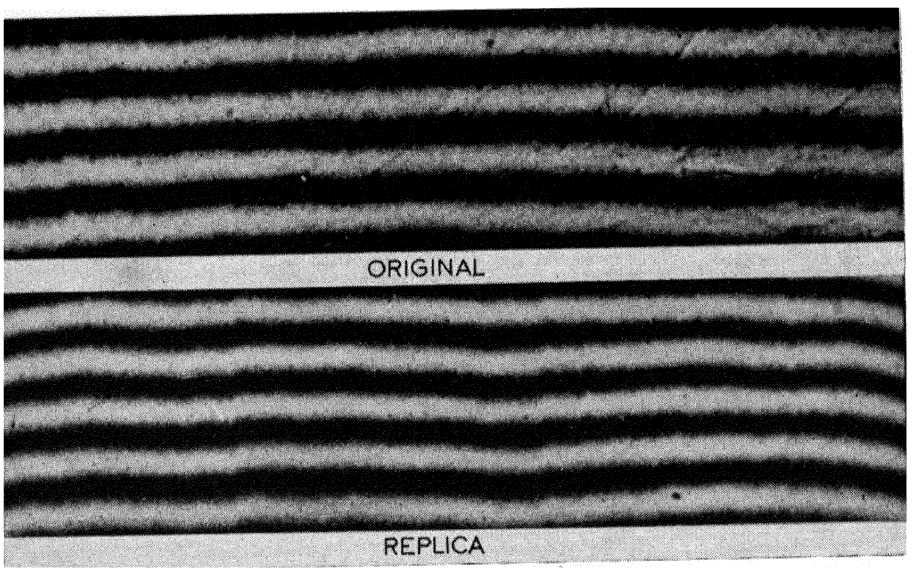

Fig. 28. Wave-front interferogram of a 5-year old replica grating (replica) produced from an 8-inch M.I.T. grating (original) of which the wave-front interferogram is also shown for comparison. The remarkable fidelity and stability characteristic of modern grating replication methods appears from this comparison of the two interferograms, both obtained in 5461 Å at 23.5° in autocollimation.

ments such as the SISAM spectrometer described by CONNES [1957, 1958] (in which two gratings are placed in the two arms of a Michelson–Twyman–Green interferometer) and in the multislit modulation spectrometer described by GIRARD [1960] (and comparable to an arrangement first suggested by GOLAY [1951, 1953]). Even though the simplicity of the grating spectrometers might appear to be somewhat lost in these arrangements, the additional gain in flux may exceed 100 in certain cases and should prove to be significant in special applications.

§ 6. Replica Gratings

Outstanding replicas of the high-resolution M.I.T. gratings have now been produced for several years by both Bausch & Lomb, Inc., of Rochester, New York, and the Jarrell–Ash Company of Newtonville, Mass. Both companies have, of course, been producing replicas of their own gratings. The relative quality of replicas and originals, as well as the permanence of replica gratings are of obvious interest. Fig. 28 shows an interferogram of an early M.I.T. 8-inch grating (original) ruled in May, 1956, as well as a recent interferogram of the now 5-year-old replica of that grating produced shortly after the grating had been ruled. Both interferograms are taken at a comparatively low angle (23.5°) where the departure of the fringes from straightness as a result of possible flatness deformations appears more than twice as strongly as at the angles around 64° where the gratings are normally used. This sensitive test of a replica produced in the early stages of the development of contemporary replication methods serves to illustrate the remarkable fidelity and stability of modern replica gratings. More recently the replication methods have attained a degree of perfection such that entire series of replicas cannot be distinguished from each other or indeed from the master grating from which they have been produced. In one instance, over 100 good replicas of a concave grating are reported to have been produced (SINTIRIS [1961]). In fact, points of superiority to the master grating are generally found in replica gratings as a result of the groove-inversion characteristic of replication (RICHARDSON [1960], SINTIRIS [1961]).

The details of the successful replication processes are particular to the methods developed in different laboratories, but it is well known that a replica grating consists of a thin layer of an aluminized plastic resin, such as Epoxy or Laminac, molecularly adherent to a perfectly flat (or perfectly spherical) optical glass blank (for plane or concave

gratings respectively). The evaporated aluminum layer with which the plastic is usually covered is similar to the layer used in original rulings. The clean separation of the replicas from the master ruling without deformation appears to be at the root of a successful replication.

§ 7. Further Improvements in the Quality and Blaze of Diffraction Gratings

Experience has shown that the achievement of an outstanding high-resolution grating in the presence of all the difficulties involved may still be considered as a singular accomplishment, even with the help of interferometric control. In fact, it has generally appeared to be more difficult to obtain sufficiently flat aluminum coatings than to maintain the regularity of spacing to a corresponding uniformity. The attainment of coatings flat to $\frac{1}{10}$ visible fringe or better, on blanks 6 × 12 inch in size or larger, at thicknesses from 3 to 30μ or more for gratings and echelles would indeed lead to a further significant advance in high-resolution grating spectroscopy.

The design and numerous very significant spectroscopic advantages of echelle-gratings were first described by HARRISON [1949], and subsequently expanded in many papers (HARRISON and BAUSCH [1950], HARRISON *et al.* [1952], HARRISON *et al.* [1953], HARRISON and STROKE [1960]). The comparable advantages of echelette-gratings have been described even earlier by WOOD [1947]. In fact, the ruled echelettes obtained on the M.I.T. engine (HARRISON [1959]) with spacing constants from 75 to 30 grooves/mm invariably show more uniform wave fronts than comparable gratings, undoubtedly also because of the considerably shorter time in which they were ruled. At the ruling speed which may be some 3 to 4 times greater for an echelle than for a grating, the dynamical conditions of the engine under interferometric control, and of the diamond, may indeed be more favorable, and the temperature-control problems are considerably reduced in rulings lasting only one day or so, rather than four or five days as is the case for 10-inch wide gratings.

For hfs studies, ruled echelettes blazed at 64° or 76°, with spacing constants of the order of 100 or 75 grooves/mm, still have a very great free spectral range even in monochromators, and the deep-groove sides characteristic of echelles can lead to a considerably more efficient light concentration in the orders of interest than even in well blazed gratings.

A theory of the distribution of light among the various orders, as a function of groove shape, angle of incidence, and wavelength in particular, should be at the root of new developments in the blazing of gratings. That discrepancies between observed and calculated energy distribution with order exist was recently again emphasized by MADDEN and STRONG [1958], for the case when calculations are carried out on the basis of 'scalar' approximation of diffraction. In fact, no satisfactory general solution of the problem of light distribution among orders exists yet for gratings having grating constants comparable to the wavelength. This is the case for which the electromagnetic character of diffraction starts to manifest itself predominantly (MARÉCHAL and STROKE [1959], STROKE [1960]). This is indeed also the case of infrared gratings, in particular, in which the problem of blaze as a function of groove shape and uniformity takes on an even greater importance than the grating spacing regularity (which appears considerably better when measured in the long wavelengths). A solution for the electromagnetic boundary-value problem of a perfectly conducting, sinusoidally 'corrugated' grating (Lord RAYLEIGH [1907a], U. FANO [1938], SENIOR [1959]) has been recently given, completely and rigorously, by STROKE [1960], for both polarizations in the incident beam ($\boldsymbol{E}$ and $\boldsymbol{H}$ parallel to the groove length in the incident plane waves), for any angle of incidence, and without any restrictions on groove spacing and groove depth in particular. Approximate electromagnetic solutions which may apply with sufficient rigor under certain restricted conditions of shallow echelette gratings had also been previously given by MEECHAM [1956] as well as by ROHRBAUGH, HATCHER, and their associates [1958] in particular. In addition, recent reviews of the state of solution of grating-diffraction problems and collections of references were given by STROKE [1960], in connection with his work, as well as by MILLAR [1961] in connection in particular with a solution of the problem of scattering by gratings of elliptical cylinders, and by TWERSKY [1956, 1960] in connection with a solution of the problem of scattering by gratings of cylinders. Even though it is not rigorously nor generally applicable, scalar diffraction theory has been used for many years, and continues to be used for the calculation of blaze, and in particular to account for some of 'Wood's anomalies' (WOOD [1902, 1912, 1935], Lord RAYLEIGH [1907b], INGERSOLL [1920], PALMER [1952, 1956, 1961]). As shown by the electromagnetic treatments of grating-diffraction problems, these irregularities in the distribution of light among orders

and with polarization are simply consequences of the electromagnetic character of diffraction. An electromagnetically predicted anomaly, according to which a grating or non-periodic structure of rectangular steps (an integral number of half-wavelengths deep, in normal incidence) may show no 'diffraction' at all in the classical sense, and behave as a perfect mirror, has been described and verified in the microwave domain by MARÉCHAL and STROKE [1959], STROKE [1960]. Advances in ruling techniques which should permit further improvements in the blaze of gratings and the speed of ruling are also under intensive study in a number of laboratories, in particular with the help of electron microscopes (HANSEN and VOLKMANN [1961]). The correlation between electron-micrographs of the groove shapes and light-intensity distributions in the spectrum is proving to be invaluable in the attainment of very well blazed gratings (STROKE [1963], STROKE and JARREL [1963]).

Acknowledgements

Much invaluable assistance and inspiration has been received in this work from many people, in several forms. A part has been especially acknowledged in the references, but particular thanks are due here again to: F. Abelès, J. E. Archer, A. Arnulf, H. W. Babcock, J. G. Baker, E. F. Barker, L. C. Bradley, III, R. Chabbal, J. Champeny, J. Connes, P. Connes, Wm. Culver, S. P. Davis, F. Denton, J. W. Evans, P. Fleury, M. Françon, G. Hansen, G. R. Harrison, P. Jacquinot, R. F. Jarrell, W. Kallenbach, A. Kastler, T. Kitayama, E. Klippenberg, R. C. Lord, A. Maréchal, J. Millot, Wm. MacArthur, E. L. O'Neill, G. Pieuchard, H. M. Randall, D. K. Rice, D. Richardson, A. Rubinowicz, R. A. Sawyer, J. C. Simon, G. Sintiris, H. H. Stroke, J. Strong, N. Sturgis, K. L. van der Sluis, H. Volkmann, Y. Yamada, J. Yena.

I am also grateful to the Research Laboratory of Electronics, Massachusetts Institute of Technology, and to its director, Professor H. J. Zimmermann for assistance in the preparation of this article, and to the Journal of the Optical Society of America for permission to adapt some pertinent sections which I first developed in the December 1961 issue of that journal.

References

ALLEN, H. S., 1902, Phil. Mag. *3*, 92; 1903, *ibid.* *6*, 559.

ANDERSON J. A., 1922, J. Opt. Soc. Am. *6*, 434; "Glazebrook's Dictionary of Applied Physics", p. 30.

ANDERSON, J. A. and C. M. SPARROW, 1911, Astrophys. J. ***33***, 338.
ARSAC, J., 1959, Optica Acta ***6***, 103; Transformation de Fourier et Théorie des distributions (Dunod, Paris).
BABCOCK, H. D. and H. W. BABCOCK, 1957, J. Opt. Soc. Am. ***41***, 776.
BABCOCK, H. W., 1962, J. Opt. Soc. Am. ***52***.
BARAKAT, R., 1961, Progress in Optics, Vol. I, ed. E. Wolf (North-Holland Publishing Co. Amsterdam) p. 69.
BARKER, E. F. and H. M. RANDALL, 1961, private communication.
BARRELL, H. and J. E. SEARS, 1939, Phil. Trans. A***238***, 1.
BAUSCH and LOMB INC., 1961, Rochester, N.Y., private communications.
BJÖRKLUND, O., 1958, Ark. Fysik ***13***, 185.
BORN, M. and E. WOLF, 1959, Principles of Optics (Pergamon Press, London, New York).
BRACEWELL, R. N., January 1961, IRE Trans. AP-9, No. 1, p. 49.
CHABBAL, R., 1957, thesis, The Sorbonne (Paris); 1958, Revue d'Optique, ***37***, 49, 336 and 501; 1958, J. Physique Radium, ***19***, 295.
CHABBAL, R. and P. JACQUINOT, 1961, Revue d'Optique ***40***, 157.
CONNES, J., 1960, thesis, The Sorbonne (Paris); 1961, Revue d'Optique ***40***, 45.
CONNES, P., 1956, Revue d'Optique ***35***, 37; 1958, J. Physique Radium ***19***, 262; 1957, Optica Acta (Paris) ***4***, 136; 1958, thesis, The Sorbonne (Paris).
COUDERC, A., 1937, J. Physique Radium, p. 37S.
CROSSWHITE, H. M. and W. G. FASTIE, 1956, J. Opt. Soc. Am. ***46***, 110.
CUTRONA, L. J., E. N. LEITH and L. J. PORCELLO, 1959, Proceedings of the National Electronics Conference, Vol. XV.
CUTRONA, L. J., E. N. LEITH, C. J. PALERMO and L. J. PORCELLO, June 1960, IRE Trans. IT-6, No. 3, p. 386
DITCHBURN, R. W., 1930, Proc. Roy. Irish Acad., A***39***, 58.
DJURLE, E., 1952, Ark. Fysik ***4***, 423; 1954, *ibid.* ***8***, 383.
DOSSIER, B. (ROIZEN-DOSSIER, B.), 1953, thesis, The Sorbonne (Paris); 1954, Revue d'Optique ***33***, 57, 147 and 267; 1956, Astronomical Optics (Amsterdam, North-Holland Publishing Co., p. 163.
DUFFIEUX, P. M., 1946, L'intégrale de Fourier et ses applications à l'Optique, chez l'auteur, Faculté des Sciences (Besançon).
ELIAS, P., D. GREY and D. ROBINSON, 1952, J. Opt. Soc. Am. ***42***, 127.
ELIAS, P., 1953, J. Opt. Soc. Am. ***43***, 229.
EVANS, J. W., 1961, private communication.
FANO, U., 1938, Ann. Physik ***32***, 393.
FASTIE, W. G. and W. M. SINTON, 1952, J. Opt. Soc. Am. ***42***, 483(A).
FASTIE, W. G., 1952, J. Opt. Soc. Am. ***42***, 641 and 647.
FEHRENBACH, CH., 1960, private communication.
FELLGETT, P., 1951, thesis, Cambridge University (Cambridge, England); 1958, J. Physique Radium ***19***, 187 and 237.
GALE, H. G., 1937, Astrophys. J. ***86***, 437.
GERASIMOV, F. M., 1954, Bulletin of the USSR Academy of Sciences, Physical Series ***18***, No. 6, 345.
GERASIMOV, F. M., I. A. TEL'TEVSKII, S. S. NAUMOV, S. N. SPIZHARSKII and S. V. NESMELOV, 1958, Optika i Spektroskopia ***4***, 779.
GIRARD, P., 1960, Optica Acta (Paris) ***7***, 81; 1963, Applied Optics, ***2***, 79.

GOLAY, M. J. E., 1951, J. Opt. Soc. Am. ***41***, 468; 1953, *ibid.* ***43***, 48(L) and 333(A).
GREENLER, R., 1955, J. Opt. Soc. Am. ***45***, 788.
HANSEN, G., 1942, Physikal. Z. ***43***, 213; 1961, private communication. The author is grateful to Professor Dr. G. HANSEN for several private communications describing the history and progress of grating ruling at CARL–ZEISS in Oberkochen, Württ.
HARRISON, G. R., 1949, J. Opt. Soc. Am. ***39***, 413. (This paper gives an excellent review of the development of the ruling art up to that time, and a complete collection of references); 1950, Physics Today ***3***, 6.
HARRISON, G. R. and C. L. BAUSCH, 1950, Proceedings of the London Conference of the Optical Institute (Chapman and Hall, Ltd. London).
HARRISON, G. R., J. E. ARCHER and J. CAMUS, 1952, J. Opt. Soc. Am. ***42***, 706.
HARRISON, G. R., S. P. DAVIS and H. J. ROBERTSON, 1953, J. Opt. Soc. Am. ***43***, 853.
HARRISON, G. R. and G. W. STROKE, 1955, J. Opt. Soc. Am. ***45***, 112.
HARRISON, G. R., N. STURGIS, S. C. BAKER and G. W. STROKE, 1957, J. Opt. Soc. Am. ***47***, 15.
HARRISON, G. R., 1958, Proc. Am. Phil. Soc. ***102***, 438.
HARRISON, G. R., N. STURGIS, S. P. DAVIS and Y. YAMADA, 1959, J. Opt. Soc. Am. ***49***, 205.
HARRISON, G. R., 1959, private communications.
HARRISON, G. R. and G. W. STROKE, 1960, J. Opt. Soc. Am. ***50***, 1153.
HULL, R. J. and H. H. STROKE, 1960, Bull. Am. Phys. Soc. ***5***, 412; 1961, J. Opt. Soc. Am. ***51***, 1203.
HULTHÈN, E. and H. NEUHAUS, 1954, Ark. Fysik ***8***, 343.
HULTHÈN, E. and U. UHLER, 1952, Ark. Fysik ***3***, 393.
INGALLS, A. G., 1952, Scientific American ***186***, 45.
INGELSTAM, E. and E. DJURLE, 1952, Ark. Fysik ***4***, 423; 1953, *ibid.* ***6***, 463; 1953, J. Opt. Soc. Am. ***43***, 572.
INGERSOLL, L. R., 1920, Astrophys. J. ***51***, 129.
JACQUINOT, P. and C. DUFOUR, 1948, Jl. Recherches CNRS ***6***, 91.
JACQUINOT, P., 1950, Proc. Phys. Soc. B***63***, 969.
JACQUINOT, P., 1954, XVIIe Congrès du G.A.M.S. (Paris); 1958, J. Physique Radium ***19***, 223; 1960, Optica Acta (London) ***7***, 291.
JACQUINOT, P., 1954, J. Opt. Soc. Am. ***44***, 761.
JACQUINOT, P., 1960, Repts. Progr. in Phys., Vol. XXIII, 267.
JARRELL, R. F., 1960, "Gratings, Production of" in The Encyclopedia of Spectroscopy (Reinhold Publishing Corp., New York), p. 173.
JARRELL–ASH COMPANY, Newtonville, Mass., 1961, private communications.
JAVAN, A., 1960, in Quantum Electronics, ed. C. H. Townes (Columbia University Press, New York), p. 564.
JAVAN, A., W. R. BENNETT and D. R. HERRIOTT, 1961, Phys. Rev. Letters ***6***, 106.
JENKINS, F. A. and L. W. ALVAREZ, 1952, J. Opt. Soc. Am. ***42***, 699.
KOPPELMANN, G. and K. KREBS, 1961, Optik ***8***, 349 and 358.
LOHMANN, A., 1959, Optica Acta (London) ***6***, 175.
LORD, R. C. and T. K. MCCUBBIN, 1955, J. Opt. Soc. Am. ***45***, 441.
MADDEN, R. P. and J. STRONG, 1958, Appendix P. in Classical Optics, by J. Strong (Freeman and Company, San Francisco, California) p. 597.

MASCART, E., 1889, Traité d'Optique, Vol. I. (Gauthier-Villars, Paris) p. 373.
MARÉCHAL, A., 1947, thesis, The Sorbonne (Paris); 1947, Revue d'Optique ***26***, 257; 1948, *ibid.* ***27***, 73 and 269.
MARÉCHAL, A. and M. FRANÇON, 1960, Diffraction, Structure des Images, Influence de la Cohérence de la Lumière (Ed. Revue d'Optique, Paris).
MARÉCHAL, A. and G. W. STROKE, 1959, Compt. rend. Ac. Sc. ***249***, 2042.
MEECHAM, W. C., 1956, J. Appl. Phys. ***27***, 361.
MEGGERS, W. F. and F. O. WESTFALL, 1950, J. Research Natl. Bureau Standards ***44***, 447.
MERTON, T. R., 1950, Proc. Roy. Soc. A***201***, 187; *see also* L. SAYCE.
MICHELSON, A. A., 1903, Astrophys. J. ***18***, 278; 1912, Nature ***88***, 362; 1927, Studies in Optics (University of Chicago Press, Chicago) p. 86.
MILLAR, R. I., 1961, Can. J. Phys. ***39***, 81 and 104.
O'NEILL, E. L., 1957, Selected Topics in Optics and Communication Theory (Boston University).
PALMER, C. H., 1952, J. Opt. Soc. Am. ***42***, 269; 1956, *ibid.* ***46***, 50; 1961, *ibid.* ***51***, 1438(L).
PEIRCE, C. S., 1879, Am. J. Mathem. ***2***, 330.
PIERCE, A. K., 1957, J. Opt. Soc. Am. ***47***, 6.
RAYLEIGH, Lord, 1874, Phil. Mag. ***47***, 81 and 193; 1888, Wave Theory (Ency. Britt., 9th edit. Vol. 24); 1907a, Proc. Roy. Soc. (London) *A* ***79***, 399; 1907b, Phil. Mag. ***14***, 60.
RANDALL, H. M., 1939, J. Appl. Phys. ***10***, 768; 1954, J. Opt. Soc. Am. ***44***, 97.
RANK, D. H. and T. A. WIGGINS, 1952, J. Opt. Soc. Am. ***42***, 983.
RANK, D. H., A. H. GUENTHER, C. R. BURNETT and T. A. WIGGINS, 1957, J. Opt. Soc. Am. ***47***, 631.
RANK, D. H., J. N. SHEARER and J. M. BENNETT, 1955, J. Opt. Soc. Am. ***45***, 762.
RICHARDSON, D., 1960, private communication.
ROHRBAUCH, J. H. and R. D. HATCHER, 1958, J. Opt. Soc. Am. ***48***, 704.
ROHRBAUCH, J. H., C. PINE, W. G. ZOELLNER and R. D. HATCHER, 1958, J. Opt. Soc. Am. ***48***, 710.
ROIZEN–DOSSIER, B., *see* B. DOSSIER.
ROWLAND, H. A., The Physical Papers, 1902 (The Johns Hopkins University Press, Baltimore) p. 525; 1893, Phil. Mag. (5), XXXV, 397.
SAYCE, L. A., 1953, in "Endeavour", p. 210.
SCHAWLOW, A. L. and C. H. TOWNES, 1958, Phys. Rev. ***112***, 1940.
SENIOR, T. B. A., 1959, Can. J. Phys. ***37***, 787.
SHEARER, J. N., T. A. WIGGINS, A. H. GUENTHER and D. H. RANK, 1956, J. Chem. Phys. ***25***, 724.
SHENSTONE, A. G., 1960, Discussion of Paper 5–4, National Physical Laboratory Symposium No. 11, Interferometry (London, Her Majesty's Stationery Office) p. 431.
SIEGBAHN, M., 1930, Zeits. f. Physik ***62***, 435; 1930, Kosmos ***8***, 186; 1940, K. Svenska Vetens Kapsa Kademiens Arbok, 151.
SIEGBAHN, M. and T. MAGNUSSON, 1935, Zeits. f. Physik ***95***, 133.
SINTIRIS, G., 1961, private communication.
SPARROW, C. M., 1919, Astrophys. J. ***49***, 65.

STROKE, G. W., 1952, J. Opt. Soc. Am. ***42***, 879(A); 1955, *ibid.* ***45***, 30; 1957, *ibid.* ***47***, 1097; 1958, *ibid.* ***48***, 276; 1961, *ibid.* ***51***, 1321; 1961, *ibid.* ***51***, 1340; 1960, thesis, The Sorbonne (Paris); 1960, Revue d'Optique ***39***, 291; 1960, Paper 5–1 in National Physical Laboratory Symposium No. 11, Interferometry (London, Her Majesty's Stationery Office) p. 223–244; August, 24, 1959, Paper No. 5, Fifth Conference of the International Commission of Optics, Stockholm; 1958, J. Physique Radium ***19***, 415; 1960, *ibid.* ***21***, p. 57S; 1963, Proceedings of the Third International Conference on Quantum Electronics, Paris; 1964, "Diffraction Gratings" in Handbuch der Physik, Vol. ***29***, edited by S. Flügge, Springer-Verlag, Heidelberg (in preparation).

STROKE, G. W. and H. H. STROKE, October 1958, Quart. Rep. Mass. Inst. Technol. Research Lab. of Electronics, p. 54; 1963, J. Opt. Soc. Am. ***53***.

STROKE, G. W. and R. F. JARRELL, 1963, Applied Optics ***2***.

STRONG, J., 1951, J. Opt. Soc. Am. ***41***, 3; 1960, *ibid.* ***50***, 1148. (This paper also gives an excellent history of the ruling of gratings at the Johns Hopkins University.)

TOLANSKY, S., 1947, High Resolution Spectroscopy (Methuen and Co. Ltd., London).

TWERSKY, V., 1956, Proc. IRE Trans. PGAP, *AP-4*, p. 330; 1960, J. Research National Bureau Standards ***64D***, 715.

VOLKMANN, H., 1961, private communication.

WADSWORTH, F. L. O., 1895, Astrophys. J. ***2***, 264.

WOLF, E., 1951, Proc. Roy. Soc. A***204***, 533; 1951, Rept. Progr. in Phys. ***14***, 95; 1953, J. Opt. Soc. Am. ***43***, 218; 1959, Proc. Roy. Soc. A***253***, 349. *See also* M. BORN and E. WOLF, (1959), as well as R. BARAKAT, 1961.

WOOD, R. W., 1924, Phil. Mag. ***48***, 497; 1947, J. Opt. Soc. Am. ***37***, 733.

II

THE METROLOGICAL APPLICATIONS OF DIFFRACTION GRATINGS

BY

J. M. BURCH

National Physical Laboratory, Teddington, Middlesex, England

CONTENTS

§ 1. Introduction to Moiré Fringe Techniques and their Applications

1.1. HISTORY OF DEVELOPMENT

It has long been known that juxtaposition of two gratings of similar pitch can result in the formation of a moiré fringe pattern, the shape of which can be used for example to assess any irregularities of ruling (RAYLEIGH [1874]). During the past decade, however, moiré fringe patterns have found new and valuable application as a means for measuring displacement (GUILD [1956, 1960]). The principle employed is that, if a short 'index' grating and a long 'measuring' grating are mounted adjacent to each other on the two components whose relative movement is to be measured, then a simple optical system will produce a pattern of moiré fringes whose changes can be converted into nearly sinusoidal fluctuations of photoelectric current. Provided that accurate linear or radial gratings of known pitch are employed, these sinusoidal signals provide instantaneous and continuous measurement of displacement or rotation, in a form especially convenient for modern electronic data-handling systems. Furthermore, because each moiré signal is derived by averaging the effect of a large number of rulings, the measuring errors encountered are extremely small and are easily calibrated because of their smoothness.

It seems clear in retrospect that three main factors were responsible for the sudden emergence of moiré fringemeasuring techniques:

Firstly, from 1951 onwards new concepts in machine tool control were introduced by the electronic engineers of Ferranti Ltd. Edinburgh. The basis of the Ferranti system (WILLIAMSON [1954]) was that digital instructions produced by an electronic computer were compared continuously with digital measurements of position of the machine tool components. Moiré fringecounting methods were envisaged, but ordinary printers' screens would have been too coarse to provide the measuring accuracy needed for most engineering applications.

During this same period, however, as a result of suggestions made by Sir Thomas Merton, methods were being developed at the National Physical Laboratory (NPL) for making plastic diffraction gratings by replication from a helically turned master ruling (MERTON [1950]). By 1952 large numbers of Merton-NPL gratings had been made available for infra-red spectroscopy, with pitches ranging from 1000 lines/inch to 10 000 lines/inch and with any desired sawtooth profile (DEW and SAYCE [1951], HALL and SAYCE [1952], DEW [1952, 1953]).

Thirdly, in order to assess the fidelity of replicas made by these Merton-NPL processes, Guild had found it convenient to examine them in transmission by moiré fringe methods. In the course of this work, indeed, he had already formulated simple but rigorous optical conditions whereby satisfactory moiré patterns could be obtained even from the finest transparent rulings (GUILD [1956]).

From these beginnings, and with the establishment of close collaboration between Ferranti Ltd. and NPL, it was possible to proceed at once to the design of suitable metrological rulings and photoelectric reading-heads (SAYCE [1953]). A reversible photoelectric counter was soon devised by Ferranti Ltd. (WILLIAMSON, SHEPHERD and WALKER [1953]), and the new digital measuring transducers were applied by them successfully to a number of complete machine tool systems (KERMACK and OGDEN [1957], WILLIAMSON [1958], FARMER [1956, 1958]).

In the operation of these systems, since each positional variable of the machine was controlled by its own set of recorded instructions, even the most complicated three-dimensional shapes could be fabricated once a suitable programme had been prepared by the computer. During 1955, however, it became apparent that, for certain special machine tools where the movement of two components must be maintained in a fixed ratio, much simpler methods could be adopted for handling the moiré fringe information. All that was necessary was to arrange for the two moving components to generate moiré fringe signals of nominally the same frequency, and then to use a phase discriminator and servo-system to keep the two components locked in step.

Pioneered both at NPL (BLAKE and SAYCE [1958]) and at the National Engineering Laboratory, East Kilbride, Glasgow (TIMMS [1959]), this kind of analogue system is now being used for monitoring and controlling such operations as thread-grinding or gear-hobbing on specially designed machines (LESLIE [1961]).

With the stimulus of these machine tool applications, considerable effort was devoted to the production of improved linear gratings at NPL (DEW [1956]) and of radial gratings at NEL (TIMMS and GRAHAM [1962]). As linear gratings with 6 350 lines/inch (2500 lines/cm) became available, moiré fringe systems with a measuring accuracy of a micron were applied to new duties, such as processing at high speed the scientific data recorded on photographic plates, for example from bubble-chambers and spectrographs (BUTLER [1958], BOVEY [1960]).

In 1957 it became apparent that the increasing demand for very long and accurate gratings with a relatively coarse spacing could not readily be satisfied by existing mechanical processes of ruling and replication, and several photographic methods of manufacture were introduced (BURCH [1958, 1959, 1960]). As a result of collaboration between NPL and Technicolor (Gr. Britain) Ltd., a range of photographic masters 3 ft long was produced at NPL and subsequently used by Technicolor Ltd. to manufacture reflection gratings on stainless steel tape in continuous lengths of up to 14 ft and with up to 1000 lines/inch.

Meanwhile, in order to take full advantage of the accuracy offered by these relatively coarse photographic gratings, electronic equipment was devised for interpolating to much smaller fractions of a moiré fringe (BARBER and ATKINSON [1959], FROST-SMITH [1960]). In the original Ferranti counter, only four counts per fringe were obtained, but analogue (DAVIES, ROBBINS, WALLIS and WILDE [1960], WALKER [1961]) and digital (SHEPHERD [1961]) methods of subdividing to a fiftieth or even a hundredth of a fringe were soon developed as an alternative. The present position is that, by employing reflection gratings of either 100 l.p.i. or 1000 l.p.i. in conjunction with one of these fringe interpolating systems, a precision adequate for any normal industrial purpose can be obtained (WALKER [1961], SHEPHERD [1961], DAVIES [1961]).

For more refined applications, however, where a measuring error of 10^{-4} inch cannot be tolerated, it is necessary to use instead a pair of transmission gratings, produced either by the Merton-NPL process (DEW [1956]) or by the new photographic methods. In Ferranti equipment for high-speed recording of scientific data, the tendency remains to use finely spaced Merton-NPL replicas in a purely digital system with one count per micron displacement. In metrological work, on the other hand, it is sometimes more convenient to dispense with counters and use analogue methods of fringe interpolation with photo-

graphic gratings of perhaps 1000 lines per inch. In applications involving uniform relative motion, for example, a measuring accuracy of a few microinches (GUILD [1960] p. 188, HALL and STANLEY [1960]) has been obtained by dynamic phase comparison methods. Another common requirement is to measure changes of stationary position, and for this purpose McIlraith has introduced during the past year a photoelectric galvanometer bridge technique whereby positional settings can be made at any desired portion of a moiré fringe cycle. At the time of writing, this elegant and simple method has already achieved an accuracy of ± 2.5 microinches, and further improvement is to be expected. When fringes are interpolated with this precision the whole number of fringes is usually known in advance, but if necessary this number too could be obtained explicitly by purely visual read-out (GUILD [1960] p. 198) from an auxiliary vernier fringe system. For laboratory purposes, therefore, the full accuracy of the moiré technique can now be obtained without the expensive electronic equipment which was its early concomitant.

Where measurements are made over ranges greater than about half an inch, the accuracy obtained depends also on the residual irregularities of the long measuring grating. With gratings currently available, a smooth progressive error of up to ± 20 microinches per foot may be encountered, but in suitably designed equipment it is possible to eliminate this by calibration so that the residual error is determined, as with any scale, by the thermal or secular stability of the supporting material.

When radial gratings are used for angular measurement, similar considerations apply with regard to fringe interpolation, since it is usual to make them with a peripheral spacing of not more than about 1000 lines per inch. Gratings made at NEL are already available with ± 2 seconds of accumulated pitch error, but, as will be seen below, considerable further improvement should be possible in the future because of the self-calibrating and self-correcting properties of the moiré technique.

In succeeding sections some further account will be given of these developments, but the reader or prospective user who needs detailed information should also refer elsewhere, in particular to the two monographs on moiré fringe measurement which have been written by GUILD [1956, 1960].

1.2. INFORMATION OBTAINABLE FROM MOIRÉ FRINGES

When two printer's screens are placed together with their lines approximately parallel and viewed in transmitted light, the moiré pattern which is seen is much coarser in structure than the individual lines, and can be regarded as a pattern of spatial beats, generated between two nearly identical periodicities. In the case of Merton-NPL gratings containing perhaps 5000 transparent rulings per inch, the lines themselves are invisible to the eye, but a simple spectroscopic observing system suffices to produce satisfactory moiré fringes, and the concept of a spatial beat or difference frequency is still a useful one. Furthermore, whatever the periodicity of the scales involved, the moiré fringe pattern, as in ordinary optical interference, conveys several distinct types of information simultaneously.

Consider first the fringes produced by two linear gratings of perfectly regular spacing; if one grating is slightly coarser in pitch than its fellow, then there must be a linear variation in phase across the moiré pattern in a direction perpendicular to the rulings, and a set of so-called 'vernier' fringes is observed running parallel to the rulings. If, on the other hand, the two gratings are identical in pitch but one of them is twisted slightly, so that the rulings intersect at an angle, this introduces a linear variation of phase along the rulings, and 'tilt' fringes are again observed, this time running perpendicular to the rulings. In addition to these two orthogonal tilt effects, if one grating is displaced in a direction perpendicular to its rulings by a distance x' the phase of the fringe pattern at any chosen point of the stationary grating must change by exactly $2\pi x'/w$ where w is the width of a single ruling of the moving grating. Every time the displacement amounts to one complete ruling-width w, the whole moiré pattern undergoes one complete cycle of fluctuation. It is usual to say that each fringe moves across the pattern so as to replace its neighbour, but in practice the gratings are often identical and adjusted to parallelism, so that the fringe pattern is 'fluffed-out' to an infinite width; under such conditions there is no fringe motion to be detected, but the brightness of the whole of the pattern fluctuates simultaneously in response to a displacement.

It may also happen that the periodicity of one or both gratings forming a moiré pattern is not perfectly regular, and information about these irregularities is then conveyed by the kinks and distortions of the fringe contours. The fringes are indeed somewhat analogous to those seen when testing an imperfect flat against a horizontal master

flat in a Fizeau interferometer. In flat-testing the phase of the fringe pattern depends on height measured in half-wavelengths, whereas for an imperfect grating the phase observed depends on the lateral displacement of each ruling from its correct position, measured this time in ruling-widths.

In conclusion, a general expression will be given for the phase of a moiré fringe pattern formed by two gratings A and B whose ruling errors are $W_A(x, y)$ and $W_B(x, y)$, where x is measured perpendicular and y parallel to the rulings. It will be assumed that A has an average pitch distance $w_A = 1/N_A$ and remains stationary, but is twisted through a very small angle α, while B has an average pitch of $w_B = 1/N_B$ and has been translated through a distance x' in the x direction. Under these conditions the phase angle $\psi_{AB}(x, y, \alpha, x')$ determining the position of each moiré fringe will be

$$\begin{aligned}\psi_{AB}(x, y, \alpha, x') &= 2\pi[W_A(x, y) + N_A(x + y\alpha) - W_B(x - x', y) - N_B(x - x')] \\ &= 2\pi[W_A(x, y) - W_B(x - x', y) + (N_A - N_B)x + \alpha N_A y + N_B x']. \qquad (1)\end{aligned}$$

In most metrological applications a photocell integrates this phase over an appreciable aperture, and most of the relatively small phase variations contributed by the first four terms are averaged out, leaving the simplified relation

$$\begin{aligned}\psi(x') &= \arg \iint \exp i\psi_{AB}(x, y, \alpha, x')\, dx\, dy \\ &= 2\pi[\overline{W_B(-x')} + N_B x']. \qquad (2)\end{aligned}$$

In eq. (2) $\overline{W_B(-x')}$ represents a smoothed progressive error which becomes appreciable only when grating B moves over a distance x' comparable with or greater than the x-range summed by the photocell. In practical applications a change of 2π radians in ψ nearly always corresponds to the occurrence of a single approximately sinusoidal fluctuation of intensity, but much more complicated fringe shapes are also possible, as has been shown exhaustively by GUILD [1956].

This review is concerned more particularly with the implications of eq. (2), but it is also obvious from eq. (1) that by detailed analysis of the shape of a moiré fringe pattern a great deal of information about ruling error can be extracted. If for example two imperfect metrological gratings are intercompared with various amounts of lateral shear x', the ruling errors of both gratings can be separated and established. Once a grating has been calibrated in this way, it can be used to check

a whole series of further gratings, e.g. for accidental errors which may occur in a replication process or in photomechanical reproduction. For such procedures the modern tendency is to use photoelectric rather than visual methods for setting on the fringe pattern, and it is found that in the internal calibration of 1000 l.p.i. masters, for example, the r.m.s. residual errors do not exceed ten microinches (BURCH [1960]).

Let us now consider the metrological information which can be extracted from a pair of suitably mounted identical gratings. A moiré fringe system could in principle be devised to measure any uniform mode of relative displacement, the most general example being a screw displacement (which would entail similar helices ruled on a pair of coaxial cylinders). If for practical ease of manufacture we demand that both gratings shall have plane surfaces which remain parallel and almost in contact, there remain available only two degrees of freedom for translation and one for rotation, and the following measuring systems are possible.

a) *Displacement*

If it is desired to measure linear displacement of a carriage, then the usual practice is to construct a 'reading-head' which contains an illuminating system, a photoelectric viewing system, and a short linear 'index' grating. This reading-head is then clamped to the moving carriage and arranged to slide past a long stationary 'measuring' grating. An alternative but equivalent possibility is to place the measuring grating on the carriage and to keep the reading-head stationary.

When properly designed and adjusted, such a system will give sinusoidal moiré signals containing anything from 10 to 10 000 cycles per inch of displacement. For Merton-NPL replicas the pitch of the gratings is usually made a little finer than desired, and final adjustment of the effective pitch is obtained by slightly skewing both gratings with respect to the direction of motion, so as to increase their effective pitch by a small cosine correction factor. For gratings of photographic manufacture this procedure is unnecessary.

b) *Straightness*

In addition to measuring displacement of a carriage, moiré fringes can also be used to measure its departure from straightness. This requires that the index and measuring gratings shall be ruled with lines running parallel to the direction of the slide, so that the long

grating then becomes a multiple straight-edge. No straight-edge gratings have so far been produced, but with photographic manufacture it would be possible to mount them on the same piece of glass or tape as the displacement measuring grating and to obtain both signals simultaneously from a composite reading-head. If a straight-edge grating is 'read' by two separate reading-heads some distance apart then any tilting of the carriage can also be deduced, so that if necessary a complete servo-control of the carriage can be established.

c) *Rotation*

Reference has already been made to the possibility of measuring rotation of a shaft or table by means of radial gratings, which contain a large number of rulings disposed radially like the spokes of a wheel. In this case the index grating need be only a small peripheral portion of a complete radial grating, but it is very desirable to eliminate residual errors of centring by using two such index gratings disposed 180° apart and taking the mean of the two signals produced. Satisfactory compensation is then obtained provided that the centring error does not exceed about one eighth of the peripheral ruling width.

d) *Centring error*

By using circular or zonal gratings, in which all the rulings are concentric circles, it should also be possible to measure the centring errors of the rotating spindle referred to above, and a servo-system could presumably be made to control such errors, e.g. by varying the fluid pressure in a number of hydrostatic bearing pads. Here again photographic manufacture would make it possible to combine radial and circular gratings on a common disc, but so far this has not been done. The only application of circular gratings so far reported has used them in a very different manner, as axicon devices for measuring alignment at a distance (DYSON [1958], UKITA and TSUJIUCHI [1958]).

Of the four systems described above, a) and c) are part of current practice, but b) and d) still await development; production of suitable straight-edge and zonal gratings would not be difficult, but has not so far been undertaken.

In conclusion, it should perhaps be mentioned that moiré fringes have many uses beyond the strictly metrological applications which are the subject of this article. They can for example function as variable sine-wave test objects in measurement of frequency response (LOHMANN [1959]), in multiplex spectroscopy (MERZ, YOUNG and

ARMITAGE [1961]), or in an optical analogue computer (HOWELL [1959]). By combining the moiré principle with Fresnel diffraction (LOHMANN [1961]), or with a two-beam interferometer (BURCH and PALMER [1961]) spectroscopic information may be obtained.

The spatial beat principle has found spectacular application in electron microscopy, where, as a result of superposing two similar crystal lamellae, a dislocation in one of them can be revealed even though the lattice structure is too fine to be resolved (BASSET, MENTER and PASHLEY [1958]).

§ 2. The Formation of Moiré Fringe Signals

2.1. INTENSITY MODULATION BY A PAIR OF COARSE GRATINGS

When light passes in succession through two coarse gratings A and B both of which consist of alternate opaque lines and transparent spaces, the amount of light which emerges clearly depends on whether or not the spaces are aligned in phase with each other. In order, however, to determine quantitatively the intensity profile of the moiré fringes produced, we need to consider the transmission averaged over a relatively large number of individual rulings; this is especially true in most metrological applications where a photocell may be arranged to average the light from the whole of the index grating. Furthermore, even in visual observation, the moiré fringes have a decidedly unsatisfactory appearance unless the eye is at such a distance as to make the individual lines almost too fine to be resolved.

Let $f_A(x)$ denote the intensity transmission coefficient of the index grating A, and let $f_B(x)$ denote the corresponding coefficient for the measuring grating B. It is assumed for the present that f_A and f_B do not vary along the length of each line. If collimated light of unit intensity is incident on to the gratings then for a relative displacement x' the intensity of light emerging (in all directions) and collected by the detector will be $f_C(x')$ where

$$f_C(x') = \int_{x_1}^{x_2} f_A(x)\, f_B(x - x')\, dx. \tag{3}$$

In this equation x_2 and x_1 represent the region of grating A which is being summed by the eye or detector. By making $f_A(x)$ vanish outside these limits, we can extend the limits of integration to $\pm\infty$, and eq. (3) then states that the fringe profile $f_C(x')$ is the resultant of the grating functions f_A and f_B. It follows from the convolution

theorem that if $g_A(k)$ and $g_B(k)$ denote exponential Fourier transforms of f_A and f_B, then the photoelectric intensity signal f_C will have a Fourier transform $g_C(k)$ where

$$g_C(k) = g_A(k)\, g_B(-k). \tag{4}$$

It is no exaggeration to say that eq. (4) is the fundamental basis of the moiré technique. In addition to predicting the detailed fringe profile of a visually observed pattern, or the harmonic content of the corresponding photoelectric signals, it underlines also the fact that each grating acts as a filter to suppress any periodic or random errors in its fellow. If for example the variation of transmission for each grating is approximately sinusoidal, with a pitch distance w, then $g_A(k)$ and $g_B(k)$ will contain principal peaks at spatial periodicities $k = 0$ and $k = \pm 2\pi/w$, together with much smaller peaks and background due to unwanted periodic errors or random errors. In the signal spectrum $g_C(k)$, the latter will be greatly reduced by comparison with the principal peaks of wanted periodicity. The purification of a spatial frequency spectrum here obtained by averaging a moiré pattern is in fact closely analogous to the narrowing of frequency response which can be obtained by cascading a pair of selective filters, for example in a radio circuit or in a double-stage monochromator.

This result has been obtained for a pair of linear gratings, whose periodicity must be expressed by a Fourier integral. For the special case where a photocell collects and integrates all of the light transmitted by the annular periphery of a pair of radial gratings, the integrals are replaced by Fourier series, and eq. (4) then represents a discrete set of equations applied to the corresponding Fourier coefficients.

If an unwanted 'ghost' peak due to periodic error is to appear in the moiré signal output, it must necessarily have been present in both $g_A(k)$ and $g_B(-k)$; when gratings A and B are similar, this condition is satisfied, so that the peak emerges with its intensity (relative to the main peak) squared, but it is interesting to note that the resultant modulation of the main signal is then one of amplitude only which usually has no effect on subsequent electrical squaring or discriminating circuits. Injurious phase modulation of the output signal occurs only when a phase error in one grating is combined with an amplitude error of the same period in the second grating. If for example one imperfect radial grating is rotated steadily with respect to an exactly similar grating, residual grating errors and errors of centring may

indeed cause some fluctuations in the amplitude of the main signal, but there should be virtually no distortion of phase, and substantially perfect performance should be obtained provided that none of these errors exceeds the Rayleigh limit of one quarter of a peripheral division (BURCH [1959]).

In linear measurement, convenience usually dictates that a long measuring grating shall be scanned by a relatively short index grating A. Curtailment of the length of A is equivalent to an amplitude modulation which broadens the peaks of $g_A(k)$ at $k = \pm 2\pi/w$; this has the result that any close-spaced phase modulation sidebands in $g_B(k)$, which are produced by progressive or long-period irregularities in B, and are really the Fourier transform of $\overline{W}_B$ in eq. (2), are no longer rejected by the filtering action of $g_A(k)$. If grating A is eventually reduced to a single slit, the filtering action disappears entirely, and the full errors of B appear in the output.

In most of the new photographic methods of grating manufacture a triple filtering action of this kind is built into the process, and rapid periodic errors are completely eliminated. This is also true of recent Merton-NPL rulings DEW [1962] produced under moiré fringe servo-control, so that in most modern apparatus the importance of using a wide index grating is no longer quite so great. Nevertheless, in special applications where exceptional local smoothness of measuring is needed, for example if moiré fringes are used to control a ruling engine, it remains sound practice to employ an index area as large as possible. As a further insurance against intrusion of rapid random errors, due for example to severe local defects or abrasions, the boundary of the illuminated area of A should be made diffuse rather than sharp so as to produce an apodizing effect. In general, however, such blemishes on a grating become obvious to the eye long before they distort the phase of the integrated signal of a photocell by more than a few microinches, even with a normal index area of perhaps 0.5 cm^2.

2.2. FRINGES FORMED BY FINE GRATINGS IN A SPECTROSCOPIC OBSERVING SYSTEM

If two fine gratings are superposed, the moiré pattern which is seen depends not only on the gratings themselves and on their relative position, but also on the direction from which they are illuminated and viewed. With transparent phase gratings, in particular, there can be no absorption of energy, and no fringes at all will be observed unless some degree of collimation has been employed. For a full

treatment of these matters the fundamental work of GUILD [1956] must be consulted, but some of his results are summarized below.

Let both gratings have the same spacing w, and let collimated light of wavelength λ be incident upon the first grating in a principal plane and at angle θ_1 to the grating normal. The first grating, here assumed to be of unlimited extent, produces a discrete set of diffracted orders, the pth of which is incident upon the second grating at angle θ_2 where $w\,(\sin\theta_1 - \sin\theta_2) = p\lambda$.

A further decomposition takes place on traversal of the second grating, and each of the two-fold family of wavefronts which emerges is termed an 'order-sequence', specified by two integers p and q which represent the order of diffraction which has taken place at the first and second gratings respectively. The angle θ_3 at which a given order-sequence (p, q) emerges is given by $w(\sin\theta_1 - \sin\theta_3) = (p+q)\lambda$, and it follows that all order-sequences for which $(p + q) = r$ emerge in the same resultant direction as if a single grating had produced an rth order diffraction. This family of order-sequences is termed the rth order-group (Fig. 1).

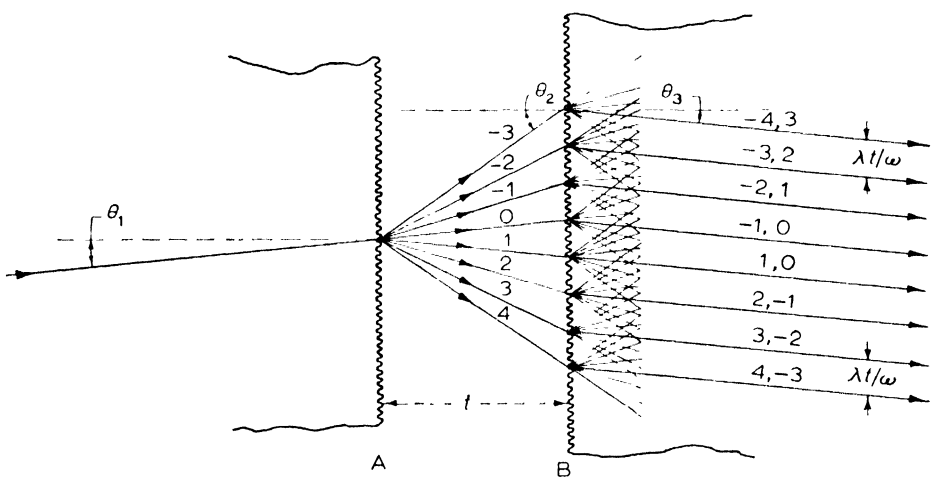

Fig. 1. Illustration of diffracted order-sequences belonging to the first order-group

If phase gratings of fine pitch are being employed, then the first optical condition which must be fulfilled by the moiré fringe observing system is that it shall be collimated so as to accept only the members of a single order-group. For metrological applications the first order-group is almost invariably selected, and under these conditions the moiré fringe amplitude is the vector resultant of the

individual disturbances contributed by the several order-sequences of that group, *viz.*: $(n, 1-n)(n-1, 2-n) \ldots (2, -1)(1, 0)(0, 1)(-1, 2)$ etc.

The amplitude associated with each of these component disturbances is determined largely by the groove-form of the gratings employed, but their phase relationships also depend on other factors such as the separation and mutual alignment of the gratings and the wavelength and orientation of the 'spectroscopic' viewing and illuminating systems. If a pair of gratings is chosen arbitrarily and viewed in the above type of spectroscopic arrangement, then moiré fringes are almost always observed, but their waveform and behaviour is often complicated and unprofitable. Guild has shown that, in order to ensure fringes which are suitable for measurement, there are two further optical precautions which must be taken.

The first precaution is to use gratings which are 'blazed' so as to concentrate as much of the light as possible into two adjacent orders, in most cases, the zero order and one preferred first order. A slightly less favourable possibility is to blaze a single order so that it is much brighter than all the others. The object of using blazed gratings is to ensure that the order-group employed is dominated by two adjacent order-sequences [usually (0,1) and (1,0)] so that the fringe pattern is virtually sinusoidal and the higher harmonics are small.

The second precaution is to arrange that the second grating and the viewing direction have mirror symmetry with the first grating and illuminating direction respectively. For the gratings this is ensured by using two gratings of similar groove-form (derived from the same original master) and using them similarly oriented, while for the illuminating and viewing systems it is necessary to arrange that the order-group selected is being transmitted at the 'minimum deviation' angle. In this way complete symmetry of phase and amplitude is obtained between the order-sequences emerging on either side of the grating normal, and the advantages obtained are firstly that the fringe-shape is symmetrical and secondly that variations in the gap-thickness between the gratings, which in practice always occur when one grating is moved past the other, are without any effect on the phase of the fundamental fringe-period. If higher harmonics are appreciable, however, their coefficients will fluctuate and distort the positions of the fringe-shoulders, causing error if only one of the shoulders is being used for measurement (McILRAITH [1961]).

For most moiré fringe systems the above may be summarized into two main requirements.

(1) The spectroscopic viewing and illuminating systems should be arranged to collect the preferred first order-group at minimum deviation (Fig. 2).
(2) The gratings used should be similar, similarly oriented, and blazed so that the (0,1) and (1,0) order-sequences predominate.

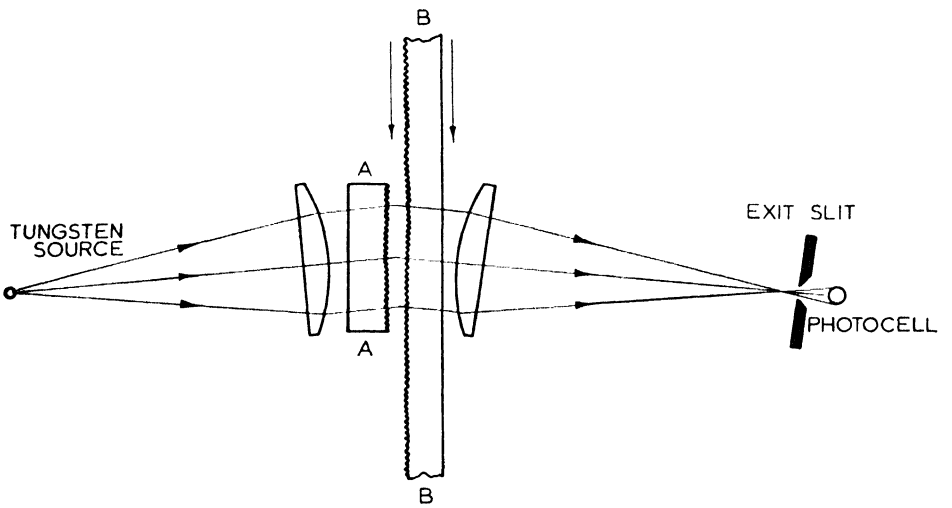

Fig. 2. Arrangement of simple spectroscopic reading-head set to receive first order-group at angle of minimum deviation. Index and long grating are interchangeable.

In practical systems arranged to satisfy these conditions a satisfactorily close approximation to a two-beam fringe pattern is obtained. With wedge-shaped rulings designed for double-order blaze, the unwanted order-sequences do in fact contribute appreciable amplitude to the disturbance (the theoretical amplitude of the $(n, 1-n)$ and $(1-n, n)$ order-sequences being $[2/(2n-1)\pi]^2$), but Guild has shown that the effect of a finite gap-thickness, used in white light with slits of finite width, is such as to attenuate the higher harmonics of the fringe pattern without affecting too seriously the visibility of the fundamental period.

Let us now consider the form of moiré signal to be expected from the above spectroscopic system. Let $\phi_A(x)$ denote the complex amplitude transmission coefficient of index grating A, and similarly let $\phi_B(x)$ denote the complex transmission coefficient for the measuring grating B. As before let $\gamma_A(k)$ and $\gamma_B(k)$ denote corresponding exponential Fourier transforms in terms of a spatial periodicity variable k; $\gamma_A(k)$ is obviously the Fraunhofer diffraction spectrum of grating A in the sense that a plane wavefront of unit amplitude incident on

A at angle θ_1 and observed at an emergent angle θ_2 will produce an amplitude distribution

$$\gamma_A\left[\frac{2\pi\,(\sin\theta_2 - \sin\theta_1)}{\lambda}\right] = \gamma(k_2 - k_1), \text{ where } k = \frac{2\pi \sin\theta}{\lambda}.$$

If the grating B is superposed on A with negligible gap-thickness but relative displacement x', then the integrated amplitude collected by the detector C will be

$$\phi_C(x') = \int_{-\infty}^{\infty} \phi_A(x) \exp(-ik'x)\, \phi_B(x - x')\, dx, \tag{5}$$

where the phase factor $\exp(-ik'x)$ represents the tilt introduced between illuminating and observing systems.

Again by virtue of the convolution theorem, this amplitude ϕ_C will have a Fourier transform $\gamma_C(k)$ where

$$\gamma_C(k) = \gamma_A(k)\, \gamma_B(k' - k). \tag{6}$$

For gratings of indefinite extent and perfectly regular periodicity, the diffraction spectra $\gamma(k)$ vanish except when $k = 2\pi p/w$ gives an integral pth order of diffraction, and equation (6) then becomes equivalent to the discrete order-sequence treatment of Guild. The effects of a finite gap-thickness t are readily included, and provided that the angles of diffraction are small the equation can be rewritten.

$$\gamma_C(k) = \gamma_A(k) \exp\left[\frac{it\lambda k(k' - k)}{4\pi}\right] \gamma_B(k' - k). \tag{7}$$

Equation (7) illustrates the symmetry between order-sequences on either side of the grating normal (for which (k) and $(k' - k)$ must be interchanged), but this symmetry is incomplete unless γ_A and γ_B represent similar groove-forms similarly oriented.

Equations (6) and (7) show that, as far as the removal of error sidebands is concerned, a spectroscopic system achieves the same double filtering action as was produced by eq. (4). On the other hand, as far as the harmonic content of the photoelectric signal $g_C(k)$ is concerned, it must be remembered that the intensity spectrum $g(k)$ corresponding to any amplitude spectrum $\gamma(k)$ is given by the equation

$$g(k) = \int \gamma(l) \cdot \gamma^*(l - k)\, dl, \tag{8}$$

so that there is no one-to-one correspondence between the peaks of

$\gamma_C(k)$ and the peaks of $g_C(k)$. Indeed it often happens that an amplitude fluctuation containing only odd harmonics is converted into an intensity pattern with appreciable even harmonic content (for example in three-beam interference). Where fringe interpolation is contemplated, it is very desirable to avoid any even harmonics, and in a simple intensity system this can be ensured once and for all and irrespective of non-uniformity of the long grating B, by choosing a suitable index grating A to act as a spatial filter (McIlraith [1961]); in a spectroscopic system, however, removal of even harmonic cannot be accomplished except in conjunction with specified properties of the long-grating, and for large carriage displacement the unavoidable changes which occur in gap or grooveform may then reintroduce the trouble. Over short distances of displacement, or in digital systems producing only four counts per fringe, the distortion encountered is entirely negligible, but for most fringe interpolating systems, as used for example in machine tools or in photograph grating manufacture by moiré fringe control, an intensity system is now more generally preferred.

A final point which perhaps deserves to be mentioned in connection with spectroscopic systems is that, since the gap (t) between the gratings amounts to only a few thousandths of an inch, the variations in optical thickness of the plate glass blanks on which metrological gratings are usually supported produce almost the same phase change in all the interfering order-sequences and do not distort the phase of the output signal. This is because they are sheared laterally by only $\lambda t/w$ between each order-sequence. If a monochromatic light source is used, then the exit slit of the spectroscopic observing system should be made slightly larger than the entrance slit so as to allow for the slight deviations of the emergent order-group; with the usual tungsten incandescent source this is unnecessary.

2.3. NON-SPECTROSCOPIC SYSTEMS USING FRESNEL DIFFRACTION

In non-spectroscopic systems requiring high accuracy, it is usual to employ gratings with about 1000 lines per inch in conjunction with silicon photocells which collect all the light emerging from the second grating. Because of Fresnel diffraction effects, however, the intensity distribution produced by the first grating in the plane of the second depends also on the finite gap-thickness t employed. If the first grating is illuminated at normal incidence, then the amplitude of the distur-

bance reaching the plane of the second grating will have the modified Fourier transform

$$\gamma_{At}(k) = \gamma_A(k) \exp\left[\frac{-2\pi i t}{\lambda}\left\{1 - \left(1 - \frac{k^2\lambda^2}{4\pi^2}\right)^{\frac{1}{2}}\right\}\right]. \tag{9}$$

Provided that only small angles of diffraction are being considered, so that $\sin\theta = k\lambda/2\pi \ll 1$, the phase factor in eq. (9) may be simplified to give

$$\gamma_{At}(k) = \gamma_A(k) \exp\left[-\frac{it\lambda k^2}{4\pi}\right]. \tag{10}$$

If eq. (10) is used with eq. (8) to compute the corresponding intensity distribution $g_{At}(k)$ produced in the plane of the second grating, then by substituting $g_{At}(k)$ for $g_A(k)$ in eq. (4) the modified form of the moiré signal can be calculated.

For each pth order of diffraction, the phase factor in eq. (10) takes the value $\Delta_p = \pi t\lambda p^2/w^2$ radians; it follows that if the gap-thickness t increases from $t = 0$ to $t = w^2/\lambda$, a Fresnel image of the grating is reconstituted which closely resembles the grating except for a lateral displacement of half a ruling-width. On the other hand, by choosing intermediate values of t, considerable control over the periodic intensity distribution can be exercised. For example, if A is a pure phase grating, there is then no intensity modulation at all in the plane $t = 0$, but the phase modulation can be converted into a useful amplitude modulation by choosing and maintaining a gap-thickness $t = (n - \frac{1}{2})w^2/\lambda$, where n is a small integer. For a purely absorbing grating the preferred gap-thickness would be nw^2/λ, but for most photographic variable density gratings of about 1000 l.p.i. the emulsion surface also possesses slight phase corrugations, and this unfortunately brings all the planes of optimum intensity modulation to a position slightly closer to the first grating where $t = (n-0.1)w^2/\lambda$. It is preferable that the surface of the second grating should not depart from the optimum plane by more than $\pm 0.15\, w^2/\lambda$, and five sixths of the region corresponding to $n = 0$ is therefore physically inaccessible. For a 1000 l.p.i. grating scanned by a silicon photocell at an effective wavelength of 0.8 micron, the requirement $t < 0.0016''$ would be difficult to satisfy without danger of abrasion, but the alternative range from $0.024''$ to $0.032''$ (corresponding to $1.15 > n > 0.85$) gives easier operation and better performance. For a grating with 500 lines per inch or less, however, around $n = 0$ a gap-thickness of $0.006''$ is permissible, whereas to operate with the first Fresnel image

across gap-thicknesses of 0.120″ or more would create difficulties in collimation.

Familiar from the defocussing method of obtaining 'phase contrast' in a microscope, these Fresnel images have advantages of convenience not only in moiré fringe reading equipment but also for purposes of photographic reproduction on to a sensitive emulsion (BURCH [1960]). In general, the intensity distribution produced in the first Fresnel image of a photographic grating contains appreciable second harmonic, but this can be removed, at some cost to contrast of the main signal, by arranging for the incident illumination to subtend a finite angle of approximately $(\lambda/1.6w)$ radians at the first grating. The optimum gap-thickness is then reduced to about $0.8\ w^2/\lambda$, but this value should be adjusted finally by experiment until maximum modulation of the fundamental signal has been obtained (MCILRAITH [1961]).

2.4. FRINGES OBTAINED WITH AN INTERVENING IMAGING SYSTEM

Instead of relying on Fresnel diffraction to recreate at a convenient distance an image of the first grating, it is possible to separate the gratings altogether by interposing an imaging system. This method is not often adopted because it is less compact and demands great rigidity of mounting, but several interesting properties arise.

Firstly, if the imaging system is an afocal one which brings the diffracted spectrum $\gamma_A(k)$ to an intermediate focus, then by means of opaque masks all but two of the diffracted orders can be eliminated. In this case the two beams which are allowed to reach the second grating produce a purely sinusoidal intensity pattern, and the output signal is also a pure sine wave, irrespective of the properties of the second grating and detector system (provided that the latter is electrically linear) (Fig. 3). The system is then functioning as a true two-beam interferometer, as may be verified by optically retarding one of the two beams emerging from the mask. Indeed, by inserting a small plane mirror in such a position, extremely small rotations of 10^{-11} radians or less have been converted into measurable photo-electric signals (JONES and RICHARDS [1959]).

By comparison with line-standards, a measuring grating is liable to be distorted by flexure since its measuring surface is not in a neutral plane. If a sufficiently stable cement could be found, the use of a grating stiffened by side pieces or sandwiched between two equal transparent silica plates might become attractive, necessitating

recourse to an imaging system. For fringe interpolation in the metrological laboratory, the advantage of eliminating all harmonics might outweigh the considerable difficulties incurred with regard to rigidity and off-axis aberrations. If the two beams allowed through the mask are circularly polarized in opposite directions, a rotating analyser may be used for fringe interpolation (BURCH [1958]).

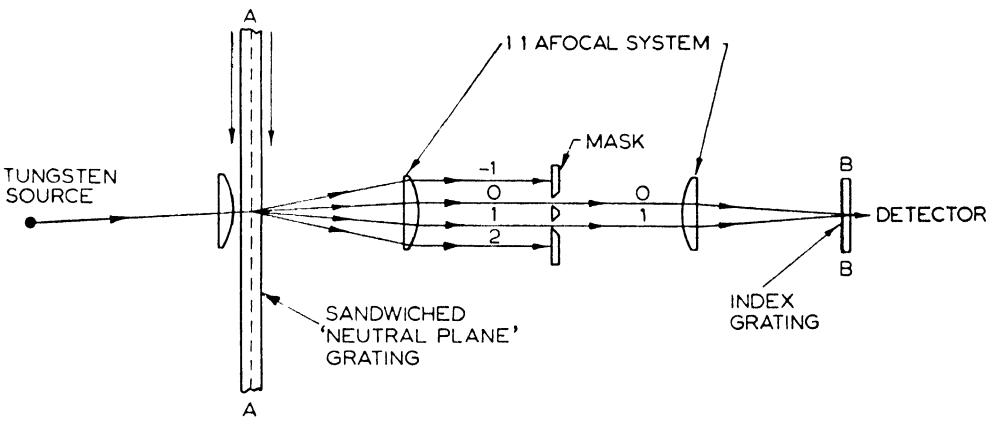

Fig. 3. Production of purely sinusoidal moiré fringes by a masked afocal imaging system. Path of one set of diffracted rays only is indicated.

By arranging for the same grating to be imaged back on to itself, the following self-compensating measuring systems can be devised:

a) By using a linear grating at the focus of an autocollimating system of -1 magnification, sensitivity to linear displacement can be doubled whilst parallelism of the two superposed images is automatically ensured. Arranging a spherical mirror with a plano-convex lens to form an afocal monocentric system with zero Seidel aberration, the author's colleague Dr. D. A. Palmer successfully obtained 28 800 sinusoidal signals per inch of displacement (PALMER [1960], see also DYSON [1959]).

b) It is likewise possible to image one portion of a radial grating on to a diametrally opposite portion and thereby to obtain doubled sensitivity of angular measurement, even when several fringes of centring error are present. This method is however difficult to apply in the presence of a central light-obstructing shaft.

c) Another system, due to the author's colleague Mr. J. W. Gates, is the optical equivalent of a sine-bar and might be useful for analogue-to-digital conversion purposes. One portion of a large linear grating is imaged on to a distant portion of the same

grating in such a way that the phase of the signal is unaffected by any translational movement but depends on the sine of the relative orientation between the grating and the imaging system.

Reference was made above to the fact that, when masks are being used in the imaging system, the disturbance reaching the second grating is indistinguishable from a two-beam interference pattern. A further possibility in this direction is to dispense with the first grating altogether, and to generate a similar fringe pattern by means of monochromatic light in an amplitude-splitting two-beam interferometer. By comparing the spatial periodicity of the grating with that of the fringes it is possible on the one hand to assess the errors of the grating and on the other, by Fourier transformation of the moiré pattern, to obtain the spectrum of the light source employed (BURCH and PALMER [1961]; see also Fig. 4).

2.5. SOURCES OF MEASURING ERROR

In any measuring system the sources of error may be internal or external; internal errors of a moiré fringe system are associated with the performance either of the gratings or of the source-detector combination and subsequent electrical circuits, but external errors can also arise, usually because the value given by the measuring output, instead of being a unique function of the variable required, is also determined to some degree by unwanted variables. For example, if linear gratings are being used to measure the axial translation of a lathe-tool, errors will be introduced by any yawing or pitching of the lathe-saddle unless the gratings are mounted accurately in line with the tool-point. In practice this may be impossible, and the alternative solution of mounting a pair of moiré fringe systems symmetrically on either side of the tool-point is also awkward to arrange. On the other hand, if the errors are not changing very rapidly it may be possible to measure continuously all the variables involved and use a computer to work out and apply the necessary corrections to the main output (LEETE [1961]). When a radial grating is scanned by a pair of reading-heads disposed at 180°, the two signals should be weighted equally if the requirement is to measure pure rotation, but if single-flank measurements are being made on the periphery of a gearwheel of finite radius in a direction perpendicular to the line joining the reading-heads, then a different weighting of the signals may give better compensation for centring error.

External error of this kind is liable to occur with any type of measuring device, and the moiré fringe technique is less susceptible to it than, for example, an optical length-measuring interferometer. If moiré fringes are produced by a pair of perfect gratings they measure pure displacement in ruling-widths x'/w, but the Michelson fringes always measure $x'\mu \cos\theta/\lambda$ where μ represents atmospheric refractive index, $\cos\theta$ an obliquity effect, and λ the wavelength of a coherent source or detector. Moiré fringes are immune from the effects of unsteady air since the two paths compared are always short and their lateral separation $\lambda t/w$ is even smaller. Mechanical vibration is a problem which has been reduced by the introduction of gratings with coarser pitch together with faster photoelectric circuits. The use of glass gratings to measure metal components may lead to thermal expansion errors, but for really accurate work a thermostatically controlled enclosure is in any case essential. Where long metal tape reflection gratings are used, there is less need to work at a particular temperature, but the differing thermal time-lags of different components of a machine will still cause error if it is exposed to the usual diurnal temperature variations.

The effects of ruling error have already been considered, both in terms of the spatial periodicity approach, which gives insight into the nature of the moiré fringe averaging process, and in terms of the lateral displacements themselves. Quantitative estimates of measuring error for a given pair of gratings are more easily obtained in terms of the latter (eq. (2)). Questions of flexural and secular stability will be considered in § 3.1. below.

Moiré fringe measurements are of course subject to many other sources of internal error, but space prevents giving these more than passing mention.

a) Misalignment of the illuminating system, in conjunction with changes of gap-thickness.
b) Variations of either grooveform or gap, producing slight changes in the even harmonic content of the signal.
c) Slow electrical drifts in lamp brightness, detector response, or triggering level of subsequent circuits.
d) Electrical non-linearity, in detector or subsequent circuits, generating spurious even harmonics.
e) Distortion of phase relationship between the detectors of a multi-phase reading-head, due to tilt of carriage or defocusing of light source.

f) Miscounts due to rapid vibration.
g) Background noise and quantum fluctuation in ultra-fast measurement.

For a discussion of these errors and their remedy, reference should be made either to GUILD [1960] or to MCILRAITH [1961]. There is however reason to suppose that, by correct design, their cumulative effect can be reduced to the point where the accuracy of measurement is governed by the external and grating errors already discussed.

§ 3. Design of Moiré Fringe Equipment

3.1. METROLOGICAL GRATINGS AND THEIR PROPERTIES

This section is intended only to summarize in general terms some of the information which a designer needs to consider before deciding what sort of moiré fringe measuring system to adopt. Particularly in the case of linear measurement, a considerable variety of metrological gratings is now available, and, since they all offer a useful accuracy, the choice is more usually dictated by the circumstances in which the information is required. If for example it is required merely to record at high speed a whole series of positional measurements, it may be best to use a purely digital system with fine Merton-NPL replicas scanned by a spectroscopic reading-head. If on the other hand the movements of a machine are to be controlled continuously by a pre-existing programme of instructions, it may be more convenient to use a fringe interpolating system in which servo-control is exercised by a proportional error signal. In all such projects, the moiré fringe transducer represents only a small if vital part of the equipment, and satisfactory design cannot be achieved without close collaboration between experts in the fields of optics, electronics, and data-processing or servo-engineering. In metrological work, however, the measuring speed required is usually much lower, and the approach must then be to choose those gratings and reading-systems which will minimize the errors of a careful observation.

When gratings are produced for metrological purposes by the Merton-NPL process, it is not usual to employ the elastic averaging by means of a resilient nut which is used for spectroscopic gratings. Nevertheless, now that the primary ruling lathe is itself controlled by a calibrated moiré fringe measuring system, periodic errors are negligible and the residual progressive error found in the replicas is

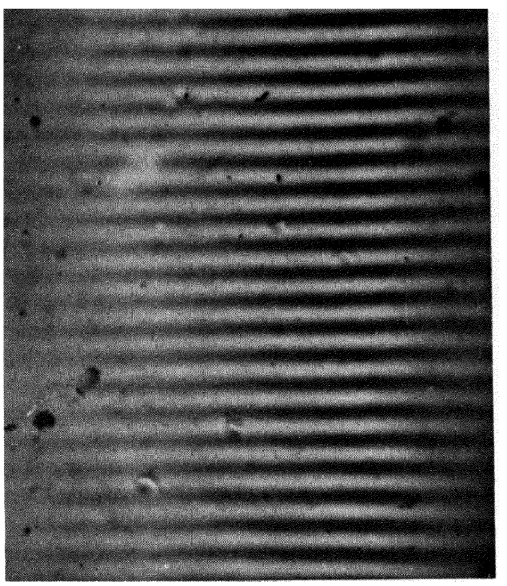

Fig. 4. Moiré pattern obtained when a photographic grating with 57 000 recorded lines per inch is compared with a fringe pattern of similar spacing produced by natural mercury green light in a two-beam interferometer.

largely attributed to random defects of the processes of replication.

These gratings take the form of thin layers of transparent resin cast on to plate glass supports which are usually $2\frac{1}{4}$ inches wide and $\frac{1}{4}$ inch thick; the index grating is normally $\frac{3}{4}$ inch in diameter. The rulings are of a prismatic sawtooth form designed to share incident light equally, as far as possible, between the zero order and one preferred first order of diffraction at the dominant wavelength of the detector (1.1μ for a germanium phototransistor and 0.8μ for a silicon photocell). Various inch and metric pitches are available from commercial licensees of the process, the most useful range being from 1000 lines per inch up to 6 350 lines per inch. If progressive error is defined as the lateral displacement of each ruling from the position which it would occupy in a perfectly regular grating of the same average pitch, then over a 10 inch length it may amount to ± 20 microinches. For longer gratings, made by casting a succession of 10 inch sections, the phasing error across a join may amount to a further ± 20 microinches, although in the most skilled hands ± 10 microinches is often achieved. It follows that if four counts per fringe are obtained from a pair of 2 500 lines/cm gratings, the full digital accuracy of ± 1 micron will be obtained over at least a 10 inch range. For use of plane 'spectroscopic' rulings, see also RASSUDOVA and GERASIMOV [1961].

With regard to photographic gratings, the three basic manufacturing processes are firstly one of direct generation by photographing a pattern of extremely fine interference fringes, secondly one of photographic copying from a master grating, using either contact printing or for finer gratings the first Fresnel image, and finally the self-improving iterative methods in which the moiré signal from a pair of imperfect gratings controls the printing of a better grating. The first two processes have been described at length elsewhere (BURCH [1958, 1959, 1960], BURCH and PALMER [1961]) and it is sufficient here to say that, by using in particular Kodak Maximum Resolution emulsion, extremely faithful recording can be achieved. In the interferometric method, a processed plate on which fringes have been recorded can be replaced afterwards on the interferometer and a moiré pattern can be formed (Fig. 4) in which the straightness or otherwise of the fringes provides a sensitive indication of any shift of the emulsion with respect to its plate glass support. Fig. 4, which is approximately life size, gives no evidence of shifts amounting to more than ± 0.1 fringewidth, which corresponds to a distance of ± 2 microinches since the grating contains 57 000 lines per inch. More recently, tests with gratings of 1000 l.p.i.

have demonstrated that, even for these relatively coarse pitches, the lateral shifts occurring are still extremely small — certainly less than ± 5 microinches.

This means that, provided that flexural distortion or secular change of the supporting glass plate can be avoided, large scale production and copying of accurate photographic gratings is a feasible proposition. In the equipment now installed at the National Physical Laboratory a calibrated master photographic grating, 3 ft long with a 1000 l.p.i. track 2 inches wide, serves to control the recording of almost any new grating desired. The master grating moves steadily on a slide lubricated with kilopoise-oil past a large reading-head with an index grating whose area is about 2 inches square, thereby generating a smoothed signal at about 33 cycles per second. Mounted in tandem with the master grating on the same moving carriage is a sensitive photographic plate (Kodak MR on blank $40'' \times 4'' \times \frac{1}{4}''$) which moves past a stationary 'printing-out' grating whose pitch is $1000 n_1/n_2$ lines per inch, where n_1, n_2 are any chosen integers. If the sine-wave is converted into pulses, and every n_2th pulse is used to trigger a flash-tube repeatedly, then, as a result of $36\,000/n_2$ overlapping exposures of the printing-out grating, a new grating 36″ long is obtained at the new desired pitch. Furthermore, provided that the residual progressive errors of the master have been determined, a phase-shifting control with a precision of ± 1 microinch can be used manually to compensate for those errors during the twenty minutes required for an exposure.

Constructed with the help of Mr. H. A. C. Stallan of Technicolor (Gr. Britain) Ltd., and Mr. N. Sibthorp of Watson Manesty Ltd., and operated by the author's colleagues Dr. A. H. McIlraith and Mr. F. C. Middleton, this apparatus has now produced several master gratings with 10, 100, 1000 lines per inch, 40, 100, and 400 lines per cm, together with composite gratings for purposes of visual read-out (GUILD [1960] p. 198). The accuracy achieved at any point in a 3 ft length is ± 20 microinches, but there is reason to believe that an improvement on this figure by a factor of two can be obtained (MCILRAITH [1961]). The machine itself, with its dynamic phase comparison system, can be used to assess the accuracy of its products by a procedure similar to those employed with line-standards.

With photographic gratings of 1000 l.p.i., it is indeed possible to use a spectroscopic system for the reading-head, but corrugation of the gelatin surface in the clear portions of the emulsion prevents the even orders of diffraction from vanishing as would be desirable. This

means that appreciable second harmonic is encountered in the signal unless the index is deliberately twisted through half a fringe or alternatively a broadened slit is employed in the collimator. Better performance is obtained by operating in a non-spectroscopic system with the first Fresnel image, and locating a silicon photocell in contact with the back of the index grating. If the line-space ratio of the latter is 1 : 1 then it is no longer necessary to take the above-mentioned two precautions against second harmonic content, and full modulation of the fundamental signal is preserved.

Extreme care must be observed in mounting gratings of this accuracy, since the measuring plane is $\frac{1}{8}$ inch away from the neutral plane of the glass. If for example any region of the plate is slightly twisted, so that the local normal to the surface rotates about the line of a ruling through an angle of one minute of arc, the progressive error thereby introduced for that region will be a displacement of $\frac{125000}{3440} = 36$ microinches. Constraints applied in the mounting should be as gentle as possible, and applied at opposite pairs of points so as to avoid introducing a couple which will produce bending. By providing such pairs of supports every six inches, the surface of the grating can be kept close to a plane, so that gap-thickness is constant, without straining the glass in the attempt to remove purely local errors. Provided that the grating takes up the same shape in use as it assumed during its photographic manufacture, no error is occasioned by the constraints. From time to time, by taking readings with a simple autocollimator on the zero order image reflected from the grating surface, a check can be made on the shape, and any necessary corrections calculated on the basis of 36 microinches per minute of deflection.

In order to establish the secular changes which may be expected in plate glass blanks of these dimensions, measurements are being made every six months by Standards Division of NPL on a series of plates, ruled with several lines at distances up to a metre. Over a period of a year a uniform expansion of one or two parts in a million has sometimes been observed, but no measurable non-uniformity has been reported. Provided therefore that calibration of absolute pitch and internal error is undertaken every six months or so, it would seem that a measuring accuracy of 1 in 10^6 could be obtained with such gratings. This fact, together with the simple laboratory interpolation techniques now being introduced, may make them an attractive substitute for existing metrological procedures. A similar and

perhaps even brighter prospect exists for angular measurement by radial gratings, available at present from NEL on blanks about $10\frac{1}{2}$ inches in diameter and typically with 32 400 divisions. Since the accuracy achieved is ± 2 seconds, which corresponds to ± 0.05 fringe, it is already necessary to use some sort of fringe interpolating method. Further improvements in accuracy are in prospect both at NEL, where gear-hobbing applications are being developed, and at NPL, where the technique is being used in a dynamic refractometer and goniometer (GUILD [1960] p. 186, BRITTAN and HABELL [1958]).

Particularly for machine tool applications, the reflection gratings now being made on stainless steel tape by Technicolor Ltd. represent a considerable advance. Their manufacture, like that of the NPL masters which preceded them, is accomplished by a photographic process of flashing under moiré fringe control, so that freedom from periodic error and from local defects such as joins is automatically achieved. Since the rulings consist eventually of alternately etched and polished steel lines, they are considerably more durable than their glass counterparts, and are not likely to break in their mountings if for example intense cold occurs during a shut-down period in a factory.

Lengths of up to 14 ft are available in standard pitches of 10, 100, and 1000 lines per inch, 4 and 40 per cm. In addition, any of the following can be provided to meet special requirements: 20, 25, 40, 50, 200, 250 per inch: 5, 10, 20, 25, 100, 400 per cm. The accuracy claimed by the makers is ± 0.0002 inch per ft run ± 0.0001 inch, but over a 10 ft run the current standard of accuracy is rather better, in that the errors do not build up beyond ± 0.001 inch. By using a fringe interpolating system with either 100 l.p.i. or 1000 l.p.i. gratings, therefore, their full accuracy can be exploited.

3.2. VISUAL AND PHOTOELECTRIC READING-HEADS

For visual read-out from a moiré fringe pattern, the precision obtainable depends very largely on how black a fringe can be produced, so that those procedures which are calculated to remove all unwanted harmonics, at the expense of some loss of contrast at the fundamental fringe period, here become inappropriate. In the multiple decade vernier system described by GUILD [1960] p. 198, gratings with 100 l.p.i. and 1000 l.p.i. gave settings correct to ± 50 microinches, which corresponds to $\pm\frac{1}{20}$ fringe. By using 1000 lines/cm gratings, again with a separation corresponding to the first Fresnel image, this

resolution could probably be improved to ± 20 microinches. The necessary composite decade gratings are made by frequency division on the NPL photoelectric-cum-photographic engine mentioned in the previous section.

For photoelectric reading-heads, an extremely thorough treatment of all practical aspects has been given by GUILD [1960] and by MCILRAITH [1961]. Except for certain applications where dynamic measurement is being performed always in the same direction, it is usual to employ a multiphase pick-up which provides directional information, e.g. by sampling both $\cos\psi$ and $\sin\psi$ (where ψ as before is the phase angle of the fringe pattern). In order to eliminate any second harmonics that may still be present, four photocells are nearly always used in opposed pairs, being positioned at points exactly 90° apart in the fringe pattern. In most spectroscopic systems, quadrature adjustment is obtained by slightly skewing the index grating, and checked by displaying the two signals on a C.R.O. Lissajous figure. When this has been done accurately a circular trace is obtained within which the spot rotates either clockwise or anticlockwise as the grating moves in either direction. In Ferranti counters, a digit is added or subtracted every time the bright spot crosses either the X or the Y axis into a new quadrant. By visual interpolation, extremely small fractions of a fringe can be determined over short periods, especially in vibration measurement (AITCHISON, BRUCE and WINNING [1959]). By employing a large cathode ray tube with gratings of 10 000 lines per inch Mr. J. Guild has been able to obtain quasi-static measurements reliable to ± 2 microinches.

When four-phase signals are to be obtained from photographic transmission or reflection gratings, the method which is now preferred is to use four small silicon photocells, produced either by Ferranti Ltd. of Manchester or by Siemens Halske Ltd., in conjunction with a specially made index grating containing four adjacent sections. In the photographic production of these sections, a lateral shift of exactly one quarter of a ruling width is introduced between each section and its neighbours. Since the four sections are displaced from each other in the direction of measurement, the phase quadrature relationship so established is unaffected by the small tilts which tend to occur at different portions of the carriage travel. Because of the separation between gratings, a small final adjustment of this quadrature relationship can be effected by slightly defocusing the tungsten light source with respect to its collimator.

Silicon cells employed in such reading-heads are previously matched in respect of their sensitivity and also of internal resistance. Their intrinsic frequency response is as high as several Mc/s, and their temperature variations from cell to cell are extremely similar. Once the amplitudes of the four photocell signals have been balanced, either optically or electrically, so as to give satisfactory push-pull operation, interpolation accuracy of $\pm\frac{1}{100}$ fringe should be possible over long periods without readjustment.

3.3. BASIC METHODS FOR HANDLING MOIRÉ FRINGE INFORMATION

Reference has already been made in § 1.1 to a laboratory method for fringe interpolation using a null-setting galvanometer bridge, and it was mentioned in the section just concluded that a four-phase reading-head could produce two reliable photoelectric signals that represent $\cos\psi$ and $\sin\psi$. McIlraith has pointed out that, by using commercially available two-gang sine-cosine potentiometers, the above pair of signals can be combined to form a single signal of the form $\sin(\psi - \beta)$ whose β value can be preset manually on the potentiometer to an accuracy of $\pm$ one thousandth of a cycle. By determining the zero-axis crossing point of this signal with a galvanometer, ψ can then be deduced with the same accuracy as β. Development of this method is proceeding, but an accuracy of ± 2.5 microinches has already been achieved.

In the Ferranti reversible counting systems, counts are generated whenever either the $\cos\psi$ or the $\sin\psi$ signal crosses zero, the sign of the count increment depending firstly on whether the other signal is positive or negative, and secondly on the direction in which the transition is made. The counting speed must be made sufficiently high so that all possible frequencies of vibration across the finite width of the transition region are within the capacity of the counter. Transistors and in-line indicators have now replaced valves and Dekatrons in the new Ferranti counters, which have a maximum speed of 40 kc/s and a working speed of 20 kc/s.

In order to achieve high speed fringe interpolation, the method adopted in the Staveley-NPL system (DAVIES, ROBBINS, WALLIS and WILDE [1960]) was to use an A.C. waveform $\sin\omega t$ as a carrier on which the wanted information $\sin\psi$ could be superposed as a phase modulation $\sin(\omega t + \psi)$. In an earlier system (BARBER and ATKINSON [1959]) this was achieved by imaging a continuously moving

grating, mounted on a rotating drum, on to a stationary index grating and also on to a movable measuring grating, thus generating sin ωt, the drum frequency, and sin $(\omega t + \psi)$ from the comparison of the drum with the moving grating. A similar system, employing a rotating multi-start spiral, was developed independently and with considerable success by Ferranti Ltd. for continuous control at a carrier frequency of $\omega/2\pi = 104$ c.p.s. (WALKER [1961]).

In the Staveley-NPL system, however, much higher carrier frequencies were achieved by the device of replacing physical movement of a grating by an electronically simulated movement of a moiré fringe pattern. If for example the four spatially phased moiré signals $(\cos\psi)(\sin\psi)(-\cos\psi)$ and $(-\sin\psi)$ are respectively multiplied by four temporally phased electrical signals $(\cos\omega t)(\sin\omega t)(-\cos\omega t)$ and $(-\sin\omega t)$, and the four product signals are then summed, the result is clearly $\cos(\omega t - \psi)$ and the desired phase modulation has been achieved. Since this would require an accurate four phase sinewave generator and devices for linear multiplication, the scientists of Staveley Research Group, Bedford devised the elegant solution of replacing the sinewaves by correspondingly phased square-waves, with the result that instead of modulating each photocell output linearly it was necessary only to switch it on and off at the carrier frequency. They showed that if the waveform derived by this sequential switch-sampling process was integrated once, then the resulting signal would pass through zero at an instant whose position within the carrier cycle was linearly related to the displacement angle ψ. This was strictly true only if the moiré fringe itself was of the triangular or serrasoidal shape associated with coarse line and space gratings, but for a pure sinusoidal moiré fringe the error occasioned would not exceed ± 0.011 fringe, and could be removed by an additional electrical filter.

By converting position angle ψ into phase angle with respect to a high frequency carrier signal, one has the possibility of using several analogue or digital methods of phase comparison to establish the fringe fraction $(\psi/2\pi)$. Working at the NPL, for example, the author's colleague Mr. E. Archbold devised a digital fringe subdivider in which the necessary four phase switching waveforms at 2 kc/s were all derived by binary subdivision from a single master oscillator at 256 kc/s. When the switch-sampled and integrated waveform crossed the zero axis, the time separation of this pulse from a 2 kc/s carrier reference pulse was determined by counting cycles of the 256 kc/s

oscillator, each count representing $\frac{1}{128}$th of a fringe. Since moreover this count was repeated at the 2 kc/s sampling rate, considerable accuracy in fringe subdivision could be obtained even when measuring on the move.

The main virtue of the switch-sampling system, however, is that it allows a simple analogue phase discriminator to compare the phase of the measuring signal $\cos(\omega t - \psi)$ with that of a command signal $\cos(\omega t - \beta)$ whose phase-modulation (β) is controlled e.g. by magnetic tape. Since in this case any error that builds up between command and slave signal does so proportionally, smooth operation of the servo is the more readily achieved in continuous contouring applications (DAVIES [1961]).

Another interesting development, by Ferranti Ltd., Edinburgh, has been the introduction of an electronically switched 'sine-cosine' potentiometer with only ten steps, which is linked to a ring counter and achieves ten counts per fringe (SHEPHERD [1961]). Perhaps the most important aspect of either system is that they enable accuracies approaching 10^{-4} inch to be obtained from the very long lengths of reflection grating which are now commercially available.

In addition to these developments in computer-controlled machine tools, the scope of simple phase comparison methods has been increased considerably by introduction of what may be termed an electronic gearbox. It sometimes happens that two moiré fringe signals representing uniform motion of two components of a machine are not identical in frequency but are in some integral ratio $m : n$. Since changing one of the gratings to a different pitch would involve extremely tedious adjustments, the alternative adopted is to turn the photoelectric sinewaves into pulse-trains and then compare the times of occurrence of the mth pulse of one train and the nth pulse of the other train (LESLIE [1956], ARCHBOLD [1962]). On the other hand, when this has been done the time intervals between the pulses compared by the discriminator are correspondingly longer by a factor n or m which may be over a hundred, so that, if the accuracy of perhaps 10^{-2} fringe which was present in the original information is to be preserved, the phase discriminator must be capable of measuring reliably to within 10^{-4} of the pulse repetition time.

By employing a balanced design in fast digital circuits this accuracy has been achieved in practice (ARCHBOLD [1962]). The resulting phase discriminator will operate at up to 100 kc/s if necessary, but its full accuracy of 10^{-4} repetition cycle is needed only when the electronic

gearbox is operating as a frequency divider. The timing accuracy required from the discriminator remains the same, since it depends only on the frequency of the original moiré signal and on the progressive errors of the gratings employed.

The performance of an electronic gearbox and discriminator system should be extremely reliable, depending as it does on transistorised digital circuits. If the associated servo-engineering problems can be solved, it may be possible to eliminate much of the mechanical complexity of modern thread-grinding and gear-hobbing equipment.

§ 4. Conclusion

The moiré fringe technique was developed very largely in response to the need of modern electronics for a transducer that would measure position continuously. More recently, however, the introduction of several new methods of handling moiré fringe information, coupled with improvements in the production of the necessary gratings, have made it possible and economic to use moiré fringes to tackle almost any metrological problem. For any particular problem, of course, there is often an effective alternative measuring system available, but this alternative is usually neither so versatile nor so easily calibrated. In machine tool applications, for example, extremely satisfactory results have been obtained by employing electromagnetic induction, either between periodically disposed electrical windings (BROUWER [1957]), or from recordings arranged on a magnetic emulsion (STEPANEK [1958]). The former type of system, however, cannot readily be adapted to recording digital measurements on a fine scale, while with the latter it is difficult to use anything but dynamic measuring methods. Both systems, it is worth noting, share with moiré fringes the principle of using one periodic scale to analyse another.

For linear measurement over distances greater than about twenty feet it may well be preferable to use interferometry with a light beam modulated at a microwave frequency (FROOME and BRADSELL [1961]), while for extreme accuracy in the laboratory over distances of one or two feet a two-beam interferometer is likely to be greatly superior, especially if a continuous-wave optical maser can be used to improve the signal/noise ratio. For angular measurement, on the other hand, the self-calibrating and error filtering properties of the moiré technique should render it, like Stepanek's method, capable of great accuracy.

In conclusion, the basic advantages of measurement by means of gratings may be summarized as follows.

a) Moiré fringe information is presented continuously, in a form convenient for purposes of recording, control or laboratory measurement, and on a scale whose sensitivity can be chosen to suit most problems.
b) The fringes are virtually achromatic and can be used to measure either length or angle, with equal sensitivity over a large measuring range.
c) Although accuracy may be limited by residual grating errors, or by flexure, creep, or thermal expansion of the material support, only smooth progressive errors can occur.
d) In angular measurement these errors can, if necessary, be averaged out altogether, and in linear measurement the establishment or re-establishment of an error curve is not a formidable task since the number of points to be calibrated is small.

Acknowledgements

The author is grateful to Mr. A. T. Shepherd of Ferranti Ltd., to Mr. R. W. Wilde of Staveley Research Dept., and to many of his colleagues in Light Division NPL for helpful discussions. Particular acknowledgement is made to Mr. J. Guild and Dr. A. H. McIlraith for permission to refer to hitherto unpublished work.

List of Symbols

w	pitch distance of grating, or width of a single ruling
A, B	stationary and moving gratings (interchangeable)
x	position in plane of grating, measured perpendicular to rulings
y	position in plane of grating, measured parallel to rulings
x'	relative displacement of B with respect to A
N	number of rulings per unit length $(=1/w)$
α	small angle at which two juxtaposed sets of rulings are intersecting
$W(xy)$	lateral displacement of rulings at (xy) from position which they would occupy in a perfectly regular grating of the same average pitch

ψ	phase angle determining a moiré fringe pattern
$f(x)$	intensity transmission coefficient of grating surface
k	spatial periodicity variable measured in radians phase change per unit displacement
$g(k)$	Fourier transform of $f(x)$
θ	angle formed in a principal plane between grating normal and direction of propagation
p, q, r	integral orders of diffraction specifying an order-sequence or order-group
λ	wavelength of light employed
$\phi(x)$	complex amplitude transmission coefficient of grating surface
$\gamma(k)$	Fourier transform of $\phi(x)$ (i.e. Fraunhofer diffraction spectrum)
t	gap thickness, or separation between two juxtaposed gratings A and B
n	integral order of Fresnel image (changes by unity for a gap change $\Delta t = w^2/\lambda$)
ω	angular frequency of A.C. carrier wave
β	phase angle of moiré fringe pattern which is being demanded

References

AITCHISON, T. W. A., I. W. BRUCE and D. S. WINNING, 1959, J. Sci. Instrum. ***36***, 400.

ARCHBOLD, E., 1962, J. Sci. Instrum. ***39***, 107.

BARBER, D. L. A. and M. P. ATKINSON, 1959, J. Sci. Instrum. ***36***, 501.

BASSETT, G. A., J. W. MENTER and D. W. PASHLEY, 1958, Proc. Roy. Soc. A ***246***, 345.

BLAKE, D. V. and L. A. SAYCE, 1958, Trans. Soc. Instrum. Tech. ***10***, 190.

BOVEY, L., 1960, Research ***9***, 363.

BRITTAN, K. W. and K. J. HABELL, 1958, Optics in metrology, Symposium Brussels (1960 Pergamon Press, London) 141.

BROUWER, F., 1957, Electrical Manufacturing ***1***, 138.

BURCH, J. M., 1958, Optics in metrology, Symposium Brussels (1960 Pergamon Press, London) 361.

BURCH, J. M., 1959, NPL Symposium on Interferometry Paper 3.3 (1960 HMSO, London) 181.

BURCH, J. M., 1960, Research ***13***, 2.

BURCH, J. M. and D. A. PALMER, 1961, Optica Acta ***8***, 73.

BUTLER, C. C., 1958, Inaugural lecture as Professor of Physics, University of London. Distributed by The Modern Book Co. Ltd., Praed St., London, W2.

DAVIES, B. J., 1961, Int. J. Mach. Tool Des. Res. ***2***, 111.
DAVIES, B. J., B. C. ROBBINS, C. WALLIS and R. W. WILDE, 1960, Proc. I.E.E., ***107***B, 624.
DEW, G. D., 1952, J. Sci. Instrum. ***29***, 277.
DEW, G. D., 1953, J. Sci. Instrum. ***30***, 229.
DEW, G. D., 1956, J. Sci. Instrum. ***33***, 348.
DEW, G. D., 1962, J. Sci. Instrum. ***39***, 141.
DEW, G. D. and L. A. SAYCE, 1951, Proc. Roy. Soc. A ***207***, 278.
DYSON, J., 1958, Proc. Roy. Soc. A ***248***, 93.
DYSON, J., 1959, J. Opt. Soc. Am. ***49***, 713.
FARMER, P. J., 1956, Aircraft Production, ***18***, 256.
FARMER, P. J., 1958, Aircraft Production, ***20***, 174.
FROOME, K. D. and R. H. BRADSELL, 1961, J. Sci. Instrum., ***38***, 458.
FROST-SMITH, E. H., 1960, Times Science Review ***35***, 3.
GUILD, J., 1956, The Interference Systems of Crossed Diffraction Gratings: Theory of Moiré Fringes (Monographs on the Physica and Chemistry of Materials, Clarendon Press, Oxford).
GUILD, J., 1960, Diffraction Gratings as Measuring Scales (Oxford Univ. Press).
HALL, R. G. N. and L. A. SAYCE, 1952, Proc. Roy. Soc. ***215***, 536.
HALL, R. G. N. and V. W. STANLEY, 1960, Microtechnic ***14***, 293.
HOWELL, B. J., 1959, J. Opt. Soc. Am. ***49***, 1012.
JONES, R. V. and J. C. S. RICHARDS, 1959, J. Sci. Instrum. ***36***, 90.
KERMACK, G. S. and H. OGDEN, 1957, J. Roy. Aero. Soc. ***61***, 609.
LEETE, D. L., 1961, Int. J. Mach. Tool Des. Res. ***1***, 293.
LESLIE, W. H. P., 1956, Electrical Energy, ***1***, 2.
LESLIE, W. H. P., 1961, Int. J. Mach. Tool Des. Res. ***2***, in the press.
LOHMANN, A., 1959, Optica Acta ***6***, 37.
LOHMANN, A., 1961, London Conference on Optical Instruments and Techniques (Chapman and Hall, London, in the press).
MCILRAITH, A. H., 1961, NPL Light Division Report Li/3.
MERTON, Sir Thomas, 1950, Proc. Roy. Soc. A ***201***, 187.
MERZ, L., N. O. YOUNG and J. ARMITAGE, 1961, London Conference on Optical Instruments and Techniques (Chapman and Hall, London, in the press).
PALMER, D. A., 1960, J. Sci. Instrum. ***37***, 261.
RASSUDOVA, G. N. and F. M. GERASIMOV, 1961, Optics and Spectroscopy ***11***, 136.
RAYLEIGH, Lord, 1874, Phil. Mag. ***47***, 81 and 193.
SAYCE, L. A., 1953, Endeavour ***12***, No. 48, 210.
SHEPHERD, A. T., 1961, Int. J. Mach. Tool Des. Res. ***3***, in the press.
STEPANEK, K., 1958, Proceedings of International Measurements Conference, November 1958, Budapest.
TIMMS, C., 1959, Viscount Nuffield Lecture, Production Engineer, pp. 321 and 403.
TIMMS, C. and R. M. GRAHAM, 1962, NEL Report (in press).
UKITA, Y. and TSUJIUCHI, J., 1958, Optics in metrology, Symposium Brussels (1960 Pergamon Press, London) 314.
WALKER, G. S., 1961, Int. J. Mach. Tool Des. Res. ***3***, in the press.
WILLIAMSON, D. T. N., 1954, Machinery Lloyd (European Edn.) ***26***, 51.
WILLIAMSON, D. T. N., 1958, Control, 1, 19 and 70.
WILLIAMSON, D.T. N., A.T. SHEPHERD and G. S. WALKER, 1953, Brit. Pat. 760, 321.

III

DIFFUSION THROUGH NON-UNIFORM MEDIA

BY

R. G. GIOVANELLI

National Standards Laboratory Chippendale, N.S.W., Australia

CONTENTS

§ 1. Introduction

The prime purpose of diffusion theory is to describe the intensity of diffuse radiation in media of given elementary properties under given conditions of irradiation. By now, many of the bulk properties of *uniform* diffusing media have been fairly well established. These include the diffuse reflection characteristics of semi-infinite media, the reflection and transmission properties of parallel layers, and the radiant intensities within media of a wide range of shapes when irradiated externally or from sources distributed through the medium. On the whole, however, non-uniform diffusers have been much less studied, though the vast majority of diffusers fall into this class: e.g. imperfectly mixed paints, clouds, the solar photosphere and chromosphere, soils, timbers.

The basic properties of a diffusing medium are its scattering coefficient σ and absorption coefficient α, so defined that fractions $\sigma\,ds$ and $\alpha\,ds$ are respectively scattered and absorbed from a beam of radiation in traversing an elementary path ds. The coefficient for attenuation is the sum of these two, $\kappa = \sigma + \alpha$; while often-used ratios are the albedo for single scattering $\omega_0 = \sigma/\kappa$ and the scattering parameter $\lambda = 1 - \omega_0 = \alpha/\kappa$. In the general case, the angular distribution of light scattered from a pencil of rays is non-isotropic; but if it is at least statistically symmetrical about the direction of the pencil of rays, it may be described in terms of a phase function $p(\cos\Theta)$, where $p(\cos\Theta) \cdot d\omega/4\pi$ is the fraction of the radiation entering an element of solid angle $d\omega$ after scattering through an angle Θ.

The liberation of radiation within the medium may be due to thermal emission or other self-luminous processes, or to scattering from a separate beam of radiation not forming part of the diffuse radiation field; the latter process occurs, for example, when a beam of collimated light falls on a diffuser. The liberation of radiation in all forms can be represented by a single function, the ratio of the emission

per unit volume and solid angle to the attenuation coefficient. Most authors include *all* the scattered radiation in the emission, this function then being called the source function. For some purposes it is more convenient to exclude from the emission the component due to the scattering of the diffuse radiation, in which case the function might be distinguished by the name 'emission function', S; this emission is usually regarded as isotropic, though this is not strictly true for any component due to scattering from an incident beam of radiation.

The intensity of diffuse radiation I, which is a function of position and direction, is such that $I\mathrm{d}\omega$ is the radiant energy per second crossing unit area normally into $\mathrm{d}\omega$. The elementary equation of radiative transfer describes gains and losses in an elementary path $\mathrm{d}s$:

$$\mathrm{d}I = -\kappa I\mathrm{d}s + \sigma\,\mathrm{d}s\int_{4\pi} Ip(\cos\Theta)\frac{\mathrm{d}\omega}{4\pi} + \kappa S\mathrm{d}s. \tag{1.1}$$

In the special case of isotropic scattering, $p(\cos\Theta) = 1$, and

$$\mathrm{d}I = -\kappa I\mathrm{d}s + \sigma\,\mathrm{d}s\int_{4\pi} I\frac{\mathrm{d}\omega}{4\pi} + \kappa S\mathrm{d}s. \tag{1.2}$$

Even for uniform media, the integral equation of radiative transfer (1.2) has been solved *exactly* only for a very few cases; the intensity in an infinite medium with a point source, and therefore, by integration, for any given distribution of sources (MARSHAK, BROOKS and HURWITZ [1949]); the distribution of light escaping at the surface of a semi-infinite medium when (a) the surface is irradiated uniformly externally, or (b) the radiation has penetrated through the medium from effectively infinite depth (CHANDRASEKHAR [1950]); formal or, in some cases, detailed solutions for the reflection and transmission properties of plane-parallel layers (e.g. CHANDRASEKHAR [1950]), though the solutions are of great complexity.

The earliest work in radiative transfer was carried out in connection with the diffusion of radiation through stars. To make progress, scattering was assumed isotropic, and various approximations were introduced, of which the best compromise between consistent success and ease of numerical evaluation was (and still is) that of Eddington. In the one-dimensional problems with which he was concerned, the intensity I can be expanded in a series of Legendre polynomials

$$I = \sum_{n=0}^{\infty} I_n P_n(\mu). \tag{1.3}$$

With the sole approximation that the coefficient I_2 is negligible, eq. (1.2) reduces to the simple Milne-Eddington equation

$$\frac{1}{3}\frac{\partial^2 J}{\partial z^2} = \kappa^2(\lambda J - 4\pi S), \tag{1.4}$$

in which J, the total intensity, is $\int_{4\pi} I \mathrm{d}\omega$.

Eddington's approximation is immediately justifiable when α/σ is very small or $\omega_0 \backsim 1$, for then the radiation field is in any case nearly isotropic (and I_2 consequently small) except for very near the surface; this holds good also for a medium in, or nearly in, radiative equilibrium. A direct theoretical test of eq. (1.4) can be made in the case of the reflectance of a uniform semi-infinite medium, this depending solely on the ratio α/σ. Results obtained on Eddington's approximation are compared in Fig. 1 with exact solutions obtainable from Chandrasekhar.

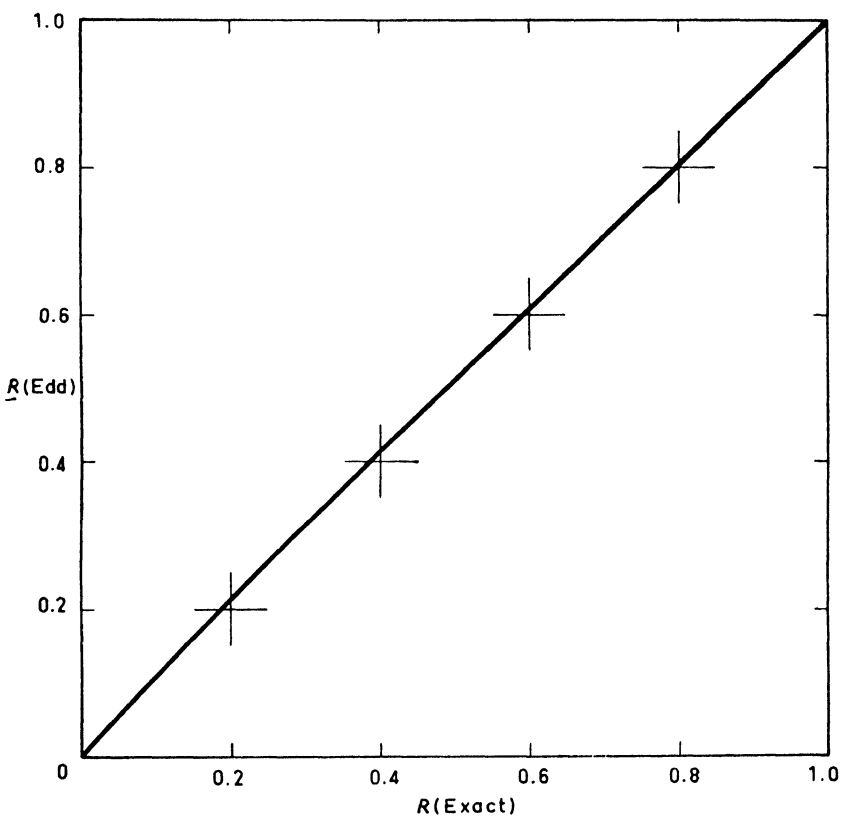

Fig. 1. Diffuse reflectance of a uniform semi-infinite isotropically scattering medium computed on the Eddington approximation, R(Edd.), as compared with Chandrasekhar's exact result (normal incidence, air matrix).

The agreement is extremely good for high reflectances, and still satisfactory for quite low reflectances.

The adequacy of the assumption of isotropic scattering in predicting the behaviour of real media may be checked by measuring the reflectance of a medium of known absorption and scattering properties. For satisfactory dispersion, the particles must be suspended in a liquid matrix, and this involves additional calculations to take account of internal surface reflections (e.g. GIOVANELLI [1955]). BLEVIN and BROWN [1961] find that for a wide range of mixtures of pigment particles, reflectances can be predicted remarkably well by assuming isotropic scattering.

The reflectance of a semi-infinite *uniform* medium depends solely on the *ratio* between the absorption and scattering coefficients α and σ, and not on their individual values. What happens if, in a *non-uniform* semi-infinite medium, the individual values of α and σ vary with position but their ratio is constant throughout? In the extreme case where the absolute values drop to zero in places, the surface might contain cavities, for example in the form of deep vertical louvres, a structure known to have intrinsically low overall reflectance. So at least in some instances, variations in internal structure, even subject to the condition $\alpha/\sigma = \text{constant}$, have profound effects on optical characteristics.

Exact discussions of the radiation escaping from plane-parallel non-uniform media have been given recently by SOBOLEV [1956], UENO [1960] and BUSBRIDGE [1961], though the practical difficulties of evaluating solutions have been found exceedingly great. It is not surprising, therefore, that greatest progress in studying non-uniform media has been in the direction of approximate solutions, mostly based on an extension of the Eddington approximation. Thus in the simple case of diffusion through a medium whose properties vary only in depth, the approximate equation (1.4) holds in the readily amenable form

$$\frac{1}{3}\frac{\partial^2 J}{\partial \tau^2} = \lambda J - 4\pi S, \tag{1.5}$$

where $d\tau = -\kappa dz$ is an element of optical depth. For constant λ, all the results for uniform media are applicable directly.

The first treatment of a more complex medium was in GIOVANELLI's [1957] discussion of the reflectance of a semi-infinite medium in which α/σ was constant throughout, the particles being aggregated into

randomly distributed spheres, all of equal diameters. The method used was cumbersome, but showed that drastic changes in reflectance were involved in going from a uniform semi-infinite medium to one in the form of large, well-spaced aggregates, falling, for example, from 95 to 65 per cent, or from 50 to 25 per cent. The physical reason is that each cluster acts as a scattering centre of lower albedo than that of the individual particles.

A more flexible and powerful method became available when GIOVANELLI [1959] derived a differential equation analogous to eq. (1.4), valid for non-uniform media. WILSON [1960, 1961, 1962a,b] has used this equation to study a number of model media, and has developed techniques for interpreting observations of non-uniform media in terms of their structures. These developments are summarized in the following sections.

§ 2. The Equation of Radiative Transfer in Non-uniform Media

In its most general form, I may be expanded in a series of spherical harmonics

$$I = \sum_{n=0}^{\infty} [I_n P_n(\mu) + \sum_{m=1}^{n} (a_n{}^m \cos m\phi + b_n{}^m \sin m\phi) P_n{}^m(\mu)], \quad (2.1)$$

the $P_n{}^m(\mu)$ being associated Legendre functions, and I_n, $a_n{}^m$ and $b_n{}^m$ the various amplitudes. With the sole approximation that the coefficients I_2, $a_2{}^1$ and $b_2{}^1$ are zero, Giovanelli showed that eq. (1.2) reduces to

$$\tfrac{1}{3}\nabla^2 J = \frac{1}{3\kappa}\nabla J \cdot \nabla\kappa + \kappa^2(\lambda J - 4\pi S), \quad (2.2)$$

the generalized equation of radiative transfer corresponding to the Milne-Eddington equation. The above approximation is a direct generalization of that of Eddington, and is expected to lead to results for non-uniform media having the same degree of validity as those obtained from the Eddington approximation in one-dimensional cases.

In the case of a uniform medium, $\nabla\kappa$ is zero, and eq. (2.2) reduces to eq. (1.4). For problems involving variations of κ with z only, eq. (2.2) reduces to

$$\frac{1}{3\kappa^2}\left(\frac{\partial^2 J}{\partial x^2} + \frac{\partial^2 J}{\partial y^2}\right) + \frac{1}{3}\frac{\partial^2 J}{\partial \tau^2} = \lambda J - 4\pi S \quad (2.3)$$

which is identical with eq. (1.5) for one-dimensional diffusion.

Subject to the same approximation as eq. (2.2), the total flux per unit area in the direction whose unit vector is $\boldsymbol{n}$, is

$$F_{\boldsymbol{n}} = -\frac{1}{3\kappa}\,\boldsymbol{n}\cdot\nabla J, \tag{2.4}$$

the corresponding generalization of the well-known result for a uniform medium.

§ 3. Model Problems

The main importance of studying model media is to obtain a feeling for the subject generally, a background of knowledge which can provide insight for more complex problems. Model media can also be important for the allocation of design tolerances.

All the model problems solved so far have been for media in which the non-uniformities can be treated as small perturbations. Examples are set out below.

3.1. INFINITE SINUSOIDAL MEDIA WITH SOURCES AT INFINITY

Consider an infinite absorbing and scattering medium with small sinusoidal variations of κ and λ, in phase, in say the x direction. Then

$$\kappa = \kappa_0 + \kappa_1 \cos lx,$$

$$\lambda = \lambda_0 + \lambda_1 \cos lx,$$

κ_1/κ_0 and λ_1/λ_0 being small, and l being an inverse measure of the structure size of the medium. For a distributed source at $z = \infty$, the radiation field clearly has an exponential distribution along the z direction and, apart from a common exponential factor, the angular and spatial distributions of the radiation are preserved as z varies. In the x direction, the intensity variation may include harmonics of the fundamental spatial frequency, so J takes the form

$$J = \sum_{n=0}^{\infty} j_n \,\mathrm{e}^{-\gamma z} \cos nlx. \tag{3.1}$$

The method of solution for γ and for the j_n is to substitute eq. (3.1) in the equation of radiative transfer (2.2) in which, since all sources are at infinity, the emission function S is now zero. Separate equations are extracted for the various harmonic components, and these can be solved simultaneously. In practice, only a small number of harmonic components j_n can be retained. This represents a serious limitation

to the method, but for small perturbations of κ and λ, the distortion terms j_n, $n \geqq 2$, may generally be neglected. In the physically significant case where the structure is not too coarse, $l^2 \gg (3\kappa_0^2\lambda_1 + 6\kappa_0\kappa_1\lambda_0)$, it is found that

$$\frac{j_1}{j_0} = -\frac{3\kappa_0^2\lambda_1 + 6\kappa_0\kappa_1\lambda_0}{l^2}, \qquad (3.2)$$

$$\gamma = \kappa_0(3\lambda_0)^{\frac{1}{2}}.$$

The negative sign shows that the total intensity (or radiation density) is greater in regions of attenuation minima, or of scattering parameter minima. The intensity variations are linear with fluctuations of κ and of λ, and decrease rapidly as l increases, i.e. as the size of the fluctuations decreases.

3.2. SEMI-INFINITE SINUSOIDAL MEDIA

A simple type of semi-infinite medium has properties with small sinusoidal variations in a direction parallel to the surface, but constant with depth. GIOVANELLI [1959] discussed the total intensity distribution in a self-luminous medium of this type in which the emission function was also allowed to vary slightly, in phase with the other properties:

$$\kappa = \kappa_0 + \kappa_1 \cos lx,$$
$$\lambda = \lambda_0 + \lambda_1 \cos lx,$$
$$S = S_0 + S_1 \cos xl.$$

The solution to the equation of radiative transfer is carried out along the lines of § 3.1. The z direction being taken along the outward normal, J is expressed in the form

$$J = \sum_{n=0}^{\infty} j_n(z) \cos nlx,$$

the coefficients $j_n(z)$ being functions of depth. General solutions follow readily on neglecting the small distortion terms $j_n(z)$, $n \geqq 2$. These general solutions have to be fitted to the boundary conditions, one of which is that deep within the medium the $j_n(z)$ remain finite (it will be noted from eq. (2.2) that deep in a uniform medium $J = 4\pi S/\lambda$).

The surface boundary condition is of considerable interest. In the present problem, there is no inward flux at the surface, whence

$$0 = \int_0^{2\pi}\int_0^{-1} I\mu \,\mathrm{d}\mu\,\mathrm{d}\phi = \pi I_0 - \frac{2\pi}{3} I_1, \qquad (3.3)$$

provided I_n is negligible for $n = 2, 4, 6 \ldots$ But on the approximations leading to eq. (2.2),

$$\kappa I_1 = -\frac{\partial I_0}{\partial z},$$

whence it follows that at the surface

$$\kappa J = -\frac{2}{3}\frac{\partial J}{\partial z}. \tag{3.4}$$

In particular, eq. (3.4) holds for $\cos lx = \pm 1$, yielding two independent boundary conditions which suffice to complete the solution. It may be noted that the boundary condition eq. (3.4) depends on eq. (3.3), and this involves more restrictive approximations than does the equation of radiative transfer; hence the solution is likely to be most in error near the boundary. This is just as in the well-studied cases of one-dimensional diffusion where, however, the errors have proven to be small (e.g. Fig. 1).

The solution of the semi-infinite medium problem is rather complicated, but the following results emerge:

a) Deep within the medium, there are lateral fluctuations of total intensity

$$\frac{j_1}{j_0} = \frac{3\kappa_0^2(\lambda_0 S_1 - \lambda_1 S_0)}{S_0(l^2 + 3\kappa_0^2\lambda_0)}, \tag{3.5}$$

while, as in the uniform case, $j_0 = 4\pi S_0/\lambda_0$. For very coarse structures, eq. (3.5) becomes

$$\frac{j_1}{j_0} = \frac{\lambda_0 S_1 - \lambda_1 S_0}{\lambda_0 S_0}, \qquad (l^2 \ll 3\kappa_0^2\lambda_0)$$

as might have been anticipated; for very fine structures, j_1/j_0 tends to zero inversely as l^2.

b) At the surface, the fluctuations of total intensity depend linearly on κ_1, λ_1 and S_1, and for fine structures they again tend to zero inversely as l^2. The relationship is

$$\begin{aligned}\frac{j_1}{j_0} = {} & [c(a + l^2)\{\kappa_0 + \tfrac{2}{3}(a + l^2)^{\frac{1}{2}}\}]^{-1} \\ & \times [-2\kappa_0 a l^{-2} bc\{1 - (1 + l^2/a)^{\frac{1}{2}}\} - 2\kappa_0 bc + \kappa_0 ad(1 + l^2/a) \\ & - \kappa_1 ac(1 + l^2/a) + \tfrac{2}{3}(a + l^2)^{\frac{1}{2}}(ad - 2bc)],\end{aligned} \tag{3.6}$$

where

$$a = 3\kappa_0^2\lambda_0^2$$
$$b = 3\kappa_0\kappa_1\lambda_0 + \tfrac{3}{2}\kappa_0^2\lambda_1,$$
$$c = 12\pi\,\kappa_0^2 S_0,$$
$$d = 12\pi(2\kappa_0\kappa_1 S_0 + \kappa_0^2 S_1).$$

The following table sets out, for various structure sizes, the values of j_1/j_0 at the surface due to variations in only one of the quantities κ, λ or S, as derived from eq. (3.6).

Structure size	j_1/j_0 for variations alone in		
	κ	λ	S
$l^2 \ll a$ (coarse)	$-\dfrac{\kappa_1}{\kappa_0 + \frac{2}{3}\sqrt{a}} \cdot \dfrac{l^2}{4a}$	$-\dfrac{\lambda_1}{2\lambda_0}\dfrac{4\lambda_0 + \sqrt{3\lambda_0}}{2\lambda_0 + \sqrt{3\lambda_0}}$	$\dfrac{S_1}{S_0}$
$l^2 = a$	$-\dfrac{\kappa_1}{\kappa_0 + \frac{2}{3}\sqrt{2}}(3-2\sqrt{2})$	$-\dfrac{\lambda_1}{2\lambda_0}\dfrac{2-\sqrt{2}+2\sqrt{6\lambda_0}}{1 + \frac{2}{3}\sqrt{6\lambda_0}}$	$\dfrac{S_1}{S_0\sqrt{2}} \cdot \dfrac{\kappa_0 + \frac{2}{3}\sqrt{a}}{\kappa_0 + \frac{2}{3}\sqrt{2a}}$
$l^2 \gg a$ (fine)	$-\dfrac{\kappa_1}{\kappa_0 + \frac{2}{3}l}$	$-\dfrac{\lambda_1}{\lambda_0}\dfrac{a(\kappa_0 + 2l)}{l^2(\kappa_0 + \frac{2}{3}l)}$	$\dfrac{S_1\sqrt{a}}{S_0 l} \cdot \dfrac{\kappa_0 + \frac{2}{3}\sqrt{a}}{\kappa_0 + \frac{2}{3}l}$

The interesting result emerges that for fine enough structures, greater changes are produced in the total intensity at the surface by a given fractional change in attenuation alone than by the same fractional changes in S or λ alone; though for coarse structures, variations in attenuation coefficient alone have negligible influence on the total intensity at the surface.

3.3. CONSERVATIVE SINUSOIDAL-EXPONENTIAL MEDIA

In a conservative (i.e., scattering but non-absorbing) medium with all sources at infinity, λ and S are both zero; in radiative equilibrium, $\lambda J = 4\pi S$. In both cases, eq. (2.2) simplifies to

$$\kappa\nabla^2 J = \nabla J \cdot \nabla\kappa. \tag{3.7}$$

This is the equation for constant flux.

WILSON [1960] has studied this problem in a medium where the attenuation coefficient has small sinusoidal variations in the x direc-

tion, and an exponential variation with depth

$$\begin{aligned} \kappa &= \kappa_0 \, \mathrm{e}^{-\nu z}(1 + \zeta \cos lx) \qquad (z < 0), \\ &= 0 \qquad\qquad\qquad\qquad (z > 0). \end{aligned} \tag{3.8}$$

The surface lies in the plane $z = 0$, the positive z direction being outwards, as before. The significance of a medium of this type is as a model of a stellar atmosphere in radiative equilibrium. The simplest stellar model, in which the attenuation coefficient tapers off exponentially to zero, corresponds to the limit where κ_0 tends to zero. A non-zero value of κ_0 provides a simple model for an atmosphere whose attenuation coefficient initially increases rapidly with depth, and then more slowly in accordance with eq. (3.8).

The solution to the intensity distribution is

$$J(x, z) = 3F_0 \left[\tfrac{2}{3} + \frac{\kappa_0}{\nu} (\mathrm{e}^{-\nu z} - 1) - \frac{\zeta}{\tfrac{3}{2} + p/\kappa_0} \mathrm{e}^{pz} \cos lx \right], \tag{3.9}$$

where F_0 is the mean flux per unit area across a layer parallel to the surface, and

$$p = \tfrac{1}{2}[-\nu + (\nu^2 + 4l^2)^{\frac{1}{2}}].$$

In particular,

$$\frac{j_1}{j_0} = -\frac{\zeta \kappa_0}{\kappa_0 + \frac{2}{3}p}$$

at the surface. As before, the negative sign shows that an intensity maximum is associated with an attenuation minimum.

From the total intensity distribution it is easy, in principle, to calculate the directional intensity. The radiation scattered into unit solid angle by unit volume of medium is $\kappa J/4\pi$, and along a given path s the directional intensity becomes

$$I = \frac{1}{4\pi} \int_0^{s_0} \kappa J \exp\left(-\int_0^s \kappa \, \mathrm{d}s\right) \mathrm{d}s, \tag{3.10}$$

the upper limit s_0 being at the relevant boundary of the medium. Except in very special cases, eq. (3.10) requires numerical evaluation. For the intensity along the normal at the surface, direct integration shows that $I_1/I_0 = -\kappa_1/\kappa_0$ for $\nu/l \gg 1$, i.e., for a medium whose density increases greatly in a distance equal to the structure size; but in the same direction $I/I_0 = -0.6\kappa_1/\kappa_0$ for $\nu/l \ll 1$ or for $\kappa_0/l \ll 1$. Fig. 2 shows Wilson's numerical values of the directional intensity at the

surface for a medium tapering off to $\kappa_0/l = 10^{-5}$ (i.e., to negligible density). The angles from the vertical, θ, are in a plane at right angles to the structure; the abscissa gives ν/l. For $\nu/l \ll 1$, the contrast is

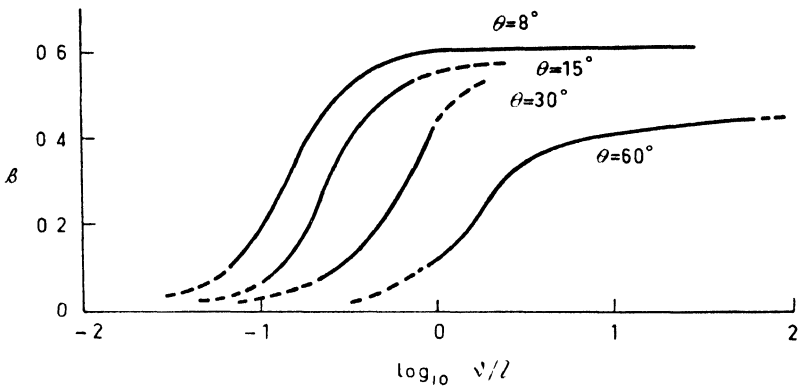

Fig. 2. The directional intensity at the surface of a semi-infinite sinusoidal-exponential medium, $\kappa = \kappa_0 e^{-\nu z}(1 + \zeta \cos lx)$, $(z < 0)$. β is the ratio of I/I_0 to ζ, the curves being for various angles to the normal. All cases are for a medium tapering off effectively to zero density $(\kappa_0/l = 10^{-5})$.

small even as close as 8° to the normal; as might be expected, the effect of structure is apparent only very close to the normal. For ν/l large, the contrast changes relatively slowly with direction.

§ 4. The Interpretation of Observations

An important application of radiative transfer theory is in interpreting observed surface intensities in terms of the elementary properties of the medium. A variation of intensity across the surface implies that either the medium is irradiated non-uniformly or that it possesses a non-uniform internal structure. The question arises how best to proceed in the interpretation of such observations. While solutions to model problems such as discussed in § 3 can help, it must be remembered that the equation of radiative transfer is non-linear, and that intensity fluctuations due to various harmonic components of the medium structure are not additive. To get around this, WILSON [1961, 1962a] has developed two separate techniques (described below in §§ 4.1 and 4.2) for solving the equation of radiative transfer, given the distribution of total intensity throughout the medium. An expression for the latter may be derived in part from observations of the intensity at the surface; though for the intensity distribution within the medium, which is usually unobservable directly, use must be made

of previous knowledge of types of behaviour. The methods have the advantage, too, of making otherwise difficult problems tractable. As in § 3, they are restricted to two-dimensional problems.

4.1. RADIATIVE EQUILIBRIUM, OR CONSERVATIVE MEDIA WITH ALL SOURCES AT INFINITY

For such cases, Wilson commenced by rewriting eq. (2.2), or (3.7), in the form

$$\nabla \cdot \left(\frac{1}{\kappa} \nabla J\right) = 0. \tag{4.1}$$

When J and κ are point functions of two variables only (e.g. x and z, or r and z for an axially symmetric model), eq. (4.1) becomes

$$\frac{\partial}{\partial x}\left(\frac{1}{\kappa}\frac{\partial J}{\partial x}\right) + \frac{\partial}{\partial z}\left(\frac{1}{\kappa}\frac{\partial J}{\partial z}\right) = 0,$$

which is a necessary and sufficient condition for the existence of a function $\phi(x, z)$ such that

$$\begin{aligned} \frac{\partial \phi}{\partial z} &= \frac{1}{\kappa}\frac{\partial J}{\partial x} + \psi(z), \\ \frac{\partial \phi}{\partial x} &= -\frac{1}{\kappa}\frac{\partial J}{\partial z} + \eta(x), \end{aligned} \tag{4.2}$$

where $\psi(z)$ and $\eta(x)$ are arbitrary functions of one variable. If $\phi(x, z)$ can be found, $\kappa(x, z)$ can be determined from eq. (4.2), $\psi(z)$ and $\eta(x)$ being chosen so that κ is unique.

Eliminating κ, eq. (4.2) yields

$$\frac{\partial \Phi}{\partial z} \Big/ \frac{\partial \Phi}{\partial x} = -\frac{\partial J}{\partial x} \Big/ \frac{\partial J}{\partial z} \tag{4.3}$$

where

$$\frac{\partial \Phi}{\partial z} = \frac{\partial \phi}{\partial z} - \psi(z) \quad \text{and} \quad \frac{\partial \Phi}{\partial x} = \frac{\partial \phi}{\partial x} - \eta(x).$$

Thus

$$\Phi(x, z) = \phi(x, z) + X(x) + Z(z), \tag{4.4}$$

where X and Z are again arbitrary functions of one variable. Then from eq. (4.3), it follows that, if $J(x, z) =$ constant defines a family

of curves in the x, z plane, $\Phi(x, z) =$ constant defines an orthogonal family. Given $J(x, z)$, therefore, $\Phi(x, z)$ and hence $\phi(x, z)$ and $\kappa(x, z)$ may always be found to within arbitrary functions of one variable, and an accurate solution of the equation of radiative transfer is available. However, the function chosen for $J(x, z)$ may be (and usually is) incompatible simultaneously with radiative equilibrium and with the surface boundary condition. In this case the arbitrary functions $\eta(x)$ and $\psi(z)$ may require modification so that neither the equation of radiative transfer nor the boundary condition is satisfied exactly, but each holds approximately to the same order of accuracy.

4.1.1. *Conservative Sinusoidal-Exponential Media*

As illustration, the case discussed in § 3.3 can be considered in reverse, J now being given as

$$J(x, z) = A\, \mathrm{e}^{-\nu z} + B + C\, \mathrm{e}^{\nu x} \cos lx. \tag{4.5}$$

It is required to find the distribution of attenuation coefficient compatible with this intensity distribution.

From the gradient of the family of curves $J(x, z) =$ constant, the differential equation for the orthogonal family is derived, its solution giving the family of curves $\Phi(x, z) =$ constant. Substitution in eq. (4.2), via eq. (4.4), leads to two separate equation for κ, one involving $\eta(x)$ and the other $\psi(z)$. In this case, a unique function for κ is obtained only if $\eta(x)$ and $\psi(z)$ are both zero; but then the boundary condition eq. (3.4) is satisfied only to zero order in $C/(A + B)$. Hence no exact solution of the equation of radiative transfer satisfies the boundary condition even to the first order, and it is necessary to consider approximate solutions.

If the ratio C/A is small, it is found that κ takes the approximate form, correct to first order terms,

$$\kappa = \kappa_0\, \mathrm{e}^{-\nu z}[1 + \xi\eta(x)],$$

where ξ is of order C/A and $\eta(x)$ is arbitrary but of order not greater than unity. The form of eq. (4.5) suggests the choice

$$\eta(x) = \cos lx;$$

the boundary conditions are then also found satisfied correct to the first order, provided that

$$\xi = \frac{C}{A + B}\left(1 + \frac{2p}{3\kappa_0}\right)$$

and that B is related to A by

$$B = A\left(\frac{2\nu}{3\kappa_0} - 1\right).$$

This provides a satisfactory first order solution.

4.1.2. *Axially Symmetric Media*

An important problem in solar physics is the structure of a sunspot. As a first step towards the solution of this problem (ignoring departures from radiative equilibrium), consider the distribution of attenuation coefficient when the surface intensity has a radially symmetrical distribution with a central minimum and a finite limit as r approaches infinity, the radial dependence of $J(r, z)$ decreasing with depth. A function of this type is

$$J = A\,\mathrm{e}^{-\nu z} + B + C\,\mathrm{e}^{pz - kr^2}, \tag{4.6}$$

where A is positive, C negative, and p and k are positive.

It turns out that no exact or analytically continuous first order solution is obtainable valid over the range $0 \leqq r < \infty$, but that an approximate solution may be obtained with the discontinuous function

$$\begin{aligned} \kappa &= \kappa_0\,\mathrm{e}^{-\nu z - kr^2}, \qquad (0 \leqq r \leqq R) \\ \kappa &= \kappa'_0\,\mathrm{e}^{-\nu z}, \qquad (r > R) \end{aligned} \tag{4.7}$$

where

$$\kappa'_0 = \frac{2}{3}\frac{\nu}{1 + B/A}.$$

The solution is correct to the first order over the range $0 \leqq r \leqq R$, provided

$$A\left(1 - \frac{2\nu}{3\kappa_0}\right) + B + C\left(1 + \frac{2p}{3\kappa_0}\right) = 0$$

and

$$A\left(1 - \frac{2\nu\,\mathrm{e}^{kR^2}}{3\kappa_0}\right) + B + C\left(\mathrm{e}^{-kR^2} + \frac{2p}{3\kappa_0}\right) = 0.$$

The solution is continuous at $r = R$ provided R is chosen to satisfy $\kappa'_0 = \kappa_0\,\mathrm{e}^{-kR^2}$. The partial derivative is discontinuous at this point, but the discontinuity is small if R is large.

4.2. SEMI-INFINITE MEDIA IN THE ABSENCE OF RADIATIVE EQUILIBRIUM OR WITH GROSS VARIATIONS

Let $4\pi\varepsilon$ be the excess of emitted over absorbed-power per unit volume, so that

$$4\pi\varepsilon = 4\pi\kappa S - \kappa\lambda J.$$

Then (2.2) becomes

$$\nabla \cdot \left(\frac{1}{\kappa}\nabla J\right) = -12\pi\varepsilon. \tag{4.8}$$

If $\kappa^{-1}\nabla J$ is finite and differentiable within a finite volume V, integration of (4.8) and application of Gauss's theorem yields

$$\int \frac{1}{\kappa}\nabla J \cdot \mathrm{d}\boldsymbol{S} = -12\pi \int \varepsilon \mathrm{d}V, \tag{4.9}$$

where $\mathrm{d}\boldsymbol{S}$ is an element of the surface enclosing V, and the left and right hand integrals are taken over the surface and volume respectively. If there are no variations in the y direction, V is conveniently a cylinder of unit length and of section bounded by the lines L_1, L_2, L_3 and L_4 shown in Fig. 3. L_2 is the curve through the point B(x, z), whose

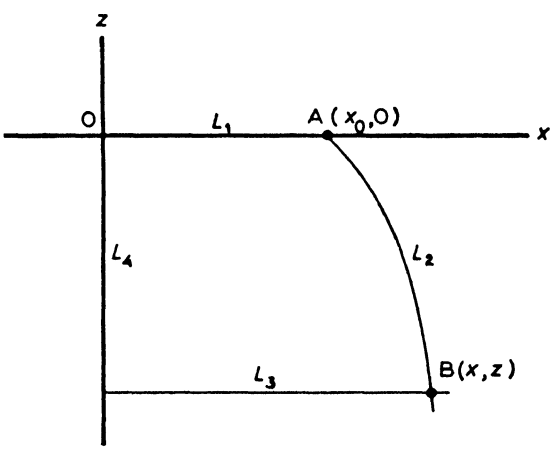

Fig. 3. Section of the volume of integration in the x–y plane.

tangent is everywhere parallel to ∇J, and is thus the locus of points (x', z') satisfying

$$\frac{\mathrm{d}z'}{\mathrm{d}x'} = \frac{\mathrm{d}J/\mathrm{d}z}{\mathrm{d}J/\mathrm{d}x}. \tag{4.10}$$

The point A$(x_0, 0)$ is determined by the intersection of L_2 with the x-axis; x_0 is a function of (x, z), and x' a function of (x, z, z'). Then

$\nabla J \cdot \mathrm{d}\boldsymbol{S}$ vanishes along L_2 and, if the intensity distribution is symmetrical about the z-axis, along L_4 also. So (4.9) reduces to

$$\int_0^{x_0} \left(\frac{1}{\kappa}\frac{\mathrm{d}J}{\mathrm{d}z}\right)_{z=0} \mathrm{d}x - \int_0^{x} \left(\frac{1}{\kappa}\frac{\mathrm{d}J}{\mathrm{d}z}\right)_{z=z} \mathrm{d}x = -12\pi \int_z^0 \int_0^{x'} \varepsilon \,\mathrm{d}x\,\mathrm{d}z.$$

The surface boundary condition (3.4) may be substituted directly into the first integral, whence

$$-\tfrac{3}{2}\int_0^{x_0} J_{z=0}\,\mathrm{d}x - \int_0^{x} \left(\frac{1}{\kappa}\frac{\mathrm{d}J}{\mathrm{d}z}\right)_{z=z} \mathrm{d}x = -12\pi \int_z^0 \int_0^{x'} \varepsilon \,\mathrm{d}x\,\mathrm{d}z.$$

Differentiating partially with respect to x yields

$$\frac{1}{\kappa(x,z)}\frac{\mathrm{d}J(x,z)}{\mathrm{d}z} + \tfrac{3}{2}J(x_0,z)\frac{\partial x_0}{\partial x} = 12\pi \int_z^0 \varepsilon(x',z)\frac{\partial x'}{\partial x}\,\mathrm{d}z,$$

where $\partial x_0/\partial x = (\partial x'/\partial x)_{z=0}$. Hence the solution follows:

$$\kappa(x,z) = \frac{-\tfrac{2}{3}\,\mathrm{d}J(x,z)/\mathrm{d}z}{J(x_0,0)\,\partial x_0/\partial x - 8\pi \int_z^0 \varepsilon(x',z)\,\partial x'/\partial x\,\mathrm{d}z}. \tag{4.11}$$

If J and ε are known throughout the medium, the attenuation coefficient can be calculated from (4.11). Only in the simplest cases can an explicit functional relation be found between x_0 and (x, z). For gross variations, x_0 and $\partial x_0/\partial x$ must be tabulated against x, y and a numerical solution obtained.

4.2.1. *Conservative Media with Gross Periodic-Exponential Variations*

As example, WILSON [1962b] has considered the attenuation coefficient in a semi-infinite medium in radiative equilibrium ($\varepsilon = 0$) in which the total intensity is given by

$$J = A\mathrm{e}^{-\nu z}(1 + \beta \cos lx),$$

where β need no longer be small: $0 \leqq \beta < 1$.

From (4.10) and (4.11) the solution is

$$\kappa = \frac{2}{3}\,\frac{\nu \mathrm{e}^{-\nu z}(1 + \beta \cos lx)}{1 + \beta \cos lx_0}\,\frac{\partial x}{\partial x_0}, \tag{4.12}$$

the curve L_2 being given by the solution of

$$\frac{\mathrm{d}z'}{\mathrm{d}x'} = \frac{\nu}{\beta l}\,\frac{1 + \beta \cos lx'}{\sin lx'}$$

which passes through (x, z). Thus

$$\frac{\tan \frac{1}{2} lx'}{\tan \frac{1}{2} lx} \left(\frac{\sin lx'}{\sin lx}\right)^{\beta} = \exp\left[\frac{\beta l^2}{\nu} (z' - z)\right].$$

Since $x' = x_0$ when $z' = 0$, x_0 is given by

$$\tan \tfrac{1}{2} lx_0 \cdot (\sin lx_0)^{\beta} = \tan \tfrac{1}{2} lx \cdot (\sin lx)^{\beta} \exp\left(-\frac{\beta l^2}{\nu} z\right). \tag{4.13}$$

Partial differentiation with respect to x yields

$$\frac{\partial x_0}{\partial x} = \left(\frac{\sin lx}{\sin lx_0}\right)^{\beta-1} \frac{\tan \frac{1}{2} lx}{\tan \frac{1}{2} lx_0} \frac{1 + \beta \cos lx}{1 + \beta \cos lx_0} \exp\left(-\frac{\beta l^2}{\nu} z\right)$$

$$= \frac{\sin lx_0}{\sin lx} \frac{1 + \beta \cos lx}{1 + \beta \cos lx_0},$$

so that the solution (4.12) becomes

$$\kappa = \tfrac{2}{3} \nu e^{-\nu z} \cdot \frac{\sin lx}{\sin lx_0}. \tag{4.14}$$

For given values of x and z, (4.13) may be solved for x_0 numerically or graphically, and κ tabulated from (4.14).

Wilson has obtained results for the case $\nu = l$ and a range of β. For $\beta = 0.5$, Fig. 4 plots the values of κ^*, the ratio of κ to $\frac{2}{3}\nu e^{-\nu z}$,

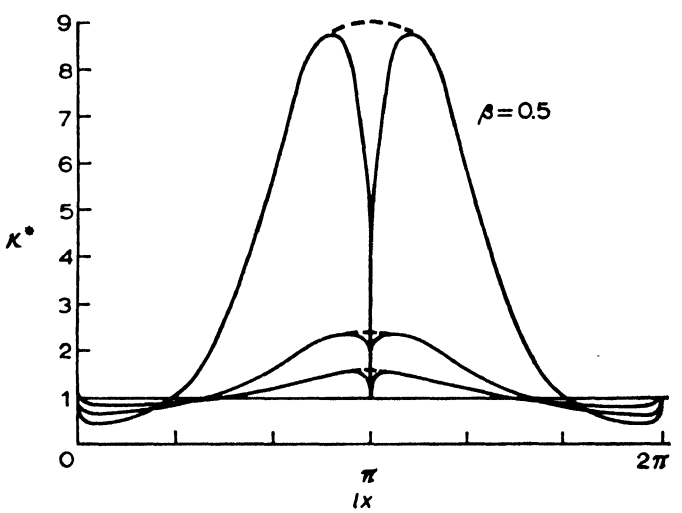

Fig. 4. κ^* as a function of lx for the case $\nu = 1$, $\beta = 0.5$ (§ 4.2.1). The high, medium and low curves in central ranges of lx are for $\nu z = -1.0$, -0.4 and -0.2 respectively; i.e., the higher curves correspond to greater depths. The broken lines eliminate the artificial cusps at $lx = \pi$, as described in the text; similar broken lines should eliminate the cusps at $lx = 0, 2\pi$, but have been omitted for clarity of the diagram.

the latter being the attenuation when $\beta = 0$. The cusps at $lx = 0$, π, 2π arise from logarithmic infinities in the solution at these points due to the sinusoidal form of J. Since the transfer equation itself involves a second-order approximation, the cusps are almost certainly artificial; the adopted solution is the smooth continuation of the curves shown by the broken lines.

The solutions found are reasonably sinusoidal for $\beta = 0.1$, but not for larger values. As shown for small perturbations in § 3.1, an intensity maximum corresponds to an attenuation minimum. The ratio of the amplitude of κ^* to its mean increases with depth, as does the mean itself; moreover, for a given mean attenuation coefficient, large perturbations reduce the mean intensity gradient required for a given flux.

4.2.2. *Media in the Absence of Radiative Equilibrium*

An extension of the above analysis to non-conservative media is straightforward though more tedious. WILSON [1962a] has shown that, assuming small perturbations, it is possible in this way to derive the structure of granulation in the solar photosphere, using the granulation contrast at several different angles from the normal to the sun's surface, i.e., at different distances from the centre of the sun's disk.

§ 5. Discussion

It is a fair summary of the present position to say that, subject to an approximation equivalent to the well-tried Eddington approximation, a differential equation of radiative transfer exists which is capable of solution in a wide range of multi-dimensional radiative transfer problems. In most of the examples treated to date the variations within the medium have been small, though at least one method is available for handling gross variations. A common feature in all solutions has been the significance of structure, be it variation of scattering coefficient or absorption coefficient, or both, on the radiant intensities.

The most interesting mathematical feature has been the strength of methods in which the structure of the medium is deduced from the intensity distribution. This is particularly fortunate as in many cases the solution required would be that corresponding to observed surface intensities.

In a medium having gross variations of attenuation coefficient (its

substance being aggregated into randomly spaced spheres), the effective value of α/σ has been found greater than for a uniform medium of the same material; so that the reflectance of a semi-infinite medium is reduced, in some instances greatly, by large non-uniformities. On the contrary, small perturbations in structure can be shown to have no effect, to a first approximation, on the mean reflectance of a semi-infinite medium. Analogous conclusions apply to the effects of structure on the penetration of radiation through a medium.

In view of the difficulties in obtaining exact solutions for uniform media or for one-dimensional problems, it appears unlikely that more accurate methods for handling non-uniform media will become available for some time; though because of the reliability of the Eddington approximation in other contexts, this can scarcely be regarded as a serious difficulty.

Application of these methods to the formation of spectral lines in some types of non-uniform media is straightforward provided scattering is coherent. Non-coherent scattering introduces considerable difficulties, though in some cases numerical solutions are practicable. For the time being, progress in this direction is likely to be slow.

To date remarkably small demand has been made for theories of non-uniform radiative transfer. In at least one case, a basis has been provided for understanding the non-reproducibility of particular processes in a pigment industry. In astrophysics, in the simple case of photospheric structure, difficulties of securing reliable observations of intensity variations across granules at present outweigh those of handling the relevant theory.

References

BLEVIN, W. R. and BROWN, W. J., 1961, J. Opt. Soc. Am. ***51***, 975.

BUSBRIDGE, I. W., 1961, Astrophys. J. ***133***, 198.

CHANDRASEKHAR, S., 1950, Radiative Transfer (London, Oxford University Press).

GIOVANELLI, R. G., 1955, Optica Acta ***2***, 153.

GIOVANELLI, R. G., 1957, Aust. J. Phys. ***10***, 337.

GIOVANELLI, R. G., 1959, Aust. J. Phys. ***12***, 164.

MARSHAK, R. E., H. BROOKS and H. HURWITZ, 1949, Nucleonics ***4***, No. 5, 10.

SOBOLEV, V. V., 1956, Doklady Akad. Nauk SSSR ***111***, 1000.

UENO, S., 1960, Astrophys. J. ***132***, 729.

WILSON, P. R., 1960, Aust. J. Phys. ***13***, 461.

WILSON, P. R., 1961, Aust. J. Phys. ***14***, 57.

WILSON, P. R., 1962a, Mon. Not. R. Astr. Soc. ***123***, 287.

WILSON, P. R., 1962b, Mon. Not. R. Astr. Soc. ***124***, 383.

IV

CORRECTION OF OPTICAL IMAGES BY COMPENSATION OF ABERRATIONS AND BY SPATIAL FREQUENCY FILTERING

BY

JUMPEI TSUJIUCHI

The Government Mechanical Laboratory, Suginami-ku, Tokyo

CONTENTS

§ 1. Introduction

The disturbing effects of aberrations on image formation in optical systems is well known, and efforts are being made to reduce its amount in designing and in the production of optical instruments. In practice, however, many technical difficulties have to be surmounted and as a rule one has to be contented with some residual aberrations. Then, if no due care is taken, the residual aberrations are very likely to impair the sharpness of image to such an extent that either the optical system becomes unserviceable or, that in the case of simultaneous focussing on two objects at different distances from the objective, disturbing effects are produced, unless the relative aperture is reduced. If, in such cases, the aberration could be minimized by some simple means, for example by reduction of the relative aperture, there will be no longer any difficulties to be met; but in most cases, use of such methods is not appropriate. What is thus required are techniques by means of which correcting the aberrant image under given conditions of relative aperture, focusing and so on can be attained.

For this purpose, two different methods are considered: in the first method the aberration is compensated by the use of an optical filter at the pupil of the objective. In fact, we find successful examples of the filter for this type of compensation in the correcting plate of the Schmidt Camera and the aspheric mirror for the reflecting objective of microscopes used in the ultraviolet region (MIYATA, YANAGAWA and NOMA [1952]). The second method consists of applying double diffraction (Abbe's experiment) to correction of photographic images. The possibility of this method was first pointed out by MARÉCHAL and CROCE [1953], and the improvement of image contrast, the correction in a special case of double image and the removal of the trace of screen mesh from a printed image, etc. were made by the application of this method. The same problem was also

studied by O'NEILL [1956], who succeeded in obtaining images that originally were submerged in optical noise.

In the present article the application of these two methods is studied in relation to correction of optical images formed by an aberrant objective.

§ 2. Correction of Aberrant Images by Aberration Compensating Filter

2.1. INTRODUCTION

For compensating aberrations by a filter placed in front of the pupil of an optical system used under incoherent illumination, phase filter which introduces inverse phase retardation of wave aberration of the system (such as the correcting plate of the Schmidt Camera) is most desirable. But from the point of view of practical applications this method is usually very difficult to be realized, except for special cases.

On the other hand, if a filter with a certain absorption distribution is placed in front of the pupil, the real part of the pupil function is modulated and some change will be caused in the image characteristics. If we choose a suitable form of the distribution, we can expect that the aberration is compensated by such a filter in an appropriate manner. Similarly, if a filter has a distribution of discrete phase retardations of amount π, which alters the sign of real part of the pupil function, such a filter may be expected to compensate the aberration; moreover, it will be more easily realizable than the phase filter, such as the correcting plate of a Schmidt Camera, which introduces continuous phase retardation by the form of the dictated aberrant wavefront.

Attempts have been made to change the image quality by the application of such filters in such a way as to make particular features more conspicuous. As for the filter, the high precision focusing filters by Mlle DOSSIER, JACQUINOT, MARÉCHAL et PIEUCHARD [1951], the filter for apodisation by Mlle DOSSIER [1954] and LANSRAUX [1953a,b], and the coated microscope objective by OSTERBERG, WILKINS and WISSLER [1949, 1950] are now known, and with any one of them, the optical system is aberration-free.

The subject which is treated in the following sections is the application of such filters to optical systems with aberrations; and the use of specially designed absorption filters, phase filters with the retardation of π and of their combination, for the compensation of aberrations and for improvement on the image (TSUJIUCHI [1957, 1958]), is studied.

2.2. CHOICE OF FILTER

In Fig. 1, let O be the object plane, E the exit pupil plane, O′ the image plane. Suppose that the optical system is symmetrical about the optical axis and that it is isoplanatic over the whole working field. The radial coordinate r in the plane E and w in the plane O′ are defined as follows:

$$\begin{aligned} r &= \sqrt{x^2 + y^2}, & w &= \sqrt{u^2 + v^2}, \\ x &= X/L, & u &= k\alpha U, \\ y &= Y/L, & v &= k\alpha V, \\ \alpha &= L/B, & k &= 2\pi/\lambda, \end{aligned} \tag{2.1}$$

where (X, Y) and (U, V) are the geometrical coordinates in the planes E and O′ respectively, L the geometrical radius of the pupil and B the distance between E and O′. If the optical system has the wave

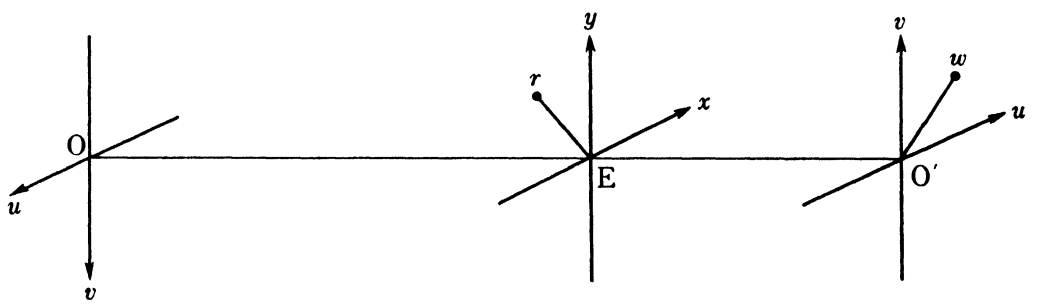

Fig. 1

aberration $W(r)$, the pupil function, which is defined as the amplitude distribution in the pupil plane when a point source is taken as an object, is given by

$$f(r) = \exp \mathrm{i}kW(r). \tag{2.2}$$

If we imagine now a filter of amplitude transmission factor $t(r)$ placed at the pupil of the objective, the pupil function of this system becomes

$$f_t(r) = t(r)\, f(r). \tag{2.3}$$

When the objective has no aberrations, the pupil function becomes constant; hence in order to remove the harmful effect of aberrations on the image, $t(r)$ must take the form:

$$t(r) = \exp\,[-\mathrm{i}kW(r)] = \cos kW(r) - \mathrm{i} \sin kW(r). \tag{2.4}$$

Such a filter is a phase filter which gives inverse phase retardation to

that of the wave aberration such as seen in the correcting plate of a Schmidt Camera. The preparation of a filter of this type is very difficult except in special cases.

Recently, an interesting solution for this difficulty by the use of a Fresnel lens was suggested by MIYAMOTO [1961]. On the assumption that the wave aberration $W(r)$ is

$$0 \leqq W(r) \leqq m\lambda,$$

the pupil is divided into m zones by Fresnel's condition

$$(i-1)\lambda \leqq W(r) \leqq i\lambda, \qquad i = 0, 1, 2, \ldots m.$$

The Fresnel lens can be so made that it shifts the wavefront by the amount $W(r)-(i-1)\lambda$ in the ith zone $(i = 0, 1, \ldots m)$, and the amount of phase retardation in each zone is smaller than 2π. This Fresnel lens can be regarded as a phase filter which satisfies the condition (2.4). The preparation of such a lens is relatively easy because only small amounts of phase retardation are required.

But this phase filter introduces continuous phase retardation even though it is limited within a narrow zone; hence precise retardation is still difficult to be obtained.

To avoid this difficulty a filter, whose amplitude transmission factor is real, may be used, though the compensation may not be so effective as with filter of the type (2.4), mentioned above. Hence a filter whose amplitude transmission factor is given by

$$t(r) = \frac{1}{1+p}\{p + \cos[kW(r) + \delta]\} \tag{2.5}$$

is suggested where p and δ are both positive parameters.

The first parameter p represents the effect of intrinsic aberration on the image when the filter is on, and eq. (2.5) implies that, as p becomes smaller, the compensation effect increases. When $p \geqq 1$, $t(r)$ is always positive, the filter is simply absorptive, $p = 1$ gives the most suitable condition

$$t(r) = \tfrac{1}{2}\{1 + \cos[kW(r) + \delta]\} \tag{2.6}$$

for the filter to be absorptive (TSUJIUCHI [1957]).When $p<1$, $t(r)$ has a negative part, and the filter is composed of an absorption filter and a transparent phase filter which gives the phase retardation π. In this case, $p = 0$ gives the best condition,

$$t(r) = \cos[kW(r) + \delta], \tag{2.7}$$

for the compensation (TSUJIUCHI [1958]). The second parameter δ relates to how much the effect of intrinsic aberration is reduced by use of the filter; it depends on the value of p and the type the intrinsic aberration.

2.3. EFFECTS OF ABERRATION COMPENSATION

2.3.1. *Absorption Filter*

Suppose that the aberration is limited to the spherical type, namely, to spherical aberration and defocussing, and that the image formation is in monochromatic light. If a filter with transmission function (2.6) is used, the pupil function becomes according to eqs. (2.3) and (2.6)

$$f_t(r) = \tfrac{1}{2}\{\exp \mathrm{i}kW(r) + \tfrac{1}{2}\exp \mathrm{i}[2kW(r) + \delta] + \tfrac{1}{2}\exp \mathrm{i}\delta\}. \quad (2.8)$$

For studying the effect of filter on an aberrant system, the Strehl definition which gives the intensity at the centre of the point image and is expressed by

$$I_t(0) = |2\int_0^\infty f_t(r) r \,\mathrm{d}r|^2$$

affords a useful criterion. On the other hand, the total light flux that passes through this system is reduced because of the absorption of the filter, and if the total light flux without the filter is taken as unity, the total light flux available in the presence of the filter is

$$T_t = 2\int_0^1 t^2(r) r \,\mathrm{d}r. \quad (2.9)$$

Hence the evaluation of the image obtained by the use of this filter can be made by the Strehl definition which is normalized by means of the factor, defined in eq. (2.9):

$$I_0 = I_t(0)/T_t \quad (2.10)$$

and the value of δ that makes the filter reduce the effect of intrinsic aberration most effectively can be found as that value which makes I_0 maximum. This value is calculated as a root of the equation

$$\frac{\mathrm{d}I_0}{\mathrm{d}\delta} = 0. \quad (2.11)$$

To simplify the calculation, representation of the aberrations by

means of circle polynomials (ZERNIKE and NIJBOER [1949]), *viz.* expansion of the form

$$kW(r) = \sum_{n=0}^{n} \beta_{2n} R_{2n}^{0}(r), \tag{2.12}$$

is very useful. As an example, the simplest case of aberration caused by defocussing may be considered. In this case

$$\begin{aligned} W(r) &= br^2, \\ kW(r) &= \beta R_2{}^0(r) + \beta, \\ \beta &= \tfrac{1}{2}kb. \end{aligned} \tag{2.13}$$

From eqs. (2.8), (2.10) and (2.12), we have

$$\frac{\tfrac{1}{4} + \left(\frac{\sin\beta}{\beta}\right)^2 + \tfrac{1}{4}\left(\frac{\sin 2\beta}{2\beta}\right)^2 + \frac{\sin 2\beta}{2\beta}\left(1 + \frac{\sin 2\beta}{2\beta}\right)\cos(\beta+\delta) + \tfrac{1}{2}\frac{\sin 2\beta}{2\beta}\cos 2(\beta}{\tfrac{3}{2} + 2\frac{\sin\beta}{\beta}\cos(\beta+\delta) + \tfrac{1}{2}\frac{\sin 2\beta}{2\beta}\cos 2(\beta+\delta)} \tag{2.14}$$

and the values of δ that make I_0 extreme are obtained from (2.11). It is then found that

$$\begin{aligned} \delta_1 &= 2n\pi - \beta, \\ \delta_2 &= (2n+1)\pi - \beta = \delta_1 + \pi, \end{aligned} \tag{2.15}$$

where n is an integer including 0. Fig. 2 shows the relation between b and I_0 for δ_1, δ_2, and also the case without filter. The filter characterized by δ_1 makes the Strehl definition I_0 maximum and that characterized

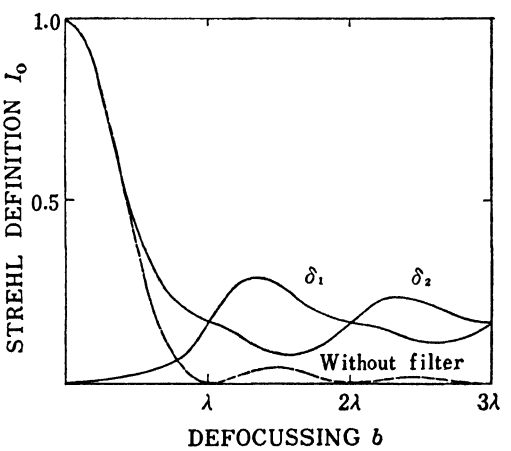

Fig. 2. Relation between the defocussing and the Strehl definition when an aberration-compensating filter is used.

by δ_2 makes it minimum when $2n\lambda < b < (2n + 1)\lambda$, whereas when $(2n + 1)\lambda < b < 2(n + 1)\lambda$ the relation becomes reversed, and the definition obtained by any arbitrary value of δ lies between these extrema. It is found that the definition with a suitable filter is larger than that without filter, or in other words, such a filter can correct the aberrant images.

When $b = n\lambda$, the Strehl definition with the filter becomes independent of the amount of aberration and the value of δ, and has the constant value 0.167. If b becomes very large, any arbitrary choise of δ hardly causes deviations of I_0 from the value 0.167, and the filter becomes similar in form to the Fresnel zone plate.

2.3.2. *Complex Filter*

The second type of the filter whose transmission function is of the form indicated by eq. (2.7) is realized by the combination of an absorption filter mentioned above and a phase filter with transparent thin film layer that causes discrete phase retardation of π.

In the case of spherical type aberrations, the pupil function becomes according to (2.3) and (2.7)

$$f_t(r) = \tfrac{1}{2}\{\exp(-i\delta) + \exp i[2kW(r) + \delta]\}, \tag{2.16}$$

and according to eqs. (2.9), (2.10), (2.12) and (2.16) the Strehl definition becomes

$$I_0 = \frac{1 + A_2^2 + \tilde{A}_2^2 + 2A_2 \cos 2(\beta_0 + \delta) - 2\tilde{A}_2 \sin 2(\beta_0 + \delta)}{2[1 + A_2 \cos 2(\beta_0 + \delta) - \tilde{A}_2 \sin 2(\beta_0 + \delta)]} \tag{2.17}$$

where

$$\begin{aligned} A_m &= 2\int_0^1 \cos m \sum_{n=1}^{n} \beta_{2n} R_{2n}^0(r)\, r\, dr. \\ \tilde{A}_m &= 2\int_0^1 \sin m \sum_{n=1}^{n} \beta_{2n} R_{2n}^0(r)\, r\, dr. \end{aligned} \tag{2.18}$$

From (2.11) one then obtains the relation

$$\tan 2(\beta_0 + \delta) = -\tilde{A}_2/A_2, \tag{2.19}$$

and

$$\begin{aligned} \delta_1 &= \tfrac{1}{2}\tan^{-1}(-\tilde{A}_2/A_2) - \beta_0 + n\pi, \\ \delta_2 &= \delta_1 + \tfrac{1}{2}\pi. \end{aligned} \tag{2.20}$$

These values of δ give the extrema of the definition

$$I_0 = \tfrac{1}{2}[1 + \sqrt{A_2^2 + \tilde{A}_2^2}], \tag{2.21}$$

in which + (−) corresponds to the maximum (minimum), and the maximum of I_0 is obtained for $\delta = \delta_1$ when $A_2 > 0$, and for $\delta = \delta_2$ when $A_2 < 0$.

In the case of defocussing shown by eq. (2.13), we have for the maximum value of I_0,

$$I_0 = \tfrac{1}{2}\left[1 + \left|\frac{\sin 2\beta_0}{2\beta_0}\right|\right], \tag{2.22}$$

where

$$\delta_1 = \begin{cases} n\pi - \beta_0, & \text{for } \dfrac{\sin 2\beta_0}{2\beta_0} > 0, \\ (n + \tfrac{1}{2})\pi - \beta_0 & \text{for } \dfrac{\sin 2\beta_0}{2\beta_0} < 0. \end{cases} \tag{2.23}$$

The curve 2 of Fig. 3 shows the Strehl definition I_0 with defocussing b corresponding to the most favorable value of δ. As seen from eq. (2.22), I_0 is always larger than 0.5 when δ is suitably chosen; it tends to converge to 0.5 with increasing b and becomes eventually independent of the value of δ. Thus, this filter is expected to correct aberrant images more effectively than the absorption filter represented by the curve 1 of Fig. 3.

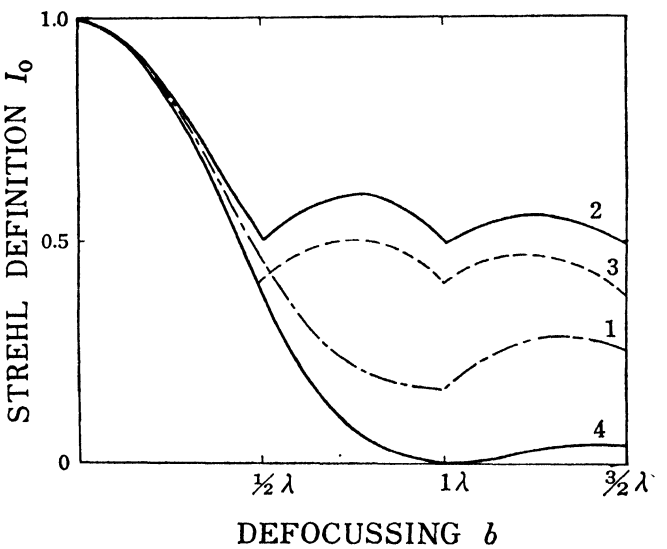

Fig. 3. Effects of different filters on aberration compensation
1. With an absorption filter, 2. With a complex filter,
3. With a phase filter, 4. Without filter

2.3.3. *Phase Filter*

As seen in the above, a considerable effect in compensating the aberration can be attained by the use of a filter with transmission function of the form (2.7). But the realization of such combination of absorption and phase retardation is very troublesome; a filter, simpler in form, easily realizable and equally effective, is required.

A filter which has the amplitude transmission factor of rectangular wave form (Fig. 4) derived from sinusoidal fundamental (2.7) is now considered. Such a filter can be represented as a phase filter which gives phase retardation $P(r)$ to the wave front passing through it, where

$$P(r) = \begin{cases} 0 & \text{for} \quad \cos\left[kW(r) + \delta\right] > 0, \\ \pi & \text{for} \quad \cos\left[kW(r) + \delta\right] < 0. \end{cases} \tag{2.24}$$

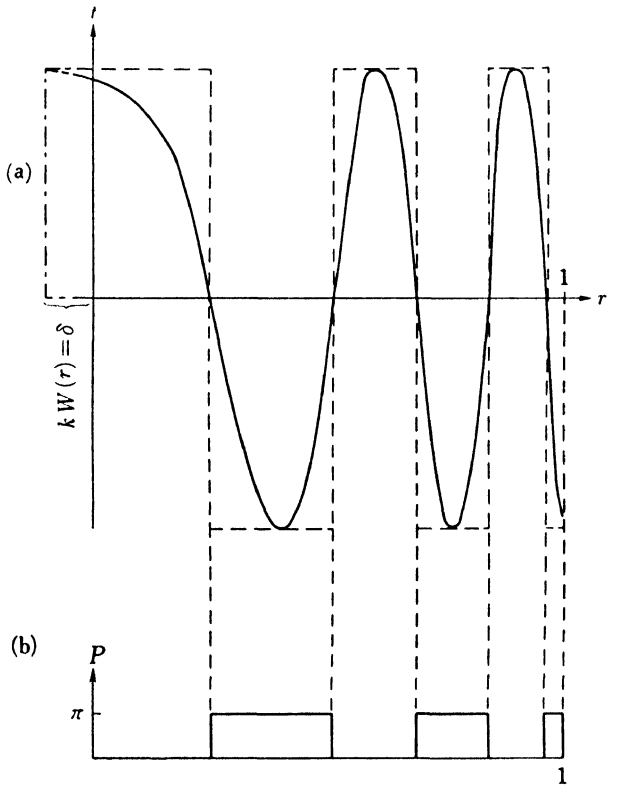

Fig. 4. Relation between complex filter and phase filter

If $W(r)$ is a monotonic function, eq. (2.24) can be expressed by

$$t(r) = P(r) = \frac{4}{\pi} \sum_{m=0}^{\infty} (-1)^m \frac{1}{2m+1} \cos\left\{(2m+1)kW(r) + \delta\right\}. \tag{2.25}$$

According to eq. (2.3) the pupil function becomes

$$f_t(r)=\frac{2}{\pi}\sum_{m=0}^{\infty}\frac{(-1)^m}{2m+1}\{\exp \mathrm{i}[2(m+1)kW(r)+\delta]+\exp-\mathrm{i}[2mkW(r)+\delta]\}. \quad (2.26)$$

If the aberration is large, the Strehl definition becomes according to eqs. (2.10), (2.18) and (2.26)

$$\begin{aligned} I_0 = \frac{4}{\pi}\{&A_0^2 + \tilde{A}_0^2 + A_2^2 + \tilde{A}_2^2 + 2(A_0A_2 - \tilde{A}_0\tilde{A}_2)\cos 2(\beta_0+\delta) \\ &-2(\tilde{A}_0A_2 + A_0\tilde{A}_2)\sin 2(\beta_0+\delta) - \tfrac{2}{3}[(A_2^2 - \tilde{A}_2^2)\sin 2(2\beta_0+\delta) \\ &+ (A_0A_2 + \tilde{A}_0\tilde{A}_2)\cos 2\beta_0 + (\tilde{A}_0A_2 - A_0\tilde{A}_2)\sin 2\beta_0] \\ &+ \tfrac{1}{9}(A_2^2 + \tilde{A}_2^2)\}. \end{aligned} \quad (2.27)$$

Using eq. (2.11), the best value of δ is found to be given by

$$\tan 2(\beta_0+\delta) = \frac{A_0\tilde{A}_2 + \tilde{A}_0A_2 - \frac{1}{3}(A_2 - \tilde{A}_2)\cos 2\beta_0}{\tilde{A}_0\tilde{A}_2 - A_0A_2 + \frac{1}{3}(A_2 - \tilde{A}_2)^2\sin 2\beta_0}. \quad (2.28)$$

When A_2 and $\tilde{A}_2$ are small enough in comparison with A_0, square terms of A_2 and $\tilde{A}_2$ can be neglected comparatively and eq. (2.28) becomes approximately

$$\tan^{-1} 2(\beta_0+\delta) = -\tilde{A}_2/A_2. \quad (2.29)$$

This expression has the same from as eq. (2.19), and the best value of δ becomes the same as given by eq. (2.20). This implies that this phase filter is almost as effective as a complex filter. But with the best value of δ the Strehl definition becomes approximately

$$I_0 = \left(\frac{2}{\pi}\right)^2\{1 + 2\sqrt{A_2^2 + \tilde{A}_2^2} - \tfrac{2}{3}(A_2\cos 2\beta_0 - \tilde{A}_2\sin 2\beta_0)\}, \quad (2.30)$$

which is about 80 % of the value corresponding to the case of the complex filter.

If $W(r)$ is the aberration which represents defocussing, we obtain

$$I_0 = \left(\frac{2}{\pi}\right)^2\left\{1 + 2\left|\frac{\sin 2\beta}{2\beta}\right| - \frac{2}{3}\frac{\sin 4\beta}{4\beta}\right\}. \quad (2.31)$$

Fig. 3 shows the results obtained by the use of these filters with the best value of δ to reduce effects of defocussing. Curve 1 corresponds to the absorption filter (2.6), curve 2 to the complex filter

(2.7), curve 3 to the phase filter (2.24) and curve 4 corresponds to the case when no filter is present. This means that the complex filter is most effective, but the filter (2.24), which is better than the absorption filter (2.6), can be used as a practical substitute for the complex filter.

2.4. CHARACTERISTICS OF IMPROVED IMAGES

As explained in § 2.3, three types of filters are considered for the compensation of aberration, among which the complex filter (2.7) and the phase filter (2.24) are important for practical use. The image characteristics, in cases when these two filters are used will be now discussed.

2.4.1. *Complex Filter*

If the aberration $W(r)$ is sufficiently large, the result becomes almost independent of the value of δ and we can use the filter with the transmission function $t(r) = \cos kW(r)$. The amplitude distribution of a point image is given by the Hankel transformation of the pupil function $f_t(r)$, viz.†

$$A_t(w) = \mathfrak{H}[f_t(r)] \tag{2.32}$$

and we have from eq. (2.16)

$$A_t(w) = \tfrac{1}{2}[A_0(w) + A_2(w)], \tag{2.33}$$

where $A_0(w)$ and $A_2(w)$ are the amplitude distributions of an aberration-free objective and of an objective with aberration $2W(r)$ respectively. The intensity distribution becomes

$$I_t(w) = |A_t(w)|^2. \tag{2.34}$$

Since $W(r)$ is large, the interference term $A_0(w)A_2(w)$ in $|A_t(w)|^2$ can be neglected within the approximation of geometrical optics. We thus finally obtain

$$I_t(w) = \tfrac{1}{4}[|A_0(w)|^2 + |A_2(w)|^2] \tag{2.35}$$

which shows that the image is a superposition of two images: one is $A_0(w)$ which is aberration-free and the other is $A_2(w)$ which is the image of an objective with the aberration twice as large as the original aberration.

† $\mathfrak{H}[f_t(r)] = 2\int_0^1 f_t(r)\, J_0(wr)\, r\, dr$, where J_0 is the Bessel function of the first kind and zero order.

The transfer function of this system is obtained by means of the Hankel transformation of the intensity distribution $I_t(w)$, viz.

$$\begin{aligned} H_t(r) &= \mathfrak{H}[I_t(w)]/T_t \\ &= \tfrac{1}{4}[H_0(r) + H_2(r)]/T_t, \end{aligned} \tag{2.36}$$

where r is the spatial frequency, $H_0(r)$ is the transfer function of an aberration-free objective, and $H_2(r)$ is the transfer function of the objective with the aberration twice as large as its original. Since from eq. (2.9) one obtains for T_t

$$T_t = 2\int_0^1 |f_t(r)|^2 r\,\mathrm{d}r = \tfrac{1}{2},$$

we finally have

$$H_t(r) = \tfrac{1}{2}[H_0(r) + H_2(r)]. \tag{2.37}$$

2.4.2. *Phase Filter*

In the case of the phase filter, the amplitude distribution of a point image is given by eqs. (2.26) and (2.32) as

$$A_t(w) = \frac{2}{\pi}\left[A_0(w) + \sum_{n=1}^{\infty}(-1)^n\left(\frac{1}{2n-1} - \frac{1}{2n+1}\right)A_{2n}(w)\right]. \tag{2.38}$$

The intensity distribution of the image can be calculated by eq. (2.34), and when the aberration $W(r)$ is sufficiently large, each interference term $A_0(w)\,A_{2n}(w)$ will hardly contribute to the structure of the image, and we may assert that the sum of these interference terms appears as a sufficiently large patch of light with uniform intensity distribution. We have then

$$I_t(w) = \left(\frac{2}{\pi}\right)^2\left[\left|A_0(w)\right|^2 + \sum_{n=1}^{\infty}\left(\frac{1}{2n-1} - \frac{1}{2n+1}\right)^2\left|A_{2n}(w)\right|^2 + 1\right], \tag{2.39}$$

and therefore the transfer function is given by

$$\begin{aligned} H'_t(r) &= \mathfrak{H}[I_t(w)] \\ &= \left(\frac{2}{\pi}\right)^2\left[1 + \sum_{n=1}^{\infty}\left(\frac{1}{2n-1} - \frac{1}{2n+1}\right)^2 H_{2n}(r) + \delta(r)\right]. \end{aligned} \tag{2.40}$$

In the case of defocussing, the transfer function is calculated by the approximation of geometrical optics. If the aberration is expressed as eq. (2.13),

$$kW(r) = 2\beta r^2$$

and if a point source gives as its image a uniform circular patch of light with the radius

$$w_0 = \left[\frac{\mathrm{d}kW(r)}{\mathrm{d}r}\right]_{r=1} = 4\beta, \tag{2.41}$$

then the transfer function is given by

$$H(r) = \frac{2J_1(8n\beta r)}{8n\beta r}, \qquad n = 0, 1, 2, \ldots. \tag{2.42}$$

In Fig. 5, the transfer functions $H(r)$, $H_t(r)$ and $H_t'(r)$ are represented by three curves. In the high frequency region, the transfer function of a compensated system rises remarkably as compared with the original uncompensated system. On the other hand, in the very low frequency

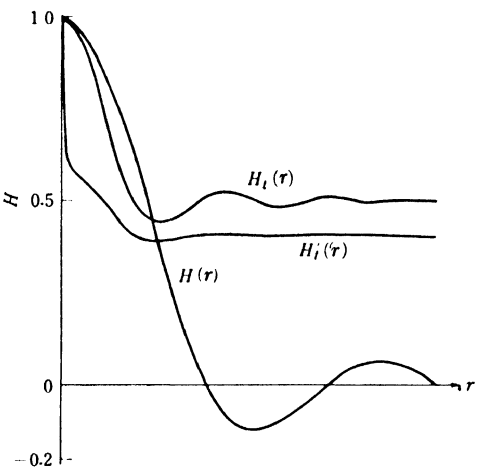

Fig. 5. Change of the transfer function by the use of an aberration-compensating filter.

region except for $r = 0$, it falls especially when the filter is a phase filter, and this fall affects the image characteristics by lowering the contrast.

It is also seen that the zero and negative values of the original transfer function rise to about 0.5 for the filter (2.7) and to 0.4 for the filter (2.24), because the absolute value of $H_2(r)$ in eqs. (2.37) and (2.40) is so small that the final value of the transfer function is obscured by that of the aberration-free system.

2.5. CONSTRUCTION OF FILTERS

In order to construct the complex filter of amplitude transmission factor

$$t(r) = \cos\left[kW(r) + \delta\right],$$

it is advisable to consider a combination of two filters shown in Fig. 6. One is an absorption filter of the intensity transmission factor

$$t^2(r) = \cos^2 [kW(r) + \delta] \tag{2.43}$$

and the other is a phase filter of the phase retardation shown by eq. (2.24) as

$$P(r) = \begin{cases} 0 & \text{for} \quad \cos [kW(r) + \delta] > 0, \\ \pi & \text{for} \quad \cos [kW(r) + \delta] < 0. \end{cases}$$

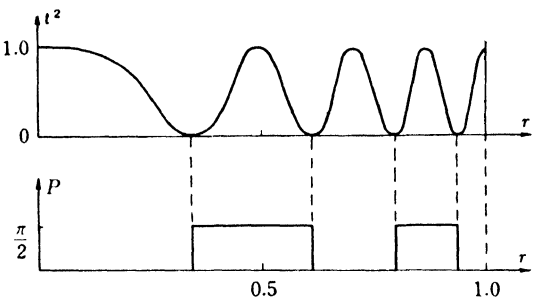

Fig. 6. Characteristics of a complex filter

The latter is none other than the phase filter, the characteristics of which are discussed in § 2.4.2.

The construction of these filters will now be discussed.

2.5.1. *Absorption Filter*

The absorption filter is made photographically with ease by the use of Twyman's lens interferometer. If the objective in question is placed in a testing beam of the interferometer and optical axes of the testing and reference beams are made to coincide exactly at the beam splitter, the amplitude distribution of the interferogram is expressed by

$$\tfrac{1}{2}[\exp \mathrm{i}2kW(r) + \exp \mathrm{i}\varepsilon]$$

where ε is the phase difference between these two beams. The intensity distribution is given by

$$F(r) = \cos^2 [kW(r) - \tfrac{1}{2}\varepsilon].$$

If these interference fringes are recorded on the photographic emulsion with $\gamma = 1$, the intensity transmission function of the positive image becomes

$$t^2(r) \propto \cos^2 [kW(r) - \tfrac{1}{2}\varepsilon], \tag{2.44}$$

which is the same expression as eq. (2.43), and the best value of ε can be obtained by adjusting the optical path difference between the two beams in the interferometer.

The practical method of constructing the filter is as follows: The objective, on which the filter is to be applied, is set in the Twyman's lens interferometer, and the phase difference ε between the two beams is so chosen that the value of δ calculated from the aberration of the objective becomes most favorable. If the radius of the photographed interferogram coincides exactly with that of the objective and $\gamma = 1$ is retained, the plate-positive (or negative provided δ is given due consideration) of the interferogram may be used as an absorption filter.

2.5.2. *Phase Filter*

As can be seen from eq. (2.24), the phase filter is composed of several annular zones with transparent thin film on each, which gives the retardation of π, and $\cos kW(r)$ is negative in these zones. The zones are prepared by vacuum deposition of evaporated magnesium fluoride MgF_2 or other suitable substances. This group of concentric zones comprises every other transparent zone of the above-mentioned absorption filter or the allocation of the zones is determined by calculating the aberration.

The preparation process of the phase filter is as follows.† In a circle representing the pupil of the objective, concentric circles are drawn with radii which divide the circle in proportion to the values of $r_n (n = 1, 2, \ldots)$ given by the relation $\cos kW(r_n) = 0$, and the annular zones where the thin film layers are to be deposited; in other words zones where $\cos [kW(r) + \delta] < 0$ holds, are blackened and other zones are whitened. This pattern is then photographed in a size exactly equal to the pupil of the objective. The photo-negative thus prepared is laid on a glass plate of a well polished surface; is chemically silvered and is treated with photosensitive glue; and exposed to light. Since the exposed glue becomes insoluble in water, a warm water bath makes the unexposed glue dissolve, leaving bright silver annular zones. The silver layer on these zones is first dissolved in an acid bath leaving naked glass surfaces, and the remained exposed glue is then dissolved in an acetic acid bath. After the vacuum deposition of evaporated MgF_2

† The same method is found in the study of ENNOS [1960] relating to the preparation of a phase grating.

over the whole surface, the glass plate is left again in an acid bath which dissolves away the silver layer zones, removing the MgF_2 films deposited on them. A phase filter with annular zones of phase retarding film is thus prepared.

For this filter, the phase difference π is independent of its sign, therefore the zones where $\cos[kW(r) + \delta] > 0$ holds, can be processed as above instead of the zones where $\cos[kW(r) + \delta] < 0$ holds.

The optical thickness nd of the thin deposited film is given by

$$nd = \frac{n}{n-1}\frac{\lambda}{2}, \tag{2.45}$$

where n is the refractive index of the film. $n = 1.38$ at $\lambda = 546\,\mathrm{m}\mu$ for MgF_2 gives the thickness $nd = 1.8\lambda$. As this optical thickness is 7 times that of the anti-reflecting film ($nd = 0.25\lambda$), the required thickness is easily obtained by observing the successive changes of surface color during the vacuum deposition; for every addition of the thickness of one non-reflecting layer produces a characteristic color on the surface. Hence, for film deposition, it is advisable to prepare in advance seven samples of surfaces, vacuum deposited from once to seven times of anti-reflecting layer; thus may then be used for checking the deposition process by color.

2.5.3. *Practical Filter*

For practical use, the two filters mentioned above are combined. They are combined in such a way that not only their corresponding zones exactly coincide (Fig. 6), but the absorptive layer of the absorption filter is in close contact with the film of the phase filter; for otherwise, the two filters would influence the image independently lessening the compensation effect.

The surface of a photographically prepared absorption filter is not optically flat; the transmitted light suffers phase disturbance. Therefore, in combining the filters, a small amount of ceder oil or dibutyl phthalate is used in between to compensate for the unevenness of the surface. The equation (2.45), which gives the thickness of deposited film on the phase filter, is then modified to

$$nd' = \frac{n}{n_0 - n}\frac{\lambda}{2}, \tag{2.46}$$

where n_0 is the refractive index of the intervening substance.

However, we have seen in § 2.3.3 that the phase filter nearly equals the complex filter in effectiveness. Therefore in practice, one does not have to venture on such a technically difficult task of combining the two filters.

2.6. APPLICATION OF THE FILTER

2.6.1. *Filter of Two Foci*

If an objective which has the aberration of defocussing, represented by eq. (2.13)

$$kW(r) = 2\beta r^2$$

and a filter which has the amplitude transmission factor

$$t(r) = \cos 2\beta' r^2 \tag{2.47}$$

are used together, the Strehl definition becomes similar to eq. (2.17), viz.

$$= \frac{\left(\frac{\sin(\beta'+\beta)}{\beta'+\beta}\right)^2 + \left(\frac{\sin(\beta'-\beta)}{\beta'-\beta}\right)^2 + 2\frac{\sin(\beta'+\beta)}{\beta'+\beta}\frac{\sin(\beta'-\beta)}{\beta'-\beta}\cos 2(\beta+\delta)}{2\left[1+\frac{\sin 2\beta'}{2\beta'}\cos 2(\beta'+\delta)\right]}. \quad (2.$$

When β' is sufficiently large, I_0 becomes independent of the value of δ and we have then for a suitable value of δ,

$$I_0 = \frac{1}{2}\left[\frac{\sin^2(\beta'+\beta)}{(\beta'+\beta)^2} + \frac{\sin^2(\beta'-\beta)}{(\beta'-\beta)^2}\right]. \tag{2.49}$$

When β is regarded as variable, I_0 has two maxima, at $\beta = \beta'$ and $\beta = -\beta'$. In Fig. 7, curve 1 shows the result when $\beta' = 2\pi$, and it is

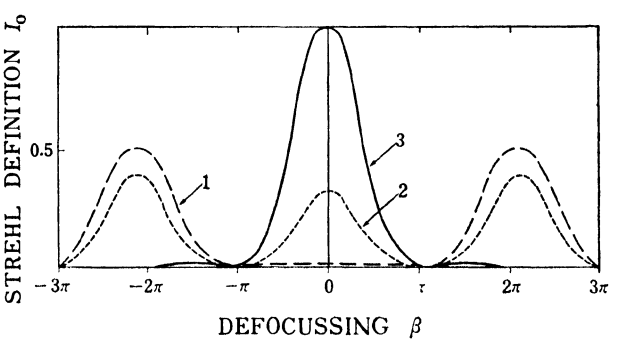

Fig. 7. Filters of two foci and three foci
1. Filter of two foci, 2. Filter of three foci,
3. Ordinary objective

seen that this filter has an effect of splitting the focus of an objective into two, formed at positions corresponding to $\beta = \beta'$ and $\beta = -\beta'$.

Because of this property, we call the filter the 'filter of two foci'. The Strehl definition at the point $\beta = \beta'$ or $\beta = -\beta'$ becomes

$$I_0 = \tfrac{1}{2}\left[1 + \frac{\sin^2 2\beta'}{(2\beta')^2}\right] \tag{2.50}$$

and I_0 can always be above 0.5 in this system. If this filter is used with an objective, two foci, in front and rear of the proper focus, will be formed; and inversely if an image plane is fixed, images of two objects separated one behind the other will be in the same plane.

No doubt, the filter of two foci can be effectively realized by a phase filter. The Strehl definitions at each of the new separated foci becomes 0.4.

2.6.2. *Filter of Three Foci*

If p in eq. (2.5) becomes $\frac{1}{2}$ and $W(r)$ represents defocussing, I_0 becomes for a large aberration and for a suitable value of δ

$$I_0 = \frac{\dfrac{\sin^2\beta}{\beta^2} + \dfrac{\sin^2(\beta+\beta')}{(\beta+\beta')^2} + \dfrac{\sin^2(\beta-\beta')}{(\beta-\beta')^2}}{3 + 4\dfrac{\sin\beta'}{\beta'} + 2\dfrac{\sin 2\beta'}{2\beta'}}; \tag{2.51}$$

I_0 has a maximum value 0.33 for $\beta = 0$, $\beta = \beta'$ and $\beta = -\beta'$, and it is seen that the focus of the objective is split into three (Fig. 7, curve 2). This filter is called 'filter of three foci'.

The filter of three foci can be realized by the use of a phase filter. Let

$$P = 2\pi q \tag{2.52}$$

be the phase retardation given by the film of the phase filter where q is a parameter which is proportional to the optical thickness. The Strehl definition of the phase filter compensating defocussing of amount $n\lambda$ is calculated from the expression

$$\begin{aligned} I_t(0) = \Bigg| & 2\int_0^{r_1} \exp i\beta' r^2 r\,dr + \ldots + 2\int_{r_{2n-2}}^{r_{2n-1}} \exp i\beta' r^2 r\,dr \\ & + \exp i2\pi q\left[2\int_{r_1}^{r_2} \exp i\beta' r^2 r\,dr + \ldots + 2\int_{r_{2n-1}}^{1} \exp i\beta' r^2 r\,dr\right]\Bigg|^2 \\ = & \left(\frac{4n}{2\beta'}\right)^2 \left(\frac{1-\cos 2\pi q}{2}\right), \end{aligned} \tag{2.53}$$

where $r_1, r_2, \ldots, r_n$ are the radii of the borders of annular film layers (Fig. 8), and

$$2\beta' = kn\lambda = 2\pi n.$$

We thus have

$$I_t(0) = \left(\frac{2}{\pi}\right)^2 \left(\frac{1 - \cos 2nq}{2}\right). \tag{2.54}$$

On the other hand, at the proper focus $\beta = 0$, we have by setting $\beta' = 0$ in eq. (2.53),

$$I_t(0) = \tfrac{1}{2}[1 + \cos 2\pi q]. \tag{2.55}$$

The three foci are obtained when the values of I_t at $\beta = 0$, $\beta = +\beta'$

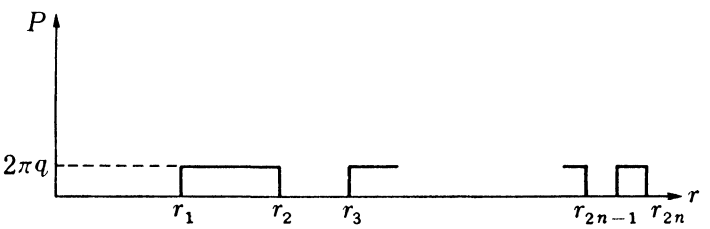

Fig. 8

and $\beta = -\beta'$ are made equal, and the best value of q is determined from the relation

$$\cos 2\pi q = \frac{1 - 4/\pi^2}{1 + 4/\pi^2}. \tag{2.56}$$

This gives $q = 0.32 = 0.64 \times 0.5$, which corresponds to 0.64 times of the film thickness of filter of two foci and it gives $I_t = 0.29$.

2.7. EXPERIMENTS

Fig. 9 shows a phase filter of two foci corresponding to $\beta' = 5\pi$, prepared for a pupil of 30 mm diameter. It was used with a photographic objective of focal length $f = 135$ mm (1 : 4), and a scale placed slanting near the focus of a collimator of focal length $f = 1875$ mm was photographed. The image is shown in Fig. 10. Two foci separated in the image space of the objective are clearly shown.

Fig. 11 shows the result obtained with a phase filter of two foci, of 30 mm diameter, corresponding to $\beta' = 20\pi$ used with a photographic objective of focal length $f = 135$ mm (1 : 4). The pictures of a gatepost and a house shown in (a) have respectively $\pm 20\lambda$ of defocussing.

On the filtered image (b), these two objects are well in focus. But owing to drop in the value of the transfer function in the very low frequency region, contrast of the image is not sufficient.

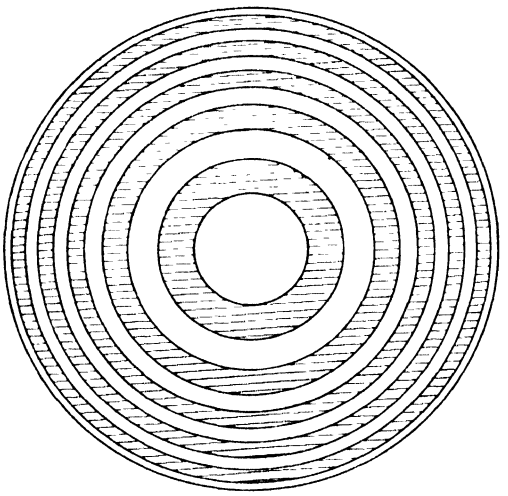

Fig. 9. An example of phase filter of two foci ($\beta' = 5\pi$). Thin film layer of MgF_2 is deposited by vacuum evaporation on hatched zones.

2.8. CONCLUSION

The principles and construction of filters of absorption and phase retarding characteristics and their combination, designed for the compensation of aberrations have been outlined. Such filters are easily prepared. The compensation effect is notable. Such filters could also be used in the ultraviolet and infrared spectral regions.

Filters for compensating effects of defocussing, when used on an ordinary objective, can give two or three independent foci which enable the depth of focus to be increased. An application of the filter of two foci is found in metrology in testing the straightness of lines and edges (UKITA and TSUJIUCHI [1960]).

As explained before, these filters, which change negative and zero values of transfer function into positive values, are useful in metrology in which high resolution is required. However, drop in values of the transfer function in the low frequency region deprives the image of its contrast that is needed in photography.

As will be shown in § 4, the shortcoming of these filters, when used with photo-objectives in particular, can be made up by the use of double diffraction method. This combination of the filters and the double diffraction method is expected to afford further useful applications.

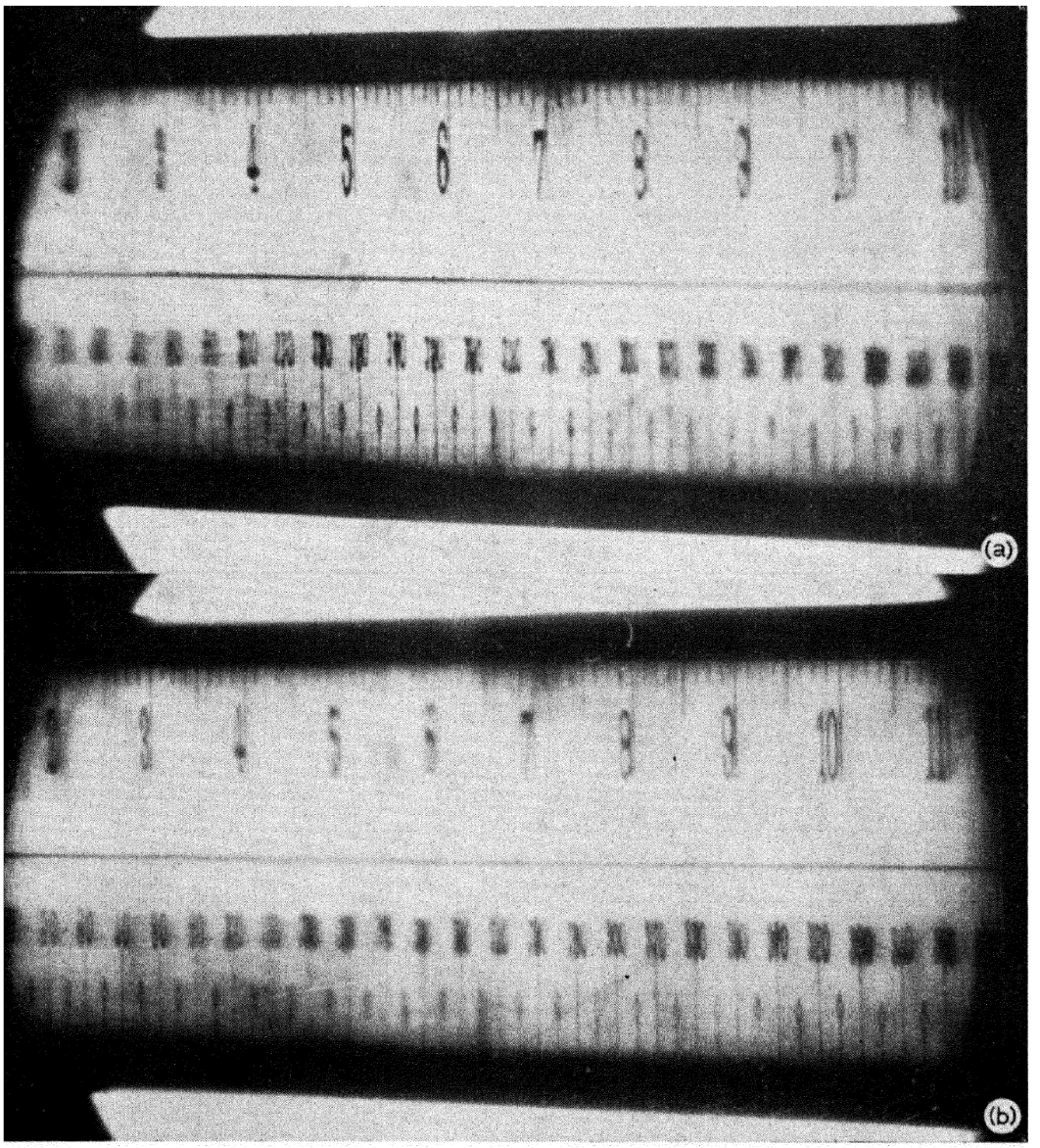

Fig. 10. Separation of focus by the use of filter of two foci
(a) Image by an ordinary objective
(b) Image by the use of filter of two foci

Fig. 11. An example of image obtained by the use of filter of two foci
(a) Image by an ordinary objective with $\beta = \pm 20\pi$
(b) Image by the use of filter of two foci ($\beta' = 20\pi$)

§ 3. Correction of Aberrant Images by Double Diffraction Method

3.1. INTRODUCTION

Another way of correcting aberrant images is by spatial frequency filtering, processed photographically. This method is called the *method of double diffraction.*

Such an application of double diffraction was first studied by MARÉCHAL and CROCE [1953] and by Prof. Maréchal's collaborators. They succeeded in intensifying the photographic image contrast (MARÉCHAL, CROCE and DIETZEL [1958]); correction of double image (CROCE [1956]); elimination of trace of screen mesh from printed image (Mme MARQUET [1959]).O'NEILL [1956] also discussed this method and used it to eliminate optical noise from photographic images.

In the following, theoretical account of this method will be given and illustrated by results of experiments.

3.2. PRINCIPLES OF THE METHOD

Fig. 12 illustrates the optical system with which the image is photographed. (x, y), (u_1, v_1) and (u_2, v_2) are rectangular coordinates set on pupil plane E, object plane I and image plane I′ respectively with

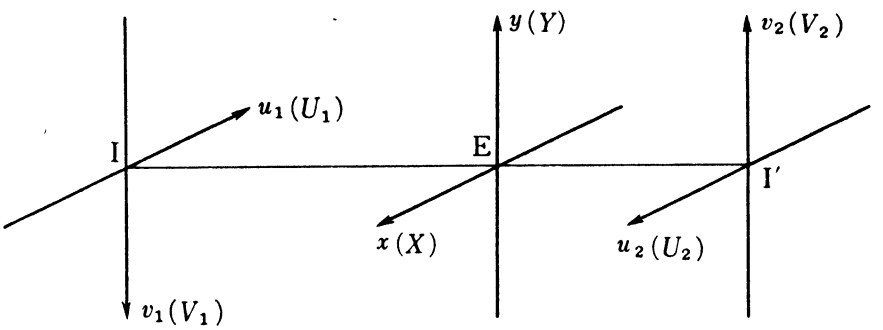

Fig. 12

their origins on the optical axis and the axes x, u_1, u_2 parallel with one another. Let (X, Y), (U_1, V_1) and (U_2, V_2) be the geometrical representations of the coordinates (x, y), (u_1, v_1) and (u_2, v_2) respectively, L the maximum aperture in the E plane, A the distance between I and E, B the distance between E and I′, m_{12} the magnification of the image. Then, similarly to eq. (2.1), we have the following equations

$$\begin{aligned} &x = X/L, && u_1 = k\alpha_1 U_1, && u_2 = k\alpha_2 U_2, \\ &y = Y/L, && v_1 = k\alpha_1 V_1, && v_2 = k\alpha_2 V_2, \\ &U_2/U_1 = V_2/V_1 = m_{12}, && \alpha_1 = L/A, && \alpha_2 = L/B. \end{aligned} \tag{3.1}$$

Consider an object with the light intensity distribution represented by $g(u_1, v_1)$. Its Fourier transformation becomes †

$$G(x, y) = \mathfrak{F}[g(u_1, v_1)], \tag{3.2}$$

and represents the spectral density of the object; (x, y) is called the *spatial frequency*. When the light intensity distribution on the image of a point source on I is represented by $h(u_2, v_2)$, and there is isoplanatism for all the images formed on the I′ plane, the image of $g(u_1, v_1)$ under incoherent illumination is represented by

$$g'(u_2, v_2) = g(u_1, v_1) * h(u_2, v_2), \tag{3.3}$$

where the symbol $*$ represents convolution ††. Then by the theorem of Parseval we have

$$G'(x, y) = G(x, y) \cdot H(x, y), \tag{3.4}$$

where $G(x, y)$, $G'(x, y)$ and $H(x, y)$ are obtained by Fourier transformations of $g(u_1, v_1)$, $g'(u_2, v_2)$ and $h(u_2, v_2)$ respectively.

Here, a photographic negative to record the image $g'(u_2, v_2)$ is considered. For the value of γ to remain constant, contrast of the image must be sufficiently low, and this can be realized if $g(u_1, v_1) + a$ is the light intensity distribution of the object; a is a constant which is sufficiently larger than the amplitude of the fluctuations of $g(u_1, v_1)$. The object $g(u_1, v_1) + a$ gives the image $g(u_1, v_1) * h(u_2, v_2) + a$ except for the peripheral part of the field, and the density distribution of the negative image becomes approximately

$$d(u_2, v_2) = \log_{10} [g'(u_2, v_2) + a]. \tag{3.5}$$

If this negative is placed in a uniform light beam, the distribution of amplitude transmission becomes

$$o(u_2, v_2) = [g'(u_2, v_2) + a]^{-\gamma/2} \tag{3.6}$$

and, as a is sufficiently large in comparison with the amplitude of the fluctuations of $g(u_2, v_2)$, we have finally

$$o(u_2, v_2) = 1 - \frac{\gamma}{2a} [g(u_1, v_1) * h(u_2, v_2)]. \tag{3.7}$$

Double diffraction treatment of this negative is made with the

† $\mathfrak{F}[g(u_1, v_1)] = \int\int_{-\infty}^{+\infty} g(u_1, v_1) \exp [-\mathrm{i}(u_1 x + v_1 y)] \mathrm{d}u_1 \mathrm{d}v_1.$

†† $g(u_1, v_1) * h(u_2, v_2) = \int\int_{-\infty}^{\infty} g(u_1 + u_2, v_1 + v_2) h^*(u_2, v_2) \mathrm{d}u_1 \mathrm{d}v_1.$

arrangement shown in Fig. 13. Point source S has its image S′ formed by a collimator O_1, the negative P to be treated is placed just behind collimator O_1, and correction filter F is placed at the plane of spectra S′. A second collimator O_2 is placed close behind the filter F so as to form the image of P at image plane P′.

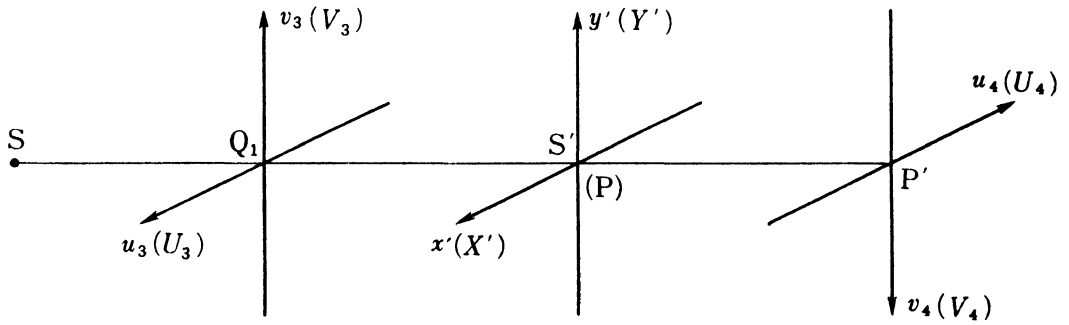

Fig. 13

By setting rectangular coordinates (u_3, v_3), (u_4, v_4) and (x', y') on planes P, P′ and S′ respectively, we have similarly to eq. (3.1)

$$\begin{aligned} x' &= X'/L', \qquad y' = Y'/L', \\ u_3 &= k\alpha_3 U_3, \qquad v_3 = k\alpha_3 V_3, \qquad \alpha_3 = L'/A', \\ u_4 &= k\alpha_4 U_4, \qquad v_4 = k\alpha_4 V_4, \qquad \alpha_4 = L'/B', \\ U_4/U_3 &= V_4/V_3 = m_{34}, \end{aligned} \tag{3.8}$$

where (U_3, V_3), (U_4, V_4) and (X', Y') are geometrical representations of (u_3, v_3), (u_4, v_4) and (x', y') respectively, A' the distance between P and S′ and L' is the maximum radius of F.

If the negative obtained above is so placed that (U_2, V_2) coincides with (U_3, V_3), the following relations hold:

$$\begin{aligned} U_2 &= U_3, \qquad \frac{u_2}{u_3} = \frac{v_2}{v_3} = \frac{\alpha_2}{\alpha_3}, \\ V_2 &= V_3, \qquad \frac{x}{x'} = \frac{y}{y'} = \frac{\alpha_3}{\alpha_2}. \end{aligned} \tag{3.9}$$

The amplitude distribution of the image of S formed on the plane of S′ gives the spectral density of the image recorded on the negative. It may be calculated by the Fraunhofer diffraction formulae and one obtains

$$\begin{aligned} O(x', y') &= \mathfrak{F}[o(u_3, v_3)] \\ &= K(x', y') - \frac{\gamma}{2a}\,\mathfrak{F}[g(u_1, v_1) * h(u_3, v_3)] \\ &= K(x', y') - \frac{\gamma}{2a}\,G(x', y') \cdot H(x', y'). \end{aligned} \tag{3.10}$$

Here $G(x', y')$ is the spectral density of the object, $H(x', y')$ is the transfer function of the objective which is used and

$$K(x', y') = \frac{\sin u_0 x'}{u_0 x'}\,\frac{\sin v_0 g'}{v_0 y'} \tag{3.11}$$

assuming that the negative is of rectangular form of the dimension $2u_0 \times 2v_0$, which is sufficiently large in comparison with the region of distribution of $h(u_3, v_3)$.

When the filter has the amplitude transmission factor $t(x', y')$, the filtered spectrum becomes

$$\begin{aligned} O_F(x', y') &= O(x', y')\, t(x', y') \\ &= K(x', y')\, t(x', y') - \frac{\gamma}{2a}\,G(x', y')\, H(x', y')\, t(x', y'). \end{aligned} \tag{3.12}$$

If $t(x', y')$ is chosen so that

$$H(x', y')\, t(x', y') = \text{const.} \tag{3.13}$$

in the spatial frequency region necessary for the formation of fine image, eq. (3.12) becomes

$$O_F(x', y') = \frac{K(x', y')}{H(x', y')} = \frac{\gamma}{2a}\,G(x', y'). \tag{3.14}$$

As the dimension of the negative is sufficiently large in comparison with the region of distribution of $h(u_3, v_3)$, the region of distribution of $K(x', y')$ is limited to the very narrow region neighbouring the origin of frequency $x' = y' = 0$, and in this region, $H(x, y) = 1$ can be assumed. We then have

$$O_F(x', y') = K(x', y') - \frac{\gamma}{2a}\,G(x', y'). \tag{3.15}$$

The amplitude distribution in the image formed on the plane P′ becomes

$$\begin{aligned} o'(u_4, v_4) &= \mathfrak{F}[O_F(x', y')] \\ &= \text{const.} \times \left[1 - \frac{\gamma}{2a}\,g(u_4, v_4)\right] \end{aligned} \tag{3.16}$$

and photographic emulsion with γ' of the negative placed at the plane P′ records the image, the density distribution of which is represented by

$$d'(u_4, v_4) = \gamma' \log_{10} |o(u_4, v_4)|^2. \tag{3.17}$$

If the developed positive is placed in a uniform light beam the intensity distribution of the image then obtained becomes

$$\begin{aligned} g''(u_4, v_4) &= \text{const.} \times [1 - \frac{\gamma}{2a} g(u_4, v_4)] \\ &= \text{const.} \times [a + \gamma\gamma' g(u_4, v_4)]. \end{aligned} \tag{3.18}$$

The above expression is free from the effect of aberrations; the effect of aberration on the original negative is entirely eliminated. If $\gamma\gamma' = 1$, the expression (3.18) is none other than the intensity distribution of the object except for the magnification of the images.

In order to realize the correction filter, two cases are considered:

i) The case of positive $H(x, y)$

When the transfer function is positive in the frequency region necessary for the formation of fine image, we have from (3.13)

$$t(x', y') = \frac{1}{c} \frac{1}{H(x', y')} \tag{3.19}$$

and this amplitude distribution can be used as a simple absorption filter. Here c is a constant defined by

$$c = 10^{D_0/2}, \tag{3.20}$$

where D_0 is the maximum density at $x' = y' = 0$.

ii) The case of partially negative $H(x, y)$

In a practical optical system, if the aberration or defocussing is somewhat large, it is more appropriate to assume that $H(x, y)$ becomes zero for several frequencies (x_n, y_n) and that it becomes negative in certain regions $(x_n < x < x_{n+1}, y_n < y < y_{n+1})$. The relation (3.19) cannot therefore be valid for such frequencies. It means that the spectral density at (x_n, y_n) cannot pass the objective and the photographed image does not include such components.

For these reasons, such photographic images are useless for the restoration of spectral density of the object. Then a filter is considered, the transmission function of which is defined by eq. (3.19) except for the neighbourhood of (x'_n, y'_n). Fig. 14 shows an example of such a filter in the case of defocussing: (a) represents the transfer function

of an objective with large amount of defocussing, (b) the transmission function of a filter defined by eq. (3.19) except for the neighbourhood of (x'_n, y'_n). If c is a constant defined by eq. (3.20), we obtain the corrected spectrum

$$H_F(x', y') = \begin{cases} 1 & \text{for } |H(x', y')| \geqq 1/c \\ cH(x', y'), & \text{for } |H(x', y')| < 1/c. \end{cases} \tag{3.21}$$

For the region $H(x', y') < 0$, use of a phase filter of discrete phase retardation π (§ 2.5.2) shown in (c) is very effective. A corrected spectrum

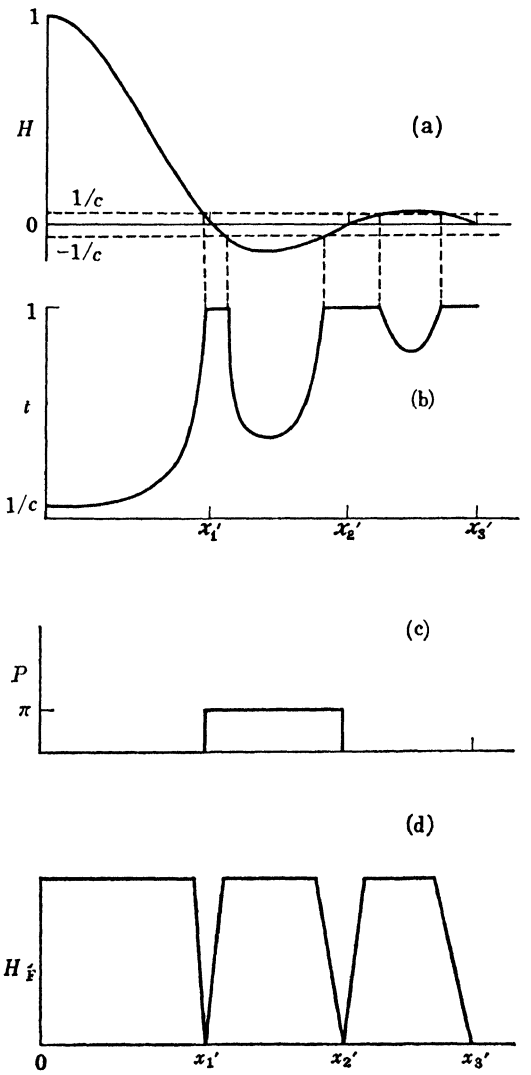

Fig. 14. Correction filter for a partially negative transfer function
(a) Transfer function to be corrected
(b) Amplitude transmission factor of absorption filter
(c) Phase retardation of phase filter
(d) Transfer function corrected by (b) and (c)

by the combination of an absorption and a phase filter is shown in (d). It is seen that the corrected spectrum becomes 1 and the condition (3.17) is satisfied except for the neighbourhood of the frequencies (x'_n, y'_n). But the influence of the discontinuity of spectral density in the neighbourhood of (x'_n, y'_n) on the corrected image has to be considered.

3.3. POSITIVE $H(x, y)$

3.3.1. *Principles*

As an example of a positive transfer function, an astigmatic image (the transfer function of the aberrant direction which is represented by a Gaussian curve sloping downward in the low frequency region) will be examined (TSUJIUCHI [1960a]). Fig. 15 shows the arrangement

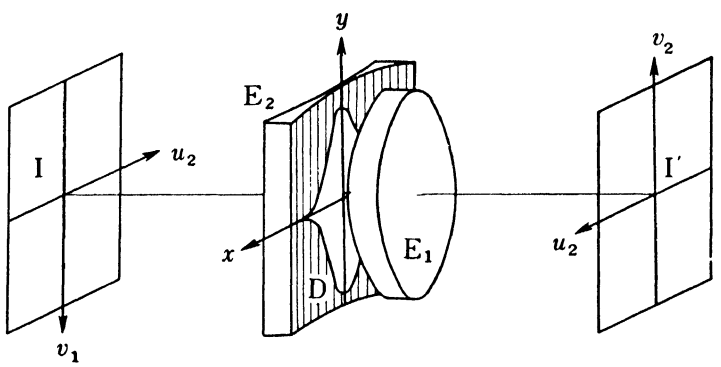

Fig. 15. Optical system for the preparation of a negative which is to be corrected.

for obtaining such an image: it is composed of a well-corrected objective E_1, a cylindrical concave lens E_2 and a diaphragm D with aperture bordered by two curves

$$y = \pm\, \mathrm{e}^{-\pi x^2}, \tag{3.22}$$

the y-axis being taken parallel to the geometrical axis of the cylindrical lens. The image plane is in the position where the image would be formed if the cylindrical lens was removed.

By the approximation of geometrical optics, the point source becomes a line-shaped image along the u_2-axis and its intensity distribution becomes proportional to the aperture of the y-direction of the diaphragm. A brief calculation gives the intensity distribution of the image as

$$h(u_2, v_2) = c' \exp\left[-\pi (f_2/kL^2)^2\, u_2^2\right], \tag{3.23}$$

where $-f_2$ is the focal length of the cylindrical lens and c' is a constant. Then the transfer function becomes

$$\begin{aligned} H(x, y) &= \exp\left[-(1/4\pi)(kL^2/f_2)^2 x^2\right] \\ &= \exp\left[-(1/\pi)(BL/f_2)^2 N^2\right], \end{aligned} \tag{3.24}$$

where N is the spatial frequency in lines/mm defined by

$$x = \frac{\lambda}{\alpha} N. \tag{3.25}$$

If the 'negative' (3.23) is placed at the position P (Fig. 13), the amplitude transmission factor of the filter to be used in this experiment becomes by eqs. (3.8), (3.9) and (3.19)

$$t(X', Y') = \frac{1}{c} \exp\left[(1/4\pi)(kL^2 B/f_2 A')^2 X'^2\right], \tag{3.26}$$

when referred to geometrical coordinates in S' plane (Fig. 13).

As seen from eq. (3.26), the amplitude transmission function of the filter becomes the reciprocal of a Gaussian function, so the filter can be prepared photographically by the method used in the preparation of the negative to be corrected. A long slit along the V-axis is used in place of the object and the same diaphragm as defined by eq. (3.22) is used. If the focal length of the cylindrical lens is $-f_3$ and the distance between the objective and the image plane is B'', the intensity distribution of the image, referred to the geometrical coordinates, is expressed by

$$h'(U', V') = c' \exp\left[-\pi(f_3/LB'')^2 U'^2\right]; \tag{3.27}$$

and the amplitude transmission factor of the filter, prepared photographically by recording the image (3.27), becomes

$$\begin{aligned} t(X', Y') &= \frac{1}{c} \exp\left[\tfrac{1}{2}\pi\gamma(f_3/LB'')^2 X'^2\right], \\ c &= c'^{\gamma''/2} \end{aligned} \tag{3.28}$$

if the emulsion with γ'' is used.

Then the focal length of the cylindrical lens is determined by comparing eq. (3.26) with eq. (3.28),

$$-f_3 = -\frac{1}{2\sqrt{\gamma''}} \frac{kL^2 BB''}{\pi f_2 A'}. \tag{3.29}$$

3.3.2. *Experiments*

According to the conclusion obtained by the theoretical treatment, the following experiment was made:

A photographic objective ($f = 191$ mm, 1 : 7.5), an achromatic cylindrical lens ($-f_2 = -1540$ mm) and a diaphragm defined by eq. (3.22), ($L = 6.5$ mm), were used to prepare the negative to be corrected. As the object, a printed matter with letters of various sizes in low contrast (density contrast : 0.5 and 0.3) was used. The image was recorded on a fine emulsion and developed at $\gamma \doteqdot 1$.

To simplify the experiment, the rough estimate of distance B between the objective and the image plane was made at first so as to obtain numerical data needed for the making of a filter. The density distribution of a filter thus prepared was then measured, and on the basis of this measurement, the correct value of B was determined,

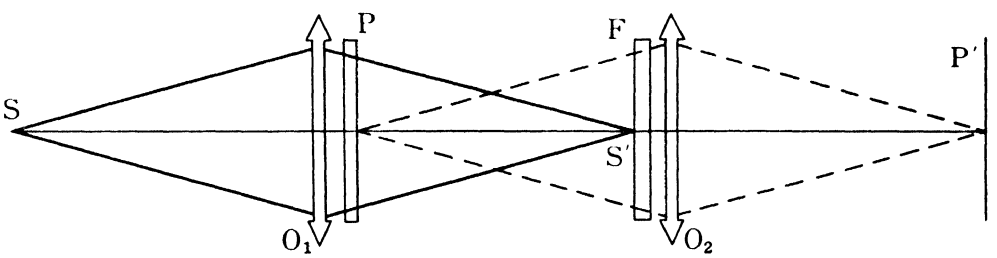

Fig. 16. Double diffraction experiment

with which the negative to be corrected was photographed. With a filter and a negative prepared in this way the experiment on double diffraction was carried out. The arrangement of the experiment is shown in Fig. 16. S is a narrow slit illuminated by a high pressure mercury lamp with a monochromatic filter ($\lambda = 546$ mμ). O_1 is a collimator which forms the image of S on correction filter F placed at S'. Negative P, which is to be corrected, is placed just behind the collimator, and objective O_2, which is placed just behind the filter, and an image of P is formed on the photographic emulsion at P'. The distance A' between P and F was made $A' = 7260$ mm, to enlarge the spectrum which is to be corrected.

The correction filter was prepared by the arrangement shown in Fig. 17. The objective and the diaphragm were those used in the preparation of the negative (Fig. 15). The focal length of the cylindrical concave lens was chosen $-f_3 = -336$ mm, which is close to the value calculated from the relation (3.29) by the use of numerical data of the experiment. The filter pattern was recorded on a fine-grain process plate of $\gamma = 4$

in two stages: first the intensity distribution (3.27); then a uniform density distribution, so as to cut off the foot of sensitometric curve of the emulsion. When the actual distribution of density was measured by a Fabry-Buisson microdensitometer, a small difference of density

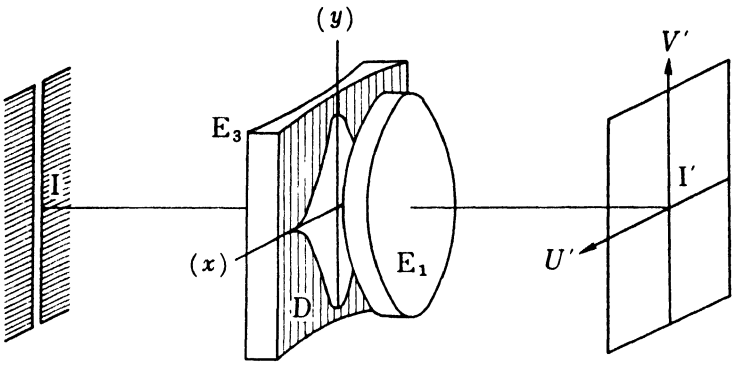

Fig. 17. Optical system for the preparation of a correction filter

distribution was found between the theoretical and measured values. This difference was canceled by changing either the transfer function of the objective or the distance B between the objective and the image in eq. (3.24).The value of B was thus determined as $B = 276$ mm.

Fig. 18 shows the transfer function of the final imaging to be-corrected.

The phase irregularity of the wavefront of the light that passed through type negative or the filter can be avoided by the use of dibutyl phthalate on the emulsion layer as explained in § 2.5.3. By this method, the phase variation was controlled not to exceed $\frac{1}{20}\lambda$.

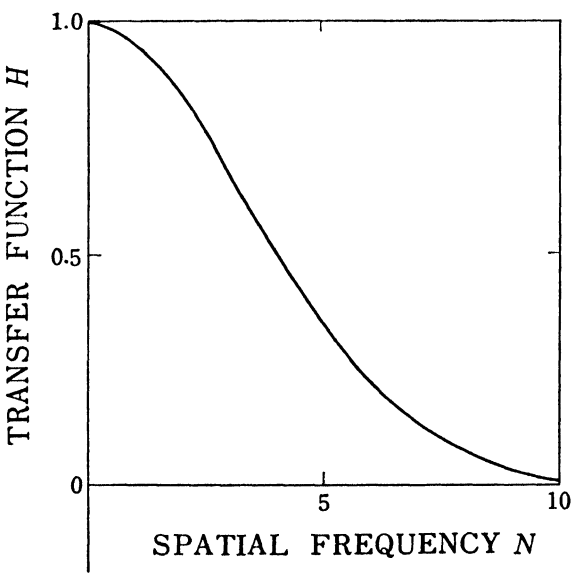

Fig. 18. Transfer function to be corrected in this experiment

3.3.3. *Results of Experiments*

The filter prepared had the amplitude transmission factor

$$t(x', y') = \begin{cases} \dfrac{1}{c} \exp qL'^2x'^2 & |x'| \leqq x'_0, \\ 1 & |x'| > x'_0, \end{cases} \tag{3.30}$$

where

$$c = 10^{D_0/2}, \qquad x' = \sqrt{\frac{\log_e c}{qL'^2}}. \tag{3.31}$$

The spectrum of the image of a point, that is the transfer function of the objective, is given by eq. (3.24) as

$$\begin{aligned} H(x', y') &= \exp\left[-q_0 L'^2 x'^2\right] \\ q_0 &= \frac{1}{4\pi}\left(kL^2/f_2\alpha_2 A'\right)^2, \end{aligned} \tag{3.32}$$

and the corrected spectrum becomes

$$H_F(x', y') = \begin{cases} \exp\left[-(q_0 - q)L'^2x'^2\right] & |x'| \leqq x'_0, \\ c \exp\left[-q_0 L'^2 x'^2\right], & |x'| > x'_0. \end{cases} \tag{3.33}$$

As this equation implies, the effect of the correction depends on the three factors c, $q_0 - q$ and L':

1. c; From eqs. (3.31) and (3.32), the frequency region in which the correction filter is effective is $x' \leqq x'_0$, and for other regions where $x' > x'_0$, the spectrum is left as it is, but as $H_F(x', y')$ is normalized at $x' = y' = 0$ where the spectrum is reduced in intensity by $1/c$, the corrected spectrum acquires a gain by the factor c for the region $x' > x'_0$ (Fig. 19). The filter is effective not only for the region $x' < x'_0$ but also for $x' > x'_0$, though the effect is more or less different. At any rate the correction on spectrum is more effective when c is large. On the other hand, largeness of c means largeness of D_0, the maximum density; difficulty of filter preparation and of visual estimation of the final corrected image make the experiment difficult.

2. $q_0 - q$; The shape of the corrected spectrum is determined by the difference $q - q_0$, and the following three cases are considered:

(1) normal-correction $q_0 = q = 0$

$H_F(x', y')$ becomes 1 for the region $x' < x'_0$, and the spectrum is perfectly corrected in this region (Fig. 19, curve 1).

(2) under-correction $q_0 - q > 0$

$H_F(x', y')$ is still a Gaussian curve though the coefficient becomes smaller for the region of $x' < x'_0$ (Fig. 19, curve 2).

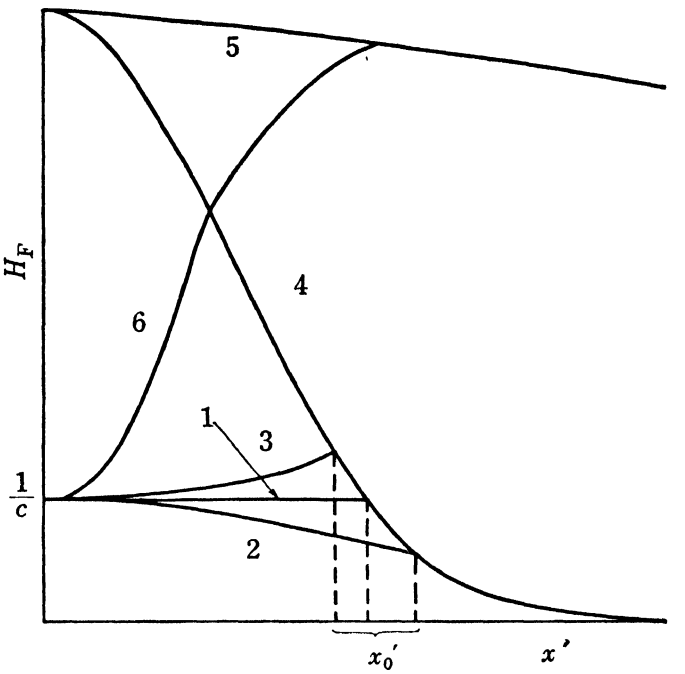

Fig. 19. Correction of a transfer function
1. Normal correction, 2. Under-correction,
3. Over-correction, 4. Original transfer function to be corrected, 5. Transfer function for defects on the negative to be corrected, 6. Transfer function 5 modulated by correction filter

(3) over-correction $q_0 - q < 0$

For the region $x' < x'_0$, $H_F(x', y')$ is no longer a Gaussian curve, and it has a maximum at $x' = x'_0$ where $H_F(x', y')$ is greater than 1 (Fig. 19, curve 3).

Fig. 20 shows the intensity distribution of the corrected images 1, 2 and 3 calculated (approximately) from the corrected spectra 1, 2 and 3 in Fig. 19 respectively. Curve 4 is the intensity distribution of the original image which is

$$h(u_4, v_4) = \exp(-x'_0 u_4 / 4 \log_e c). \tag{3.34}$$

The intensity distribution of the corrected image appears well concentrated in comparison with the original, and the improvement of the image is apparent. However a periodic structure is noticeable especially around the over-corrected image. Such periodic structure

causes parasitic images in bright or dark borders around the final image and impairs the fidelity of the image. In normal-correction, such periodic structure becomes very faint and hardly influences the final image. In under-correction, the periodic structure is almost lost but the correcting effect is not sufficient.

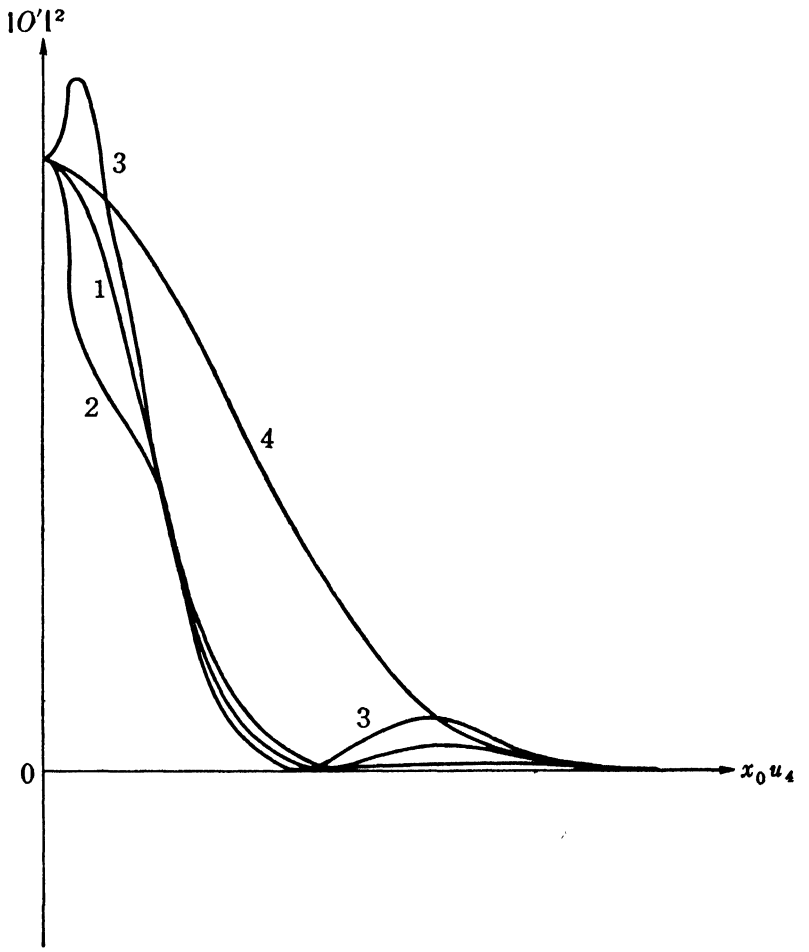

Fig. 20. Intensity distribution in corrected point image
1. Normal correction, 2. Under-correction,
3. Over-correction, 4. Original image to be corrected

3. L'; Another factor affecting the results is the dimension of the correction filter. The spatial frequencies contributing to the original image under incoherent illumination are in the range $x \leqq 2$, and those in the experiment of the double diffraction are in the range $x' \leqq 1$ because of the central coherent illumination. Therefore, the dimension of the filter, sufficient to transmit all the frequencies which

contribute to the forming of original image, is given by

$$L' = 2\frac{A'}{B}. \tag{3.35}$$

But, as the high frequency component is severely attenuated by the aberration of the objective and as the region of frequency $x' < x'_0$ in which the spectrum is effectively corrected is very narrow because of the low value of c, a few times x'_0 suffices in practice for the dimension of the filter.

Fig. 21 shows the corrected images by these experiments: (a) is the original image, (b) is a somewhat over-corrected image, and (c) is the normal corrected image. The faint border around the letters in (b) hardly appears in (c). The restoration of the original letters is conspicuous.

From these experiments we see that the restoration of the image of low contrast objects is achieved more effectively than that of high contrast objects. If the contrast of an object is high in some extent, a filter prepared according to (3.10) is no longer suitable. This is also the case when a very high 'gamma' emulsion is used for the original image formation. In these two cases, the value of q_0 in eq. (3.32) has the tendency to diminish, and over-correction results.

It is also seen that the defects on the negative such as cracks, dust, bubbles and silver grains become very noticeable in the corrected image. As these defects are on the emulsion of the negative on which the aberrant image is recorded, they are not influenced by the transfer function of the objective, that is to say, the spectrum originated from these defects can be regarded as aberration-free (Fig. 19, curve 5). This spectrum is therefore highly over-corrected (Fig. 19, curve 6) and for this reason these defects are very conspicuous; at the same time, a slight phase change that frequently accompanies these defects turns into an amplitude change as if transformed by schlieren method and becomes prominent (FRANÇON [1946]). Probably, this is in part responsible for the defects becoming very much noticeable.

Another example of image correction is shown in Fig. 22.

3.4. PARTIALLY NEGATIVE $H(x, y)$

3.4.1. *Principles*

This case will be illustrated by a defocused image photographed with an aberration-free objective (TSUJIUCHI [1960b]). The polar

coordinate r defined by eq. (2.1) is used in the pupil plane and also as spatial frequency.

For defocussing,

$$kW(r) = 2\beta r^2,$$

the transfer function is, as shown by eq. (2.42), given by

$$H(r) = \frac{2J_1(4\beta r)}{4\beta r}. \tag{3.36}$$

H becomes zero for the frequencies

$$r_n = \mu_n/4\beta, \tag{3.37}$$

where μ_n is the nth positive root of $J_1(x) = 0$, and $H(r)$ becomes negative in the region $r_{2n+1} < r < r_{2(n+1)}$.

The correction filter is prepared as mentioned in § 3.2 by a combination of an absorption filter and a phase filter. If R' is the geometrical representation of the polar coordinate r' in the plane of spectra (S′ in Fig. 13) defined by

$$R' = A' Lr/B, \tag{3.38}$$

the amplitude transmission factor of the correction filter becomes by eqs. (3.19), (3.36) and (3.38)

$$t(R') = \frac{1}{c} \frac{4\beta R'/A'L}{J_1(4\beta R'/A'L)}, \tag{3.39}$$

except for the neighbourhood of R'_n which is calculated by eqs. (3.37) and (3.38). Photographic process is used to prepare the absorption filter. As shown in Fig. 23, a photographic objective E forms the image I′ of a revolving white disc I, on which rectangular coordinates (ξ, η) are taken with O, the center of revolution, as origin. If a pair of curves

$$\eta = \pm e(\xi) \tag{3.40}$$

is drawn on the disc and the surface of the disc is blackened except in the area bordered by these curves, the revolving disc gives a light intensity distribution which is proportional to $|e(\xi)|/\xi$ provided the amplitude of variation of the curve (3.40) is small. Then, choosing the magnification of the image for the unit of (ξ, η) to coincide with that of the geometrical coordinate R' on the plane of the filter, we obtain photographically the absorption filter. The amplitude trans-

mission factor of this filter can be calculated by the formula

$$t(R') = [R'/|e(R')|]^{\gamma/2}. \tag{3.41}$$

The curves to be drawn on the disc from eqs. (3.39) and (3.41) are

$$e(R') = [J_1(4\beta BR'/A'L)]^{-2/\gamma}(4\beta BR'/A'L)^{1-2/\gamma}. \tag{3.42}$$

The phase filter is prepared by vacuum deposition of an evaporated thin film layer on concentric zones where $t(R') < 0$.

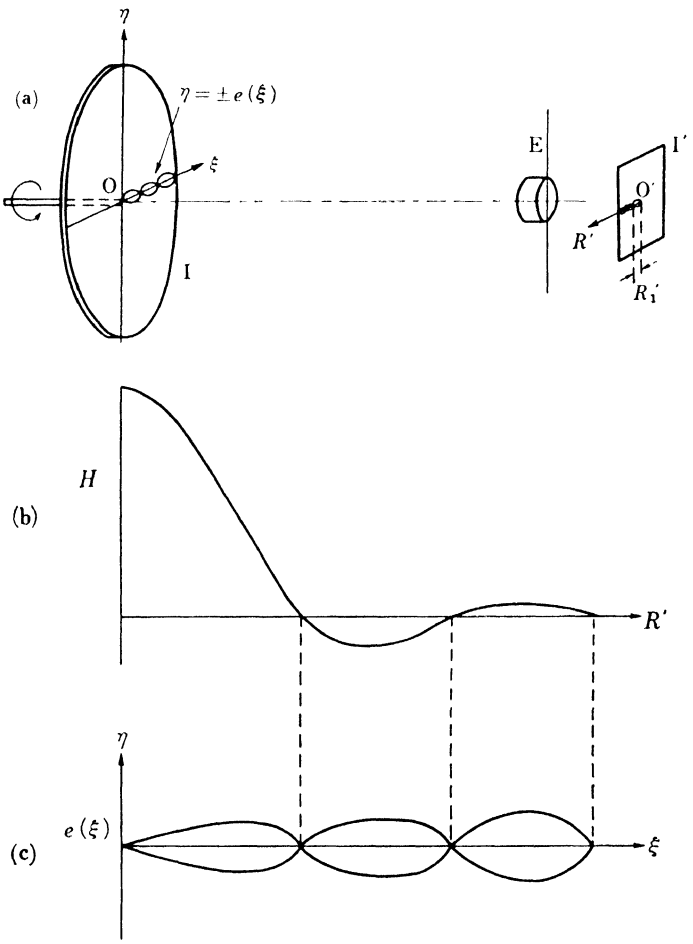

Fig. 23. Preparation of absorption filter
(a) Revolving disc
(b) Transfer function to be corrected
(c) Curves to be drawn on the disc

3.4.2. *Experiments*

According to the principle explained in the preceding § 3.4.1 the following experiments were made:

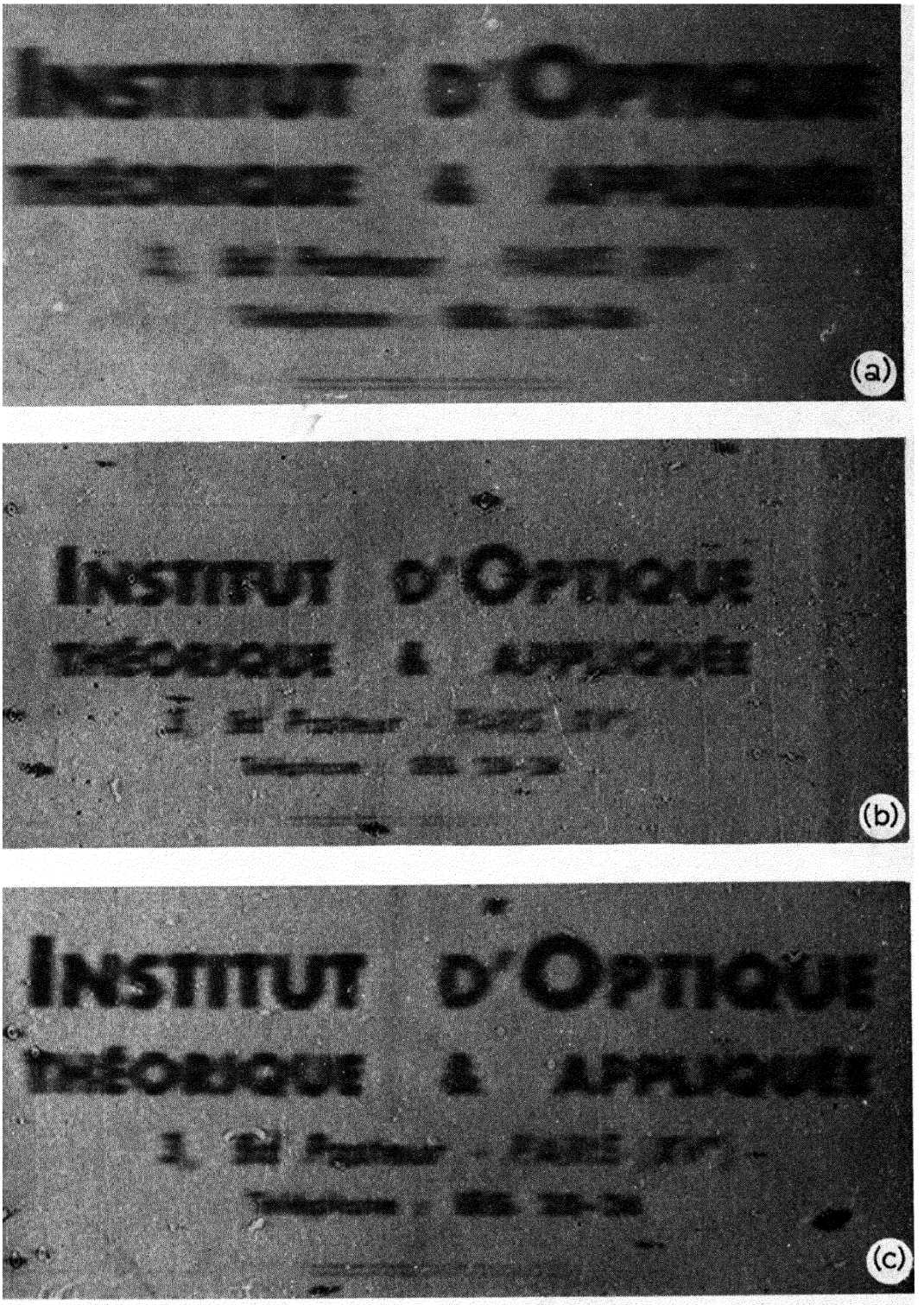

Fig. 21. Results of correction
(a) Original image to be corrected
(b) Somewhat over-corrected image
(c) Normal corrected image

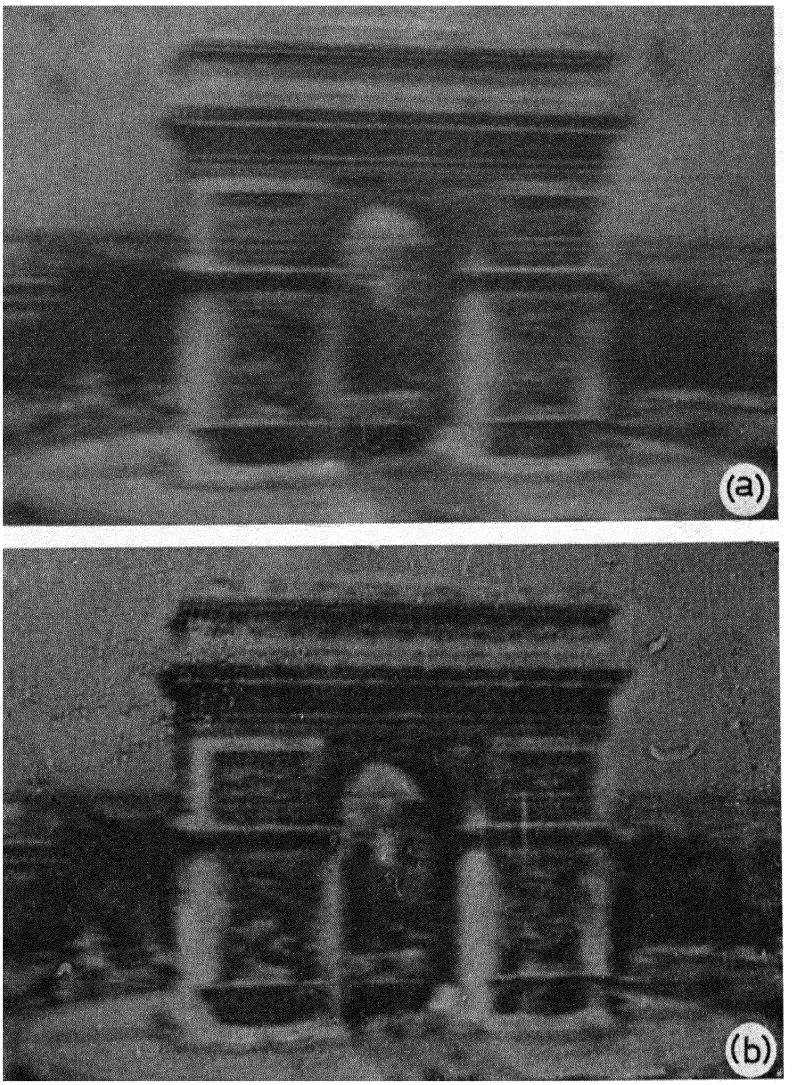

Fig. 22. An example of corrected image
(a) Original image to be corrected
(b) Corrected image

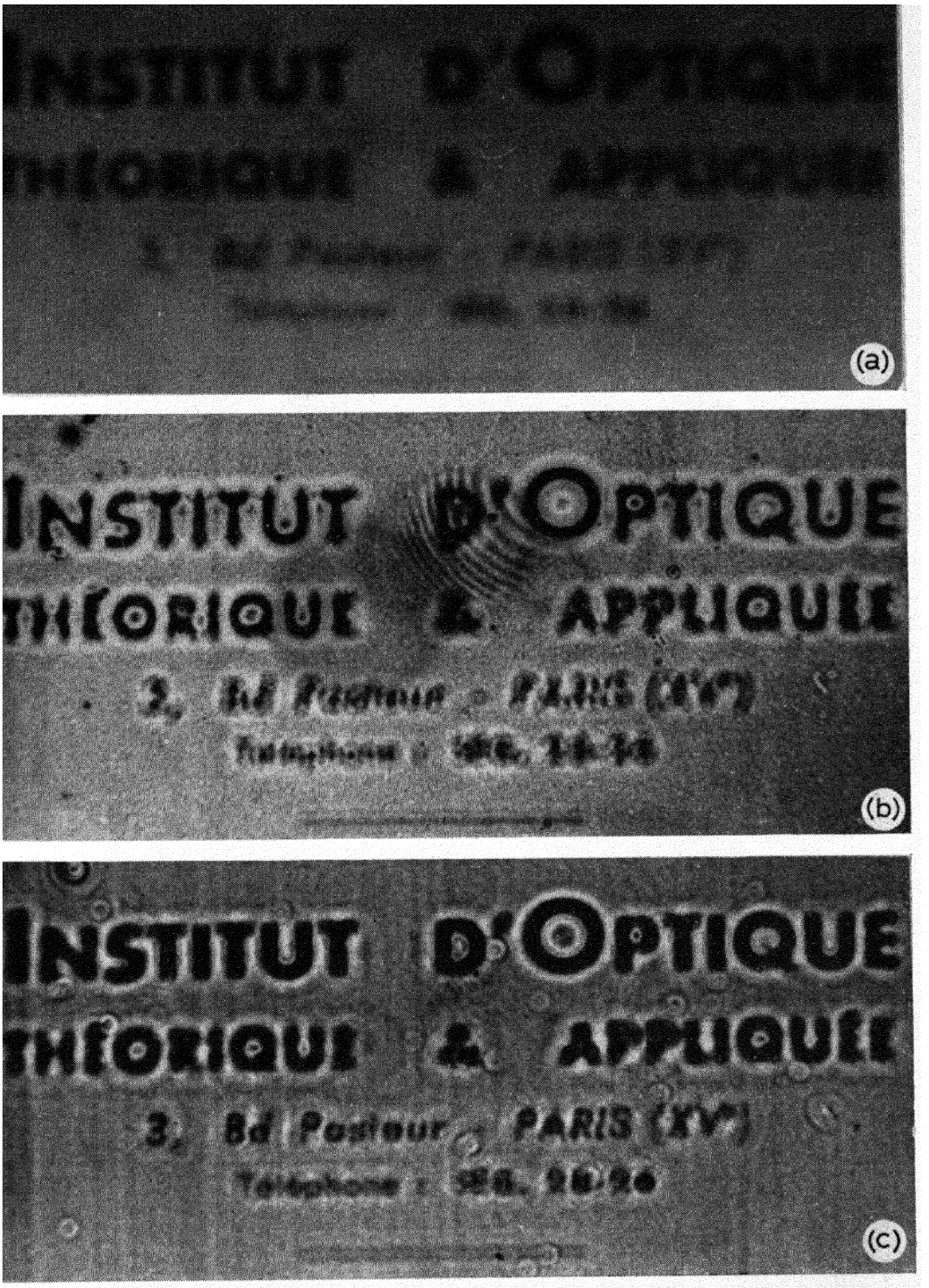

Fig. 29. Results of correction
(a) Original image to be corrected
(b) Corrected image by absorption filter alone
(c) Corrected image by combination of absorption and phase filters

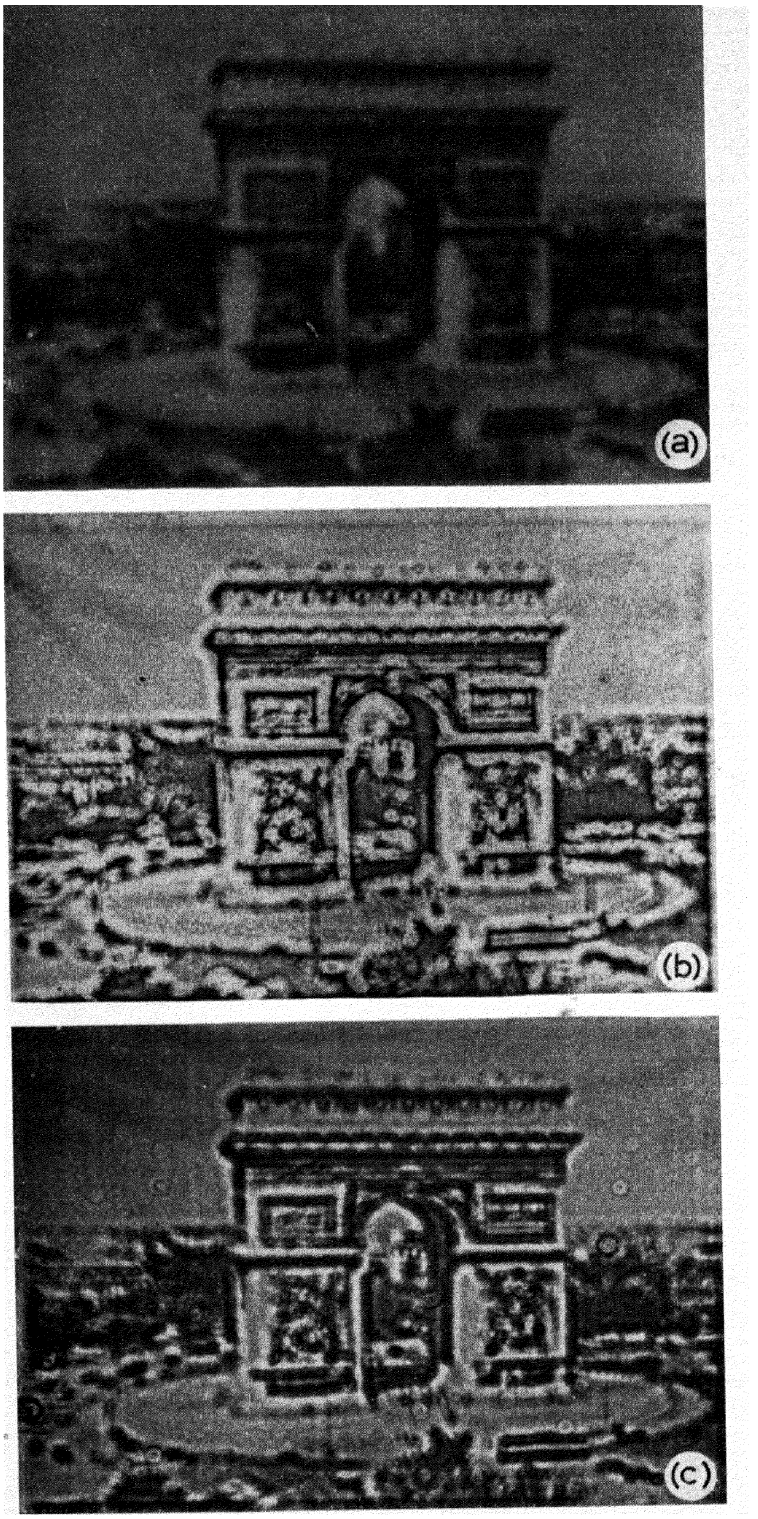

Fig. 31. An example of image correction
(a) Original image to be corrected
(b) Corrected image by absorption filter alone
(c) Corrected image by combination of absorption and phase filters

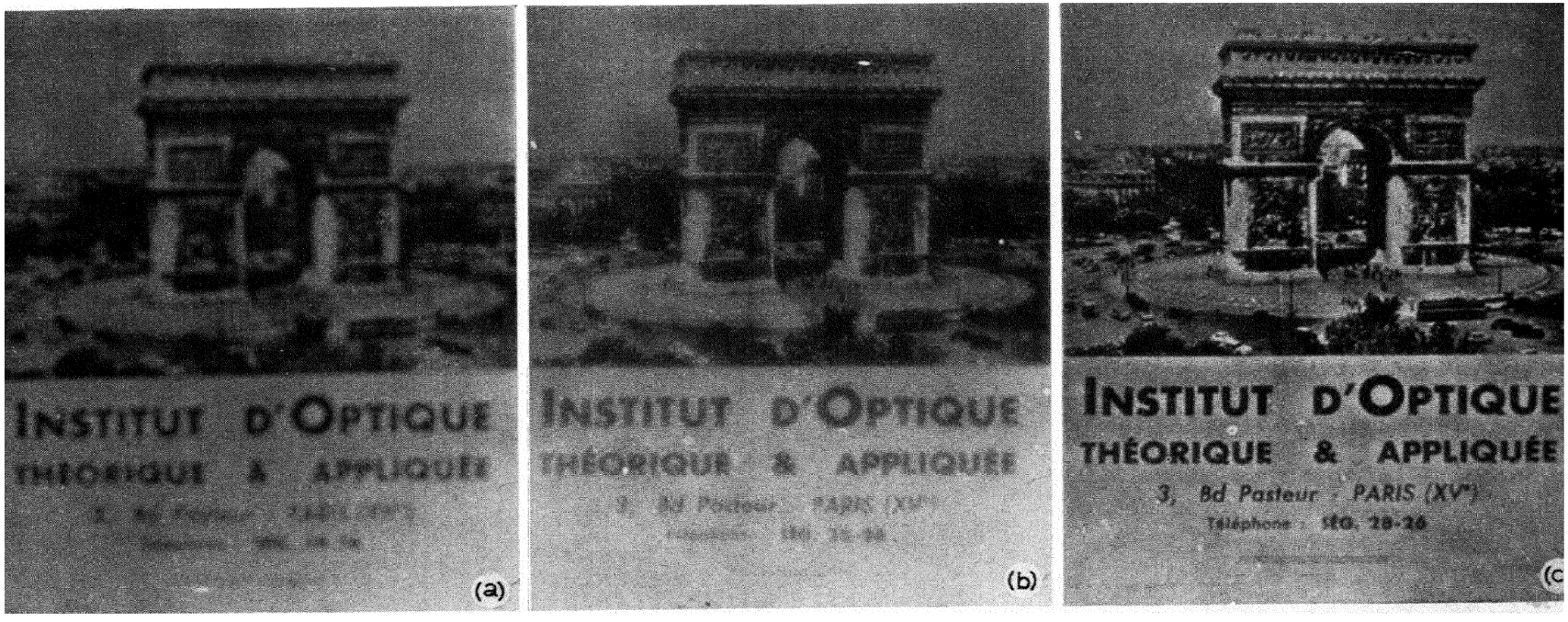

Fig. 33. Results of experiment
(a) Image obtained by a defocused objective
(b) Image obtained by the use of phase filter of two foci compensating defocussing
(c) Image (b) corrected by the method of double diffraction

The original defocused image was obtained by means of a filter of two foci made to compensate the aberration of $\beta = 20\pi$ for $L = 15$ mm. This filter was applied to a well-corrected photographic objective of $f = 200$ mm and $L = 11$ mm with resulting aberration of $\beta = 10.8\pi$. The image plane was placed at the shorter one of the two separated foci. The transfer function is shown in Fig. 24. With the filter removed, some photographs of printed matters of low contrast were taken on a fine grain emulsion of $\gamma = 1$.

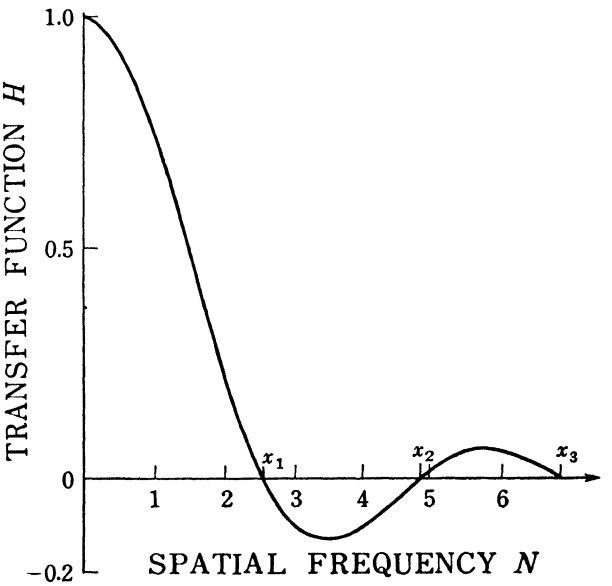

Fig. 24. Transfer function to be corrected

The experiment of double diffraction was made with the apparatus of Institut d'Optique (Paris) in which A, the distance between P and F, is variable (Fig. 16). In this experiment $A = 390$ mm was used and the radii of the zones by which phase change is effected were calculated from eqs. (3.36) and (3.37), corresponding to the experimental conditions

$$R_1 = 0.60 \text{ mm}, \quad R_2 = 1.10 \text{ mm}, \ldots.$$

If an emulsion with $\gamma = 4$ is used, the curves to be drawn on the rotatable disc become

$$e(\xi) = \pm\sqrt{\xi J_1(\xi)}. \tag{3.43}$$

Four pairs of curves

$$\pm\eta = \pm a\sqrt{\xi J_1(\xi)}, \qquad \pm\xi = \pm a\sqrt{\eta J_1(\eta)}, \tag{3.44}$$

were drawn and their image was photographed on a negative which is to be used as the absorption filter. The magnification of the image was so set that the first dark ring R'_1 became 0.60 mm. The filter thus prepared had $D_0 = 1.64$, which corresponded to $1/c = 0.15$. If we set

$$H(R'_0) = 0.15, \tag{3.45}$$

this should give the normal correction for the region $R' \leqq R'_0$ while in the region $R' > R'_0$ the spectrum remains unaltered except for a relative increase of the gain.

As the phase filter, an annular transparent thin film layer with the retardation of π shown in Fig. 25 was used. One annular zone with inner radius R'_1 and outer radius R'_2 sufficed; it corresponded to the correction of the spectrum up to R'_3. The filter was prepared by the method described in § 2.5.2.

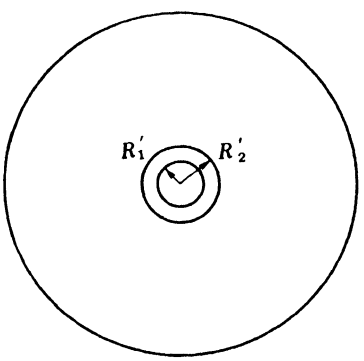

Fig. 25. Phase filter

The above two filters were combined as explained in § 2.5.3 for the double diffraction experiment. As image formation in this case was made under coherent illumination, a small distance between these two filters was allowable, for off-axial rays of light did not cause parallax detrimental to the final corrected image.

The combined filter is shown in Fig. 26. Dibutyl phthalate in thin

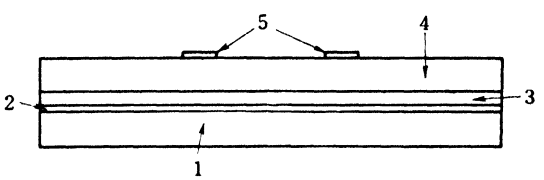

Fig. 26. The correction filter
1. Supporting glass of absorption filter, 2. Emulsion,
3. Layer of liquid, 4. Supporting glass of phase filter, 5. Thin film layer

layer was applied on the emulsion side of the absorption filter, the emulsion side being in contact with the back of the phase filter (§ 2.5.3).

3.4.3. *Results of Experiments*

Fig. 27 shows the modulation of the spectrum of a point image which is the transfer function of the used objective; (a) is the original spectrum

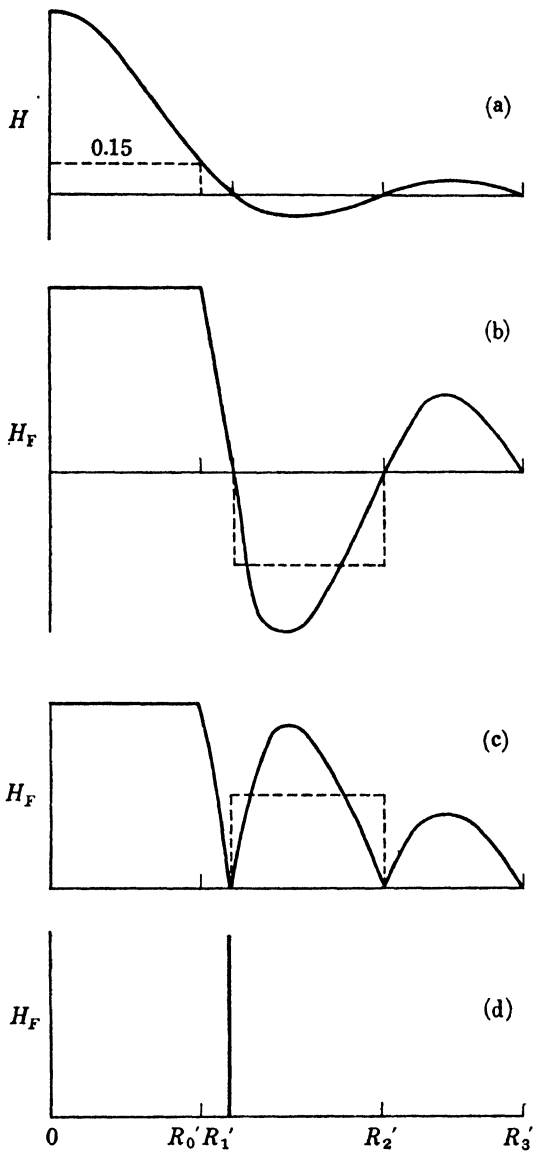

Fig. 27. Correction of the transfer function
(a) Original transfer function to be corrected
(b) Corrected by absorption filter alone
(c) Corrected by combination of absorption and phase filters
(d) Spectrum absent in corrected spectrum

to be corrected, (b) the spectrum corrected by the absorption filter alone and (c) the spectrum corrected by the combination of absorption and phase filters. As described before, normal correction is obtained only in the region $0 \leqq R' \leqq R'_0$, and in the region $R' > R'_0$ the spectrum acquires a gain by the factor c as compared with the original. It is easily understood that such modulation of spectrum improves the image. In Fig. 28, approximate results of the Hankel transfor-

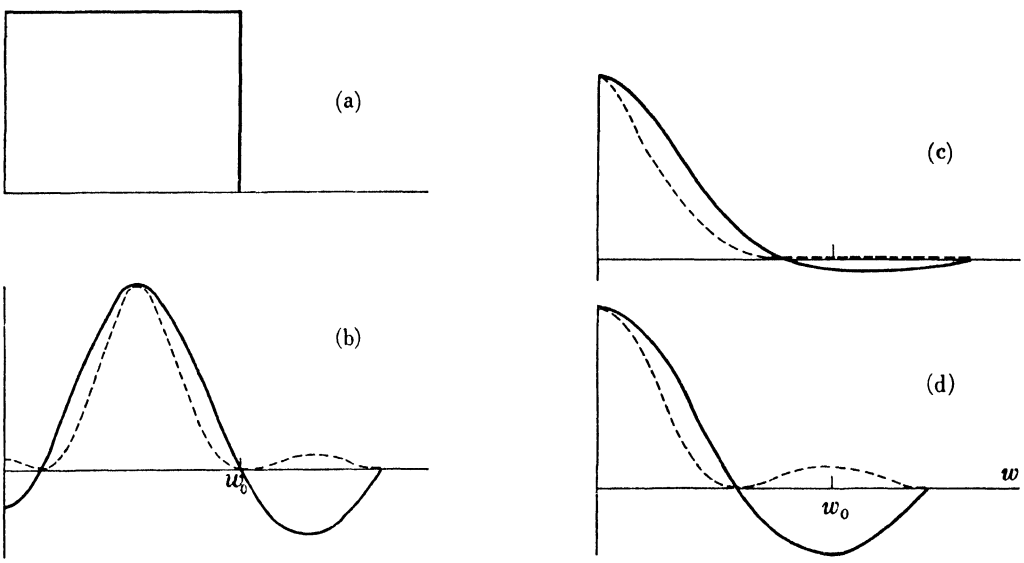

Fig. 28. Characteristics of corrected point image (amplitude distribution in full lines, intensity distribution in dotted lines)
(a) Original image to be corrected
(b) Corrected image by absorptive filter alone
(c) Corrected image by combination of absorption and phase filters
(d) Parasitic image caused by the absence of spectrum

mation of the spectra of Fig. 27 are shown. For the calculation, H_F for the region $R'_1 < R' < R'_2$ was replaced by rectangular variations represented by dotted lines shown in (b) and (c). The dotted lines were so drawn that the areas bordered by them become equal to the areas bordered by the original full curves, and the region $R' > R'_2$ is omitted. (b) is the image obtained by the absorption filter alone, (c) the image obtained by combination of the two filters, and these images were calculated on the assumption no spectrum at R'_1 is missing. The image (b) has similar characteristics to an annular image and the improvement of sharpness cannot be expected. On the other hand, in the image (c) the blur of the image is very much reduced and the improvement of sharpness is apparent.

However, because of the absence of the spectrum at $r_1(R'_1)$, the image

$$\mathfrak{G}[\delta(r - r_1)] = J_0(\mu_n w/4\beta) \tag{3.46}$$

is formed, which has a conspicuous periodic structure. μ_n is the nth positive root of $J_1(x) = 0$. The obtained image is then composed of the images (b) or (c) and (d) in proportion to their spectral densities at r_1 of the object.

The first minimum of eq. (3.46) lies near w_0, the radius of the original defocused image, where the amplitude of (b) or (c) is very small. Hence the periodic structure on the above-mentioned composed image in the neighbourhood of w_0 becomes very apparent. The ratio of (b) or (c) component to (d) component, which indicates how far the image is improved, depends on the maximum density D_0 of the absorption filter and also on the spectral density at r_1 of the object. It can be said that the influence of parasitic image on the final image depends mostly on the spectral density distribution of the object, if D_0 is somewhat large.

Fig. 29 shows the results of the experiment. (a) is the original image to be corrected, (b) corrected image by an absorptive filter alone, (c) corrected image by combination of absorption and phase filters.

In the image (b), the contrast becomes very high, but the improvement is not sufficient: letters are still blurred and appear doubled. But in (c), those letters that are undecipherable in (a) come out clearly.

But as seen in these figures, bright borders appear around the letters. These are the parasitic image owing to the absence of spectrum at R'_1. The intensity distribution across the vertical stroke of the first letter I of 'INSTITUT' in the above three cases was measured and the results are shown as the curves A, B and C in Fig. 30, corresponding to (a), (b) and (c) in Fig. 29 respectively. The bright borders are represented by steep depressions of the curves and it is ascertained that these bright borders originated from the depression of spectrum at R'_1; for their breadths and the spread of the original defocused image are nearly equal.

It should be noted that the parasitic image depends on the difference in size of the letter. This confirms that the parasitic image depends on the spectral density of the object.

Difficulties, arising from variation of the emulsion 'gamma' on which the aberrant image is recorded, and difficulties of the wave-front

of a light beam in passing through negative or filter, can be overcome by the method given in the preceding subsection. The value of 'gamma' must be assured not to differ from that used in calculation, for the dimension of the filter is too small for the density distribution to be obtained by measurement.

Another difficulty which might be expected is due to parallax. In our experiment, however, the absorption filter and the phase filter were separated by the thickness of supporting glass plate of the phase filter which was 2 mm and the aberrant negative was placed at the distance of 390 mm from the filter combination. When, as a test, the

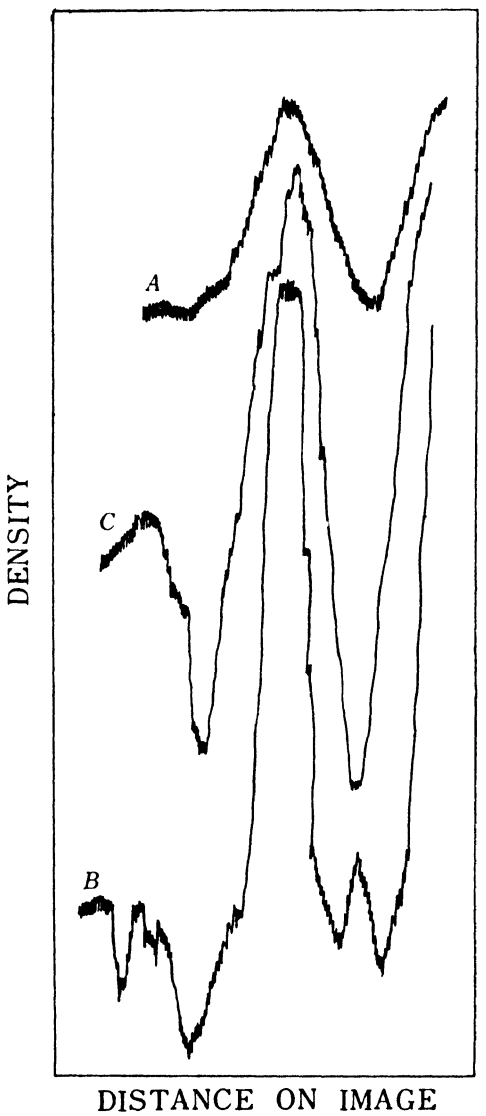

Fig. 30. Density distribution of a corrected image. Microdensitometric recording was made across the letter I of INSTITUT in Fig. 29.
A, B and C correspond respectively to (a), (b) and (c) of Fig. 29.

image of a point source was formed on the absorption filter on one occasion and on the phase filter on another, no difference was found between the two results, which confirmed that the parallax in our case was not worth detailed consideration.

3.5. CONCLUSION

The method of double diffraction was found very effective in correcting photographic images taken by an aberrant system in two cases, namely when the transfer function was positive and when it was partially negative.

An optical system can be regarded as a linear filter of spatial frequencies. In an aberrant system, the transmission characteristic — the optical transfer frunction — for high frequencies becomes low in value and sometimes phase change occurs for some frequencies, impairing the image. In other words, high frequency components in the image become very weak in comparison with low frequencies. This is analogous to the case of communication signals obtained through an electric filter; in such a case the frequency attenuation is also considerable for high frequencies.

In double diffraction experiment, spectral density of the aberrant image gives the Fraunhofer diffraction pattern of the negative, and amplitude distribution of this Fraunhofer pattern, the Fourier spectra of the image, can easily be modulated by a correction filter: an absorption filter reduces the high gain of spectra for low frequencies and a phase filter effects the reversal of the sign of these spectra.

But in the range of frequencies in which the transfer function is zero, the image gives no information on the spectral density of the object; there is no means of obtaining the spectral density from the image. The corrected image will be lacking in components at frequencies at which the transfer function becomes zero and will become more or less different from the original object. Hence the correction cannot be perfect.

On the other hand, for the aberrant image of the positive transfer function, the spectrum components for all frequencies is recorded even though it is attenuated by the aberration of the system employed. The original state of the spectra can be reproduced simply by attenuating the low frequency spectra, and a fine image should be obtained by this method.

As mentioned above, the method of double diffraction can be applied

only to the case of the positive transfer function. But, if we know in advance all about the object to be photographed — how to make up for the loss caused by the transfer function being zero — this method becomes applicable. Consider for example Fig. 29. The appearance of the bright borders around the letters is not serious, for we see at once that the object is an assemblage of letters printed on paper and the letters are those we are familiar with. However, when it comes to pictures such as those shown in Fig. 31 for example, it is usual that we have no previous knowledge about them. Therefore corrected images need to be true to their originals, and the parasitic image is a real parasite.

Furthermore, this method cannot be applied to cases where the imaging is not isoplanatic — defocused background on a portrait for example. Dust, bubbles, defects and the like on the emulsion for example, which also represent departure from isoplanatism, and their effect appears enhanced. Good care in the process of preparation is needed for the image to be free from these, otherwise avoidable, intruders. Application of a suitable liquid on the image negative (§ 3.3.2) to compensate for the thickness irregularity of the emulsion layer that causes phase disturbance is useful in this connection.

It is important to know the transfer function of the objective; this may be determined either from calculation of aberration or by direct measurement. The filter can be prepared in the way explained.

If the aberration represents a considerable amount of defocussing, the transfer function becomes invariant except for special frequencies, and the case can be treated with a single filter, simply by changing the distance between the negative and the filter. This method might possibly be used to make X-ray photographs clear, as though sharply focussed.

§ 4. Use of Aberration Compensating Filter in Double Diffraction Method

4.1. INTRODUCTION

In the preceding sections, two methods of correcting aberrant images were explained. Both methods effect good improvement, yet neither of them is perfect. To improve the correction, one may combine the two methods first by photographing the aberrant image through a compensating filter and then applying the double diffraction method to the resulting image (TSUJIUCHI [1961]).

4.2. PRINCIPLES

If the objective is considerably defocussed, the transfer function becomes of the form represented by curve 1 in Fig. 32. Eqs. (2.37) and (2.40) show that, when the complex filter is used, the transfer function becomes as represented by curve 2; and when the phase filter is used, it becomes as represented by curve 3. It is seen from these results that $H(r)$ becomes about 0.5 or 0.4 for the high frequency region, and information of the spectra which was lost by $H(r)$ becoming zero can be found again by using the aberration compensating filter. For the

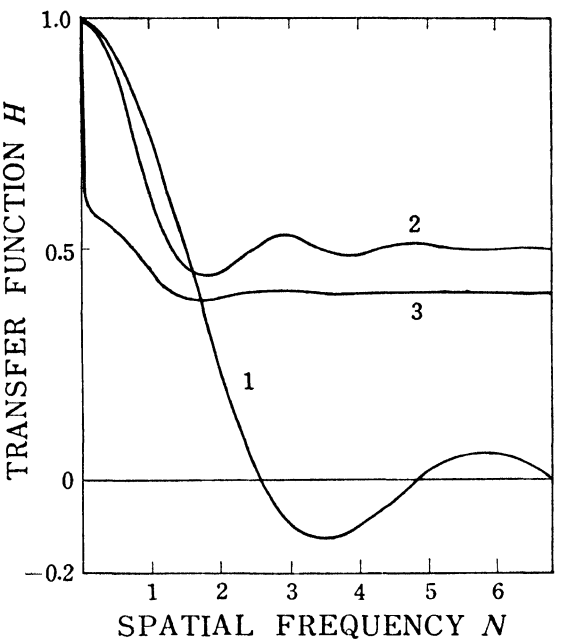

Fig. 32. Transfer functions obtained by the use of filter of two foci
1. Original transfer function of a defocused objective
2. Transfer function improved by the use of complex filter of two foci
3. Transfer function corrected by the use of phase filter of two foci

very low frequency region, the value of the revised transfer function becomes lower than the original, dropping steeply as r becomes higher.

Then if we can arrest this steep drop in value so that $H(r)$ is equalized for all the frequencies which are necessary to form the image, complete correction of the aberrant image can be expected. In this case, as $H(r)$ is always positive, appropriate correction can be made by the use of an absorption filter which lowers the high gain of the spectra in the low frequency region.

As was shown in § 2.4.2 for a defocused system with a phase filter

of two foci, the transfer function is represented by eq. (2.40):

$$H'_t(r) = \left(\frac{2}{\pi}\right)^2 [1 + \sum_{n=1}^{\infty} \left(\frac{1}{2n-1} - \frac{1}{2n+1}\right)^2 H_{2n}(r) + \delta(r)].$$

The last term $\delta(r)$ gives a uniform light distribution in the image. Hence if a photographic material of high γ is used, this term need not be taken into consideration. For $\sum H_{2_n}(r)$, $n = 1$ suffices and the amplitude transmission factor, referred to geometrical coordinates of the filter, is given by eqs. (2.40), (3.19) and (3.38) as

$$t(R') = \frac{\frac{1}{4}\pi - 1}{c} \frac{1}{1 + \frac{4}{9} \frac{2J_1(4\beta BR'/A'L)}{4\beta BR'/A'L}}. \tag{4.1}$$

This filter is easily prepared by using the photographic process given in § 3.4.1. If $\eta = e(\xi)$ is the curve drawn on the revolving disc, the curve $e(R')$ photographed on the filter emulsion is represented by

$$e(R') = \left(\frac{c}{\frac{1}{4}\pi^2 - 1}\right)^{\gamma/2} [4\beta BR'/A'L + \frac{4}{9} \frac{\gamma}{2} 2J_1(4\beta BR'/A'L)]. \tag{4.2}$$

The first term of this equation gives a uniform distribution of absorption, which is a characteristics of the filter; it can be discarded if

$$c \leqq \tfrac{1}{4}\pi^2 - 1, \tag{4.3}$$

and for the region $R' > R'_1$ where $J_1(4\beta B'R'/A'L) = 0$, such absorption is practically unnecessary.

Then we have a curve

$$e(\xi) = J_1(\xi) \tag{4.4}$$

and the curve ending at ξ_1, the first root of eq. $J_1(\xi_1) = 0$, is drawn on the disc.

4.3. EXPERIMENTS AND RESULTS

An objective $f = 200$ mm with a phase filter of two foci ($\beta = 10.9\pi$ $L = 11$ mm) was used to prepare the aberrant image. Under these given conditions, we have the transfer function shown by curve 1 in Fig. 32. An object composed of various letters and an architectural structure were photographed on very fine grain emulsion and developed with $\gamma = 1$. Phase retardation was avoided by applying dibuthyl phthalate on the emulsion side of the negative as explained before.

The double diffraction arrangement was the same as used in § 3.4. The radius R'_1 was obtained numerically from eqs. (3.37) and (3.38) as

$$R'_1 = 0.30 \text{ mm},$$

with which the magnification of the image for preparing the filter was determined.

Four pairs of curves

$$\pm\eta = \pm aJ_1(\xi), \qquad \pm\xi = \pm aJ_1(\eta) \tag{4.5}$$

given by eq. (4.4) were drawn on the disc. The area bordered by these curves were whitened and the rest blackened. With this disc revolving, and with due arrangement to fulfil the conditions $R'_1 = 0.30$ mm and $D_0 = 0.33$ given by eqs. (3.31) and (4.3), the image was photographically recorded.

Fig. 33 shows the results of this experiment: (a) is the intentionally defocused image, (b) the image formed through a phase filter of two foci that matched the objective, and (c) the corrected image obtained by the further use of double diffraction method. Fine details of the original are well restored in (b), but the contrast is very low. Improvement in (c) is striking.

4.4. CONCLUSION

The transfer function which became negative for some frequencies can always be made positive by the use of an aberration compensating filter, and the image obtained can be corrected by the double diffraction method to restore the original detail.

By this combination of the two methods, information on spectral density lost in a region of some frequencies can be found and nearly perfect restoration of original detail can be attained. This combined method shows the possibility of two object planes placed at different distances from the objective being correctly focused. It is applicable not only to the case of defocussing but to all other aberrations overcoming the difficulties met with when either one of the two methods is used singly.

§ 5. Concluding Remarks

We have seen that there are two methods of improving images formed by optical systems which suffer from aberrations: the method in which an aberration compensating filter is used and the method of double diffraction. Each of these methods has its merit and failings. However when the two methods are combined, details that are lost in the image come out well restored.

For image-forming in infrared and ultraviolet regions, well corrected objectives are not easily made because of the lack of suitable materials. In such cases, a negative may first be obtained by a single

objective lens with an aberration compensating filter and can then be corrected by the double diffraction method.

Simultaneous focusing of two or three object planes placed at different distances from the objective can be made by the use of a filter of two or three foci. A negative thus prepared is treated by the double diffraction method to obtain a clear image.

As to filters with special absorption characteristics or special phase retardations for imaging under incoherent illumination, there are a number of studies of considerable interest made by different authors, as mentioned in § 2.1 and § 3.1.

In closing, the writer wishes to emphasize that this article was written with the specific intention of compiling and explaining the means so far known for the correction and improvement on aberrant images so as to restore original detail.

References

CROCE, P., 1956, Rev. d'Opt. ***35***, 569, 642.

Mlle DOSSIER, B. JACQUINOT, A. MARÉCHAL and G. PIEUCHARD, 1951, J. Phys. Rad. [8] ***12***, 142, 565.

Mlle DOSSIER, B., 1954, Rev. d'Opt. ***33***, 57, 147, 267, 552.

ENNOS, A. E., 1960, J. Opt. Soc. Amer. ***50***, 14.

FRANÇON, M., 1946, Rev. d'Opt. ***25***, 257.

JACQUINOT, P., P. BOUGHON and Mlle B. DOSSIER, 1949, La Théorie des Images Optiques (ed. Revue d'Optique, Paris) p. 183.

LANSRAUX, G., 1953a, Diffraction Instrumentale (ed. Revue d'Optique, Paris).

LANSRAUX, G., 1953b, Rev. d'Opt. ***32***, 475.

MARÉCHAL, A. and P. CROCE, 1953, C. R. Acad. Sci. Paris ***237***, 607.

MARÉCHAL, A., P. CROCE and K. DIETZEL, 1958, Opt. Act. ***5***, hors serie 256.

Mme MARQUET, M., 1959, Opt. Act. ***6***, 404.

MIYAMOTO, K., 1961, J. Opt. Soc. Amer. ***51***, 17.

MIYATA, S., S. YANAGAWA and M. NOMA, 1952, J. Opt. Soc. Amer. ***42***, 431.

O'NEILL, E. L., 1956, IRE Trans. **I T-2**, 56.

OSTERBERG, H. and J. E. WILKINS, 1949, J. Opt. Soc. Amer. ***39***, 553.

OSTERBERG, H. and I. C. WISSLER, 1949, J. Opt. Soc. Amer. ***39***, 558.

TSUJIUCHI, J., 1957, J. Phys. Soc. Japan. ***12***, 744.

TSUJIUCHI, J., 1958, Rev. d'Opt. ***37***, 1.

TSUJIUCHI, J., 1960a, Opt. Act. ***7***, 243.

TSUJIUCHI, J., 1960b, Opt. Act. ***7***, 385.

TSUJIUCHI, J., 1961, Opt. Act. ***8***, 161.

UKITA, Y. and J. TSUJIUCHI, 1960, Optics in Metrology (Pergamon Press, London) p. 314.

WILKINS, J. E., 1950, J. Opt. Soc. Amer. ***40***, 222.

ZERNIKE, F. and B. R. A. NIJBOER, 1949, La Théorie des Images Optiques (ed. Revue d'Optique, Paris) p. 227.

V

FLUCTUATIONS OF LIGHT BEAMS

BY

L. MANDEL

Department of Physics, Imperial College, London, England

CONTENTS

§ 1. Historical Introduction

The subject of radiation fluctuations is quite an old one, whose importance has been recognized since the turn of the century; indeed it played a key role in the development of quantum statistics that followed in the period up to 1930. Later, much interest in the subject centred on the practical problem of achieving maximum detectivity in spectrometric investigations. However, with the development of some radically new techniques in the last few years, based on photoelectric detectors and fast electronic circuitry, the field has acquired a new and greatly enhanced significance. In this introductory section we shall briefly summarize the historical background leading to this development.

Like other fluctuation problems concerned with departures from equilibrium, radiation fluctuations in an enclosure can be treated by the methods of statistical mechanics. EINSTEIN [1909a, b] was the first to apply the energy fluctuation formula (cf. FOWLER [1929])

$$\overline{(\Delta E)^2} = kT^2 \frac{\mathrm{d}\bar{E}}{\mathrm{d}T} \tag{1}$$

to black body radiation in an enclosure at equilibrium temperature T. Here E is the total energy of the radiation and $\bar{E}$ the mean energy averaged over a large ensemble of similar systems. $\Delta E = E - \bar{E}$ is the deviation from the mean energy and $\overline{(\Delta E)^2}$ the variance. In the following we shall continue to denote the ensemble mean by a bar.

If equation (1) is applied to the energy $\mathrm{d}E_\nu$ of the radiation lying within a narrow frequency interval $\mathrm{d}\nu$, with $\overline{\mathrm{d}E_\nu}$ given by Planck's distribution law (PLANCK [1901]) for black body radiation in an enclosure of volume V, i.e.

$$\overline{\mathrm{d}E_\nu} = \frac{8\pi\nu^2 \mathrm{d}\nu V}{c^3} \frac{h\nu}{\exp(h\nu/kT) - 1}, \tag{2}$$

then

$$\overline{(\Delta \mathrm{d}E_\nu)^2} = h\nu\,\overline{\mathrm{d}E_\nu}\left[1 + \frac{1}{\exp(h\nu/kT) - 1}\right] = h\nu\,\overline{\mathrm{d}E_\nu} + \frac{c^3}{8\pi\nu^2 \mathrm{d}\nu V}(\overline{\mathrm{d}E_\nu})^2. \quad (3)$$

As Einstein pointed out, the second term alone follows from the classical Rayleigh-Jeans formula for radiation of long wavelengths. On the other hand, the assumption that the total energy is due to classical particles of energy $h\nu$ yields only the first term in (3). The equation (3) therefore appears to be a peculiar hybrid of contributions from classical particles and classical waves.

In the years up to about 1930 the subject of radiation fluctuations was taken up by several workers (EINSTEIN and HOPF [1910]; SMEKAL [1926]; BOTHE [1927]; FÜRTH [1928a, b]). FÜRTH [1928b] made an important generalization in showing that equation (3) can be obtained directly by the application of Bose-Einstein statistics to photons, irrespective of their spectral distribution. However, the treatments all related to a closed system rather than to a propagating light beam. Quite recently BOURRET [1960] has calculated the coherence properties of black body radiation in equilibrium in an enclosure, from which the spatial and temporal correlations of the radiation intensity fluctuations can be obtained.

In the 1940's the development and application of radiation detectors focused attention on the importance of investigating the fluctuations of propagating electromagnetic fields remote from their sources. The first fluctuation studies of BURGESS [1941, 1946] were exclusively concerned with radio waves and the noise induced in radio antennas, but later work by MILATZ and VAN DER VELDEN [1943], LEWIS [1947], JONES [1947] and FELLGETT [1949] on a variety of radiation detectors showed that the fluctuations of the radiation field imposed the ultimate limit of measurement in every case. In particular, it was shown by BURGESS [1941] and later by CALLEN and WELTON [1951], EKSTEIN and ROSTOKER [1955], and WEBER [1956] that the spectral density of the radiation fluctuations obeyed the quantum form of the well-known NYQUIST [1928] formula for JOHNSON [1928] noise. LEWIS [1947], FELLGETT [1949] and JONES [1953] also obtained expressions by a thermodynamic argument for the mean squared fluctuation $\overline{(\Delta n)^2}$ of the number of photon counts n recorded by an illuminated photocell. Although some of these expressions were later shown to be inapplicable, after some discussion (FELLGETT [1957]; TWISS and HANBURY BROWN [1957]; FELLGETT *et al.* [1959]), yet they drew

attention to the fact that the fluctuations of n depart from classical counting statistics and that $\overline{(\Delta n)^2}$ is expressible as the sum of two contributions, in close analogy with equation (3). In a very interesting paper DICKE [1954] examined the coherence and fluctuation properties of the photons emitted by an excited gas and showed how the departures from classical behaviour, such as angular correlation, arise. But, despite these publications, it was some years before the quantum mechanical features of the photo-electric counting fluctuations and their relation to the properties of the incident light were fully appreciated (cf. BRANNEN and FERGUSON [1956]).

In a review article, MACDONALD [1948] considered it "... clear a priori that no information about the energy distribution of the incident photons can be derived ..." from counting measurements with a photo-cell. Yet it now appears that an important method of determining very narrow spectral distributions is based on such measurements. In another review article in 1952 VAN DER ZIEL still regarded all photo-electrons liberated by incident radiation as statistically independent and obeying the Poisson distribution. The subject of output fluctuations of radiation detectors was reviewed and summarized by JONES [1953, 1959] (see also BOLGIANO [1961]).

Up to the early 1950's interest in the field of radiation fluctuations was largely based on the unavoidable limitations which they imposed on the accuracy of radiation measurements. However, in the years 1952–1956 Hanbury Brown and collaborators in the field of radio astronomy developed a new interferometry technique for the determination of angular diameters of radio sources (HANBURY BROWN *et al.* [1952]; HANBURY BROWN and TWISS [1954]; JENNISON and DAS GUPTA [1956]) in which the measurement of radiation fluctuations played a new and essential role. They showed, among other things, that the degree of coherence at two points in a radiation field can be inferred from correlation measurements of the fluctuating signals appearing at radio antennas placed at the two points. In a very effective laboratory experiment HANBURY BROWN and TWISS [1956a] demonstrated that the same principle is applicable to visible light also and that the output fluctuations of two photo-multipliers illuminated by coherent light beams are correlated. In the following years the effect was more thoroughly investigated experimentally by correlation (HANBURY BROWN and TWISS [1957b]; see also HARWIT [1960]) and by pulse counting techniques (TWISS *et al.* [1957]; TWISS and LITTLE [1959]; REBKA and POUND [1957]; BRANNEN *et al.* [1958]) and

applied to the astronomical problem of determining angular diameters of visible stars (HANBURY BROWN and TWISS [1956b, 1958a, b]; RATCLIFFE [1958]; HANBURY BROWN [1960]). More recently it has been shown that the fluctuations of the radiation field carry information, not only about the state of coherence of the field, but also about the state of polarization (WOLF [1960]; MANDEL and WOLF [1961b]; MANDEL [1963a]) and about the spectral distribution (FORRESTER [1961a]; SMITH and WILLIAMS [1962]; MANDEL [1962a]). Moreover measurements of intensity modulations are particularly applicable also to the light from optical masers (JAVAN *et al.* [1961, 1962]; HERRIOTT [1961, 1962]; FORRESTER [1961b]; MCMURTRY and SIEGMAN [1962]) which has rather different statistical properties. With these discoveries the subject of radiation fluctuations has acquired a new enhanced significance.

The observed correlation between the photo-current fluctuations of two photo-electric detectors immediately rules out the possibility that these currents consist of statistically independent pulses (cf. SARD [1946]) corresponding to the arrival of statistically independent photons at the photo-cathodes. PURCELL [1956] was the first to point out that the observed effects could be explained quantitatively in terms of the quantum statistical behaviour of the photons and these considerations were later followed up and extended by HANBURY BROWN and TWISS [1957a], MANDEL [1958, 1959], KAHN [1958] and FANO [1961]. In particular, it was shown that the fluctuations of the counts recorded by a photo-electric detector which is illuminated by light from a thermal source are just those to be expected from a boson assembly. This led to the identification of the natural coherence length (MANDEL [1959] but see also WOLF [1958]; WOODWARD [1953]; MANDEL and WOLF [1962]) and of the degeneracy (GABOR [1950, 1961], MANDEL [1961a, 1962b]) of a photon beam. The significant fluctuation properties were therefore recognized to be quantum statistical.

Nevertheless, as was shown by HANBURY BROWN and TWISS [1957a], WOLF [1957], JANOSSY [1957, 1959], BRACEWELL [1958], and MANDEL and WOLF [1961b] (see also SILLITO [1957]), the wave picture of light is also able to account quantitatively for many of the observed effects. It fails only in accounting for the statistical errors in the measurement of fluctuations and for those effects which, by their nature, are concerned with discrete quantum events. It is therefore convenient to begin by examining the conclusions to be drawn from the wave model

of a light beam. We shall see later that some of its limitations are removed by the introduction of the particle model, which will, of course, account for the discrete events also.

§ 2. The Wave Picture of Light

2.1. REPRESENTATION OF THE WAVE AMPLITUDE

The light waves encountered in nature invariably consist of a superposition of waves of many different frequencies ν lying within some continuous (or piecewise continuous) range $\Delta\nu$. Because there is normally no definite phase relationship between these different frequency components, the resultant real† wave amplitude $V^{(r)}(t)$ must be regarded as a stochastic time function, which can be expanded as a Fourier series in a long interval T in the form:

$$V^{(r)}(t) = \sum_n a_n \cos(2\pi nt/T) + b_n \sin(2\pi nt/T). \tag{4}$$

From the central limit theorem of statistics it might be expected that the superposition of a large number of independent frequency components, as above, will result in a Gaussian random process $V^{(r)}(t)$. Indeed, the use of the expansion (4), in which a_n and b_n are Gaussian random variables, as a representation of light waves was first suggested by RAYLEIGH [1889], who pictured the emission from a light source as a sequence of random wave trains. It was shown by EINSTEIN [1915] (see also EINSTEIN and HOPF [1910]), after some discussion with VON LAUE [1915a, b], that, for a stationary process and for sufficiently long T, the Fourier coefficients of (4) should be regarded as statistically independent Gaussian random variables with the same variance and this has been confirmed by recent work (ROOT and PITCHER [1955]). A more thorough investigation by JANOSSY [1957, 1959] based on this picture also leads to a Gaussian random process.

However this all applies to light produced mainly by spontaneous emission from sources in thermal equilibrium. When the light output is dominated by stimulated emission, as is the case for example in the recently developed optical maser (SCHAWLOW and TOWNES [1958]; MAIMAN [1960, 1961]; COLLINS *et al.* [1960]; WIEDER and SARLES [1961]; SCHAWLOW and DEVLIN [1961]; JAVAN *et al.* [1961] and many

† The superscript in $V^{(r)}(t)$ draws attention to the fact that the function is real, to distinguish it from the complex function which we shall shortly introduce.

others), saturation effects may occur and the fluctuation properties of the light may be quite different. Thus the different Fourier components of maser light are generally not statistically independent (cf. SMITH and WILLIAMS [1962]) and the light cannot be described by a Gaussian random function. At the moment there appears to be no completely adequate classical wave representation of a maser beam, although different aspects of the fluctuation properties of such radiation have been treated by many authors (cf. DICKE [1954], STRANDBERG [1957]; WEBER [1957, 1959]; SHIMODA *et al.* [1957]; SENITZKY [1959, 1960, 1961]; BARRAT *et al.* [1961]; MANDEL [1936]; WOLF [1963]; GLAUBER [1963]). To a first approximation the light probably resembles the output of a phase modulated R.F. oscillator in its statistical features.

Another example of non-thermal light is that produced by the passage of fast moving electrons close to a metallic reflection grating (SMITH and PURCELL [1953]) or through a medium of refractive index appreciably above unity as in the Čerenkov effect (cf. TORALDO DI FRANCIA [1960]).

In the following we shall mainly confine ourselves to treating light from thermal sources and take it for granted that the wave amplitude of a linearly polarized beam may be represented by a stationary Gaussian random time function of zero mean. Moreover the process will be assumed to be ergodic, so that averages over the ensemble of random functions will be equal to the corresponding time averages. For the moment we shall consider only linearly polarized light. The more general case of partial polarization will be treated separately in section 2.4.

It will be convenient to make use of the complex analytic representation of wave amplitudes which was first introduced by GABOR [1946] and has since been used in the development of coherence theory by WOLF [1955] (see also BORN and WOLF [1959]). Consider the truncated wave function $V_T^{(r)}(t)$ which is defined by

$$V_T^{(r)}(t) = \begin{cases} V^{(r)}(t), & \text{for } -\tfrac{1}{2}T \leqq t \leqq \tfrac{1}{2}T \\ 0, & \text{otherwise,} \end{cases}$$

where T is some long time interval. With the real function $V_T^{(r)}(t)$ we now associate another real function $V_T^{(i)}(t)$, which is defined as the Hilbert transform of $V_T^{(r)}(t)$:

$$V_T^{(i)}(t) = -\frac{1}{\pi}\int_{-\infty}^{\infty} \frac{V_T^{(r)}(t')}{t'-t}\,\mathrm{d}t',$$

where it is understood that the principal value of the integral is to be taken. Then the truncated complex wave function is defined by

$$V_T(t) = V_T^{(r)}(t) + iV_T^{(i)}(t)$$

and the complex function $V(t)$ is obtained from $V_T(t)$ by letting $T \to \infty$. The truncated functions are useful because they are of integrable square and therefore have well-defined integral transforms. It can be shown that $V_T(t)$ is an analytic function of t in the upper half of the complex plane (GABOR [1946]; TITCHMARSH [1948]) and that its Fourier transform $A_T(\nu)$ in the frequency domain is zero for negative frequencies† ν. The analyticity is retained also by the auto-correlation function $\Gamma_{11}(\tau)$ of $V(t)$ (BORN and WOLF [1959]), defined by:

$$\Gamma_{11}(\tau) = \overline{V(t+\tau)V^*(t)} = \lim_{T\to\infty} \frac{1}{T} \int_{-\infty}^{\infty} V_T(t+\tau)V_T^*(t)\, dt.$$

If $V_T^{(r)}(t)$ is a Gaussian random process and $V_T^{(i)}(t)$ is obtained from it by a linear transformation, it follows that $V_T^{(i)}(t)$ is also a Gaussian random process. Moreover, by letting $T \to \infty$ and taking averages over the ensemble of $V^{(r)}(t)$, it follows at once that the mean of $V^{(i)}(t)$ is zero also. It is further shown in the Appendix that the auto-correlation functions of $V^{(r)}(t)$ and $V^{(i)}(t)$ are equal and that the values of $V^{(r)}(t)$ and $V^{(i)}(t)$ at the same instant t are uncorrelated. We shall shortly have occasion to make use of these properties.

The optical wave fields encountered in practice are frequently quasi-monochromatic, i.e. the normalized spectral density $\phi_{11}(\nu)$ of the waves, defined by

$$\phi_{11}(\nu) = \Phi_{11}(\nu) \Big/ \int_{-\infty}^{\infty} \Phi_{11}(\nu)\, d\nu$$

and

$$\Phi_{11}(\nu) = \lim_{T\to\infty} \frac{1}{T} (A_T(\nu)\, A_T^*(\nu)),$$

is zero outside a narrow frequency range $\Delta\nu$ centred around some mid-frequency ν_0, with $\Delta\nu \ll \nu_0$. Under these conditions $V(t)$ can be represented as a harmonic oscillation modulated by a slowly varying envelope in the form:

† Note that in the representation used by Wolf (cf. BORN and WOLF [1959]), $V(t)$ is analytic in the lower half t-plane.

$$V(t) = U(t) \exp(2\pi i \nu_0 t), \tag{5}$$

where $U(t)$ is the envelope function, which is nearly constant over any interval short compared with $1/\Delta\nu$. To show this, consider the auto-correlation function $\Gamma_{11}(\tau)$ of $V(t)$, which is well known (cf. RICE [1944, 1945]) to be the Fourier transform of the spectral density $\Phi_{11}(\nu)$:

$$\begin{aligned}\Gamma_{11}(\tau) &= \int_0^\infty \Phi_{11}(\nu) \exp(2\pi i \nu\tau)\, d\nu \\ &= \exp(2\pi i \nu_0 \tau) \int_{-\nu_0}^\infty \Phi_{11}(\nu_0 + \nu') \exp(2\pi i \nu' \tau)\, d\nu'.\end{aligned}$$

If the wave is quasi-monochromatic the integral vanishes for any ν' which is much outside the range $\nu' \lesssim \Delta\nu$. Hence, in this range, $2\pi i \nu' \tau \ll 1$ for any $\tau \ll 1/\Delta\nu$ and it follows that

$$\Gamma_{11}(\tau) = \exp(2\pi i \nu_0 \tau)\, \Gamma_{11}(0) \tag{6}$$

for $\tau \ll 1/\Delta\nu$.

Now consider the auto-correlation function of $U(t)$. From the definition (5),

$$\overline{U(t+\tau)\, U^*(t)} = \exp(-2\pi i \nu_0 \tau)\, \Gamma_{11}(\tau)$$

and from (6),

$$= \Gamma_{11}(0), \tag{7}$$

provided $\tau \ll 1/\Delta\nu$. It follows that $U(t)$ is a slowly varying function which is nearly constant over such short time intervals τ and can therefore be interpreted as the envelope of the wave. From (5) we note that $|V(t)| = |U(t)|$ and $\arg V(t) - 2\pi i \nu_0 t = \arg U(t)$ and both are slowly varying functions. When the light waves are not quasi-monochromatic equation (5) still defines an envelope function, which ceases however to have an easily recognizable interpretation.

2.2. ENVELOPE AND INTENSITY FLUCTUATIONS

Let us now consider the fluctuations of the amplitude $|U(t)|$ of the envelope function. Since $V^{(r)}(t)$ and $V^{(i)}(t)$ are uncorrelated Gaussian random variables, with the same standard deviation σ, say, it follows that the joint probability distribution of $V^{(r)}(t)$ and $V^{(i)}(t)$ is given by

$$\begin{aligned}&p(V^{(r)}(t), V^{(i)}(t))\, dV^{(r)}(t)\, dV^{(i)}(t) \\ &\quad = \frac{1}{2\pi\sigma^2} \exp \frac{-[V^{(r)2}(t) + V^{(i)2}(t)]}{2\sigma^2}\, dV^{(r)}(t)\, dV^{(i)}(t).\end{aligned} \tag{8}$$

Now, from (5), $V(t)$ and $U(t)$ are related by:

$$\begin{aligned} |U(t)|^2 &= |V(t)|^2 = V^{(r)^2}(t) + V^{(i)^2}(t) \\ \arg U(t) &= \arg V(t) - 2\pi\nu_0 t. \end{aligned} \tag{9}$$

The joint probability distribution of $|U(t)|$ and $\arg U(t)$ then follows by a simple transformation to polar variables and we find:

$$p(|U|, \arg U)\, \mathrm{d}|U|\, \mathrm{d}(\arg U) = \frac{1}{2\pi\sigma^2} |U| \exp \frac{-|U|^2}{2\sigma^2} \mathrm{d}|U|\, \mathrm{d}(\arg U). \tag{10a}$$

Since $\arg U$ does not appear explicitly in the probability density it follows that all phase angles in the range $0 \leqq \arg U < 2\pi$ are equally probable and that the distributions of the amplitude $|U|$ and phase $\arg U$ at the same instant are statistically independent. This statistical independence does not, however, hold for the random *processes* $|U(t)|$ and $\arg U(t)$ (see, for example, DAVENPORT and ROOT [1958]; PARZEN and SHIREN [1956]). If we integrate (10a) over all phase angles we obtain the probability distribution of $|U|$ alone:

$$p|U|\, \mathrm{d}|U| = \frac{|U|}{\sigma^2} \exp \frac{-|U|^2}{2\sigma^2} \mathrm{d}|U|, \tag{10b}$$

which is the Rayleigh distribution illustrated in Fig. 1. The most probable value of the amplitude of the envelope is σ.

The instantaneous value of the wave intensity $I(t)$ is defined to be the square of the envelope amplitude:

$$I(t) = |U(t)|^2. \tag{11a}$$

$I(t)$ is therefore a slowly varying function like $U(t)$. It follows from the definition and from (9) that

$$\bar{I} = \overline{U^2} = 2\sigma^2. \tag{11b}$$

By a simple transformation of (10b) we find the probability distribution of the instantaneous intensity $I(t)$:

$$p(I)\, \mathrm{d}I = \frac{1}{\bar{I}} \exp\left(-\frac{I}{\bar{I}}\right) \mathrm{d}I, \tag{12}$$

which is the exponential distribution illustrated in Fig. 1. The nth moment of the distribution is $n!\,\bar{I}^n$ and its variance is $\bar{I}^2$. The corresponding expression $p(I)$ for unpolarized light has been given by

HURWITZ [1945], while the intermediate case of partially polarized light has been treated by BLANC-LAPIERRE [1956] and MANDEL [1963a]. We shall not consider these more general distributions here, although the second moments will be discussed in section 2.4.

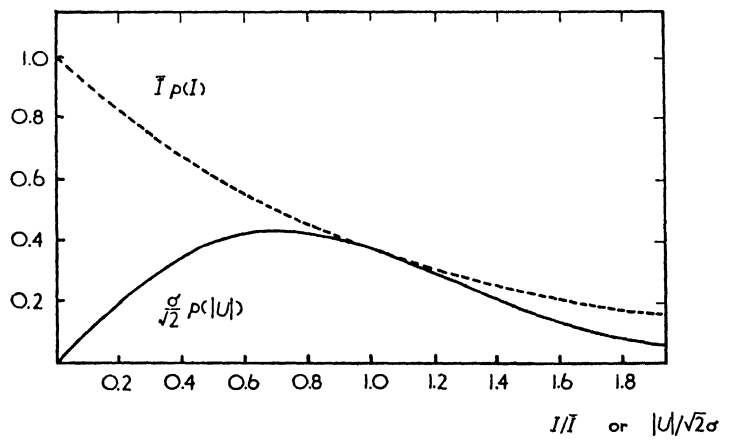

Fig. 1. The probability distributions of $|U|$ and I

It is worth noting that the two distributions (10) and (12) are universal functions depending on only one parameter and independent of the normalized spectral density of the light. In particular, the distributions continue to hold for light of arbitrarily narrow spectral extent, so that the concept of a strictly monochromatic light beam, with wave function $V(t) = \sqrt{2}\sigma \exp(2\pi i\nu t)$, is inadmissible in our representation.

As the frequencies of optical waves ($\sim 10^{15}$ c/sec) exceed the frequency limits of the fastest detectors by several orders of magnitude, the wave functions $V(t)$ are never observed and only the more slowly varying intensities or other quadratic functions of $V(t)$ can be measured experimentally. Moreover, until the recent development of the optical maser, the photon density of beams from conventional light sources was so low (cf. GABOR [1961]; MANDEL [1961a]) that the rapid variations of $V(t)$, and therefore the phase of $U(t)$ (but not phase differences) were, in principle, unobservable (see also GABOR [1950, 1961], HANBURY BROWN and TWISS [1957a]). In the following we shall therefore confine our discussion to the properties of the quadratic functions of $V(t)$, such as the light intensity. The importance of concentrating on the experimental measurables has frequently been emphasized by WOLF [1954a, b, 1955, 1956].

2.3. INTENSITY CORRELATIONS IN PARTIALLY COHERENT FIELDS

Consider two points $\boldsymbol{r}_1$ and $\boldsymbol{r}_2$ in a partially coherent optical field and let the light waves at these points be represented by the complex analytic wave functions $V_1(t)$ and $V_2(t)$. As before, we shall first of all confine ourselves to plane, linearly polarized light. The waves from a very distant source will, of course, be nearly plane.

The cross-correlation or mutual coherence function (cf. ZERNIKE [1938]; HOPKINS [1951, 1953, 1957]; WOLF [1954b, 1955]; BLANC-LAPIERRE and DUMONTET [1955]) of the light at $\boldsymbol{r}_1$ and $\boldsymbol{r}_2$ is defined by:

$$\Gamma_{12}(\tau) = \overline{V_1(t+\tau)\, V_2^*(t)} = \langle V_1(t+\tau)\, V_2^*(t)\rangle,$$

where the angular brackets denote the time average, and the normalized coherence function is:

$$\gamma_{12}(\tau) = \Gamma_{12}(\tau)/\sqrt{(\bar{I}_1\bar{I}_2)},$$

where $\bar{I}_1$ and $\bar{I}_2$ are the mean intensities at $\boldsymbol{r}_1$ and $\boldsymbol{r}_2$. Partial coherence between the light at $\boldsymbol{r}_1$ and $\boldsymbol{r}_2$ implies that there are some values of τ for which $\gamma_{12}(\tau)$ does not vanish. As has been shown (cf. HOPKINS [1951, 1953]; WOLF [1954b, 1955]), $\gamma_{12}(\tau)$ can, in principle, be determined from measurements of the interference fringes resulting from the superposition of the light at $\boldsymbol{r}_1$ and $\boldsymbol{r}_2$. The maximum value of $|\gamma_{12}(\tau)|$ as τ varies is usually known as the degree of coherence (PARRENT [1959], MANDEL and WOLF [1961a]), which has an upper bound of unity (WOLF [1955]).

We shall now show that coherence between the light at $\boldsymbol{r}_1$ and $\boldsymbol{r}_2$ implies a correlation between the intensity fluctuations, from which the degree of coherence can, in principle, be determined. From the definition of the instantaneous intensities,

$$I_1(t) = V_1(t)\, V_1^*(t)$$
$$I_2(t) = V_2(t)\, V_2^*(t),$$

it follows that the cross-correlation function of the intensities is given by:

$$\begin{aligned}\overline{I_1(t+\tau)\, I_2(t)} &= \overline{V_1(t+\tau)\, V_1^*(t+\tau)\, V_2(t)\, V_2^*(t)} \\ &= \overline{V_1^{(r)^2}(t+\tau)\, V_2^{(r)^2}(t)} + \overline{V_1^{(r)^2}(t+\tau)\, V_2^{(i)^2}(t)} \\ &+ \overline{V_1^{(i)^2}(t+\tau)\, V_2^{(r)^2}(t)} + \overline{V_1^{(i)^2}(t+\tau)\, V_2^{(i)^2}(t)}. \qquad (13)\end{aligned}$$

The four real correlation functions appearing on the R.H.S. of (13) can

be separately evaluated from the known probability distributions of $V_1^{(r)}(t)$, $V_2^{(r)}(t)$, etc. As an example consider the first term, in which $V_1^{(r)}(t+\tau)$ and $V_2^{(r)}(t)$ are both Gaussian random variates, with variances $\frac{1}{2}\bar{I}_1$ and $\frac{1}{2}\bar{I}_2$ according to (11), and with the correlation function $\overline{V_1^{(r)}(t+\tau)\,V_2^{(r)}(t)}$. It follows that $\overline{V_1^{(r)^2}(t+\tau)\,V_2^{(r)^2}(t)}$ is given by

$$\overline{V_1^{(r)^2}(t+\tau)\,V_2^{(r)^2}(t)}$$

$$= \int_{-\infty}^{\infty}\int x_1^2 x_2^2 p(x_1, x_2; \tfrac{1}{2}\bar{I}_1, \tfrac{1}{2}\bar{I}_2, \overline{V_1^{(r)}(t+\tau)\,V^{(r)}{}_2(t)})\,dx_1\,dx_2, \tag{14}$$

where $p(x_1, x_2; \frac{1}{2}\bar{I}_1, \frac{1}{2}\bar{I}_2, \overline{V_1^{(r)}(t+\tau)\,V_2^{(r)}(t)})\,dx_1\,dx_2$ is the bivariate Gaussian distribution for the variates x_1 and x_2 with the given parameters. The integral (14) is well known and can be shown to give (see LAWSON and UHLENBECK [1950]; WOLF [1957]; DAVENPORT and ROOT [1958]; BENDAT [1958])

$$\overline{V_1^{(r)^2}(t+\tau)\,V_2^{(r)^2}(t)} = \tfrac{1}{4}\bar{I}_1\bar{I}_2 + 2[\overline{V_1^{(r)}(t+\tau)\,V_2^{(r)}(t)}]^2 \tag{15}$$

and corresponding results hold for the other three terms in (13). Now it is shown in the Appendix that the real correlation functions

$$\overline{V_1^{(r)}(t+\tau)\,V_2^{(r)}(t)}$$

etc. are related to the complex function $\Gamma_{12}(\tau)$ by (cf. BUNIMOVICH [1949]):

$$\begin{aligned}
&\overline{V_1^{(r)}(t+\tau)\,V_2^{(r)}(t)} = \overline{V_1^{(i)}(t+\tau)\,V_2^{(i)}(t)} = \tfrac{1}{2}\mathscr{R}[\Gamma_{12}(\tau)] \\
&-\overline{V_1^{(r)}(t+\tau)\,V_2^{(i)}(t)} = \overline{V_1^{(i)}(t+\tau)\,V_2^{(r)}(t)} = \tfrac{1}{2}\mathscr{I}[\Gamma_{12}(\tau)],
\end{aligned} \tag{16}$$

where $\mathscr{R}[\ ]$ and $\mathscr{I}[\ ]$ denote the real and imaginary parts respectively. By substituting these results in (15) and the three corresponding equations, we finally obtain from (13),

$$\begin{aligned}
\overline{I_1(t+\tau)\,I_2(t)} &= \bar{I}_1\bar{I}_2 + |\Gamma_{12}(\tau)|^2 \\
&= \bar{I}_1\bar{I}_2[1 + |\gamma_{12}(\tau)|^2].
\end{aligned} \tag{17}$$

We may also express this result in the form of a correlation between the fluctuation of I_1 and I_2 about their mean values $\bar{I}_1$ and $\bar{I}_2$. If $\Delta I_1(t)$ and $\Delta I_2(t)$ denote the instantaneous deviations $I_1(t) - \bar{I}_1$ and $I_2(t) - \bar{I}_2$, then

$$\overline{\Delta I_1(t+\tau)\,\Delta I_2(t)} = \overline{I_1(t+\tau)\,I_2(t)} - \bar{I}_1\bar{I}_2$$
$$= \bar{I}_1\bar{I}_2\,|\gamma_{12}(\tau)|^2, \tag{18}$$

from (17). Thus, it appears that, as long as there is some coherence between the light at $\boldsymbol{r}_1$ and $\boldsymbol{r}_2$, there will be correlation between the intensity fluctuations. Moreover, the degree of coherence between points in an optical field can be explored by measuring intensity correlations as well as by examining interference fringes. This result is at the basis of correlation interferometry.

When the points $\boldsymbol{r}_1$ and $\boldsymbol{r}_2$ coincide, (17) reduces to the autocorrelation function of the intensity:

$$\overline{I_1(t+\tau)\,I_1(t)} = \bar{I}_1^2\,[1 + |\gamma_{11}(\tau)|^2], \tag{19}$$

while (18) becomes:

$$\overline{\Delta I_1(t+\tau)\,\Delta I_1(t)} = \bar{I}_1^2\,|\gamma_{11}(\tau)|^2. \tag{20}$$

In particular, for $\tau = 0$ we find the variance

$$\overline{(\Delta I_1)^2} = \bar{I}_1^2, \tag{21}$$

in agreement with the result obtained directly from the distribution (12).

2.4. THE EFFECT OF PARTIAL POLARIZATION

So far the discussion has been strictly applicable to linearly polarized light only. We shall now attempt to remove this rather strong restriction, since the light encountered in practice is usually only partially polarized or unpolarized.

A satisfactory description of a partially polarized beam, within the framework of coherence theory, appears to be a quite recent achievement. Although the first quantitative treatment of polarized light was given by Stokes in 1852, a proper understanding of the significance of the Stokes parameters for light of finite spectral range largely followed the introduction of the statistical ideas of coherence theory and of the 2×2 polarization or coherence matrix (FANO [1949, 1954]; FALKOFF and MACDONALD [1951]; WOLF [1954a, 1956, 1959]; PANCHARATNAM [1956, 1961]; WESTFOLD [1959]; ROMAN [1959]; PARRENT and ROMAN [1960]; MCMASTER [1961]). As has been pointed out (FALKOFF and MACDONALD [1951]; FANO [1954]; WOLF [1954a]; etc.); this matrix is closely related to the quantum mechanical density matrix (TOLHOEK [1956]; FANO [1957]; TER HAAR [1961]) for the

description of mixed states (compare also GABOR [1956]; GAMO [1957]). While the 2 × 2 polarization matrices are sufficient for the treatment of plane light waves, more general 3-dimensional Cartesian tensors are needed for dealing with waves of arbitrary form. These were first introduced by WOLF [1954a, 1956] and further developed by ROMAN and WOLF [1960a, b] and ROMAN [1961]. In the following we shall however confine ourselves to a discussion of plane light waves.

It will be convenient to make use of a slightly expanded notation. With each point $\boldsymbol{r}$ in a light beam we associate two scalar analytic wave functions $V_x(\boldsymbol{r}, t)$ and $V_y(\boldsymbol{r}, t)$, which represent the disturbances (electric vectors) in two perpendicular directions normal to the direction of propagation. With any two points $\boldsymbol{r}_1$ and $\boldsymbol{r}_2$ in an optical field we can then associate four cross-correlation functions:

$$\overline{V_x(\boldsymbol{r}_1, t+\tau)\, V_x^*(\boldsymbol{r}_2, t)} = \Gamma_{xx}(\boldsymbol{r}_1, \boldsymbol{r}_2, \tau)$$

$$\overline{V_x(\boldsymbol{r}_1, t+\tau)\, V_y^*(\boldsymbol{r}_2, t)} = \Gamma_{xy}(\boldsymbol{r}_1, \boldsymbol{r}_2, \tau)$$

$$\overline{V_y(\boldsymbol{r}_1, t+\tau)\, V_x^*(\boldsymbol{r}_2, t)} = \Gamma_{yx}(\boldsymbol{r}_1, \boldsymbol{r}_2, \tau)$$

$$\overline{V_y(\boldsymbol{r}_1, t+\tau)\, V_y^*(\boldsymbol{r}_2, t)} = \Gamma_{yy}(\boldsymbol{r}_1, \boldsymbol{r}_2, \tau),$$

for which we have used an obvious extension of our notation. These functions can be regarded as the elements of a τ-dependent correlation matrix $J_{12}(\tau)$ (see MANDEL and WOLF [1961b]; MANDEL [1963a]) defined by:

$$J_{12}(\tau) = \begin{bmatrix} \Gamma_{xx}(\boldsymbol{r}_1, \boldsymbol{r}_2, \tau) & \Gamma_{xy}(\boldsymbol{r}_1, \boldsymbol{r}_2, \tau) \\ \Gamma_{yx}(\boldsymbol{r}_1, \boldsymbol{r}_2, \tau) & \Gamma_{yy}(\boldsymbol{r}_1, \boldsymbol{r}_2, \tau) \end{bmatrix}, \tag{22}$$

which is a generalization of the matrix $J_{11}(0)$ introduced by WOLF [1954a, 1956, 1959] and also discussed by PARRENT and ROMAN [1960]. They showed that the expectation value $\bar{A}$ of a physical observable A connected with the light at any point, which can be represented by a 2 × 2 matrix, is given by:

$$\bar{A} = \mathrm{Tr}\,[A J_{11}(0)]. \tag{23}$$

Even when the points $\boldsymbol{r}_1$ and $\boldsymbol{r}_2$ coincide and when $\tau = 0$, the matrix (22) is not uniquely defined until the directions of the x and y axes are specified. The maximum value of the degree of coherence (cf. MANDEL and WOLF [1961a]) between the x and y components of the wave is the degree of polarization P (cf. WOLF [1959]; PARRENT

and ROMAN [1960]), which may be expressed in terms of the rotational invariants of the matrix $J_{11}(0)$ in the form:

$$P = \sqrt{\left[1 - \frac{4\,|J_{11}(0)|}{\mathrm{Tr}^2\,[J_{11}(0)]}\right]}, \tag{24}$$

where $|J_{11}(0)|$ is the determinant of the matrix. It is characteristic of natural or unpolarized light that the off-diagonal elements of $J_{11}(\tau)$ vanish for all directions of the axes, while the diagonal elements are always equal, so that $\mathrm{Tr}^2\,[J_{11}(0)] = 4\,|J_{11}(0)|$ and $P = 0$.

Now consider the instantaneous intensity $I(\boldsymbol{r}, t)$ at a point $\boldsymbol{r}$ in a partially polarized beam of light. From the definitions of $V_x(\boldsymbol{r}, t)$ and $V_y(\boldsymbol{r}, t)$ it follows that

$$I(\boldsymbol{r}, t) = |V_x(\boldsymbol{r}, t)|^2 + |V_y(\boldsymbol{r}, t)|^2,$$

which may be written

$$I(\boldsymbol{r}, t) = I_x(\boldsymbol{r}, t) + I_y(\boldsymbol{r}, t), \tag{25}$$

where $I_x(\boldsymbol{r}, t)$ and $I_y(\boldsymbol{r}, t)$ are the partial intensities associated with the x and y components of the electromagnetic wave. Now from the results of the previous section, particularly from equation (18), it follows that, as long as the degree of coherence $|\gamma_{xy}(\boldsymbol{r}, \boldsymbol{r}, 0)|$ between the x and y components

$$|\gamma_{xy}(\boldsymbol{r}, \boldsymbol{r}, 0)| = \frac{|\Gamma_{xy}(\boldsymbol{r}, \boldsymbol{r}, 0)|}{\sqrt{(\bar{I}_x(\boldsymbol{r})\,\bar{I}_y(\boldsymbol{r}))}} \tag{26}$$

does not vanish, there will be correlation between the fluctuations of $I_x(\boldsymbol{r}, t)$ and $I_y(\boldsymbol{r}, t)$, given by

$$\overline{\Delta I_x(\boldsymbol{r}, t)\,\Delta I_y(\boldsymbol{r}, t)} = \bar{I}_x(\boldsymbol{r})\,\bar{I}_y(\boldsymbol{r})\,|\gamma_{xy}(\boldsymbol{r}, \boldsymbol{r}, 0)|^2. \tag{27}$$

Thus, by splitting a beam of light with a half silvered mirror and correlating the intensity fluctuations emerging from mutually orthogonal polarizers placed in each beam, $|\gamma_{xy}(\boldsymbol{r}, \boldsymbol{r}, 0)|$ can be measured. The maximum value of $|\gamma_{xy}(\boldsymbol{r}, \boldsymbol{r}, 0)|$ as the polarizers are rotated, while remaining orthogonal, is the degree of polarization P.

Most frequently, however, particularly in the astronomical applications of correlation methods, the light beams to be correlated are not fully polarized. We must therefore generalize our results so as to include this possibility. By using (25), we can expand the intensity cross-correlation function at two points $\boldsymbol{r}_1$ and $\boldsymbol{r}_2$ in an optical field as follows:

$$\overline{I(\boldsymbol{r}_1, t+\tau)\, I(\boldsymbol{r}_2, t)} = \sum_i \sum_j \overline{I_i(\boldsymbol{r}_1, t+\tau)\, I_j(\boldsymbol{r}_2, t)}, \tag{28}$$

where i, j stand for the labels x, y. But, from the general relation (17),

$$\overline{I_i(\boldsymbol{r}_1, t+\tau)\, I_j(\boldsymbol{r}_2, t)} = \bar{I}_i(\boldsymbol{r}_1)\, \bar{I}_j(\boldsymbol{r}_2) + |\Gamma_{ij}(\boldsymbol{r}_1, \boldsymbol{r}_2, \tau)|^2,$$

so that

$$\overline{I(\boldsymbol{r}_1, t+\tau)\, I(\boldsymbol{r}_2, t)} = \bar{I}(\boldsymbol{r}_1)\, \bar{I}(\boldsymbol{r}_2) + \sum_i \sum_j |\Gamma_{ij}(\boldsymbol{r}_1, \boldsymbol{r}_2, \tau)|^2 \tag{29a}$$

and

$$\begin{aligned}\overline{\Delta I(\boldsymbol{r}_1, t+\tau)\, \Delta I(\boldsymbol{r}_2, t)} &= \sum_i \sum_j |\Gamma_{ij}(\boldsymbol{r}_1, \boldsymbol{r}_2, \tau)|^2 \\ &= \sum_i \sum_j \bar{I}_i(\boldsymbol{r}_1)\, \bar{I}_j(\boldsymbol{r}_2)\, |\gamma_{ij}(\boldsymbol{r}_1, \boldsymbol{r}_2, \tau)|^2. \end{aligned} \tag{29b}$$

These are the generalizations of equations (17) and (18). Although the x, y directions appear explicitly on the R.H.S., the equations are, of course, independent of the choice of axes. This can be seen by writing (29b) in the form:

$$\overline{\Delta I(\boldsymbol{r}_1, t+\tau)\, \Delta I(\boldsymbol{r}_2, t)} = \mathrm{Tr}\, [J_{12}(\tau)\, J_{12}^{\dagger}(\tau)], \tag{30}$$

where $J_{12}^{\dagger}(\tau)$ is the Hermitian conjugate of $J_{12}(\tau)$. Equation (30) shows at once that the intensity correlation does not depend on the choice of x, y axes, since it is given by the trace of a Hermitian matrix.

As a first application of equations (29) suppose that the two partially coherent beams are completely unpolarized. Then $|\gamma_{ij}(\boldsymbol{r}_1, \boldsymbol{r}_2, \tau)| = 0$ for $i \neq j$ and $\bar{I}_x(\boldsymbol{r}_1) = \bar{I}_y(\boldsymbol{r}_1) = \frac{1}{2}\bar{I}(\boldsymbol{r}_1)$, etc. Moreover, we may suppose that (cf. MANDEL and WOLF [1961b]):

$$\gamma_{xx}(\boldsymbol{r}_1, \boldsymbol{r}_2, \tau) = \gamma_{yy}(\boldsymbol{r}_1, \boldsymbol{r}_2, \tau) = \gamma(\boldsymbol{r}_1, \boldsymbol{r}_2, \tau).$$

Under these conditions equations (29) reduce to

$$\overline{I(\boldsymbol{r}_1, t+\tau)\, I(\boldsymbol{r}_2, t)} = \bar{I}(\boldsymbol{r}_1)\, \bar{I}(\boldsymbol{r}_2)[1 + \tfrac{1}{2}\, |\gamma(\boldsymbol{r}_1, \boldsymbol{r}_2, \tau)|^2] \tag{31a}$$

and

$$\overline{\Delta I(\boldsymbol{r}_1, t+\tau)\, \Delta I(\boldsymbol{r}_2, t)} = \tfrac{1}{2}\bar{I}(\boldsymbol{r}_1)\, \bar{I}(\boldsymbol{r}_2)\, |\gamma(\boldsymbol{r}_1, \boldsymbol{r}_2, \tau)|^2, \tag{31b}$$

which can be compared with (17) and (18). It will be seen that the correlation of the fluctuations has just half the value for polarized light. As the light beams encountered in practice are frequently unpolarized, equations (31) will be applicable more often than (17) and (18).

As we might expect, the intensity correlation for partially polarized light is intermediate between the foregoing values. It has been more fully investigated by MANDEL and WOLF [1961b]. As an example, let us consider the case in which the two beams are coherent but each is partially polarized in the same way. We may express this by writing (see MANDEL and WOLF [1961a])

$$\gamma_{ij}(\boldsymbol{r}_1, \boldsymbol{r}_2, \tau) = \gamma_{ij}(\boldsymbol{r}_1, \boldsymbol{r}_1, \tau - \eta) = \gamma_{ij}(\boldsymbol{r}_2, \boldsymbol{r}_2, \tau - \eta), \tag{32}$$

where η represents a possible time shift introduced between the coherent beams at $\boldsymbol{r}_1$ and $\boldsymbol{r}_2$. With this substitution (29b) becomes:

$$\overline{\Delta I(\boldsymbol{r}_1, t + \tau)\, \Delta I(\boldsymbol{r}_2, t)} = \sum_i \sum_j \bar{I}_i(\boldsymbol{r}_1)\, \bar{I}_j(\boldsymbol{r}_2)\, |\gamma_{ij}(\boldsymbol{r}_1, \boldsymbol{r}_1, \tau - \eta)|^2. \tag{33}$$

The directions of the x, y axes are still arbitrary. Let us now choose them in such a manner that

$$\begin{aligned} \bar{I}_x(\boldsymbol{r}_1) &= \bar{I}_y(\boldsymbol{r}_1) = \tfrac{1}{2}\bar{I}(\boldsymbol{r}_1) \\ \bar{I}_x(\boldsymbol{r}_2) &= \bar{I}_y(\boldsymbol{r}_2) = \tfrac{1}{2}\bar{I}(\boldsymbol{r}_2). \end{aligned} \tag{34}$$

As WOLF [1959] has shown, this can always be done and the degree of coherence $|\gamma_{xy}(\boldsymbol{r}_1, \boldsymbol{r}_1, 0)|$ or $|\gamma_{xy}(\boldsymbol{r}_2, \boldsymbol{r}_2, 0)|$ between the x and y components of each beam will then be a maximum and equal to the degree of polarization P. With the choice $\tau = \eta$, equation (33) then reduces to

$$\overline{\Delta I(\boldsymbol{r}_1, t + \eta)\, \Delta I(\boldsymbol{r}_2, t)} = \tfrac{1}{2}\bar{I}(\boldsymbol{r}_1)\, \bar{I}(\boldsymbol{r}_2)\, (1 + P^2). \tag{35}$$

A formula of this type was first deduced by WOLF [1960] on the particle picture of a light beam. It expresses the interesting result that the intensity correlation depends on the degree of polarization P and that P can, in principle, be found from correlation measurements of the partially polarized beams (cf. also BLANC-LAPIERRE [1956] and MANDEL [1963a]). The experiment suggested earlier in this section for finding the degree of polarization can therefore also be performed without the use of any polarizers. This was first pointed out by WOLF [1960] and might prove to be a valuable technique for wave-lengths at which polarizers are not readily available.

When $\boldsymbol{r}_1$ and $\boldsymbol{r}_2$ coincide in the above formulae, we obtain expressions for the intensity auto-correlations. Thus, from (35),

$$\overline{(\Delta I(\boldsymbol{r}, t))^2} = \tfrac{1}{2}\bar{I}^2(\boldsymbol{r})(1 + P^2), \tag{36}$$

since η is necessarily zero, while, from (31),

$$\overline{\Delta I(\boldsymbol{r}, t+\tau)\,\Delta I(\boldsymbol{r}, t)} = \tfrac{1}{2}\bar{I}^2(\boldsymbol{r})\,|\gamma(\boldsymbol{r}, \boldsymbol{r}, \tau)|^2 \tag{37}$$

for unpolarized light.

In the following we shall mainly confine ourselves to a discussion of unpolarized light beams, which are most frequently encountered in practice. We shall then revert to the earlier, more abbreviated notation, in which the position $\boldsymbol{r}$ of each point does not appear explicitly in the correlation functions.

2.5. THE SPECTRAL DENSITY OF THE INTENSITY FLUCTUATIONS

By using equation (37) we can immediately write down the value of the normalized auto-correlation function $\lambda_{11}(\tau)$ of the light intensity fluctuations $I(t)$, which is defined by:

$$\begin{aligned}\lambda_{11}(\tau) &= \overline{\Delta I(t+\tau)\,\Delta I(t)} \,/\, \overline{(\Delta I(t))^2} \\ &= |\gamma_{11}(\tau)|^2.\end{aligned} \tag{38}$$

Thus it appears that $\lambda_{11}(\tau)$ and $|\gamma_{11}(\tau)|$ are very simply related. We note that, as usual, the phase of $\gamma_{11}(\tau)$ does not enter into the description of the fluctuation properties.

The normalized spectral density $\psi_{11}(\nu)$ of the intensity fluctuations is then simply the Fourier transfrom of $\lambda_{11}(\tau)$, so that, from (38),

$$\psi_{11}(\nu) = \int_{-\infty}^{\infty} |\gamma_{11}(\tau)|^2 \exp(2\pi i\nu\tau)\,\mathrm{d}\tau. \tag{39}$$

If we now apply the Wiener-Khintchine theorem to the Fourier transform pair $\gamma_{11}(\tau)$ and $\phi_{11}(\nu)$, (39) can be expressed in terms of the auto-correlation of $\phi_{11}(\nu)$ in the form:

$$\psi_{11}(\nu) = \int_{0}^{\infty} \phi_{11}(\nu'+\nu)\phi_{11}(\nu')\,\mathrm{d}\nu'. \tag{40}$$

This equation directly relates the spectral densities of $I(t)$ and of $V(t)$. It should be noted that the derivation was based on the properties of Gaussian light and that the relation is not necessarily valid for maser light. Of course while $\phi_{11}(\nu)$ uniquely determines $\psi_{11}(\nu)$ the converse is not necessarily true (but see WOLF [1962] and KANO and WOLF [1962]). The reason for this asymmetry appears to be the fact that the fluctuations of $I(t)$ carry less information about $V(t)$ than the fluctuations of $V(t)$. In particular, no information about the phase of $V(t)$ appears to be derivable from intensity correlation or fluctuation measurements (but cf. GAMO [1962]).

FORRESTER [1961] and WOLF [1962] have considered the problem of calculating $\phi_{11}(\nu)$ from $\psi_{11}(\nu)$ and given examples of the relation between them (cf. MANDEL [1962a]. Fig. 2, which is based on Forrester's results, shows that $\psi_{11}(\nu)$ is generally a broader distribution

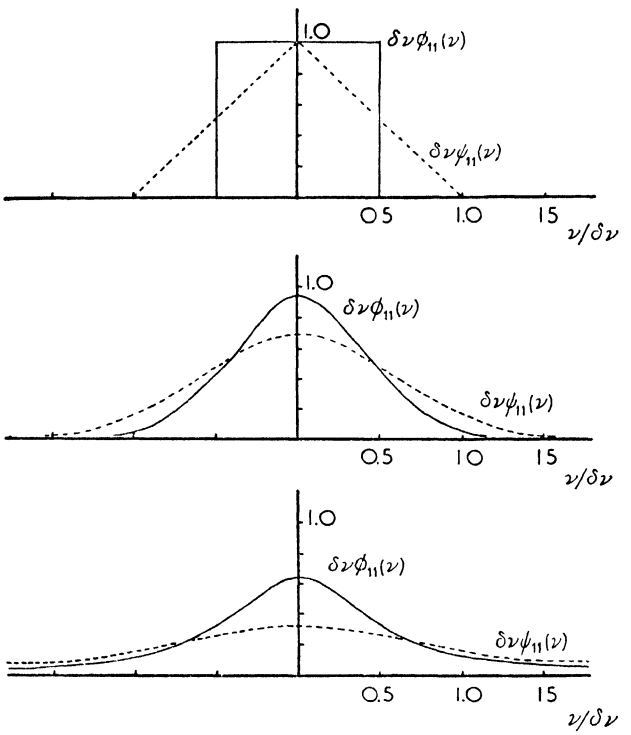

Fig. 2. The relation between the normalized spectral densities $\psi_{11}(\nu)$ and $\phi_{11}(\nu)$, for a rectangular, a Gaussian and Lorentzian spectral profile $\phi_{11}(\nu)$ ($\delta\nu$ is the spectral width at half maximum height).

than $\phi_{11}(\nu)$, although the spectral range is of the same order in both cases. We shall return to this point in section 3.5, when the problem of determining $\phi_{11}(\nu)$ will be taken up.

§ 3. Practical Applications of Fluctuation Measurements

3.1. THE MEASUREMENT OF INTENSITY CORRELATION

The problem now arises how the intensity correlations implied by (18) and (31) are to be measured in practice. In the spectral region of radio waves the procedure is fairly obvious, since square law detectors for extracting the intensity modulation $I(t)$ of a radio wave are well-known electronic devices. It is only necessary to set up two radio antennas followed by square law detectors and to multiply the

signals from these together in an electronic correlator, whose output is then averaged and recorded. The credit for pioneering this technique and applying the principles embodied in equations (18) and (31) to the study of astronomical problems belongs to Hanbury Brown and collaborators (Hanbury Brown *et al.* [1952]; Hanbury Brown and Twiss [1954]; Jennison and Das Gupta [1956]).

Once the validity of the principle was established for radio waves the question arose whether a similar technique could be applied to the study of optical fields. The only known light detectors with a sufficiently high speed of response were photo-electric detectors and the photo-currents delivered by such detectors were demonstrably proportional to the intensity of the incident light. Nevertheless, some doubts remained whether the foregoing simple wave theory was applicable to the signals obtained from photo-electric detectors, in which the quantum nature of the radiation is very evident. It was well known that the output of a photo-emissive detector consists of short current pulses.

To resolve this question the experiment illustrated in Fig. 3 was set up by Hanbury Brown and Twiss [1956a, 1957b]. Light from a

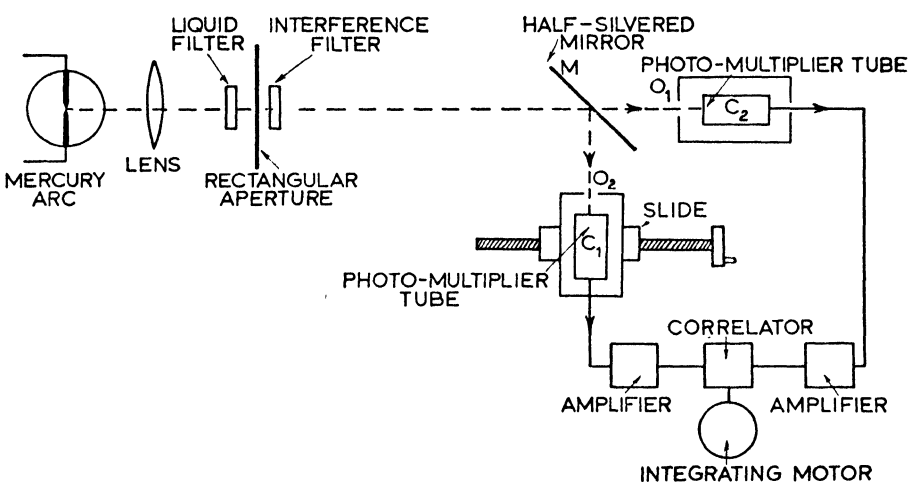

Fig. 3. The apparatus used by Hanbury Brown and Twiss for the demonstration of correlation between the intensity fluctuations of coherent light beams (reproduced from a paper by Hanbury Brown and Twiss, Nature **177**, 28, 1956).

mercury arc was filtered and split into two beams by a half silvered mirror and fell on the photo-cathodes of two photo-multiplier tubes,

one of which was movable across the beam. As this photo-multiplier moved, the degree of coherence $|\gamma_{12}|$ at the two photo-cathodes varied in a predictable manner that was calculable from the geometry of the arrangement. The electrical signals from the two photo-multipliers were fed into the electronic circuits illustrated in block form in Fig. 4.

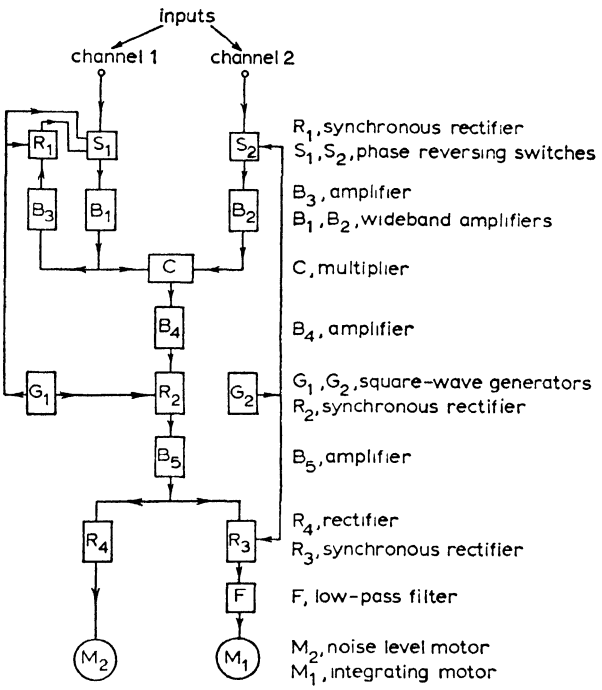

Fig. 4. Block diagram of the correlator used by Hanbury Brown and Twiss (reproduced from a paper by HANBURY BROWN and TWISS, Proc. Roy. Soc. A*243*, 300, 1957).

The signals were amplified by wide band amplifiers B_1 and B_2 of approximately 40 Mc/sec bandwidth and multiplied together in the multiplier C. From here, after further amplification and filtering, the output was fed to an integrating motor which indicated the correlation. The function of the various synchronous rectifiers and phase reversing switches was simply to reduce the random drifts in the output to an acceptable value.

With this equipment the intensity correlation was measured for various positions of the movable photo-multiplier and compared with the theoretical values calculated from the geometry, the spectral distribution of the light and the electrical characteristics of the circuits. The results are summarized in Fig. 5, in which the full curve gives the square of the degree of coherence calculated from theory. The ex-

perimental values deduced from the measured correlation, after making due allowance for the spectral distribution of the light and for the

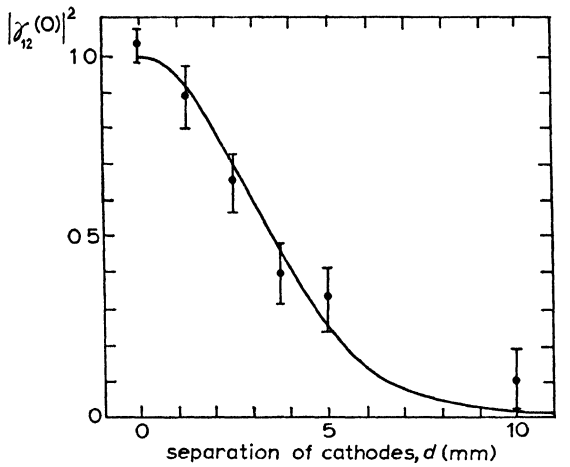

Fig. 5. The experimental and theoretical values of $|\gamma_{12}(0)|^2$ for different separations between the photo-cathodes (reproduced from a paper by HANBURY BROWN and TWISS, Proc. Roy. Soc. A*243*, 307, 1957).

electrical characteristics of the circuits are shown with their associated probable errors. It will be seen that the agreement is very reasonable, but that the statistical errors are large. Evidently there is correlation in the outputs of the photo-multipliers, but the correlation is a small effect superimposed on much larger uncorrelated fluctuations.

We see therefore that equations (31), while embodying the principle of the phenomenon, are not yet adequate to describe fully the results of the experiment. There are two reasons for this:

(a). There is no reference to the large fluctuations in the output of a photo-multiplier. These arise mainly from the shot noise of the photo-current and can be regarded as an aspect of the quantum nature of the radiation. This feature cannot, therefore, emerge from our simple wave representation without further assumptions.

(b). Equation (31) refers to correlation of the instantaneous intensities $I(t)$. Although $I(t)$ changes slowly compared with the extremely rapidly varying wave function $V(t)$, yet its fluctuations are normally too rapid for an electronic correlator (and perhaps even for the output of a photo-multiplier) to follow. Roughly speaking, the frequency spread of the fluctuations of $I(t)$ is of the same order as the frequency spread $\Delta\nu$ of the incident light. Even for the narrowest natural spectral lines $\Delta\nu$ is of the order several 100 Mc/sec and for most other light beams it is likely

to be several orders of magnitude greater. The signal on which the electronic correlator operates is therefore already some short time average of $I(t)$.

3.2. CORRELATION BETWEEN BAND LIMITED SIGNALS

In order to examine the implication of this last point, suppose that the signal currents $S_1(t)$ and $S_2(t)$ to be correlated are proportional, not to the light intensities $I_1(t)$ and $I_2(t)$, but to local time averages of $I_1(t)$ and $I_2(t)$ taken over some short time T, which has the nature of a 'resolving time'. Then

$$\begin{aligned} S_1(t) &= \frac{\alpha_1}{T}\int_{-\frac{1}{2}T}^{\frac{1}{2}T} I_1(t+t')\,\mathrm{d}t' \\ S_2(t) &= \frac{\alpha_2}{T}\int_{-\frac{1}{2}T}^{\frac{1}{2}T} I_2(t+t')\,\mathrm{d}t', \end{aligned} \tag{41a}$$

where the constants α_1 and α_2, which relate the photo-current to the incident light intensity, represent the photo-sensitivities of the photo-cathodes. These relations between the signal currents $S_1(t)$ and $S_2(t)$ and the light intensities $I_1(t)$ and $I_2(t)$ are, of course, still simple idealizations of the physical situation. In particular, they imply that any time lags (or rather variations in time lag) in the photo-emission process itself are negligible. It has been shown experimentally (FORRESTER *et al.* [1955]; MCMURTRY and SIEGMAN [1962]) that any such lags are certainly less than 10^{-10} sec. For simplicity, we assume here that α is constant over the spectral range $\Delta\nu$ of the incident light. From the definitions (41a) it follows that

$$\begin{aligned} \bar{S}_1 &= \alpha_1 \bar{I}_1, \\ \bar{S}_2 &= \alpha_2 \bar{I}_2. \end{aligned} \tag{41b}$$

Consider now the correlation between $S_1(t)$ and $S_2(t)$ for zero time shift τ, which normally yields the maximum value. From (41a),

$$\begin{aligned} \overline{S_1(t)\,S_2(t)} &= \frac{\alpha_1\alpha_2}{T^2}\int_{-\frac{1}{2}T}^{\frac{1}{2}T}\int \overline{I_1(t+t')\,I_2(t+t'')}\,\mathrm{d}t'\,\mathrm{d}t'' \\ &= \frac{\alpha_1\alpha_2}{T^2}\int_{-\frac{1}{2}T}^{\frac{1}{2}T}\int \overline{I_1(t+t'-t'')\,I_2(t)}\,\mathrm{d}t'\,\mathrm{d}t'', \end{aligned}$$

so that, in view of (31) and (41b),

$$\overline{\Delta S_1(t)\,\Delta S_2(t)} = \frac{1}{2}\frac{\bar{S}_1\bar{S}_2}{T^2}\iint_{-\frac{1}{2}T}^{\frac{1}{2}T} |\gamma_{12}(t'-t'')|^2\,\mathrm{d}t'\,\mathrm{d}t''. \tag{42}$$

Now it has been shown that, in many physical situations, the coherence possesses a certain cross-spectral purity, which makes the normalized coherence function reducible to the product of two simpler functions (MANDEL [1961b]) as follows:

$$\gamma_{12}(\tau) = \gamma_{12}(0)\,\gamma_{11}(\tau). \tag{43}$$

If we use $T\xi(T)$ to denote the double integral

$$\iint_{-\frac{1}{2}T}^{\frac{1}{2}T} |\gamma_{11}(t'-t'')|^2\,\mathrm{d}t'\,\mathrm{d}t'',$$

which can also be expressed as a single integral in the form (cf. RICE [1944, 1945]; DAVENPORT and ROOT [1958]):

$$T\xi(T) = 2\int_0^T (T-t')\,|\gamma_{11}(t')|^2\,\mathrm{d}t',$$

where $\xi(T)$ is a function of T and has the dimension of time, then, by substituting (43) in (42) we obtain:

$$\overline{\Delta S_1(t)\,\Delta S_2(t)} = \tfrac{1}{2}\bar{S}_1\bar{S}_2[\xi(T)/T]\,|\gamma_{12}(0)|^2. \tag{44}$$

This differs from (31), when $\tau = 0$, only by the inclusion of the factor $\xi(T)/T$. Since $|\gamma_{11}(\tau)| \leqq 1$, it follows from the definition of $\xi(T)$ that $\xi(T) \leqq T$. It can easily be shown (MANDEL [1958, 1959]) that $\xi(T) \approx T$ when $T \ll 1/\Delta\nu$, but that $\xi(T)$ tends to an upper limit $\xi(\infty)$ when T becomes large compared with $1/\Delta\nu$. This upper limit is given by

$$\xi(\infty) = \int_{-\infty}^{\infty} |\gamma_{11}(\tau)|^2\,\mathrm{d}\tau.$$

Since $|\gamma_{11}(\tau)|$ vanishes for $|\tau|$ much greater than about $1/\Delta\nu$, it follows that $\xi(\infty)$ will itself be of order $1/\Delta\nu$. In fact, as has been shown (MANDEL [1959]), there are good reasons for recognizing $\xi(\infty)$ as the coherence time of the light (but see also WOLF [1958]; WOODWARD [1953]; MANDEL and WOLF [1962]). The exact form of $\xi(T)$ depends on $|\gamma_{11}(\tau)|$ and therefore on the spectral distribution $\phi_{11}(\nu)$ of the light.

Some examples for three different spectral profiles are shown in Fig. 6.

With this interpretation we can readily see the significance of the factor $\xi(T)/T$ in (44). When the resolving time T is short compared with the coherence time, $\xi(T)/T \approx 1$, since the signal $S(t)$ will faith-

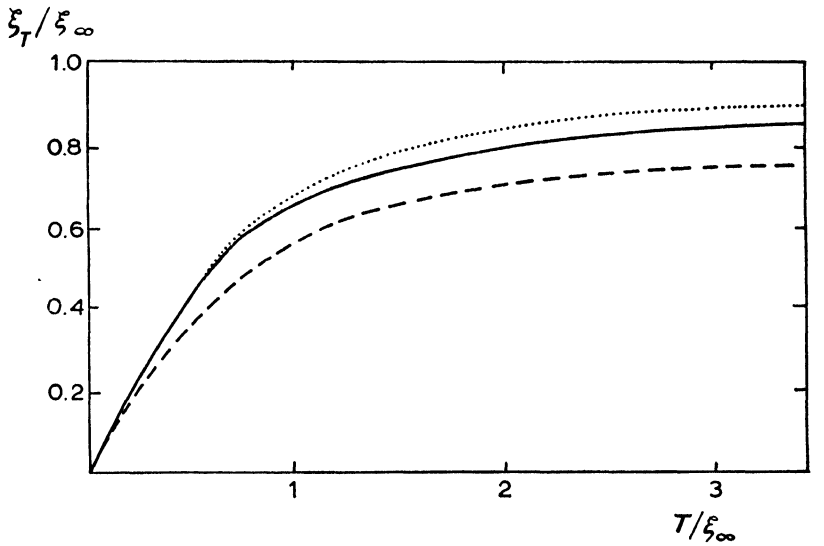

Fig. 6. The variation of $\xi(T)$ with T for three different spectral distributions of r.m.s. width $\Delta\nu$ (the full curve corresponds to a rectangular profile, the dotted curve to a Gaussian profile and the broken curve to a rectangular doublet).

fully follow the intensity $I(t)$. When the resolving time T is long compared with the coherence time of the light, as is normally the case, the signal $S(t)$ is unable to follow the intensity $I(t)$ and the observed correlation is reduced by the factor $\xi(\infty)/T$. To make the correlation observable it is therefore important to keep the resolving time short.

However, the foregoing discussion, while giving some insight into the significance of correlating time averaged signals derived from the instantaneous intensities $I_1(t)$ and $I_2(t)$, still does not describe the experimental situation. In practice, the signals to be correlated are derived from band limited electronic amplifiers, characterized by a certain frequency response $B(\nu)$, whose bandwidth $\delta\nu$ is usually much below the bandwidth $\Delta\nu$ of the light. It is, of course, quite legitimate to incorporate the electrical characteristics of the photo-multiplier within the response function $B(\nu)$. While the operation of such a filter does bear some analogy to time averaging, it is not described by the integrals (41a). The theory applicable to this situation was first

given by HANBURY BROWN and TWISS [1957a]. Here we shall adopt a somewhat simpler treatment.

If $S(t)$ is the output of any linear filter circuit whose input is $\alpha I(T)$, which here has the nature of a photo-current, it is well known that $S(t)$ and $I(t)$ can be related by a convolution integral of the form:

$$S(t) = \alpha \int_0^\infty I(t - t')\, b(t')\, \mathrm{d}t', \tag{45}$$

in which $b(t)$ is the response of the system to a short impulse at $t = 0$, and is the Fourier transform of $B(\nu)$ (cf. SOLODOVNIKOV [1960]). We can therefore write down the correlation between two signals $S_1(t)$ and $S_2(t)$ derived from two identical filters with correlated inputs $\alpha_1 I_1(t)$ and $\alpha_2 I_2(t)$. Thus:

$$\begin{aligned}\overline{S_1(t)\, S_2(t)} &= \alpha_1\alpha_2 \iint_0^\infty \overline{I_1(t - t')I_2(t - t'')}\, b(t')\, b(t'')\, \mathrm{d}t'\, \mathrm{d}t'' \\ &= \alpha_1\alpha_2 \iint_0^\infty \overline{I_1(t + t'' - t')\, I_2(t)}\, b(t')\, b(t'')\, \mathrm{d}t'\, \mathrm{d}t''. \end{aligned} \tag{46}$$

Now, from the definition (45) it follows that

$$\begin{aligned}\bar{S}_1 &= \alpha_1 \bar{I}_1 \int_0^\infty b(t')\, \mathrm{d}t' \\ \bar{S}_2 &= \alpha_2 \bar{I}_2 \int_0^\infty b(t')\, \mathrm{d}t', \end{aligned} \tag{47}$$

so that, by using (31a), (43) and (47) in (46) we obtain:

$$\begin{aligned}\overline{\Delta S_1(t)\, \Delta S_2(t)} &= \tfrac{1}{2}\alpha_1\alpha_2 \bar{I}_1 \bar{I}_2\, |\gamma_{12}(0)|^2 \iint_0^\infty |\gamma_{11}(t'' - t')|^2\, b(t')\, b(t'')\, \mathrm{d}t'\, \mathrm{d}t'' \\ &= \tfrac{1}{2}\alpha_1\alpha_2 \bar{I}_1 \bar{I}_2\, |\gamma_{12}(0)|^2 \int_0^\infty \int_{-t'}^\infty |\gamma_{11}(t''')|^2 b(t')\, b(t' + t''')\, \mathrm{d}t'''\, \mathrm{d}t'. \end{aligned} \tag{48}$$

Now $|\gamma_{11}(\tau)|$ vanishes for $|\tau|$ much in excess of $1/\Delta\nu$. On the other hand, if the highest frequency passed by the electrical filter is still small compared with the bandwidth $\Delta\nu$ of the light, as is normally the case, then $b(t)$ is nearly constant over intervals of order $1/\Delta\nu$.

Hence, for those values of t''' for which the integrand in (48) does not vanish, $b(t' + t''') \approx b(t')$ and we may write:

$$\overline{\Delta S_1(t)\,\Delta S_2(t)} = \tfrac{1}{2}\alpha_1\alpha_2\bar{I}_1\bar{I}_2\,|\gamma_{12}(0)|^2\int_0^\infty\int_{-\infty}^\infty |\gamma_{11}(t''')|^2\,b^2(t')\,\mathrm{d}t'''\,\mathrm{d}t',$$

since the range of t' for which the integrand is non-zero is so much greater than the range of t'''. Therefore,

$$\overline{\Delta S_1(t)\,\Delta S_2(t)} = \tfrac{1}{2}\alpha_1\alpha_2\bar{I}_1\bar{I}_2\,|\gamma_{12}(0)|^2\,\xi(\infty)\int_0^\infty b^2(t')\,\mathrm{d}t' \qquad (49)$$

and, provided $\bar{S}_1$ and $\bar{S}_2$ are not zero, this can be put in the form

$$\overline{\Delta S_1(t)\,\Delta S_2(t)} = \tfrac{1}{2}\bar{S}_1\bar{S}_2\,|\gamma_{12}(0)|^2\,\xi(\infty)\,\frac{\int_0^\infty b^2(t')\,\mathrm{d}t'}{\left[\int_0^\infty b(t')\,\mathrm{d}t'\right]^2},$$

with the help of (47). Now the ratio

$$\left[\int_0^\infty b(t')\,\mathrm{d}t'\right]^2 \Big/ \int_0^\infty b^2(t')\,\mathrm{d}t' = T'$$

is a rough measure of the time spread of the impulse response function $b(t)$ and therefore has the nature of a 'resolving time' T'. With this understanding we may therefore rewrite the equation in the form:

$$\overline{\Delta S_1(t)\,\Delta S_2(t)} = \tfrac{1}{2}\bar{S}_1\bar{S}_2[\xi(\infty)/T']\,|\gamma_{12}(0)|^2, \qquad (50)$$

which is in complete analogy with equation (44).

If the amplifier does not pass D.C. and $\bar{S}_1$ and $\bar{S}_2$ are zero, equation (50) is, of course, inapplicable and we have to return to (49). However, by applying Parseval's theorem to the integral and writing it in the form:

$$\int_0^\infty b^2(t')\,\mathrm{d}t' = \int_{-\infty}^\infty |B(\nu)|^2\mathrm{d}\nu = B^2\delta\nu,$$

where $\delta\nu$ is the effective bandwidth of the amplifier and B has the nature of a mean amplification averaged over all frequencies, equation (49) can be expressed in a form resembling (50):

$$\overline{\Delta S_1(t)\,\Delta S_2(t)} = \tfrac{1}{2}\bar{s}_1\bar{s}_2[\xi(\infty)\delta\nu]\,|\gamma_{12}(0)|^2.$$

The quantities $\bar{s}_1 = \alpha_1\bar{I}_1B$ and $\bar{s}_2 = \alpha_2\bar{I}_2B$ measure the mean outputs of the amplifiers and are analogous to $\bar{S}_1$ and $\bar{S}_2$.

We have so far always made the simplifying assumption that the quantum sensitivity α of the photo-electric detector is constant over

the spectral range $\Delta\nu$ of the incident light. Let us now briefly examine the more general case when α varies with frequency as $\alpha(\nu)$. This problem was first treated by HANBURY BROWN and TWISS [1957a].

We can always resolve the incident light wave $V(t)$ into a series of Fourier components, each of which has an infinitesimal frequency range $d\nu$, by writing

$$V_T(t) = \int_0^\infty A_T(\nu) \exp(2\pi i\nu t)\, d\nu.$$

The truncated functions introduced in section 2.1 are used to ensure that the Fourier integral exists. Then we can account for the frequency variation of the detector sensitivity $\alpha(\nu)$ by associating a response $\sqrt{\alpha(\nu)}$ with each Fourier component of $V_T(t)$. This ensures that the detector response to one Fourier component is of the form $\alpha(\nu)$ times the intensity of the component. While this method of accounting for the frequency variation of $\alpha(\nu)$ is plausible, it cannot be strictly justified except by a more detailed examination of the photo-electric effect, which requires a quantum treatment.

The instantaneous signal $S(t)$ emerging from the detector is now given by an equation of the form (45) but with $\alpha I(t)$ replaced by

$$\alpha I(t) \to \lim_{T\to\infty} \int_0^\infty \int_0^\infty \sqrt{[\alpha(\nu)\alpha(\nu')]}\, A_T(\nu)\, A_T^*(\nu') \exp 2\pi i(\nu - \nu')t\, d\nu d\nu'.$$

This generalized value of $\alpha I(t)$ is simply the instantaneous light intensity that would be obtained if the light waves were passed through an optical filter of transmission $\sqrt{\alpha(\nu)}$. With this understanding all the foregoing results may be generalized in a simple formal way.

Thus consider the generalization of the mean counting rate $\alpha\bar{I}$ of the photo-detector. By applying the above rule we find

$$\alpha\bar{I} \to \bar{I} \int_0^\infty \alpha(\nu)\, \phi_{11}(\nu)\, d\nu,$$

since the spectral density $\bar{I}\phi_{11}(\nu)$ has to be replaced by $\bar{I}\phi_{11}(\nu)\,\alpha(\nu)$. This may also be written in the form

$$\alpha\bar{I} \to \bar{\alpha}\bar{I},$$

where $\bar{\alpha}$ is the mean quantum sensitivity of the detector averaged over the spectral distribution $\phi_{11}(\nu)$.

As another example consider the generalization of the correlation

formula (49), when both photo-detector sensitivities are subject to the same frequency variation, i.e. when $\alpha_1(\nu) = \text{constant} \times \alpha_2(\nu)$. Since the normalized spectral density $\phi_{11}(\nu)$ has to be replaced by

$$\phi_{11}(\nu) \to \frac{1}{\bar{\alpha}_1}\phi_{11}(\nu)\alpha_1(\nu) = \frac{1}{\bar{\alpha}_2}\phi_{11}(\nu)\alpha_2(\nu) = \frac{1}{\sqrt{(\bar{\alpha}_1\bar{\alpha}_2)}}\phi_{11}(\nu)\sqrt{[\alpha_1(\nu)\alpha_2(\nu)]},$$

it follows that $\xi(\infty)$ in (49) becomes:

$$\xi(\infty) = \int_0^\infty \phi_{11}^2(\nu)\,\mathrm{d}\nu \to \frac{1}{\bar{\alpha}_1\bar{\alpha}_2}\int_0^\infty \phi_{11}^2(\nu)\,\alpha_1(\nu)\,\alpha_2(\nu)\,\mathrm{d}\nu.$$

With the additional replacement of $\alpha_1\bar{I}_1$ by $\bar{\alpha}_1\bar{I}_1$ and $\alpha_2\bar{I}_2$ by $\bar{\alpha}_2\bar{I}_2$ we obtain the following generalization of equation (49):

$$\overline{\Delta S_1(t+\tau)\,\Delta S_2(t)} = \tfrac{1}{2}\bar{I}_1\bar{I}_2\,|\gamma_{12}(0)|^2\int_0^\infty \phi_{11}^2(\nu)\,\alpha_1(\nu)\,\alpha_2(\nu)\int_0^\infty b^2(t')\,\mathrm{d}t'. \quad (51)$$

For simplicity we shall revert to the simple case $\alpha(\nu) = \text{constant}$ in future discussions, but, with the help of the foregoing formal rule, the results can always be generalized without difficulty.

3.3. THE PROBLEM OF NOISE

Let us now briefly turn to the question of the fluctuations of the signals $S_1(t)$ and $S_2(t)$ to be correlated. If we put $S_1(t) = S_2(t)$ in the foregoing analysis, we obtain an expression for the variance of $S(t)$ which, according to (49) is given by:

$$\overline{(\Delta S_{\mathrm{W}}(t))^2} = \tfrac{1}{2}\alpha^2\bar{I}^2\xi(\infty)\int_0^\infty b^2(t')\,\mathrm{d}t'$$

$$= \alpha^2\bar{I}^2\xi(\infty)\int_0^\infty |B(\nu)|^2\,\mathrm{d}\nu, \quad (52)$$

where $B(\nu)$ is the Fourier transform of $b(t)$. These fluctuations, which are based on the relation (37), are entirely attributable to the intensity fluctuations of the incident light waves and are therefore labelled by the suffix W. There are, however, additional fluctuations in the output signal $S(t)$ due to the shot noise of the photo-current, or, as it might be expressed, due to the quantum nature of the incident radiation. Moreover, the amplification processes in the photo-multiplier and in subsequent amplifiers also introduce additional noise, although these contributions are normally small compared with the fluctuations of the photo-current itself.

In speaking of shot noise fluctuations we are, in a sense, abandoning the standpoint of our wave representation, in which both the light intensity $I(t)$ and the signal $S(t)$ derived from it are regarded as continuous time functions. This is a basic limitation of the wave picture.

Let us now calculate the shot noise fluctuations and then combine them with those given by equation (52). Suppose that a coherent, unpolarized light beam of intensity $I(t)$, measured in photons per sec, is incident on a photo-cathode of quantum sensitivity α electrons per photon. If we disregard thermal emission, the mean photo-current will be $\alpha\bar{I}$ measured in electrons per sec, and it is well-known (cf. RICE [1944]; FÜRTH and MACDONALD [1947]; FÜRTH [1948]) that, after passing through an electrical filter of transmission $B(\nu)$, the associated shot noise fluctuations are given by:

$$\overline{(\Delta S_{\mathrm{P}}(t))^2} = 2\alpha\bar{I}\int_0^\infty |B(\nu)|^2 \mathrm{d}\nu. \tag{53}$$

These fluctuations due to the particle properties must be regarded as random and uncorrelated with those given by (52), so that the total observed signal fluctuation is simply the sum of the two:

$$\begin{aligned}\overline{(\Delta S(t)^2} &= \overline{(\Delta S_{\mathrm{W}}(t))^2} + \overline{(\Delta S_{\mathrm{P}}(t))^2} \\ &= 2\alpha\bar{I}[1 + \tfrac{1}{2}\alpha\bar{I}\xi(\infty)]\int_0^\infty |B(\nu)|^2 \mathrm{d}\nu. \end{aligned} \tag{54}$$

Because of the manner in which the shot noise fluctuations are introduced here, the superposition expressed by equation (54) cannot be completely justified. It may, however, be regarded as the analogue for a beam of radiation of the Einstein equation (3) for radiation in an equilibrium enclosure. In both cases the contributions due to classical particles and classical waves are additive.

HANBURY BROWN and TWISS [1957a] have called the contribution $\overline{\Delta^2 S_{\mathrm{W}}(t)}$ arising from the wave nature of the light the wave interaction noise and it is clear that the wave fluctuations are responsible for the observed intensity correlation in coherent beams. The effect may therefore properly be called a wave effect. As we shall see later, the particle picture leads to similar results, but to a slightly different interpretation.

By making use of the relations (49) and (54) we can write down an expression for the normalized signal correlation coefficient ρ:

$$\rho = \frac{\overline{\Delta S_1(t)\,\Delta S_2(t)}}{\sqrt{[\overline{(\Delta S_1(t))^2}\,\overline{(\Delta S_2(t))^2}]}}$$

$$= \frac{\frac{1}{2}\sqrt{(\alpha_1\alpha_2\bar{I}_1\bar{I}_2)}\xi(\infty)}{\sqrt{[1+\frac{1}{2}\alpha_1\bar{I}_1\xi(\infty)]}\sqrt{[1+\frac{1}{2}\alpha_2\bar{I}_2\xi(\infty)]}}\,|\gamma_{12}(0)|^2 \qquad (55a)$$

or

$$\rho = \frac{\frac{1}{2}\alpha\bar{I}\xi(\infty)}{1+\frac{1}{2}\alpha\bar{I}\xi(\infty)}\,|\gamma_{12}(0)|^2, \qquad (55b)$$

when $\alpha_1\bar{I}_1 = \alpha_2\bar{I}_2 = \alpha\bar{I}$. It is clear, therefore, that the observability of the correlation depends not only on the degree of coherence $|\gamma_{12}(0)|$ but also on the factor $\frac{1}{2}\alpha\bar{I}\xi(\infty)$, which gives half the average number of photo-electrons emitted in a time equal to the coherence time by a coherently illuminated photo-cathode. As we shall see later in discussing the photon picture, this factor plays the role of a degeneracy parameter δ in the counting statistics.

For radio waves detected with a square law detector, for which α may be interpreted as the aerial plus receiver efficiency, $\alpha\bar{I}\xi(\infty)$ is usually a very large number, perhaps of order 10^{11} (cf. HANBURY BROWN and TWISS [1957a]; GABOR [1961], so that ρ may have values close to unity when the beams are practically coherent. On the other hand, it has been shown (GABOR [1961]; MANDEL [1961a]) that $\alpha\bar{I}\xi(\infty)$ is very much less than unity for practically all light beams, so that ρ will normally be extremely small. This explains at once why the correlation was so much more difficult to observe with light than with radio waves. From (54) the smallness of $\frac{1}{2}\alpha\bar{I}\xi(\infty)$ implies that the wave interaction noise, also called the excess photon noise, is very small compared with the shot noise. The problem of detecting this excess noise directly in single beam measurements has been discussed by ALKEMADE [1959].

The situation has, however, been changed by the recent development of the optical maser (SCHAWLOW and TOWNES [1958]; MAIMAN [1960, 1961]; COLLINS *et al.* [1960]; WIEDER and SARLES [1961]; SCHAWLOW and DEVLIN [1961]; JAVAN *et al.* [1961]; and many others). In this device repeated stimulated photo-emission in a resonant cavity formed by the plates of a Fabry-Perot interferometer, leads to the emergence of an extended coherent beam of light of great intensity. From recent measurements (COLLINS *et al.* [1960]; NELSON and COLLINS [1961]) on the stimulated emission from ruby it has been shown that $\alpha\bar{I}\xi(\infty)$ may be of order 10^7 (MANDEL [1961a])

and still higher values have been obtained in the infra red from the gas maser (JAVAN *et al.* [1961, 1962]; HERRIOTT [1961, 1962]). It might appear then that the intensity correlation effect should be very readily observable with maser beams. However we must remember that equations (55) apply to light from thermal sources, i.e. Gaussian light. Because of saturation effects in the source, maser light has amplitude stabilization properties and very small intensity fluctuations. For this reason it is possible that the intensity correlation of partially coherent maser beams will be difficult to observe despite the photon degeneracy. In fact it has not yet been reported.

3.4. STELLAR CORRELATION INTERFEROMETRY

It is clear from the relation (49) that the measurement of intensity correlation at two points in an optical field can be used to obtain the degree of coherence at these points and hence to explore the coherence properties of the field.

Now there is an important connection between the coherence function $\gamma_{12}(\tau)$ at two points $\boldsymbol{r}_1$ and $\boldsymbol{r}_2$ in a field and the intensity distribution of the incoherent source producing the field, which was first established for $\tau = 0$ by VAN CITTERT [1934] and ZERNIKE [1938] and later extended by HOPKINS [1951, 1953] and WOLF [1954b]. If the source is very distant and the two points are in a plane normal to the direction of the light from the source, then the function $\gamma_{12}(0)$ is simply related to the two-dimensional Fourier transform of the intensity distribution across the source (see also BORN and WOLF [1959]). It follows that the intensity distribution, and particularly the angular dimensions of a distant star, for example, can be studied by measuring $\gamma_{12}(0)$ for a range of points $\boldsymbol{r}_1$ and $\boldsymbol{r}_2$.

This, of course, is the principle of the stellar interferometer developed by MICHELSON [1920] (see also MICHELSON and PEASE [1921]) and shown in Fig. 7. Starlight arriving at two mirrors M_1 and M_2 is directed by further mirrors M_3 and M_4 to a common point P within a telescope, where interference fringes are formed. As the visibility of these fringes, for equal beam intensities, is given by the degree of coherence $|\gamma_{12}(0)|$ at the mirrors M_1 and M_2 and as the position of the fringes is related to the phase of $\gamma_{12}(0)$ (cf. BORN and WOLF [1959]), it follows that $\gamma_{12}(0)$ can be obtained from measurements of the interference pattern. The measurements are then repeated for different separations of the mirrors M_1 and M_2. Since stellar sources usually have approximate circular symmetry it is sufficient to explore $\gamma_{12}(0)$ for points along

one line. Fig. 8 shows the expected variation of fringe visibility or degree of coherence as a function of the separation $|\boldsymbol{r}_1 - \boldsymbol{r}_2| = d$ for a circular disc source with three different intensity distributions. It will be seen that the degree of coherence falls to zero for a separation of the order λ/θ, which allows a direct estimate of the angular diameter θ to be made. It means, however, that sources of very small angular diameter require a very great point separation $|\boldsymbol{r}_1 - \boldsymbol{r}_2|$ to be resolved.

By mounting their interferometer on the 100 inch reflector of the Mount Wilson Observatories, MICHELSON and PEASE [1921] succeeded

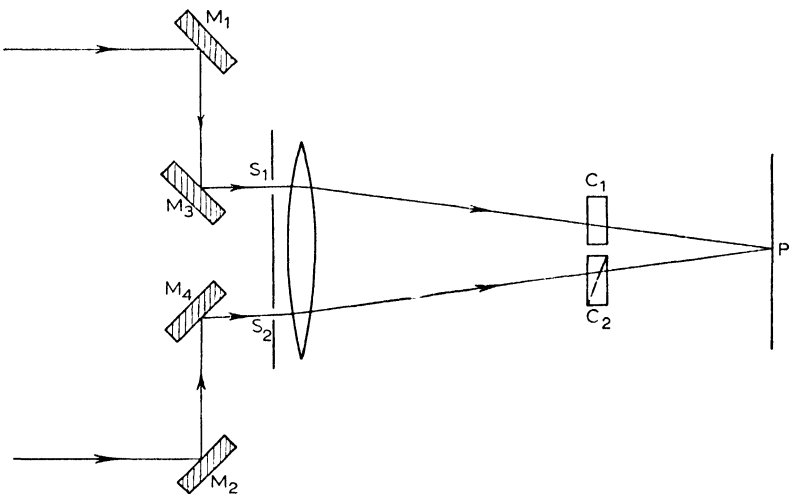

Fig. 7. Michelson's stellar interferometer (reproduced from BORN and WOLF, "Principles of Optics", p. 274, 1959, Pergamon Press).

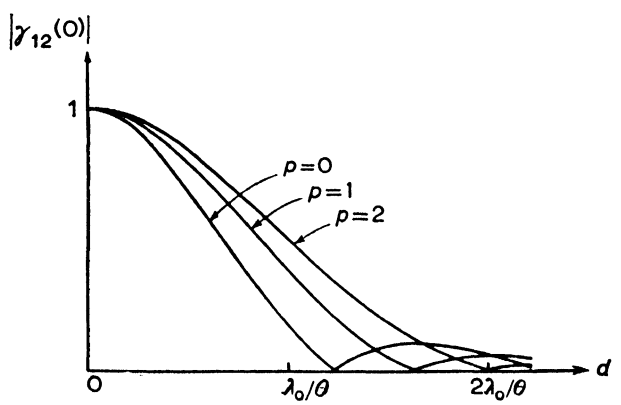

Fig. 8. The variation of the degree of coherence $|\gamma_{12}(0)|$ with aperture separation d for a circular disc source of angular diameter $\theta = 2\beta_0$, with intensity distribution proportional to $(\beta_0^2 - \beta^2)^p$, where β is the angular radius from the centre (reproduced from BORN and WOLF, "Principles of Optics", p. 273, 1959, Pergamon Press).

in measuring fringes up to a mirror separation of about 6 m, which corresponds to a minimum measurable angular diameter of about 0.02 seconds of arc. This was sufficient to examine a number of giant stars, but quite inadequate for the great majority of near stars.

The operation of an interferometer with such great arm lengths proved to be very difficult, due partly to the disturbing effects of atmospheric turbulence and partly to the mechanical difficulties of keeping path differences constant to a fraction of a wavelength. The plates C_1 and C_2 were used to compensate for these variations. It is significant that a later attempt to use a baseline of 15 m had to be abandoned.

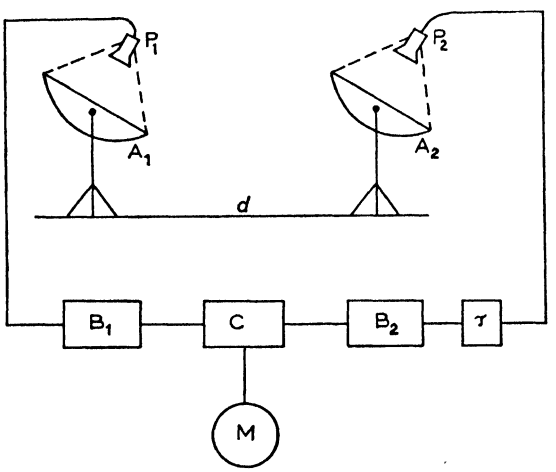

Fig. 9. Schematic diagram of the stellar intensity interferometer (A, mirrors; B, amplifiers; C, multiplier; M, integrator; P, photo-tubes; τ, delay line) (reproduced from a paper by HANBURY BROWN and TWISS, Proc. Roy. Soc. A*248*, 201, 1958).

As the degree of coherence can be derived also from intensity correlation experiments, it is natural to attempt the measurement of stellar angular diameters with the new techniques. This was done by Hanbury Brown, Twiss and collaborators, first for radio sources, using micro waves and later for the star Sirius, using visible light (HANBURY BROWN and TWISS [1956b, 1958a, b]). The apparatus, which has been called an intensity interferometer, is illustrated schematically in Fig. 9.

By means of two large reflectors A_1 and A_2 (which were search light mirrors) the light was focused on to two similar photomultipliers P_1 and P_2. The signals from these were passed to a correlator of the type illustrated in Fig. 4, which is shown in greatly simplified form in Fig. 9. The correlation was examined for different separations of

the detectors, in analogy with the Michelson stellar interferometer. A delay line inserted in one of the channels compensated for any difference in the arrival times of the light at the two mirrors and so permitted both mirrors to function at the same height. The results of the experiment are shown in Fig. 10. The full curve shows the expected variation of the correlation for an angular diameter of 0.0069 seconds of arc. Thus the angular resolution of the Michelson-Pease instrument was exceeded with much simpler optical equipment.

Since this system operates on the intensity $I(t)$ of the light, unlike a conventional interferometer which operates on the wave function $V(t)$, it appears that some information about the phase of $V(t)$ is discarded. This is also evidenced by the foregoing theory which shows

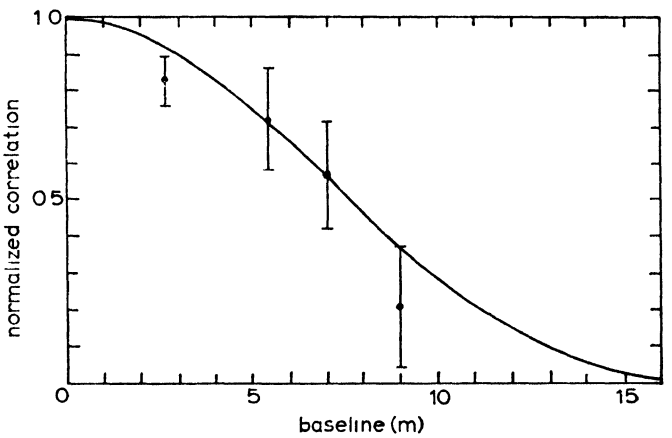

Fig. 10. The variation of the measured and theoretical values of $|\gamma_{12}(0)|^2$ with baseline length for Sirius A. The theoretical angular diameter was taken to be 0.0069 seconds of arc (reproduced from a paper by HANBURY BROWN and TWISS, Proc. Roy. Soc. A*248*, 235, 1958).

that only the modulus of $\gamma_{12}(0)$ is obtained from the measurement. However, in some respects this characteristic is a valuable feature of the method. Since the variations of $I(t)$ are so much slower than those of $V(t)$ and since the amplifiers restrict the bandwidths of the signals $S(t)$ to be correlated still further, it follows that small variations in optical path difference will not affect the measurements. This holds both for atmospheric fluctuations and for mechanical disturbance of the detectors. Thus, with amplifiers of 100 Mc/sec bandwidth, optical path variations of a few cm can be tolerated, which makes the use of baselines of many metres length quite feasible. Moreover, the effects of atmospheric phase dispersion and amplitude scintillation can be shown (HANBURY BROWN and TWISS [1958a]) to become unimportant

and, since no precise imaging is required, angular scintillation is unimportant also. HANBURY BROWN [1960] has recently given details of the very large correlation interferometer which is being set up in Australia, with a baseline up to nearly 200 m.

The two main disadvantages of the correlation technique, as compared with interferometry, are both revealed by equation (49); the correlation depends on the square of the intensities and it yields only the modulus of the coherence function $\gamma_{12}(\tau)$. This latter point would be unimportant if the source were known to be symmetric or if the phase of the coherence function could otherwise be derived from the modulus. WOLF [1962] has recently pointed out that the phase of $\gamma_{12}(\tau)$ might perhaps be derivable from the modulus because of the analytical properties of $\gamma_{12}(\tau)$. A suggestion for obtaining phase information from correlation measurements by injecting a coherent light background, or alternatively by measuring 3-point correlations, has recently been made by GAMO [1961, 1962]. The dependence on the square of the intensity limits the usefulness of the technique to the brighter stars. By using low quality reflectors of diameter 6 m in the new large instrument, it is hoped to make measurements on stars down to the 3rd photographic magnitude (HANBURY BROWN [1960]).

3.5. THE DETERMINATION OF SPECTRAL LINE PROFILES

We have already seen in section 2.5 that there is a simple relation between the spectral densities of the light and of the intensity fluctuations, so that fluctuation measurements carry information about the spectral distribution of the radiation field as well as the state of coherence and polarization. In this section we shall consider in a little more detail how the spectral distribution may be obtained. The problem has been discussed by FORRESTER [1961a, b], GIVENS [1961], WOLF [1962] and MANDEL [1962a].

It is clear from equation (37) that $|\gamma_{11}(\tau)|$, but not $\arg \gamma_{11}(\tau)$, is obtainable from measurements of the auto-correlation of the intensity fluctuations $\overline{\Delta I(t+\tau)\,\Delta I(t)}$ as a function of τ. These measurements do not, therefore, determine $\gamma_{11}(\tau)$, or the normalized spectral density $\phi_{11}(\nu)$, uniquely. However, from the Fourier transform relationship between $\gamma_{11}(\tau)$ and $\phi_{11}(\nu)$, we can write:

$$\gamma_{11}(\tau) = \int_0^\infty \phi_{11}(\nu) \exp(2\pi i \nu \tau)\, d\nu \tag{56}$$

$$= \exp(2\pi i \nu_0 \tau) \int_{-\nu_0}^{\infty} \phi_{11}(\nu_0 + \nu') \exp(2\pi i \nu' \tau)\, d\nu', \tag{57}$$

where ν_0 is the mid frequency of the spectral distribution, whose width $\Delta\nu$ is assumed to be small compared with ν_0. Now it happens that, in practice, many narrow spectral distributions $\phi_{11}(\nu)$ are nearly symmetric about ν_0, so that the integral in (57) is almost real and equal to $|\gamma_{11}(\tau)|$. We may therefore approximate $\gamma_{11}(\tau)$ by writing:

$$\gamma_{11}(\tau) \approx |\gamma_{11}(\tau)| \exp(2\pi i \nu_0 \tau), \tag{58}$$

from which it follows that the modulus of $\gamma_{11}(\tau)$ is sufficient to determine a nearly symmetrical spectral profile. But, in any case, (58) will serve as a useful first approximation when no information about $\phi_{11}(\nu)$ is available.

The function $\gamma_{11}(\tau)$ is most conveniently determined, not from auto-correlation measurements, but by dividing the light beam into two coherent beams and measuring the intensity cross-correlation of

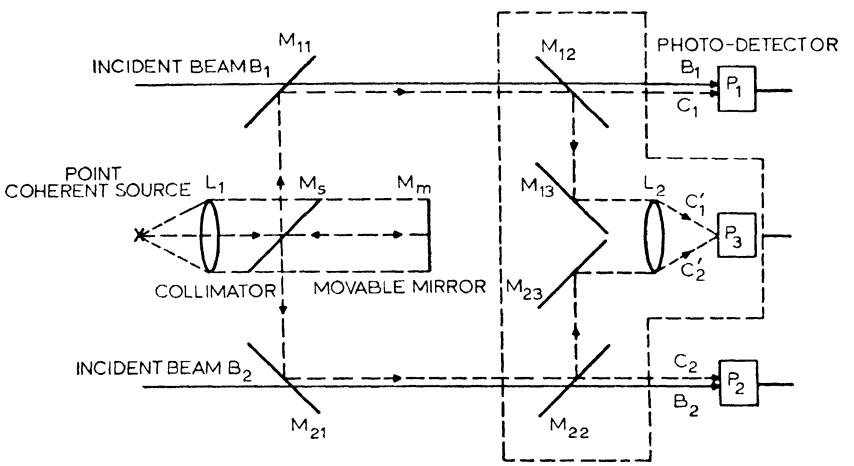

Fig. 11. Gamo's proposed experimental set-up for obtaining phase information from correlation measurements (reproduced from a paper by GAMO, Advances in Quantum Electronics, 1961, Columbia University Press, p. 255).

the two portions, as in section 3.2. The varying time delays τ can be introduced in the form of delaying cables of various lengths inserted in one channel. The approximation (58) then gives $\gamma_{11}(\tau)$ from which $\phi_{11}(\nu)$ follows by a Fourier transformation. In section 4.5 we shall encounter another approach to the determination of $|\gamma_{11}(\tau)|$, based on coincidence measurements, which is, however, comprehensible only on the particle picture of light.

GAMO [1961] has recently suggested an ingenious method, il-

lustrated in Fig. 11, for obtaining the phase of the $\gamma_{11}(\tau)$ function from correlation measurements. B_1 and B_2 are the two coherent beams to be correlated, which fall on the photomultipliers P_1 and P_2. An auxiliary source of light of accurately known normalized auto-correlation function $\gamma_{00}(\tau)$ is used to superpose two coherent beams C_1 and C_2 on B_1 and B_2, but with a variable path difference $c\theta$ produced by the movable mirror M_m. It can be shown that the cross-correlation of the intensities $J_1(t)$ and $J_2(t)$ falling on P_1 and P_2 is given by:

$$\overline{J_1(t+\tau)\,J_2(t)} = \bar{I}_1\bar{I}_2|\gamma_{11}(\tau)|^2 + \bar{I}_0{}^2\,|\gamma_{00}(\tau)|^2 + 2\bar{I}_0\sqrt{(\bar{I}_1\bar{I}_2)}\;\mathscr{R}[\gamma_{11}(\tau)\gamma_{00}{}^*(\tau+\theta)], \quad (59)$$

where $\bar{I}_1$, $\bar{I}_2$ are the mean intensities of the beams B_1 and B_2, while beams C_1 and C_2 have equal mean intensities $\bar{I}_0$. From the property (6) of the auto-correlation function $\gamma_{00}(\tau)$ we know that, for sufficiently small θ,

$$\gamma_{00}(\tau+\theta) \approx \gamma_{00}(\tau)\,\exp\,(2\pi i\nu_0\theta), \quad (60)$$

where ν_0 is the mid frequency of the known spectral distribution. Thus, from (59) and (60) it follows that variation of θ will lead to a cosine modulation of the intensity correlation $\overline{J_1(t+\tau)\,J_2(t)}$, from which the phase of $\gamma_{11}(\tau)$ can be determined. Although the method is based on correlation measurements it is, in many ways, more analogous to MICHELSON's method [1891] of obtaining spectral line shapes from visibility measurements.

So far we have been concerned with the determinative of $\gamma_{11}(\tau)$ or $|\gamma_{11}(\tau)|$, but it is equally feasible, and perhaps more convenient, to measure the spectral distribution $\psi_{11}(\nu)$ of the intensity fluctuations directly. As a first approximation, $\phi_{11}(\nu)$ is then obtained by solving the integral equation (40) with the assumption of spectral symmetry. Alternatively, $\lambda_{11}(\tau)$ can be derived from $\psi_{11}(\nu)$ and $|\gamma_{11}(\tau)|$ then follows from (38).

The distribution $\psi_{11}(\nu)$ can be measured by passing the current from the photo-detector through a sharply tuned filter (amplifier), whose transmission band is variable but very narrow compared with the spectral width of $\psi_{11}(\nu)$ (cf. MANDEL [1962a]). Then the signal $S(t)$ emerging from the filter is given by the convolution integral (45), as before. By using the well-known properties of this integral (cf. RICE [1944; 1945]; DAVENPORT and ROOT [1958]; SOLODOVNIKOV [1960]), we can immediately relate the spectral density $\chi_{11}(\nu)$ of $S(t)$ to that of $I(t)$. Thus:

$$\chi_{11}(\nu) = \alpha^2 \bar{I}^2 \, |B(\nu)|^2 \psi_{11}(\nu), \tag{61}$$

where $B(\nu)$ is the frequency response function of the filter. If the output of the filter is then fed to an electrical square law detector and meter, the mean squared signal $\overline{S^2(t)}$ can be read off. But

$$\overline{S^2(t)} = 2\int_0^\infty \chi_{11}(\nu)\, \mathrm{d}\nu$$

and, if the spectral width of $|B(\nu)|$ is very much less than that of $\psi_{11}(\nu)$, we obtain from (61)

$$\overline{S^2(t)} = 2\alpha^2 \bar{I}^2 \psi_{11}(\nu_1) \int_0^\infty |B(\nu)|^2 \, \mathrm{d}\nu, \tag{62}$$

where ν_1 is the frequency on which the filter is centred (cf. also MANDEL [1962c]). Thus $\psi_{11}(\nu)$ can, in principle, be found from a succession of measurements with sharply tuned filters centred on a number of different frequencies. Of course, in practice, electrical filters have upper frequency limits of some hundreds of megacycles per second, which limits the application of the technique to narrow emission lines.

The fluctuations given by (62) are due to the wave nature of the incident radiation and should be labelled $\overline{S_W^2(t)}$, as in section 3.3. But, as previously, the determination of $\psi_{11}(\nu)$ is complicated by the presence of the shot noise fluctuations $\overline{S_P^2(t)}$ of the photo-current,† given by equation (53). The observed fluctuations $\overline{S^2(t)}$ will be the sum of both terms. Thus:

$$\overline{S^2(t)} = 2\alpha\bar{I}[1 + \alpha\bar{I}\psi_{11}(\nu_1)] \int_0^\infty |B(\nu)|^2 \, \mathrm{d}\nu. \tag{63}$$

Since $\psi_{11}(\nu_1)$ is, at most, of the order $1/\Delta\nu$, it is clear that the practical determination of $\psi_{11}(\nu)$ again depends on the value of the parameter $\alpha\bar{I}\xi(\infty)$, which is normally very small. FORRESTER [1961a, b] has proposed an optical superheterodyne technique for improving the signal-to-noise ratio.

The tuned filter method has been used by ALFORD and GOLD [1958] to study the modulation of the spectral density which arises when coherent light beams with a large optical path difference are superposed. In these experiments a regularly pulsed light source was used, leading to a spectral modulation much in excess of the shot noise. The

† With a narrow band amplifier, the mean signal $\overline{S(t)}$ is zero, so that $\overline{(\Delta S(t))^2} = \overline{S^2(t)}$.

possibility of repeating the experiment with a steady light beam has been discussed by GIVENS [1961, 1962] and MANDEL [1962c].

For optical maser light, for which $\alpha\bar{I}\xi(\infty)$ is very large and the bandwidth very small, the tuned filter method of spectral analysis might appear to be particularly well suited. But, because of the non-Gaussian nature of maser light, the above fluctuation formulae are not directly applicable (c.f. SMITH and WILLIAMS [1962]; WOLF [1963]; MANDEL [1963b]), although they have on occasion been used. However, when two or more similar independent maser beams are superposed, the spectral density of the resulting intensity fluctuations is to a first approximation given by an expression of the form (40). Moreover equation (62) is still valid so that the foregoing method remains applicable. The superposition or beat technique has already been used by JAVAN *et al.* [1961, 1962], HERRIOTT [1961, 1962], MCMURTRY and SIEGMAN [1962] and LIPSETT and MANDEL [1963] to examine the spectral profile of a maser light beam (cf. also SANDERS [1959]).

It is interesting to note that this technique becomes easier the narrower the spectral line and is therefore well suited to take over where ordinary interferometric techniques leave off. FORRESTER [1961a] has pointed out the possibility of making an accurate frequency comparison of two optical maser emission lines at very great distances from the sources, as in interplanetary space.

§ 4. The Particle Picture

4.1. THE PHOTON WAVE FUNCTION IN CONFIGURATION SPACE AND THE PROBABILITY OF PHOTO-EMISSION

We turn now to the discussion of light fluctuations in terms of the particle picture. Since we observe only the results of the interactions of photons with the photo-detector, a meaningful discussion must refer to the interaction products, i.e. to the photo-electrons rather than to the photons themselves. The most direct approach to the problem of calculating the correlations of the fluctuations would be to compute the photo-excitation or photo-emission probabilities for atoms of the detector in terms of the configuration of the excited atoms of the source. This two-stage interaction procedure has been used by FANO [1961], but it is quite involved. Here we shall adopt a different and rather simpler approach, but the treatment should not be regarded as complete. For simplicity we shall again restrict our discussion to a plane light beam.

If a wave function in configuration space can be defined for the photons of the radiation field, then the probability of detecting a photon by its (fast) interaction at a certain point at a certain time can be computed. The possibility of giving a corpuscular interpretation to the Maxwell field equations for an electromagnetic wave in free space, by defining a photon wave function in terms of the field vectors $\boldsymbol{E}(\boldsymbol{r}, t)$ and $\boldsymbol{H}(\boldsymbol{r}, t)$ or $\boldsymbol{E}(\boldsymbol{r}, t)$ and $\dot{\boldsymbol{E}}(\boldsymbol{r}, t)$ was pointed out by LANDAU and PEIERLS [1930] (see also OPPENHEIMER [1931]). We first make a Fourier integral momentum representation of $\boldsymbol{E}(\boldsymbol{r}, t)$ in the form: †

$$\boldsymbol{E}(\boldsymbol{r}, t) = \frac{1}{(2\pi)^3}\int_{-\infty}^{\infty}\!\!\int\!\!\int [\boldsymbol{\mathscr{E}}(\boldsymbol{k}) \exp - \mathrm{i}(\boldsymbol{k}\cdot\boldsymbol{r} - ckt) + \boldsymbol{\mathscr{E}}^*(\boldsymbol{k}) \exp \mathrm{i}(\boldsymbol{k}\cdot\boldsymbol{r} - ckt)]\, \mathrm{d}\boldsymbol{k}, \tag{64}$$

where $\boldsymbol{k}$ is the wave vector whose magnitude k is the wave number $2\pi\nu/c$. The photon wave function $\psi(\boldsymbol{k}, t)$ in momentum-spin space is then defined by (cf. AKHIEZER and BERESTETSKY [1953]):

$$\psi(\boldsymbol{k}, t) = \sqrt{\left(\frac{2}{k\hbar}\right)}\, \boldsymbol{\mathscr{E}}(\boldsymbol{k}) \exp (\mathrm{i}ckt), \tag{65}$$

where $2\pi\hbar$ is Planck's constant. The Fourier transform of $\psi(\boldsymbol{k}, t)$ is $\boldsymbol{\Psi}(\boldsymbol{r}, t)$, the wave function in configuration space:

$$\boldsymbol{\Psi}(\boldsymbol{r}, t) = \frac{1}{(2\pi)^3}\int_{-\infty}^{\infty}\!\!\int\!\!\int \psi(\boldsymbol{k}, t) \exp - (\mathrm{i}\boldsymbol{k}\cdot\boldsymbol{r})\, \mathrm{d}\boldsymbol{k}. \tag{66}$$

$\psi(\boldsymbol{k}, t)$ represents a pure momentum-spin state. It can be shown (see for example AKHIEZER and BERESTETSKY [1953]) that $\psi(\boldsymbol{k}, t)$ obeys the transversality condition and a Schrödinger type equation of motion and that, with the above normalization, $\psi^*(\boldsymbol{k}, t)\cdot\psi(\boldsymbol{k}, t)\mathrm{d}\boldsymbol{k}$ can be interpreted as the probability of finding the photon in the momentum interval $\mathrm{d}\boldsymbol{k}$. Although there are some difficulties connected with the interpretation of the corresponding scalar product $\boldsymbol{\Psi}^*(\boldsymbol{r}, t)\cdot\boldsymbol{\Psi}(\boldsymbol{r}, t)\mathrm{d}\boldsymbol{r}$ as the probability of finding the photon in the space interval $\mathrm{d}\boldsymbol{r}$ (cf. LANDAU and PEIERLS [1930]; OPPENHEIMER [1931]; AKHIEZER and BERESTETSKY [1953]), for this quantity is not locally related to the field vectors, they become serious only if one attempts to localize the position of the photon within a region smaller

† To avoid convergence difficulties we assume throughout that the radiation field is large but finite in space and time. But the correlation functions can be defined even in the limit.

than the wavelength. In the following we shall be content to define the position to an accuracy of the order of a wavelength and treat $\Psi^*(\boldsymbol{r}, t) \cdot \Psi(\boldsymbol{r}, t)$ as the spatial probability density.

In a real light beam there are many photons and they are not generally in pure quantum states. Consider first the effect of the presence of many particles. For a set of non-interacting photons one can write down a symmetrized momentum-spin Schrödinger wave function, consisting of products of functions $\psi_i(\boldsymbol{k}, t)$ of the type (65) describing the individual photons (cf. AKHIEZER and BERESTETSKY [1953]). From this the probability of finding any one photon in the momentum interval $\mathrm{d}\boldsymbol{k}$ is found to be $\sum_i \psi_i^*(\boldsymbol{k}, t) \cdot \psi_i(\boldsymbol{k}, t)\mathrm{d}\boldsymbol{k}$, where the sum is to be taken over all the photons of the system.

Now suppose that the photons are in mixed quantum states. This implies that the state is describable by a statistical ensemble of Schrödinger wave functions and that all probabilities and expectation values are to be computed by averaging over the ensemble. If we now regard each photon wave function $\psi_i(\boldsymbol{k}, t)$ as a member of the same ensemble, then the probability of finding one photon in the momentum interval $\mathrm{d}\boldsymbol{k}$ is $N\overline{\psi^*(\boldsymbol{k}, t) \cdot \psi(\boldsymbol{k}, t)}\mathrm{d}\boldsymbol{k}$, where the bar denotes the ensemble average and N is the number of particles. Now from (66) the ensemble of functions $\psi(\boldsymbol{k}, t)$ generates an ensemble of functions $\Psi(\boldsymbol{r}, t)$. It follows that the probability of finding one photon within the space interval $\mathrm{d}\boldsymbol{r}$ is given by the ensemble average $N\overline{\Psi^*(\boldsymbol{r}, t) \cdot \Psi(\boldsymbol{r}, t)}\mathrm{d}\boldsymbol{r}$.

We may however picture the ensemble of $\Psi(\boldsymbol{r}, t)$ in another way. According to (65) and (66) $\Psi(\boldsymbol{r}, t)$ is expressible as an integral superposition of harmonic time functions $\exp(ickt)$ with coefficients which are members of a statistical ensemble. Such a superposition generates a random function of time (cf. DOOB [1953]; DAVENPORT and ROOT [1958]) which is analogous to the random function $V(\boldsymbol{r}, t)$ that was used in the classical representation of light. We may therefore interpret the instantaneous value $\Psi^*(\boldsymbol{r}, t) \cdot \Psi(\boldsymbol{r}, t)$ as the fluctuating probability density of finding a photon at position $\boldsymbol{r}$ at time t. As the calculation of all expectation values involves an average over the ensemble, the results will of course be identical with those obtained from the usual density matrix representation† of the mixed state (cf. FANO [1957]; TER HAAR [1961]).

† Another representation of a photon beam has been described by FALICOV [1960].

Now let us briefly consider the nature of the ensemble of the random time function $\mathcal{\Psi}(\boldsymbol{r}, t)$. If all the Fourier coefficients $\mathcal{E}(\boldsymbol{k})$ in the expansion (66) are statistically independent for different k, then by the central limit theorem of statistics the expansion (66) will generate a Gaussian random function (cf. DOOB [1953]). Since photons of different energies produced by thermal sources are normally independent, it follows that $\mathcal{\Psi}(\boldsymbol{r}, t)$ is to be regarded as a Gaussian random function for thermal light. On the other hand, in view of the saturation effects that arise in optical masers, for example, there is some statistical dependence between the Fourier components in a maser beam, and the random function $\mathcal{\Psi}(\boldsymbol{r}, t)$ is generally not Gaussian.

We note that there is a close analogy between $\mathcal{\Psi}(\boldsymbol{r}, t)$ and the function $V(\boldsymbol{r}, t)$ of the classical representation. In fact the connection can be made complete. For a plane, linearly polarized, quasi monochromatic beam of thermal light we shall see that the random functions $\mathcal{\Psi}(\boldsymbol{r}, t)$ and $V(\boldsymbol{r}, t)$ are equivalent apart from a constant, and have identical statistical properties. In the following we shall continue to use the notations $\mathcal{E}(\boldsymbol{k})$, $\psi(\boldsymbol{k}, t)$, $\mathcal{\Psi}(\boldsymbol{r}, t)$, etc. with the understanding that the functions are now members of an ensemble.

By changing the variables of integration in the integral (66) from the Cartesian components k_1, k_2, k_3 to the polar components k, Ω and using (65), we can transform the integral as follows:

$$\mathcal{\Psi}(\boldsymbol{r}, t) = \frac{\sqrt{(2/\hbar)}}{(2\pi)^3} \iint \mathrm{d}\Omega \int_0^\infty \mathrm{d}k\, k^{\frac{3}{2}}\, \mathcal{E}(k, \Omega) \exp - \mathrm{i}k(\boldsymbol{\kappa} \cdot \boldsymbol{r} - ct), \qquad (67)$$

where $\boldsymbol{\kappa}$ is the unit vector in the direction of $\boldsymbol{k}$. Since the integral over k, i.e. over frequency, extends only over positive values, it follows at once that $\mathcal{\Psi}(\boldsymbol{r}, t)$, like $V(\boldsymbol{r}, t)$, is a random function of t which is analytic in the upper half complex plane. For a linearly polarized wave $\boldsymbol{E}(\boldsymbol{r}, t)$ has a fixed direction, which we may take to be the x-direction, so that $\mathcal{\Psi}(\boldsymbol{r}, t)$ becomes a scalar function and the integral in (67) over Ω degenerates. It follows that the spectral density of $\mathcal{\Psi}(\boldsymbol{r}, t)$ is proportional to

$$k^3\, \overline{\mathcal{E}^*(k, \Omega)\mathcal{E}(k, \Omega)}.$$

where the bar denotes the ensemble average.

Now consider the spectral density of $V(\boldsymbol{r}, t)$ expressed in the same terms. We first note that, on changing the variables of integration to k, Ω in equation (64), we obtain

$$\boldsymbol{E}(\boldsymbol{r}, t) = \frac{1}{(2\pi)^3}\iint \mathrm{d}\Omega \int_0^\infty \mathrm{d}k\, k^2[\boldsymbol{\mathscr{E}}(k, \Omega) \exp - \mathrm{i}k(\boldsymbol{\kappa} \cdot \boldsymbol{r} - ct)$$

$$+ \boldsymbol{\mathscr{E}}^*(k, \Omega) \exp \mathrm{i}k(\boldsymbol{\kappa} \cdot \boldsymbol{r} - ct)]. \qquad (68)$$

For plane, linearly polarized light $\boldsymbol{E}(\boldsymbol{r}, t)$ and $\boldsymbol{\mathscr{E}}(k, \Omega)$ become scalars and the integral over Ω degenerates. Now the complex analytic function $V(\boldsymbol{r}, t)$ is derived from the real classical wave amplitude $E(\boldsymbol{r}, t)$ by suppressing the second term, which is the complex conjugate of the first, in the spectral representation (68). Hence:

$$V(\boldsymbol{r}, t) \propto \int_0^\infty \mathrm{d}k\, k^2 \boldsymbol{\mathscr{E}}(k, \Omega) \exp - \mathrm{i}k(\boldsymbol{\kappa} \cdot \boldsymbol{r} - ct)$$

and the spectral density of $V(\boldsymbol{r}, t)$ is proportional to

$$\overline{k^4\, \boldsymbol{\mathscr{E}}^*(k, \Omega)\, \boldsymbol{\mathscr{E}}(k, \Omega)}.$$

This differs from the spectral density of $\Psi(\boldsymbol{r}, t)$ only by the factor k. For quasi-monochromatic light $\overline{\boldsymbol{\mathscr{E}}^*(k, \Omega)\, \boldsymbol{\mathscr{E}}(k, \Omega)}$ vanishes except for a narrow range of k centred on some mid-frequency k_0, so that the two normalized spectral densities will be indistinguishable. It follows, therefore, that the statistical properties of $\Psi(\boldsymbol{r}, t)$ and $V(\boldsymbol{r}, t)$ similarly normalized are similar and that the probability of detecting a photon at $\boldsymbol{r}$ at time t, which is proportional to $\Psi^*(\boldsymbol{r}, t)\, \Psi(\boldsymbol{r}, t)$, is also proportional to $V^*(\boldsymbol{r}, t)\, V(\boldsymbol{r}, t) = I(\boldsymbol{r}, t)$. Photons are, of course, only detected by their interactions with charges, but, if we ignore higher order interactions, the probability that a photon of given momentum falling on a photo-cathode ejects a photo-electron will be just a constant α, representing the quantum sensitivity of the cathode. If the intensity $I(t)$ of the quasi-monochromatic light beam is measured in units of photons per second, the probability that this beam, falling on the photo-electric detector, gives rise to a count in an interval $\mathrm{d}t$, is then $\alpha I(t)\, \mathrm{d}t$.

With this approach, which was first adopted by PURCELL [1956], we have, in a sense, disposed of the need for a photon wave function. The quantity $I(t)$ bridges the gap between the particle and the wave models and many of the previous results based on the wave picture now become applicable. The two models can be seen to have much in common, but the output of a photo-detector is no longer to be regarded as a continuous function of time and meaningful questions about particle counts can now be examined.

4.2. THE PROBABILITY DISTRIBUTION OF PHOTO-ELECTRIC COUNTS

The statistics of the counts obtained with a photo-detector illuminated by a light beam are described by the probability distribution $p(n, T)$ of obtaining n counts in a time interval T. We shall now use the result of the previous section to investigate $p(n, T)$ by the method described by MANDEL [1958, 1959] based on the idea of PURCELL [1956]. A somewhat different treatment has been described by KAHN [1958].

We begin by defining a time dependent probability distribution $p(n, T, t)$, which denotes the probability that n counts, or photo-electrons, are detected in the interval t to $t + T$. Like the probability $\alpha I(t)\,\mathrm{d}t$ of detecting a count between t and $t + \mathrm{d}t$, the distribution $p(n, T, t)$ is not normally observed. However, it is not completely unphysical, since observations could, in principle, be made on a large number of coherently illuminated photo-detectors (for which $I(t)$ is the same) for a time t to $t+T$. It then follows that $p(1, \mathrm{d}t, t) = \alpha I(t)\,\mathrm{d}t$ and it is shown in the Appendix that $p(n, T, t)$ is a Poisson distribution, with parameter given by the expectation value of n in the interval t to $t+T$. This value is obviously $\alpha \int_t^{t+T} I(t')\,\mathrm{d}t'$, for $\alpha I(t)\,\mathrm{d}t$ gives the expectation value in the infinitesimal interval t to $t+\mathrm{d}t$. Thus:

$$p(n, T, t) = \frac{1}{n!}\left[\alpha \int_t^{t+T} I(t')\mathrm{d}t'\right]^n \exp\left[-\alpha \int_t^{t+T} I(t')\mathrm{d}t'\right]. \qquad (69)$$

Since $I(t)$ is a random function, the probability $p(n, T, t)$ is itself a random function and $p(n, T)$ must be obtained from $p(n, T, t)$ by taking the time or ensemble average. However, this operation does not, in general, preserve the form of the above distribution, so that the fluctuations of $I(t)$ lead to a departure from classical counting statistics.

To illustrate the method we shall first of all calculate $p(n, T)$ for intervals T which are short compared with the coherence time of the light, i.e. for $T \ll 1/\Delta\nu$. As we have seen in section 2.2, $I(t)$ does not change significantly in such a short interval and the integrals in (69) all simplify to $I(t)T$. We then obtain $p(n, T)$ from $p(n, T, t)$ by averaging over the ensemble of $I(t)$. Thus:

$$p(n, T) = \frac{1}{n!}\int_0^\infty (\alpha I T)^n \exp(-\alpha I T)\, p(I)\,\mathrm{d}I, \qquad (70)$$

where $p(I)\mathrm{d}I$ is the probability distribution of I and is given by (12)

for polarized Gaussian light. If we insert this in (70) the integrand becomes a Γ-function and we arrive at:

$$p(n, T) = \frac{1}{(1 + \alpha \bar{I} T)(1 + 1/\alpha \bar{I} T)^n}. \tag{71a}$$

Now $\alpha \bar{I} T$ is obviously the mean number of counts $\bar{n}$ obtained in the interval T, so that

$$p(n, T) = \frac{1}{(1 + \bar{n})(1 + 1/\bar{n})^n}, \tag{71b}$$

when $T \ll 1/\Delta\nu$. This will be recognized as the Bose–Einstein distribution for n indistinguishable particles in the same quantum state, or within one cell of phase space. We have therefore shown that the fluctuations of $I(t)$ in the Poisson distribution (69) lead to the Bose–Einstein distribution when $T \ll 1/\Delta\nu$. It is interesting to note that a similar approach, in a slightly different context, was long ago used by BOTHE [1927] to derive the Bose–Einstein distribution. Again it should be stressed that these conclusions apply to Gaussian light. For non-Gaussian light, as from an optical maser, $p(n, T)$ will depart from the form (71) (cf. MANDEL [1963b]).

It is not difficult to see why the photons detected in a short time interval $T \ll 1/\Delta\nu$ must be regarded as being in the same quantum state. For the uncertainty in forward momentum $h\Delta\nu/c$ of these photons must be associated with an uncertainty in position of order $c/\Delta\nu$ or an uncertainty in arrival time of order $1/\Delta\nu$ and these quantities define the extent of the unit cell of phase space. When T is long compared with $1/\Delta\nu$ we would expect the function $p(n, T)$ to represent the distribution of the n particles among several cells of phase space and this has been confirmed by MANDEL [1958, 1959].

Let us now return to the more general problem of examining $p(n, T)$ for arbitrary T. If we represent the integrals in (69) by $E(T, t)$:

$$\int_t^{t+T} I(t')\, \mathrm{d}t' = E(T, t)\ , \tag{72}$$

with

$$\bar{I} T = \bar{E},$$

where $E(T, t)$ is the classical expression for the energy received in the interval t to $t+T$, then (69) can be written:

$$p(n, T, t) = \frac{1}{n!} (\alpha E)^n \exp(-\alpha E) \tag{73}$$

and $p(n, T)$ is obtained by averaging over the ensemble of E. Unfortunately, no explicit closed expression for the probability distribution of E is available (other than an approximation, cf. RICE [1945]) so that the foregoing procedure is not easily carried out. However, we can readily derive the cumulants of the distribution $p(n, T)$. From the known properties of the Poisson distribution (73) we can write down the moment generating function $M_n(x)$ of the distribution of n (cf. KENDALL [1952]). Thus:

$$M_n(x) = \overline{\exp\,[\alpha E(e^x - 1)]},$$

where the bar denotes the ensemble average over the random variable E. But, if $M_E(x)$ is the moment generating function of the distribution of E, this equation can be written:

$$M_n(x) = M_E(\alpha e^x - \alpha), \tag{74}$$

from which we obtain

$$K_n(x) = K_E(\alpha e^x - \alpha)$$

or

$$\sum_{i=1}^{\infty} \frac{x^i}{i!} \kappa_{ni} = \sum_{i=1}^{\infty} \frac{\alpha^i (e^x - 1)^i}{i!} \kappa_{Ei}\,, \tag{75}$$

where $K_n(x)$ and $K_E(x)$ are the corresponding cumulant generating functions and the κ_{ni}, and κ_{Ei} are the cumulants of the distributions of n and E. Since the cumulants κ_{Ei} have been found by SLEPIAN [1958], the expression (75) allows us to write down the cumulants κ_{ni} of the distribution of n by comparing coefficients of x^i in the expansion of (75). It can be shown (cf. MANDEL [1959]) † that

$$\begin{aligned}
\kappa_{n1} &= \alpha\kappa_{E1} \\
\kappa_{n2} &= \alpha\kappa_{E1} + \alpha^2\kappa_{E2} \\
\kappa_{n3} &= \alpha\kappa_{E1} + 3\alpha^2\kappa_{E2} + \alpha^3\kappa_{E3} \\
\kappa_{n4} &= \alpha\kappa_{E1} + 7\alpha^2\kappa_{E2} + 6\alpha^3\kappa_{E3} + \alpha^4\kappa_{E4} \\
&\text{etc.},
\end{aligned} \tag{76}$$

where

$$\kappa_{E1} = \bar{E} = \bar{I}T$$

$$\kappa_{Ei} = (i-1)!\,\bar{I}^i \int_{-\frac{1}{2}T}^{\frac{1}{2}T}\!\!\int\!\!\cdots\!\int \gamma_{11}(t_1 - t_2)\,\gamma_{11}(t_2 - t_3)\cdots\gamma_{11}(t_i - t_1)\,dt_1\,dt_2\cdots dt_i, \tag{77}$$

for $i \geqq 2$.

† There is an error in equation (10) of the paper by MANDEL [1959] which has been corrected here.

These cumulants define the counting distribution of n and are equivalent to an explicit expression for $p(n, T)$. Two limiting cases are of particular interest. If the mean light intensity $\bar{I}$ is extremely low, all the terms in (76) tend to become small compared with the first terms $\alpha\kappa_{E1} = \alpha\bar{I}T = \bar{n}$. It follows that the cumulants of the counting distribution $p(n, T)$ all tend to $\bar{n}$, which means that the distribution becomes Poissonian (cf. KENDALL [1952]). Thus, at very low beam intensities, the photons behave like classical particles in their statistical properties. On the other hand, at high intensities, when $\alpha\bar{I}$ becomes very great, the last term becomes dominant in each equation (76), so that the distribution of n tends to become identical with the distribution of αE. Since αE is the classical integrated signal received from the photo-detector, we see how the discrete distribution of n goes over into the distribution of the continuous signal $S(t)$ given by (41), which was treated earlier. This equivalence of the fluctuations at high light intensities was, of course, to be expected from the correspondence principle.

From (76) and (77) we can write down the variance $\overline{(\Delta n)^2}$ of the counting distribution $p(n, T)$, which is identical with the second cumulant κ_{n2}. Thus:

$$\begin{aligned}\overline{(\Delta n)^2} &= \alpha\bar{I}T + \alpha^2\bar{I}^2\int_{-\frac{1}{2}T}^{\frac{1}{2}T}\int |\gamma_{11}(t_1 - t_2)|^2\,\mathrm{d}t_1\,\mathrm{d}t_2 \\ &= \bar{n}[1 + \bar{n}\xi(T)/T],\end{aligned} \tag{78}$$

where $\bar{n} = \alpha\bar{I}T$ and $\xi(T)$ is the quantity introduced earlier in section 3.2. For $T \ll 1/\Delta\nu$, this reduces to the form

$$\overline{(\Delta n)^2} = \bar{n}(1 + \bar{n}), \tag{79}$$

which is characteristic of the Bose–Einstein distribution (71). On the other hand, when $T \gg 1/\Delta\nu$, which is usually the case in practice, $\xi(T) \approx \xi(\infty)$ and

$$\overline{(\Delta n)^2} = \bar{n}[1 + \bar{n}\xi(\infty)/T]. \tag{80}$$

This is the characteristic expression for n bosons distributed among $T/\xi(\infty)$ cells of phase space (cf. FÜRTH [1928b]), so that $\xi(\infty)$ should be identified with the coherence time of the light, or $c\xi(\infty)$ with the length of the unit cell of phase space (cf. GABOR [1950, 1961]; MANDEL [1959]). Thus the coherence length of the light is the quantity in the wave picture which is complementary to the length of the phase cell in the particle picture. The departure from classical counting

statistics, for which $\overline{(\Delta n)^2} = \bar{n}$, obviously depends on the parameter $\bar{n}\xi(\infty)/T$ giving the mean number of counts per unit cell of phase space. This is the analogue of the degeneracy parameter δ encountered in quantum statistics for the number of particles in the same quantum state. As it is the departure from classical counting statistics which is responsible for the observed correlation between the outputs of coherently illuminated photo-multipliers, the parameter

$$\delta = \bar{n}\xi(\infty)/T = \alpha\bar{I}\xi(\infty)$$

is especially significant for the Hanbury Brown and Twiss effect. As has already been pointed out in section 3.3 (cf. MANDEL [1961a], GABOR [1961]), δ is much less than unity for light beams other than optical maser beams, so that the direct measurement of the excess photon noise is a difficult problem (ALKEMADE [1959]). Equation (80) which was first obtained by PURCELL [1956] is analogous to equation (54) in the (augmented) wave picture, excepted that (54) applies to unpolarized light having half the degeneracy.

4.3. CORRELATION BETWEEN COUNTING FLUCTUATIONS

The time dependent probability distribution (69) allows us to calculate the correlation of the number of counts n_1 and n_2 recorded by two photo-detectors illuminated by partially coherent light beams for a time T. We shall follow the method given by MANDEL [1958].

Let suffixes 1 and 2 refer to the outputs of the two photo-detectors respectively. Then the expectation value of the product $\overline{n_1 n_2}$ will be:

$$\overline{n_1 n_2} = \sum_{n_1=0}^{\infty} \sum_{n_2=0}^{\infty} n_1 n_2 \overline{p_1(n_1, T, t)\, p_2(n_2, T, t)}, \tag{81}$$

where p_1 and p_2 are given by (69) and the bar on the R.H.S. denotes the ensemble average over $I_1(t)$ and $I_2(t)$. If we exchange the operations of summing and ensemble averaging and insert the known mean values of the Poisson distributions (69), we obtain:

$$\begin{aligned}\overline{n_1 n_2} &= \alpha_1\alpha_2 \int_t^{t+T}\int \overline{I_1(t')\, I_2(t'')}\, \mathrm{d}t'\, \mathrm{d}t'' \\ &= \alpha_1\alpha_2 \int_0^{T}\int \overline{I_1(t + t' - t'')\, I_2(t)}\, \mathrm{d}t'\, \mathrm{d}t'',\end{aligned} \tag{82}$$

in view of the stationarity of the random processes $I_1(t)$ and $I_2(t)$.

We now make use of equation (17), together with the reduction formula (43) for cross-spectral purity, which is applicable to most experiments in which the spectral distributions of the two beams are equal. Then (82) becomes:

$$\overline{n_1 n_2} = \alpha_1\alpha_2\bar{I}_1\bar{I}_2T^2 + \alpha_1\alpha_2\bar{I}_1\bar{I}_2\,|\gamma_{12}(0)|^2\int_0^T\int |\gamma_{11}(t' - t'')|^2\,\mathrm{d}t'\,\mathrm{d}t''$$

$$= \bar{n}_1\bar{n}_2 + \bar{n}_1\bar{n}_2[\xi(T)/T]\,|\gamma_{12}(0)|^2\,, \tag{83}$$

where we have substituted $T\xi(T)$ for the double integral, as in section 3.2, and put $\alpha_1\bar{I}_1T$ and $\alpha_2\bar{I}_2T$ equal to $\bar{n}_1$ and $\bar{n}_2$, respectively. It follows that the fluctuations of n_1 and n_2 are correlated and that the correlation is given by:

$$\overline{\Delta n_1 \Delta n_2} = \overline{n_1 n_2} - \bar{n}_1\bar{n}_2$$

$$= \bar{n}_1\bar{n}_2[\xi(T)/T]\,|\gamma_{12}(0)|^2. \tag{84}$$

This formula is analogous to the correlation formula (44) in the wave picture, except that (44) applies to unpolarized light, which shows only half the correlation.

As before, it is useful to write down the normalized correlation coefficient ρ given by:

$$\rho = \frac{\overline{\Delta n_1\,\Delta n_2}}{\sqrt{[\overline{(\Delta n_1)^2}\;\overline{(\Delta n_2)^2}]}}\,,$$

which, in view of (78) and (84), becomes

$$\rho = \frac{\sqrt{(\bar{n}_1\bar{n}_2)}[\xi(T)/T]\,|\gamma_{12}(0)|^2}{\sqrt{[1 + \bar{n}_1\xi(T)/T]}\sqrt{[1 + \bar{n}_2\xi(T)/T]}} \tag{85a}$$

and, if $T \gg 1/\Delta\nu$,

$$= \frac{\sqrt{(\delta_1\delta_2)}}{\sqrt{(1+\delta_1)}\sqrt{(1+\delta_2)}}\,|\gamma_{12}(0)|^2\,, \tag{85b}$$

where δ_1 and δ_2 are the degeneracy parameters. If the intensities $\bar{I}_1$ and $\bar{I}_2$ are equal, δ_1 and δ_2 will be equal also and

$$\rho = \frac{\delta}{1+\delta}\,|\gamma_{12}(0)|^2\,, \tag{85c}$$

which is similar to the relation (55b), except that we are here considering polarized light. We note that, for non-degenerate light beams ($\delta \ll 1$), the coefficient ρ is just proportional to δ, so that the effect is not easy to observe with ordinary light sources (cf. MANDEL [1961a,

1962b]; GABOR [1961]). Nevertheless, HANBURY BROWN and TWISS [1956a] succeeded in demonstrating the effect while working with a degeneracy of the order 10^{-3}. Although $\delta \gg 1$ for maser light beams, correlation phenomena have not so far been studied with maser light. The foregoing formulae are not applicable and, as explained in section 3.3, there are good reasons for believing that the correlation would be much less than that given by (85).

4.4. PARTIALLY POLARIZED LIGHT BEAMS

After discussing fully polarized light beams, we should now generalize our results to partially polarized light, as was done in section 2.4 in terms of the wave picture. The generalization of the correlation formula (84) was first given by WOLF [1960]. More recently the distribution (71) has been generalized (MANDEL [1963a]), and shown to be of the form corresponding to n bosons distributed among $2/(1+P)$ cells of phase space, when the degree of polarization is P.

We first recall that, from equation (25), the total light intensity $I(t)$ at a point in a partially polarized beam is simply the sum of the partial intensities $I_x(t)$ and $I_y(t)$ associated with the x and y directions normal to the beam. It follows that the probability of obtaining a count from an illuminated photo-electric detector in a time interval $\mathrm{d}t$ is the sum of the corresponding probabilities of obtaining a count with the x and y polarization components. Hence, if n_x and n_y were the numbers of counts recorded by the photo-detector in a time interval t to $t+T$ due to the x and y components separately, the number n recorded when the partially polarized beam falls on the detector would be

$$n = n_x + n_y. \tag{86}$$

This relation is not completely unphysical, since the separation into x and y components could, in principle, be made. It follows that:

$$\overline{(\Delta n)^2} = \overline{(\Delta n_x)^2} + \overline{(\Delta n_y)^2} + 2\overline{\Delta n_x \Delta n_y},$$

whence, from (78) and (84),

$$\overline{(\Delta n)^2} = \bar{n}_x + \bar{n}_y + [\xi(T)/T][\bar{n}_x{}^2 + \bar{n}_y{}^2 + 2\bar{n}_x\bar{n}_y\,|\gamma_{xy}(0)|^2]. \tag{87}$$

The directions of the x and y axes have, so far, been arbitrary. However, as shown by WOLF [1959], it is always possible to choose directions for which $\bar{I}_x = \bar{I}_y = \frac{1}{2}\bar{I}$ and therefore $\bar{n}_x = \bar{n}_y = \frac{1}{2}\bar{n}$. Moreover, with this choice $|\gamma_{xy}(0)|$ has its greatest value, which can be interpreted as the degree of polarization P, so that (87) can be written:

$$\overline{(\Delta n)^2} = \bar{n}[1 + \tfrac{1}{2}(1 + P^2)\bar{n}\xi(T)/T]. \tag{88}$$

This formula, which was first derived by WOLF [1960], shows that the degree of polarization P can, in principle, be obtained from measurements of the counting fluctuations, without recourse to polarizers. An analogous expression in the wave picture has been given by MANDEL and WOLF [1961b]. In the special case when the light is unpolarized, $P = 0$ and

$$\overline{(\Delta n)^2} = \bar{n}[1 + \tfrac{1}{2}\bar{n}\xi(T)/T], \tag{89}$$

which can be compared with (78). The degeneracy parameter is halved, as is to be expected from first principles.

In order to see how equation (84) for the counting correlation should be modified when the light beams are partially polarized, let us return to equation (82) and make use of (29a). Then we find:

$$\overline{n_1 n_2} = \alpha_1\alpha_2 \bar{I}(\boldsymbol{r}_1)\,\bar{I}(\boldsymbol{r}_2)\,T^2 + \alpha_1\alpha_2 \sum_i \sum_j \bar{I}_i(\boldsymbol{r}_1)\,\bar{I}_j(\boldsymbol{r}_2) \int_0^T\!\!\int |\gamma_{ij}(\boldsymbol{r}_1, \boldsymbol{r}_2, t' - t'')|^2 \,\mathrm{d}t'\,\mathrm{d}t'', \tag{90}$$

where we have used the expanded notation of section 2.4 for clarity. The indices i, j range over x and y. Now, by making the assumption of cross-spectral purity in a strong form (cf. MANDEL [1961b]), we can write the following reduction formula for $\gamma_{ij}(\boldsymbol{r}_1, \boldsymbol{r}_2, \tau)$:

$$\gamma_{ij}(\boldsymbol{r}_1, \boldsymbol{r}_2, \tau) = \gamma_{ii}(\boldsymbol{r}_1, \boldsymbol{r}_1, \tau)\,\gamma_{ij}(\boldsymbol{r}_1, \boldsymbol{r}_2, 0). \tag{91}$$

The implications of the assumption have been discussed in more detail by MANDEL and WOLF [1961b] and MANDEL [1963a]. When this formula is substituted in (90) we obtain:

$$\overline{\Delta n_1 \Delta n_2} = \alpha_1\alpha_2 T\xi(T) \sum_i \sum_j \bar{I}_i(\boldsymbol{r}_1)\,\bar{I}_j(\boldsymbol{r}_2)\,|\gamma_{ij}(\boldsymbol{r}_1, \boldsymbol{r}_2, 0)|^2, \tag{92}$$

where we have used the results $\bar{n}_1 = \alpha_1 \bar{I}(\boldsymbol{r}_1)T$ and $\bar{n}_2 = \alpha_2 \bar{I}(\boldsymbol{r}_2)T$.

As an example of the application of equation (92) suppose that the two beams to be correlated are completely coherent, but partially polarized, so that

$$\gamma_{ij}(\boldsymbol{r}_1, \boldsymbol{r}_2, 0) = \gamma_{ij}(\boldsymbol{r}_1, \boldsymbol{r}_1, 0) = \gamma_{ij}(\boldsymbol{r}_2, \boldsymbol{r}_2, 0).$$

Suppose further that the axes are again chosen to make

$$\bar{I}_x(\boldsymbol{r}_1) = \bar{I}_y(\boldsymbol{r}_1) = \tfrac{1}{2}\bar{I}(\boldsymbol{r}_1),\ \bar{I}_x(\boldsymbol{r}_2) = \bar{I}_y(\boldsymbol{r}_2) = \tfrac{1}{2}\bar{I}(\boldsymbol{r}_2),$$

when

$$|\gamma_{xy}(\boldsymbol{r}_1, \boldsymbol{r}_1, 0)| = |\gamma_{xy}(\boldsymbol{r}_2, \boldsymbol{r}_2, 0)| = P.$$

Then, since $\gamma_{xx}(\boldsymbol{r}_1, \boldsymbol{r}_1, 0) = \gamma_{yy}(\boldsymbol{r}_2, \boldsymbol{r}_2, 0) = 1$, (92) becomes:

$$\overline{\Delta n_1 \Delta n_2} = \tfrac{1}{2}\alpha_1\alpha_2(1 + P^2)T\xi(T)\,\bar{I}(\boldsymbol{r}_1)\,\bar{I}(\boldsymbol{r}_2), \tag{93}$$

or, on putting $\alpha_1\bar{I}(\boldsymbol{r}_1)T = \bar{n}_1$ and $\alpha_2\bar{I}(\boldsymbol{r}_2)T = n_2$,

$$\overline{\Delta n_1 \Delta n_2} = \tfrac{1}{2}\bar{n}_1\bar{n}_2(1 + P^2)\xi(T)/T. \tag{94}$$

This formula was first obtained by WOLF [1960] and shows how P may be derived from correlation measurements of the counts, without the introduction of any polarizers.

Suppose, on the other hand, that the two beams to be correlated are completely unpolarized but partially coherent. Then $|\gamma_{ij}(\boldsymbol{r}_1, \boldsymbol{r}_2, 0)|$ is zero for $i \neq j$, whereas

$$|\gamma_{xx}(\boldsymbol{r}_1, \boldsymbol{r}_2, 0)| = |\gamma_{yy}(\boldsymbol{r}_1, \boldsymbol{r}_2, 0)| = |\gamma_{12}(0)|$$

and

$$\bar{I}_x(\boldsymbol{r}_1) = \bar{I}_y(\boldsymbol{r}_1) = \tfrac{1}{2}\bar{I}(\boldsymbol{r}_1)$$
$$\bar{I}_x(\boldsymbol{r}_2) = \bar{I}_y(\boldsymbol{r}_2) = \tfrac{1}{2}\bar{I}(\boldsymbol{r}_2).$$

Then (92) reduces to:

$$\begin{aligned}\overline{\Delta n_1 \Delta n_2} &= \tfrac{1}{2}\alpha_1\alpha_2 T\xi(T)\,\bar{I}(\boldsymbol{r}_1)\,\bar{I}(\boldsymbol{r}_2)\,|\gamma_{12}(0)|^2 \\ &= \tfrac{1}{2}\bar{n}_1\bar{n}_2[\xi(T)/T]\,|\gamma_{12}(0)|^2\end{aligned} \tag{95}$$

and comparison with (84) shows that the correlation for unpolarized light is halved, as expected.

§ 5. Bunching Effects and Photoelectric Coincidence Experiments

In the foregoing sections we have shown that the fluctuations of the counts recorded by a photo-detector illuminated by Gaussian light depart from classical statistics in such a way that the variance always exceeds that given by the Poisson distribution. It follows that the counts do not occur at random, but exhibit a certain clustering or bunching effect which is characteristic of boson particles. If two light beams are partially coherent, this excess photon noise will be correlated in the two beams and is therefore responsible for the intensity correlation found by HANBURY BROWN and TWISS [1956a].

The method used in section 4.2 to examine the counting distribution is quite applicable also to the calculation of the bunching effect. Consider a photo-detector illuminated by polarized light of instantaneous intensity $I(t)$. Consider two infinitesimal time intervals t to

$t + \mathrm{d}t$ and $t + \tau$ to $t + \tau + \mathrm{d}\tau$ separated by a finite interval τ. Then the probability of observing a photo-electric count at both times t and $t + \tau$ is

$$\alpha^2 I(t)\, I(t + \tau)\, \mathrm{d}t\, \mathrm{d}\tau$$

and the ensemble average of this gives the probability of finding two counts separated by an interval τ. If this is divided by the ensemble average of the probability $\alpha I(t)\, \mathrm{d}t$ of finding one count at t within $\mathrm{d}t$, we arrive at the conditional probability $p_c(\tau)\, \mathrm{d}\tau$ of obtaining a second count τ seconds after the first. Thus:

$$p_c(\tau)\, \mathrm{d}\tau = \alpha^2 \overline{I(t + \tau)\, I(t)}\, \mathrm{d}t\, \mathrm{d}\tau \,/\, \alpha \overline{I(t)}\, \mathrm{d}t \tag{96}$$

and, with the help of equation (19), we immediately obtain:

$$p_c(\tau)\, \mathrm{d}\tau = \alpha \bar{I}[1 + |\gamma_{11}(\tau)|^2]\mathrm{d}\tau. \tag{97}$$

Since $|\gamma_{11}(\tau)| \approx 1$ for $\tau \ll 1/\Delta\nu$ and $|\gamma_{11}(\tau)| \ll 1$ for $\tau \gg 1/\Delta\nu$, the conditional probability $p_c(\tau)\mathrm{d}\tau$ always starts from the value $2\alpha\bar{I}\mathrm{d}\tau$ for small τ and tends to $\alpha\bar{I}\mathrm{d}\tau$ for large τ. The chance of detecting a photon close to another one is therefore twice as great as that for classical particles. This represents the bunching phenomenon characteristic of boson particles of which we have already spoken. An example of the distribution $p_c(\tau)$ is shown in Fig. 12 for a Gaussian spectral profile. Although equation (97) holds for all intensities, the bunching phenomenon will not be very evident unless the degeneracy parameter of the counts $\delta = \alpha\bar{I}\xi(\infty)$ is at least of order unity. For $|\gamma_{11}(\tau)|$ differs appreciably from zero only for $\tau \lesssim \xi(\infty)$, so that the average number of counts δ in a time $\xi(\infty)$ should be at least of order

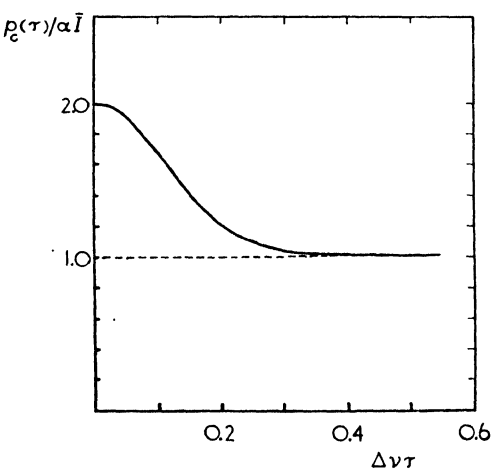

Fig. 12. The conditional probability density $p_c(\tau)$ for a Gaussian spectral distribution of r.m.s. width $\Delta\nu$

unity. Fig. 13 shows a pictorial comparison of the counting distributions to be expected with classical particles and with particles having a degeneracy $\delta \approx 1$, when the mean counting rates $\alpha\bar{I}$ are equal. The clustering is quite apparent. Of course these results will not generally hold for maser light in which intensity saturation effects occur. In such cases the counting fluctuations will probably appear to be intermediate between the two examples illustrated in Fig. 13.

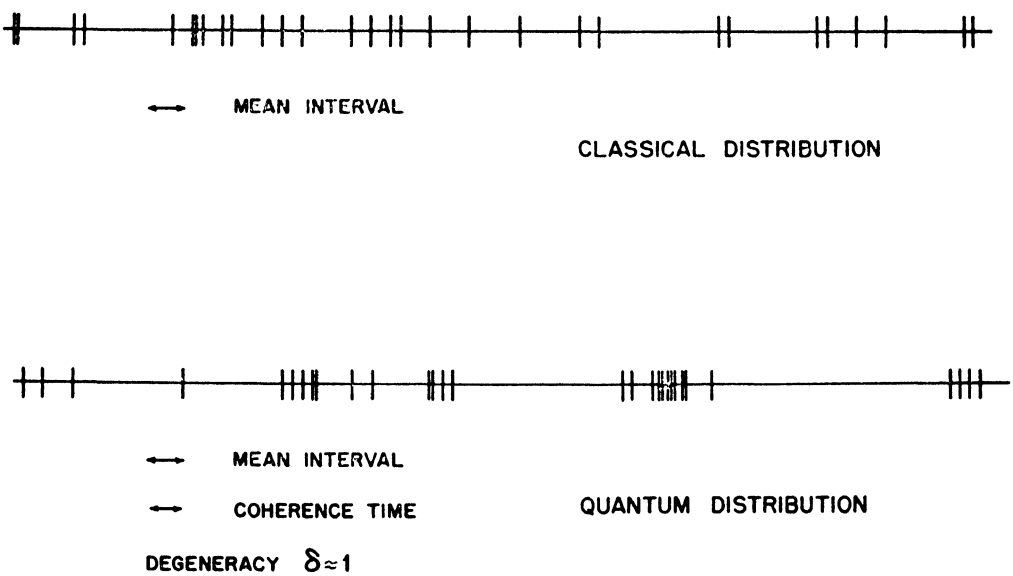

Fig. 13. An illustration of typical classical and quantum counting distributions

It is interesting to observe that the bunching in time of a photon beam is completely analogous to the well-known tendency of a photon gas (KOTHARI and AULUCK [1957]) – or indeed any boson gas (UHLENBECK and GROPPER [1932]; LONDON [1938, 1943]) – to form clusters in space. Fig. 14, which is taken from a paper by LONDON [1943], shows the mean particle density $D(r)$ of a boson gas at a distance r from another particle, and should be compared with Fig. 12. It is remarkable that, although the dimensionality of the two cases is quite different, the same clustering factor 2 is found for particles in close proximity.

The bunching phenomenon in a photon beam has also been very well analyzed by DICKE [1954] in terms of the radiation process in an excited gas. He showed that there is a correlation between the emission direction of successive photons, such that the emission probability in the same direction is nearly twice that in an arbitrary direction. This again leads to a clustering factor 2.

It is worth noting that the distribution (97) depends on $|\gamma_{11}(\tau)|$ in a simple way, so that measurements of the frequency distribution of the interval τ between pulse counts also provide information about the spectral profile of the light, as described in section 3.5. This problem is more fully discussed elsewhere (MANDEL [1962a]).

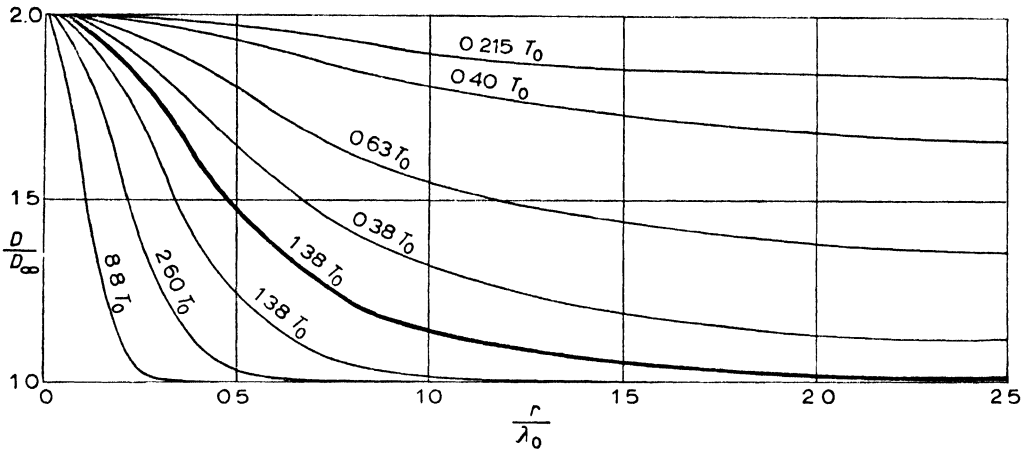

Fig. 14. The variation of density D in a Bose–Einstein gas with distance r from a given molecule, for different temperatures T and for the limit of a weak Van der Waals exchange interaction (T_0 is the condensation temperature and λ_0 is the mean De Broglie wavelength at T_0) (reproduced from a paper by LONDON, J. Chem. Phys. *11*, 212, 1943).

The foregoing photon bunching effect refers entirely to a single light beam and should be demonstrable with a single beam. However, it can easily be proved that two partially coherent beams exhibit correlated bunching effects, so that two photo-detectors illuminated by the two beams show 'counting coincidences' in excess of the random coincidences expected with classical particles.

Let $I_1(t)$ and $I_2(t)$ be the instantaneous unpolarized light intensities at the two detectors of quantum sensitivities α_1 and α_2 and suppose that the output pulses of the detectors are fed to a coincidence circuit of resolving time T. This circuit registers an output if and only if the two pulses occur within a time interval less than or equal to $\frac{1}{2}T$. The probability of obtaining a count from detector 1 at time t within $\mathrm{d}t$ is $\alpha_1 I_1(t)\mathrm{d}t$ and the probability of obtaining a count from detector 2 within the interval $t - \frac{1}{2}T$ to $t + \frac{1}{2}T$ is $\alpha_2 \int_{-\frac{1}{2}T}^{\frac{1}{2}T} I_2(t+\tau)\mathrm{d}\tau$, provided that this quantity is much less than unity. In that case the joint probability for the two counts, corresponding to a 'coincidence' within the resolving time T, is

$$\alpha_1\alpha_2 \mathrm{d}t \int_{-\frac{1}{2}T}^{\frac{1}{2}T} I_1(t)\, I_2(t+\tau)\, \mathrm{d}\tau.$$

By taking the ensemble average we arrive at the following expression for the rate R of 'coincidence counts' per second:

$$R = \alpha_1\alpha_2 \int_{-\frac{1}{2}T}^{\frac{1}{2}T} \overline{I_1(t)\, I_2(t+\tau)}\, \mathrm{d}\tau,$$

which, with the help of (31a) and the condition (43) for cross spectral purity, reduces to:

$$R = \alpha_1\alpha_2 \bar{I}_1 \bar{I}_2 [T + \tfrac{1}{2}|\gamma_{12}(0)|^2 \int_{-\frac{1}{2}T}^{\frac{1}{2}T} |\gamma_{11}(\tau)|^2 \mathrm{d}\tau]. \tag{98}$$

The integral

$$\int_{-\frac{1}{2}T}^{\frac{1}{2}T} |\gamma_{11}(\tau)|^2 \mathrm{d}\tau,$$

which we shall denote by $\zeta(T)$, is very similar to the function $\xi(T)$ previously encountered. Thus, $\zeta(T)$ obeys the two inequalities $\zeta(T) \leqq T$ and $\zeta(T) \leqq \xi(\infty)$, and $\zeta(T)$ is close to T or $\xi(\infty)$ according as $T \lessgtr 1/\Delta\nu$. If we denote the mean counting rates $\alpha_1\bar{I}_1$ and $\alpha_2\bar{I}_2$ of the two detectors by $\bar{r}_1$ and $\bar{r}_2$ respectively, then (98) can be written:

$$R = \bar{r}_1\bar{r}_2 T[1 + \tfrac{1}{2}|\gamma_{12}(0)|^2 \zeta(T)/T]. \tag{99}$$

The first term $\bar{r}_1\bar{r}_2 T$ represents the coincidence rate due to random counting rates $\bar{r}_1$ and $\bar{r}_2$, while the second term represents an excess rate due to the photon bunching, which never exceeds the first since $|\gamma_{12}(0)| \leqq 1$ and $\zeta(T) \leqq T$. This excess rate will be proportionately very small if the resolving time T of the coincidence circuit appreciably exceeds the coherence time $\xi(\infty)$ of the light, even if the beams are completely coherent. It is significant that the first two experiments performed to look for excess counting coincidences with coherent light beams (ADAMS *et al.* [1955]; BRANNEN and FERGUSON [1956]) both failed through having $\zeta(T)/T$ too small, although ADAMS *et al.* [1955] were admittedly more concerned with the beam splitting action of a half silvered mirror than with the photon bunching phenomenon. In their experiment the line width $\Delta\nu$ from a high pressure mercury lamp was of order 10^{12} c/sec and the resolving time $T \sim 4 \times 10^{-6}$ sec, giving $\zeta(T)/T \approx 2 \times 10^{-7}$. BRANNEN and FERGUSON [1956] used a similar lamp, but had a faster coincidence circuit with a resolving time $T \sim 10^{-8}$ sec, giving $\zeta(T)/T \approx 10^{-4}$.

The first successful experiment to demonstrate the excess counting coincidences with coherent beams was reported by TWISS *et al.* [1957]

and more fully described by TWISS and LITTLE [1959]. Their apparatus is shown in Fig. 15. By using the light from the green ($\lambda = 5461$ Å) line of a low pressure Hg^{198} isotope gas discharge, they were able to realize a coherence time of 0.7×10^{-9} sec. The light from the mercury lamp was passed through a filter to isolate the 5461 Å line and then to a half silvered mirror where two partially coherent beams with $|\gamma_{12}(0)|$ about 0.7 were formed. These beams fell on the two 1P21 photo-multipliers, whose output pulses were fed to a coincidence circuit with a resolving time $T \approx 7 \times 10^{-9}$ secs. Thus they achieved a value of $\frac{1}{2}|\gamma_{12}(0)|^2\zeta(T)/T$ of order 0.02. The experiment has since been successfully repeated by REBKA and POUND [1957] and BRANNEN *et al.* [1958].

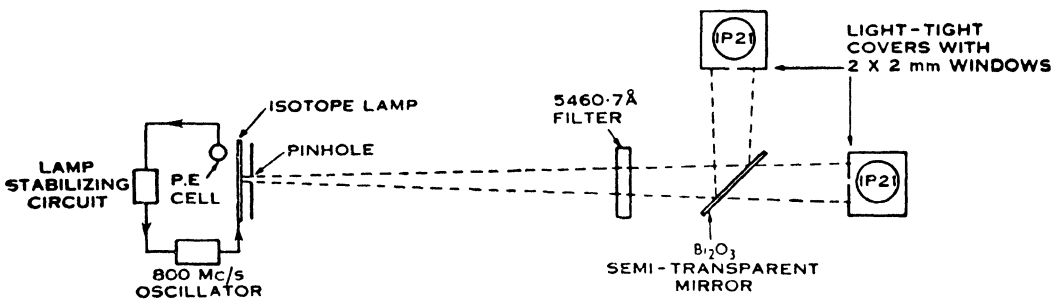

Fig. 15. The apparatus used for the demonstration of excess counting coincidences (reproduced from a paper by TWISS and LITTLE, Austr. J. Phys. *12*, 77, 1959).

In these experiments it is necessary to keep the counting rate sufficiently low to ensure that most time intervals T do not contain a counting coincidence, otherwise the percentage excess due to the photon bunching is evidently less than in equation (99). For this reason, a significant demonstration of the excess counting coincidences requires a much longer time than the signal correlation experiments described in section 3.1 (cf. HANBURY BROWN and TWISS [1956b]), in which large photo-currents can be tolerated. Nevertheless, the counting experiments provide the most direct – and perhaps also the most convincing – evidence for the departure from classical particle statistics, which has been implicit in Einstein's equation (3) for the last fifty years.

Acknowledgment

Work on this article was begun whilst the Author held a Visiting Appointment at the Institute of Optics, University of Rochester,

Rochester, N.Y., U.S.A. The work was supported by the United States Air Force, under Contract No. AF 49(638)-602 monitored by the AF Office of Scientific Research of the Air Research and Development Command.

Appendices

A. THE CONNECTION BETWEEN THE CORRELATIONS OF THE REAL AND COMPLEX WAVE FUNCTIONS

The cross-correlation of the two complex analytic wave functions $V_1(t)$ and $V_2(t)$ introduced in section 2.1 is defined by

$$\Gamma_{12}(\tau) = \overline{V_1(t+\tau)\, V_2^*(t)}.$$

In order to relate $\Gamma_{12}(\tau)$ to the correlations of the real and imaginary parts of $V_1(t)$ and $V_2(t)$ we will first show that

$$\overline{V_1(t+\tau)\, V_2(t)} = 0. \tag{A1}$$

As the random processes are assumed to be ergodic we may replace the ensemble average by a time average and write:

$$\overline{V_1(t+\tau)\, V_2(t)} = \lim_{T\to\infty} \frac{1}{T} \int_{-\frac{1}{2}T}^{\frac{1}{2}T} V_{1T}(t+\tau)\, V_{2T}(t)\, \mathrm{d}t. \tag{A2}$$

If we now introduce the Fourier transforms $A_{1T}(\nu)$ and $A_{2T}(\nu)$ of the truncated analytic functions, this becomes:

$$\begin{aligned}
&\overline{V_1(t+\tau)\, V_2(t)} \\
&= \lim_{T\to\infty} \frac{1}{T} \int_{-\frac{1}{2}T}^{\frac{1}{2}T} \int\int_0^\infty A_{1T}(\nu) A_{2T}(\nu') \exp 2\pi\mathrm{i}[\nu\tau + (\nu+\nu')t]\, \mathrm{d}\nu\, \mathrm{d}\nu'\, \mathrm{d}t \\
&= \lim_{T\to\infty} \int\int_0^\infty A_{1T}(\nu) A_{2T}(\nu') \exp(2\pi\mathrm{i}\nu\tau) \frac{\sin \pi(\nu+\nu')T}{\pi(\nu+\nu')T}\, \mathrm{d}\nu \mathrm{d}\nu' \\
&= \lim_{T\to\infty} \int_0^\infty \int_\nu^\infty A_{1T}(\nu) A_{2T}(\nu''-\nu) \exp(2\pi\mathrm{i}\nu\tau) \frac{\sin(\pi\nu''T)}{(\pi\nu''T)}\, \mathrm{d}\nu''\mathrm{d}\nu.
\end{aligned} \tag{A3}$$

Now as $T \to \infty$, the term $\sin(\pi\nu''T)/(\pi\nu''T)$ makes the integrand vanish, unless $\nu'' = 0$. But, in that case, $A_{1T}(\nu)A_{2T}(-\nu)$ vanishes, since the spectra $A_{1T}(\nu)$ and $A_{2T}(\nu)$ are zero for negative or zero frequencies. It follows that the whole integral in (A3) vanishes in the limit, so that equation (A1) holds.

Now let $V_1(t)$ and $V_2(t)$ be decomposed into real and imaginary parts as follows:

$$V_1(t) = V_1^{(r)}(t) + iV_1^{(i)}(t)$$
$$V_2(t) = V_2^{(r)}(t) + iV_2^{(i)}(t). \tag{A4}$$

Then the correlation in the complex equation (A1) splits into the sum of four terms and we obtain the following two real equations:

$$\overline{V_1^{(r)}(t+\tau)\, V_2^{(r)}(t)} = \overline{V_1^{(i)}(t+\tau)\, V_2^{(i)}(t)} \tag{A5}$$

$$\overline{V_1^{(i)}(t+\tau)\, V_2^{(r)}(t)} = -\overline{V_1^{(r)}(t+\tau)\, V_2^{(i)}(t)}. \tag{A6}$$

In particular, if $V_1(t) = V_2(t)$ and $\tau = 0$, we have from (A5) and (A6):

$$\overline{V_1^{(r)2}(t)} = \overline{V_1^{(i)2}(t)} = \tfrac{1}{2}|V_1(t)|^2 \tag{A7}$$

$$\overline{V_1^{(i)}(t)V_1^{(r)}(t)} = 0, \tag{A8}$$

so that the values of $V_1^{(r)}(t)$ and $V_1^{(i)}(t)$ at the same instant t are uncorrelated.

Now, let us similarly decompose $\Gamma_{12}(\tau)$ into the sum of four terms by using (A4). Then we find:

$$\begin{aligned}\Gamma_{12}(\tau) = {} & \overline{V_1^{(r)}(t+\tau)\, V_2^{(r)}(t)} + \overline{V_1^{(i)}(t+\tau)\, V_2^{(i)}(t)} \\ & + i\overline{V_1^{(i)}(t+\tau)\, V_2^{(r)}(t)} - i\overline{V_1^{(r)}(t+\tau)\, V_2^{(i)}(t)}\,,\end{aligned} \tag{A9}$$

which, together with (A5) and (A6), leads to:

$$\overline{V_1^{(r)}(t+\tau)\, V_2^{(r)}(t)} = \overline{V_1^{(i)}(t+\tau)\, V_2^{(i)}(t)} = \tfrac{1}{2}\mathscr{R}[\Gamma_{12}(\tau)], \tag{A10}$$

$$\overline{V_1^{(i)}(t+\tau)\, V_2^{(r)}(t)} = -\overline{V_1^{(r)}(t+\tau)\, V_2^{(i)}(t)} = \tfrac{1}{2}\mathscr{I}[\Gamma_{12}(\tau)]. \tag{A11}$$

These are the relations (16) quoted in section 2.3.

B. THE DERIVATION OF THE DISTRIBUTION $p(n, T, t)$

Let $\alpha I(t)\mathrm{d}t$ be the probability of obtaining a photo-electric count in an infinitesimal time interval t to $t + \mathrm{d}t$, when quasi-monochromatic light of intensity $I(t)$ photons per second is falling on the detector of quantum sensitivity α. Consider a finite time interval from t to $t+T$ and let $p(n, T, t)$ be the required probability of obtaining n counts in the interval. This time dependent probability is itself a random function, but one which is not usually measured, although, as has been pointed out in the text in section 4.2, it is not quite unphysical.

Let us divide the interval t to $t + T$ into $T/\Delta T$ very short intervals of length ΔT, which are labelled

$$t + i\Delta T = t_i\,, \qquad i = 0, 1, 2, \ldots, T/\Delta T.$$

Then the probability of obtaining n counts in t to $t + T$ is the product of the probabilities of obtaining a count at time t_{r_1}, a count at time t_{r_2}, . . ., a count at time t_{r_n}, multiplied by the probabilities of obtaining no counts in the remaining $T/\Delta T - n$ intervals, summed over all possible sequences of counts. Thus:

$$p(n, T, t) = \lim_{\Delta T \to 0} \sum_{r_1=0}^{T/\Delta T} \sum_{r_2=0}^{T/\Delta T} \cdots \sum_{r_n=0}^{T/\Delta T} \frac{1}{n!} \alpha^n I(t_{r_1}) I(t_{r_2}) \cdots I(t_{r_n}) \Delta T^n \times \prod_{i=0}^{T/\Delta T} [1 - \alpha I(t_i)\Delta T] / \prod_{j=1}^{n} [1 - \alpha I(t_{r_j})\Delta T]. \tag{B1}$$

We first note that, as $\Delta T \to 0$, the product

$$\prod_{j=1}^{n} [1 - \alpha I(t_{r_j})\Delta T]$$

becomes

$$1 - n\mathrm{O}[\Delta T]$$

and therefore tends to unity if n is finite. The multiple summations over $r_1, r_2, \ldots r_n$ become separable and equal to:

$$[\sum_{r_i=0}^{T/\Delta T} \alpha I(t_{r_i})\Delta T]^n,$$

which tends to $[\alpha \int_t^{t+T} I(t')\,\mathrm{d}t']^n$ in the limit $\Delta T \to 0$. The remaining product can be expanded as follows:

$$\prod_{i=0}^{T/\Delta T} [1 - \alpha I(t_i)\Delta T] = 1 - [\sum_{i=0}^{T/\Delta T} \alpha I(t_i)\Delta T] + \frac{1}{2!}[\sum_{i=0}^{T/\Delta T} \alpha I(t_i)\Delta T]^2 - \frac{1}{2!}\sum_{i=0}^{T/\Delta T} \alpha^2 I^2(t_i)(\Delta T)^2 - \frac{1}{3!}[\sum_{i=0}^{T/\Delta T} \alpha I(t_i)\Delta T]^3 + \frac{1}{3!}\sum_i \sum_j \alpha^3 I(t_i) I^2(t_j)(\Delta T)^3 + \cdots \tag{B2}$$

Now the terms in square brackets are all of order zero in ΔT, while the others are of the first or higher order in ΔT and tend to become negligible as $\Delta T \to 0$. It follows that

$$\prod_{i=0}^{T/\Delta T} [1 - \alpha I(t_i)\Delta T] \to \exp [-\sum_{i=0}^{T/\Delta T} \alpha I(t_i)\Delta T] \to \exp [-\alpha \int_t^{t+T} I(t')\,\mathrm{d}t'] \tag{B3}$$

as $\Delta T \to 0$. The limiting form of (B1) is therefore

$$p(n, T, t) = \frac{1}{n!}\left[\alpha\int_t^{t+T} I(t')\,dt'\right]^n \exp -\alpha\int_t^{t+T} I(t')\,dt', \qquad \text{(B4)}$$

which is a Poisson distribution in n with parameter $\alpha\int_t^{t+T} I(t')\,dt'$.

References

ADAMS, A., L. JANOSSY and P. VARGA, 1955, Ann. d. Phys. ***16***, 408.

AKHIEZER, A. I. and V. B. BERESTETSKY, 1953, Quantum Electrodynamics (State Technico-Theoretical Literature Press, Moscow; English translation: Office of Technical Services, Washington, D.C.).

ALFORD, W. P. and A. GOLD, 1958, Amer. J. Phys. ***56***, 481.

ALKEMADE, C. T. J., 1959, Physica ***25***, 1145.

BARRAT, J. P. and C. COHEN-TANNOUDJI, 1961, Compt. Rend. Acad. Sci. ***252***, 394.

BENDAT, J. S., 1958, Principles and Applications of Random Noise Theory (John Wiley, New York).

BLANC-LAPIERRE, A., 1956, Proceedings Internat. Congress of Math., Amsterdam 1954, Vol. ***3*** (North-Holland Publ. Co., Amsterdam).

BLANC-LAPIERRE, A. and P. DUMONTET, 1955, Rev. d'Opt. ***34***, 1.

BOLGIANO, L. P., Jr., 1961, Trans. I.R.E. MTT-***9***, 315.

BORN, M. and E. WOLF, 1959, Principles of Optics (Pergamon Press, London).

BOTHE, W., 1927, Z. f. Phys. ***41***, 345.

BOURRET, R. C., 1960, Nuovo Cimento ***18***, 347.

BRACEWELL, R. N., 1958, Proc. I.R.E. ***46***, 97.

BRANNEN, E. and H. I. S. FERGUSON, 1956, Nature ***178***, 481.

BRANNEN, E., H. I. S. FERGUSON and W. WEHLAU, 1958, Canad. J. Phys. ***36***, 871.

BUNIMOVICH, V. I., 1949, J. Tech. Phys. U.S.S.R. ***19***, 1231.

BURGESS, R. E., 1941, Proc. Phys. Soc. ***53***, 293.

BURGESS, R. E., 1946, Proc. Phys. Soc. ***58***, 313.

CALLEN, H. B. and T. A. WELTON, 1951, Phys. Rev. ***83***, 34.

COLLINS, R. S., D. F. NELSON, A. D. SCHAWLOW, W. BOND, C. G. B. GARRETT and W. KAISER, 1960, Phys. Rev. L. ***5***, 303.

DAVENPORT, W. and W. L. ROOT, 1958, An Introduction to Random Signals and Noise (McGraw-Hill, New York).

DICKE, R. H., 1954, Phys. Rev. ***93***, 99.

DOOB, J. L., 1953, Stochastic Processes (John Wiley, New York).

EINSTEIN, A., 1909a, Phys. Z. ***10***, 185.

EINSTEIN, A., 1909b, Phys. Z. ***10***, 817.

EINSTEIN, A., 1915, Ann. d. Phys. ***47***, 879.

EINSTEIN, A., 1917, Phys. Z. ***18***, 121.

EINSTEIN, A. and L. HOPF, 1910, Ann. d. Phys. ***33***, 1096.

EKSTEIN, H. and N. ROSTOKER, 1955, Phys. Rev. ***100***, 1023.

FALICOV, L. M., 1960, Nuovo Cimento ***16***, 247.

FALKOFF, D. L. and J. E. MCDONALD, 1951, J.O.S.A. ***41***, 861.
FANO, U., 1949, J.O.S.A. ***39***, 859.
FANO, U., 1954, Phys. Rev. ***93***, 121.
FANO, U., 1957, Rev. Mod. Phys. ***29***, 74.
FANO, U., 1961, Am. J. Phys. ***29***, 539.
FELLGETT, P., 1949, J.O.S.A. ***39***, 970.
FELLGETT, P., 1957, Nature ***179***, 956.
FELLGETT, P., R. C. JONES and R. Q. TWISS, 1959, Nature ***184***, 967.
FORRESTER, A. T., 1961a, J.O.S.A. ***51***, 253.
FORRESTER, A. T., 1961b, Advances in Quantum Electronics (Columbia University Press, New York) p. 233.
FORRESTER, A. T., R. A. GUDMUNDSEN and P. O. JOHNSON, 1955, Phys. Rev. ***99***, 1961.
FOWLER, R. H., 1929, Statistical Mechanics (Cambridge).
FÜRTH, R., 1928a, Z. f. Phys. ***48***, 323.
FÜRTH, R., 1928b, Z. f. Phys. ***50***, 310.
FÜRTH, R., 1948, Proc. Roy. Soc. A***192***, 593.
FÜRTH R. and D. K. C. MACDONALD, 1947, Nature ***159***, 608.
GABOR D., 1946, J. Inst. Electr. Eng. ***93*** part III, 429.
GABOR, D., 1950, Phil. Mag. Ser. 7, ***41***, 1161.
GABOR, D., 1956, Proc. Symposium on Astronomical Optics and Related Subjects, Manchester (North-Holland Publishing Co., Amsterdam).
GABOR, D., 1961, Progress in Optics (North-Holland Publishing Co., Amsterdam) ***1***, 111.
GAMO, H., 1957, J.O.S.A. ***47***, 976.
GAMO, H., 1961, Advances in Quantum Electronics (Columbia University Press) p. 255.
GAMO, H., 1962, Proceedings of the Conference on Electromagnetic Theory and Antennas, Copenhagen 1962, in press.
GIVENS, M. P., 1961, J.O.S.A. ***51***, 1030 and 1032.
GIVENS, M. P., 1962, J.O.S.A. ***52***, 225.
GLAUBER, R. J., 1963, Proc. 3rd Symp. Quantum Electronics, Paris 1963, in press.
HANBURY BROWN, R., 1960, Proc. of Symposium on Interferometry, N.P.L. (H.M.S.O., London).
HANBURY BROWN, R., R. C. JENNISON and M. K. DAS GUPTA, 1952, Nature ***170***, 1061.
HANBURY BROWN, R. and R. Q. TWISS, 1954, Phil. Mag. Ser. 7, ***45***, 663.
HANBURY BROWN, R. and R. Q. TWISS, 1956a, Nature ***177***, 27.
HANBURY BROWN, R. and R. Q. TWISS, 1956b, Nature ***178***, 1046.
HANBURY BROWN, R. and R. Q. TWISS, 1957a, Proc. Roy. Soc. A***242***, 300.
HANBURY BROWN, R. and R. Q. TWISS, 1957b, Proc. Roy. Soc. A***243***, 291.
HANBURY BROWN, R. and R. Q. TWISS, 1958a, Proc. Roy. Soc. A***248***, 199.
HANBURY BROWN, R. and R. Q. TWISS, 1958b, Proc. Roy. Soc. A***248***, 222.
HARWIT, M., 1960, Phys. Rev. ***120***, 1551.
HERRIOTT, D. R., 1961, Advances in Quantum Electronics (Columbia University Press, New York) p. 44.
HERRIOTT, D. R., 1962, J.O.S.A. ***52***, 31.
HOPKINS, H. H., 1951, Proc. Roy. Soc. A***208***, 263.

HOPKINS, H. H., 1953, Proc. Roy. Soc. A*217*, 408.
HOPKINS, H. H., 1957, J.O.S.A. *47*, 508.
HURWITZ, H. Jr., 1945, J.O.S.A. *35*, 525.
JANOSSY, L., 1957, Nuovo Cimento *6*, 111.
JANOSSY, L., 1959, Nuovo Cimento *12*, 369.
JAVAN, A., E. A. BALLIK and W. L. BOND, 1962, J.O.S.A. *52*, 96.
JAVAN, A., W. R. BENNETT Jr. and D. R. HERRIOTT, 1961, Phys. Rev. L. *6*, 106.
JENNISON, R. C. and M. K. DAS GUPTA, 1956, Phil. Mag. Ser. 8, *1*, 55.
JOHNSON, J. B., 1928, Phys. Rev. *32*, 97.
JONES, R. C., 1947, J.O.S.A. *37*, 879.
JONES, R. C., 1953, Advances in Electronics (Academic Press, New York) *5*, 1.
JONES, R. C., 1959, Proc. I.R.E. *47*, 1481.
KAHN, F. D., 1958, Optica Acta *5*, 93.
KANO, Y. and E. WOLF, 1962, Proc. Phys. Soc., *80*, 1273.
KENDALL, M. G., 1952, Advanced Theory of Statistics, 5th Ed. (C. Griffin and Co., London).
KOTHARI, D. S. and F. C. AULUCK, 1957, Current Sci. *26*, 169.
LANDAU, L. and R. PEIERLS, 1930, Z. f. Phys. *62*, 188.
LAWSON, J. L. and G. E. UHLENBECK, 1950, Threshold Signals (McGraw-Hill, New York).
LEWIS, W. B., 1947, Proc. Phys. Soc. *59*, 34.
LIPSETT M. S. and MANDEL, L., 1963, Nature *197*, 547.
LONDON, F., 1938, Phys. Rev. *54*, 947.
LONDON, F., 1943, J. Chem. Phys. *11*, 203.
MACDONALD, D. K. C., 1948, Reports on Progress in Physics *12*, 56.
MCMASTER, W. H., 1961, Rev. Mod. Phys. *33*, 8.
MCMURTRY, B. J. and A. E. SIEGMAN, 1962, Appl. Opt. *1*, 51.
MAIMAN, T. H., 1960, Nature *187*, 493.
MAIMAN, T. H., 1961, Phys. Rev. *123*, 1145.
MANDEL, L., 1958, Proc. Phys. Soc. *71*, 1037.
MANDEL, L., 1959, Proc. Phys. Soc. *74*, 233.
MANDEL, L., 1961a, J.O.S.A. *51*, 797.
MANDEL, L., 1961b, J.O.S.A. *51*, 1342.
MANDEL, L., 1962a, Proceedings of the Conference on Electro-Magnetic Theory and Antennas, Copenhagen 1962, in press.
MANDEL, L., 1962b, J.O.S.A. *52*, 1407.
MANDEL, L., 1962c, J.O.S.A. *52*, 1335.
MANDEL, L., 1963a, Proc. Phys. Soc., to be published.
MANDEL, L., 1963b, Proc. 3rd Symp. Quantum Electronics, Paris 1963, in press.
MANDEL, L. and E. WOLF, 1961a, J.O.S.A. *51*, 815.
MANDEL, L. and E. WOLF, 1961b, Phys. Rev., *124*, 1696.
MANDEL, L. and E. WOLF, 1962, Proc. Phys. Soc. *80*, 894.
MICHELSON, A. A., 1891, Nature *45*, 160.
MICHELSON, A. A., 1920, Astrophys. J. *51*, 257.
MICHELSON, A. A. and F. G. PEASE, 1921, Astrophys. J. *53*, 249.
MILATZ, J. M. W. and H. A. VAN DER VELDEN, 1943, Physica *10*, 369.
NELSON, D. F. and R. J. COLLINS, 1961, J. Appl. Phys. *32*, 739.
NYQUIST, H., 1928, Phys. Rev. *32*, 110.

OPPENHEIMER, J. R., 1931, Phys. Rev. ***38***, 725.
PANCHARATNAM, S., 1956, Proc. Ind. Acad. Sci. A***44***, 398.
PANCHARATNAM, S., 1961, Conf. Report on Communications and Information Theory Aspects of Modern Optics, Syracuse, N.Y. 1960, p. 115.
PARRENT, G. B., 1959, J.O.S.A. ***49***, 787.
PARRENT, G. B. and P. ROMAN, 1960, Nuovo Cimento Ser. 10, ***15***, 370.
PARZEN, E. and N. SHIREN, 1956, J. Math. and Phys. ***35***, 278.
PLANCK, M., 1901, Ann. d. Phys. ***4***, 553.
PURCELL, E. M., 1956, Nature ***178***, 1449.
RATCLIFFE, J. A., 1958, Reports on Progress in Physics ***19***, 188.
RAYLEIGH, 1889, Phil. Mag. Ser. 5, ***27***, 460.
REBKA, G. A. and R. V. POUND, 1957, Nature ***180***, 1035.
RICE, S. O., 1944, Bell Syst. Tech. J. ***23***, 1 and 282.
RICE, S. O., 1945, Bell Syst. Tech. J. ***24***, 46.
ROMAN, P., 1959, Nuovo Cimento ***13***, 974.
ROMAN, P., 1961, Nuovo Cimento ***20***, 759.
ROMAN, P. and E. WOLF, 1960a, Nuovo Cimento ***17***, 462.
ROMAN, P. and E. WOLF, 1960b, Nouvo Cimento ***17***, 477.
ROOT, W. L. and T. S. PITCHER, 1955, Ann. Math. Statist. ***26***, 313.
SANDERS, J. H., 1959, Nature ***183***, 312.
SARD, R. D., 1946, J. Appl. Phys. ***17***, 768.
SCHAWLOW, A. L. and G. E. DEVLIN, 1961, Phys. Rev. L. ***6***, 96.
SCHAWLOW, A. L. and C. H. TOWNES, 1958, Phys. Rev. ***112***, 1940.
SENITZKY, I. R., 1959, Phys. Rev. ***115***, 227.
SENITZKY, I. R., 1960, Phys. Rev. ***119***, 1807.
SENITZKY, I. R., 1961, Phys. Rev. ***123***, 1525.
SHIMODA, K., H. TAKAHASI and C. H. TOWNES, 1957, J. Phys. Soc. Jap. ***12***, 686.
SILLITO, R. M., 1957, Nature ***179***, 1127.
SLEPIAN, D., 1958, Bell Syst. Tech. J. ***37***, 163.
SMEKAL, A., 1926, Z. f. Phys. ***37***, 319.
SMITH, A. W. and G. W. WILLIAMS, 1962, J.O.S.A. ***52***, 337.
SMITH, J. J. and E. M. PURCELL, 1953, Phys. Rev. ***92***, 1069.
SOLODOVNIKOV, V. V., 1960, Introduction to the Statistical Dynamics of Automatic Control Systems (Dover Publications, New York).
STOKES, G. G., 1852, Trans. Cam. Phil. Soc. ***9***, 399.
STRANDBERG, M. W. P., 1957, Phys. Rev. ***106***, 617.
TER HAAR, D., 1961, Reports on Progress in Physics ***24***, 304.
TITCHMARSH, E. C., 1948, Introduction to the Theory of Fourier Integrals (Oxford, Clarendon Press).
TOLHOEK, H. A., 1956, Rev. Mod. Phys. ***28***, 277.
TORALDO DI FRANCIA, G., 1960, Nuovo Cimento ***16***, 61.
TWISS, R. Q. and R. HANBURY BROWN, 1957, Nature ***179***, 1128.
TWISS, R. Q. and A. G. LITTLE, 1959, Austr. J. Phys. ***12***, 77.
TWISS, R. Q., A. G. LITTLE and R. HANBURY BROWN, 1957, Nature ***180***, 324.
UHLENBECK, G. E. and L. GROPPER, 1932, Phys. Rev. ***41***, 79.
VAN CITTERT, P. H., 1934, Physica ***1***, 201.
VAN DER ZIEL, A., 1952, Advances in Electronics ***4*** (Academic Press, New York) 110.

VON LAUE, M., 1915a, Ann. d. Phys. ***47***, 853.
VON LAUE, M., 1915b, Ann. d. Phys. ***48***, 668.
WEBER, J., 1956, Phys. Rev. ***101***, 1620.
WEBER, J., 1957, Phys. Rev. ***108***, 537.
WEBER, J., 1959, Rev. Mod. Phys. ***31***, 681.
WESTFOLD, K. C., 1959, J.O.S.A. ***44***, 717.
WIEDER, I. and L. R. SARLES, 1961, Phys. Rev. L. ***6***, 95.
WOLF, E., 1954a, Nuovo Cimento ***12***, 884.
WOLF, E., 1954b, Proc. Roy. Soc. A***255***, 96.
WOLF, E., 1955, Proc. Roy. Soc. A***238***, 246.
WOLF, E., 1956, Proc. Symposium on Astronomical Optics and Related Subjects, Manchester (North-Holland Publishing Co., Amsterdam).
WOLF, E., 1957, Phil. Mag. Ser. 8, ***2***, 351.
WOLF, E., 1958, Proc. Phys. Soc. ***71***, 257.
WOLF, E., 1959, Nuovo Cimento Ser. 10, ***13***, 1165.
WOLF, E., 1960, Proc. Phys. Soc. ***76***, 424.
WOLF, E., 1962, Proc. Phys. Soc., ***80***, 1269.
WOLF, E., 1963, Proc. 3rd Symp. Quantum Electronics, Paris 1963, in press.
WOODWARD, P. M., 1953, Probability and Information Theory, with Applications to Radar (Pergamon Press, London) p. 117.
ZERNIKE, F., 1938, Physica ***5***, 785.

VI

METHODS FOR DETERMINING OPTICAL PARAMETERS OF THIN FILMS

BY

F. ABELÈS

Institut d'Optique and Faculté des Sciences, Paris, France

CONTENTS

§ 1. Introduction

It seems desirable to explain to the reader the spirit in which the following pages were written. Naturally, the reader will find this out for himself, if he has the courage to work himself through them, but it seems to be important that he should know that the author had a special purpose in mind. We are concerned with a review, as short as possible, of the different methods which can be used to determine the parameters which characterize optically a thin film. We will not describe any experimental arrangement and we will not give any information on the refractive indices of the substances which can be used for the production of thin films. The purpose of the present work is to show how the knowledge of the optical parameters of the film may be gained from certain measurements, and what are the necessary calculations that have to be employed for this purpose. Such knowledge is of importance because even if some experimenters have access to an electronic computer and are not afraid of long and involved calculations, there are others who prefer not to be led, for example, beyond an equation of second degree. Some of the methods indicated below have so far not been tried out, so that the following pages contain also suggestions for future research. Some results are presented here in a form slightly different from that in which they were originally given, so that the article should form a coherent ensemble in as far as notations and the methods are concerned.

1.1. DEFINITIONS AND NOTATION

A thin film is a layer with parallel faces whose thickness d is comparable to the wavelength λ of the electromagnetic radiation it receives. If $d < \frac{1}{100}\lambda$ it will be called a very thin film. If the film is homogeneous and isotropic, it is characterized by an index of refraction $\tilde{n} = n - ik$. In the case of a single film, we shall assume that

it is contained between two semi-infinite homogeneous and isotropic media whose refractive indices are n_0 and n_s. In the case of oblique incidence, the angles of refraction in the media n_0, $\tilde{n}$ and n_s are denoted by φ_0, $\tilde{\varphi}$ and φ_s respectively. These angles are related to each other by the relation of Descartes (law of refraction):

$$n_0 \sin \varphi_0 = \tilde{n} \sin \tilde{\varphi} = n_s \sin \varphi_s.$$

In the following, we shall discuss almost exclusively homogeneous and isotropic thin films. The inhomogeneous films which we will encounter will be assumed to have an index of refraction $\tilde{n}$ which is a function of the single coordinate z, where the axis Oz has the direction of the normal to the planes which limit the layer (Fig. 1).

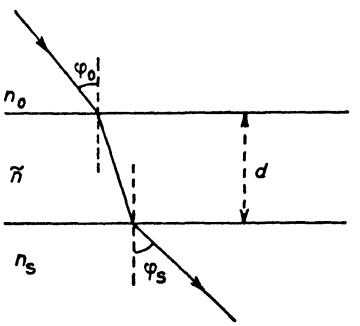

Fig. 1. Notation used in this article

We shall often encounter the angle $\eta = 2\pi d/\lambda$. This is a dimensionless number, expressed in radians.

In the case of oblique incidence we shall always find the admittance of the wave or its effective refractive index. For a plane wave with the electric vector perpendicular to the plane of incidence, the effective index of refraction is $Y = n \cos \varphi$; if the electric vector is in the plane of incidence, the effective index of refraction will be given by $Z = n/\cos \varphi$. We assume in the following that the different media have a magnetic permeability $\mu = 1$.

In the case of a thin absorbing film ($k \neq 0$), we introduce for an incident vibration *perpendicular to the plane of incidence* (*s-polarisation*), the quantity,

$$\tilde{Y} = \tilde{n} \cos \tilde{\varphi} = p - iq, \tag{1}$$

where p and q are solutions of the following system of equations:

$$p^2 - q^2 = n^2 - k^2 - n_0^2 \sin^2 \varphi_0,$$

$$pq = nk.$$

For an incident vibration *parallel to the plane of incidence* (*p-polarisation*):

$$\tilde{Z} = \tilde{n}/\cos\tilde{\varphi} = A - \mathrm{i}B, \tag{2}$$

with

$$A = p\left(1 + \frac{n_0^2 \sin^2\varphi_0}{p^2 + q^2}\right),$$

$$B = q\left(1 - \frac{n_0^2 \sin^2\varphi_0}{p^2 + q^2}\right).$$

We use quite frequently the indices $\perp$ and $\parallel$ to denote quantities which are associated with the *s*- and *p*-vibrations respectively.

1.2. GENERAL SUMMARY OF FORMULAE FOR THIN FILMS

We shall only give the formulae for normal incidence; in the case of oblique incidence the effective indices will replace the true indices with the exception of the products $\beta = \tilde{n}\eta$ where $\tilde{n}$ must be replaced by $\tilde{Y}$. We find (BORN and WOLF [1959]), if we take the incident vibration as unity, that the amplitudes of the reflected and transmitted vibrations are:

$$r = \frac{n_0 - n_s + \mathrm{i}\left(\frac{n_0 n_s}{\tilde{n}} - \tilde{n}\right)\operatorname{tg}\beta}{n_0 + n_s + \mathrm{i}\left(\frac{n_0 n_s}{\tilde{n}} + \tilde{n}\right)\operatorname{tg}\beta},$$

$$r' = \frac{n_s - n_0 + \mathrm{i}\left(\frac{n_0 n_s}{\tilde{n}} - \tilde{n}\right)\operatorname{tg}\beta}{n_0 + n_s + \mathrm{i}\left(\frac{n_0 n_s}{\tilde{n}} + \tilde{n}\right)\operatorname{tg}\beta},$$

$$t = \frac{2n_0}{(n_0 + n_s)\cos\beta + \mathrm{i}\left(\frac{n_0 n_s}{\tilde{n}} + \tilde{n}\right)\sin\beta}. \tag{3}$$

We have utilized the following notations: r if the reflected vibration occurs in the medium n_0, and r' if the vibration occurs in the medium n_s. The three numbers r, r' and t are complex. Let us set:

$$r = \mathscr{R}^{\frac{1}{2}} \exp(\mathrm{i}\delta_r), \qquad r' = \mathscr{R}'^{\frac{1}{2}} \exp(\mathrm{i}\delta_{r'}), \qquad t = |t| \exp(\mathrm{i}\delta_t).$$

The reflection and transmission factors, i.e. the energies carried by

It is easier to utilize $\sigma = 1/\lambda$ as a variable. We find then (ABELÈS [1958], KOPPELMANN and KREBS [1956], HASS, RAMSEY and THUN [1959]) that

$$\frac{d\mathscr{R}}{d\sigma} = \frac{8n_0 n_s \operatorname{tg}\beta\,(1+\operatorname{tg}^2\beta)}{[(n_0+n_s)^2+(n_0 n_s/n+n)^2\operatorname{tg}^2\beta]^2}\left\{\left(n-\frac{n_0^2 n_s^2}{n^3}\right)\operatorname{tg}\beta\frac{dn}{d\sigma}\right.$$
$$\left.+\left(\frac{n_0^2 n_s^2}{n^2}+n^2-n_0^2-n_s^2\right)\frac{d\beta}{d\sigma}\right\} \qquad (5)$$

with

$$\frac{d\beta}{d\sigma} = \beta\left(\frac{1}{n}\frac{dn}{d\sigma}+\frac{1}{\sigma}\right).$$

The smallest value of β which corresponds to $d\mathscr{R}/d\sigma = 0$ will now be nearly $\frac{1}{2}\pi$. In general, $dn/d\sigma > 0$, $d\beta/d\sigma > 0$ and for

$$n-\frac{n_0^2 n_s^2}{n^3} > 0, \qquad \frac{n_0^2 n_s^2}{n^2}+n^2-n_0^2-n_s^2 > 0,$$

we find that the equation to be solved is of the form:

$$a\operatorname{tg}\beta + b\beta = 0, \qquad (6)$$

where a and b are positive numbers. It follows that $\operatorname{tg}\beta < 0$, i.e. $\beta > \frac{1}{2}\pi$ if $\mathscr{R}$ is a maximum.

Example. Let us take a film of ZnS and let us assume that for $\lambda = 500$ mμ, $n = 2.35$ and $dn/d\sigma = 0.24\mu^{-1}$ with $n_0 = 1$, $n_s = 1.52$. We find that for this wavelength $d\mathscr{R}/d\sigma = 0$ if $\beta = 100°37'$! This means that the optical thickness of the ZnS film which is such that $\mathscr{R}(\sigma)$ is a maximum for $\lambda = 500$ mμ is

$$nd = \frac{100°37'}{360°}\lambda = 0.2795\lambda.$$

If we would have neglected the dispersion of ZnS, we would have found that $\mathscr{R}(\sigma)$ is a maximum, when $nd = 0.25\lambda$. We would have therefore made a relative error on the optical thickness of the film $\Delta(nd)/nd = 2.95/25 = 11.8\,\%$.

Let us now examine the intensity of the reflectivity for $d\mathscr{R}/d\sigma = 0$ in the case of the preceding example. We find that $\mathscr{R} = 0.316$, whereas if we had $\beta = \frac{1}{2}\pi$ we would have had $\mathscr{R}(\beta = 90°) = 0.323$. The influence of the dispersion of n still manifests itself here.

The relation (6) shows that, everything being equal, $|\operatorname{tg}\beta|$ increases proportionally to β. Hence the influence of dispersion will be weaker

with growing thickness of the films under examination. For the example which we have just given, we find that the second maximum according to a measurement of $\mathscr{R}(\sigma)$ takes place at

$$nd = \frac{273°57'}{360°}\lambda = 0.761\lambda,$$

instead of at 0.75λ if we had neglected the dispersion. This time, the relative error due to the neglection of the dispersion of n is not larger than $\Delta n/n = \frac{1}{75}$. It is difficult to give an explicit expression which permits to calculate n and d from the position and the intensity of the maximum of $\mathscr{R}$, if we take the dispersion into account. In fact, we must always determine three unknown quantities: n, $\mathrm{d}n/\mathrm{d}\sigma$ and β and the measurement in question allows the determination of only two of them.

2.1.2. *Oblique incidence*

(*a*) If the angle of incidence has a value φ_{0B} such that $\operatorname{tg}\varphi_{0B} = n/n_0$, $\mathscr{R}_{||}$, the reflectance for parallel light, becomes:

$$\mathscr{R}_{||}(\varphi_{0B}) = \left(\frac{Z_0 - Z_s}{Z_0 + Z_s}\right)^2,$$

where $Z_0 = n_0/\cos\varphi_0$, $Z_s = n_s/\cos\varphi_s$.

This shows that the film behaves as if it did not exist. This is evident because in this case there is no reflection at the air-film interface, which means that the incident wave does not find any discontinuity at this boundary.

Stated in a different manner, we can say that the impedances of the air and the film are the same. This suggests a simple method for the determination of the indices of refraction of non-absorbing substances which are deposited on any substrate. We compare the relative reflectances $\mathscr{R}_{||}$ at the uncovered surface and at the surface covered with the thin film. When they are equal, it means that the equality $n = n_0 \operatorname{tg}\varphi_0$ is verified. For the applications of this method, see for example ABELÈS [1949], POLSTER and WOODRUFF [1953], HEAVENS and SMITH [1957], TRAUB and OSTERBERG [1957], KINOSITA *et al.* [1960], KOPPELMANN and KREBS [1961]. Two facts should be emphasized about this method.

1. The measurement of φ_{0B} is not sufficient to determine at the same time n and d, because $\mathscr{R}_{||}(\varphi_{0B})$ is independent of the thickness of the

film. It is, therefore, necessary to make one additional measurement.

2. The method is valid only for homogeneous and isotropic films. It has been shown by several authors (BOUSQUET [1955 and 1957], KOPPELMANN and KREBS [1961] that, if the film is inhomogeneous, the determination of the angle, for which the reflectance $\mathscr{R}_{||}$ of the film is equal to the reflectance of the uncovered substrate, may lead, if one applies the relation $n = n_0 \operatorname{tg} \varphi_{0B}$, to completely erroneous results. The sensitivity of this method depends on the optical thickness of the film. It is a maximum if $nd \sim \frac{1}{4}\lambda$ and a minimum if $nd \sim \frac{1}{2}\lambda$. This will become clear after an examination of Fig. 2 where we have

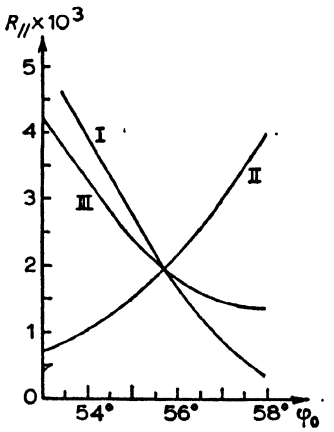

Fig. 2. Measurement of the refractive index of a thin film using Brewster's angle for the interface air-film. (I): $\mathscr{R}_{||}$ for an uncovered substrate ($n_s = 1.649$); (II): $\mathscr{R}_{||}$ for the same substrate covered by a film ($n = 1.47$) of optical thickness $nd = 147$ mμ; (III): $\mathscr{R}_{||}$ for the same film as in (II), but of optical thickness 300 mμ ($\lambda = 588$ mμ). (After KINOSITA *et al.* [1960].)

shown: in (I), $\mathscr{R}_{||}$ for an uncovered substrate ($n_s = 1.649$); in (II), $\mathscr{R}_{||}$ for the same substrate covered by a film ($n = 1.47$) of optical thickness 147 mμ; in (III), $\mathscr{R}_{||}$ for the same film as in (II), but of optical thickness 300 mμ ($\lambda = 588$ mμ). Curves (I) and (II) intersect each other almost at right angles, whereas curves (I) and (III) intersect with an acute angle. In practice, n can be determined with a probable error of $\pm$ 0.002.

(*b*) It is possible to find n and d by measuring $\mathscr{T}_{||}$ and $\mathscr{T}_{\perp}$ for a given angle of incidence φ_0. It may be shown (ABELÈS [1953b]) that $x = n^2$ is a root of the following equation:

$$b_0 x^2 + b_1 x + b_2 = 0, \tag{7}$$

where

$$b_0 = (Z_0 + Z_s)^2 - (Y_0 + Y_s)^2 - 4Z_0Z_s/\mathscr{T}_{||} + 4Y_0Y_s/\mathscr{T}_{\perp},$$
$$b_1 = [(Y_0 + Y_s)^2 - 4Y_0Y_s/\mathscr{T}_{\perp}](n_0^2 \operatorname{tg}^2\varphi_0 + n_s^2 \operatorname{tg}^2\varphi_s),$$
$$b_2 = -[(Y_0 + Y_s)^2 - 4Y_0Y_s/\mathscr{T}_{\perp}]\, n_0^2 n_s^2 \operatorname{tg}^2\varphi_0 \operatorname{tg}^2\varphi_s.$$

In order to determine the thickness of the film, we must use the following equality:

$$\operatorname{tg}^2\beta = \frac{(Y_0 + Y_s)^2 - 4Y_0Y_s/\mathscr{T}_{\perp}}{4Y_0Y_s/\mathscr{T}_{\perp} - (Y_0Y_s/Y + Y)^2} = \frac{(Z_0 + Z_s)^2 - 4Z_0Z_s/\mathscr{T}_{||}}{4Z_0Z_s/\mathscr{T}_{||} - (Z_0Z_s/Z + Z)^2}.$$

The last expression is naturally not valid for $\varphi_0 = \varphi_{0B}$. Here $Y = n\cos\varphi$ and $Z = n/\cos\varphi$. The sensitivity of the method has not yet been examined in a systematic way.

(*c*) We can also utilize the slope of the curves which show the variation of $\mathscr{R}_{||}$ and $\mathscr{R}_{\perp}$ as a function of φ_0 at the point of the abscissa $\varphi_0 = \frac{1}{2}\pi$. If we now define $p_{\perp} = \mathrm{d}\varphi_0/\mathrm{d}\mathscr{R}_{\perp}$ and $p_{||} = \mathrm{d}\varphi_0/\mathrm{d}\mathscr{R}_{||}$ at $\varphi_0 = \frac{1}{2}\pi$, we find that $x = n^2$ is a solution of a third degree equation of the form (ABELÈS [1953a]) †:

$$A_0x^3 + A_1x^2 + A_2x + A_3 = 0, \tag{8}$$

where

$$A_0 = n_0 + 4Z_sp_{||}; \qquad A_1 = -n_0^3 - 4(n_s^2Z_sp_{||} + n_0^2Y_sp_{\perp});$$
$$A_2 = -n_0n_s^2(n_s^2 - 4n_0Z_sp_{\perp}); \qquad A_3 = -n_0^2A_2.$$

If we know n, we obtain the thickness of the film from the relation

$$\operatorname{tg}^2\beta = \frac{Y_s^2 - 4n_0Y_sp_{\perp}}{4n_0Y_sp_{\perp} + n_0^2 - n^2}. \tag{9}$$

This assumes that one may perform photometric measurements for very large angles of incidence. Naturally, when $\varphi_0 = \frac{1}{2}\pi$, $\mathscr{R}_{\perp} = \mathscr{R}_{||} = 1$ regardless of what the index of refraction and the thickness of the film may be.

(*d*) The problem is somewhat more complicated with an absorbing substrate. This happens, for instance, when we investigate oxyde layers on metals. The reflection factors can be written as follows:

$$= \frac{[(Y_0 - p_s)^2 + q_s^2]Y^2 + [Y_0^2(p_s^2 + q_s^2) + Y^4 - 2Y_0p_sY^2]\operatorname{tg}^2\beta + 2(Y_0^2 - Y^2)q_sY}{[(Y_0 + p_s)^2 + q_s^2]Y^2 + [Y_0^2(p_s^2 + q_s^2) + Y^4 + 2Y_0p_sY^2]\operatorname{tg}^2\beta + 2(Y_0^2 - Y^2)q_sY}$$

while $\mathscr{R}_{||}$ is obtained from $\mathscr{R}_{\perp}$ by the usual substitutions.

† Some errors in the original article have been corrected here.

The measurement of $\mathscr{R}_\perp$ and $\mathscr{R}_{||}$ for a given angle of incidence φ_0 gives a system of two equations which are of the second degree in tg β. The elimination of this unknown leads to an algebraic equation for n^2. The mathematical problem has not yet been thoroughly investigated.

It is quite easy to understand why the problem is much more complicated now than with a non-absorbing substrate. In the latter instance, $q_s = B_s = 0$ and the expressions for $\mathscr{R}_\perp$ and $\mathscr{R}_{||}$ are simplified by the vanishing of the linear term in tg β in the numerator as well as in the denominator. This term in turn is due to the phase-change at the reflection on the dielectric-metal interface, which differs from zero or π.

It was already stated that, when $\varphi_0 = \mathrm{tg}^{-1}(n/n_0) = \varphi_{0B}$, $\mathscr{R}_{||}$ is the same for the substrate covered with a thin non-absorbing film and for the uncovered substrate. This allows the use, even in this case, of the method indicated in 2.1.2(a) for the computation of n. The measurement of $\mathscr{R}_\perp(\varphi_{0B})$ gives the thickness of the film by solving the following equation:

$$\left[\frac{Y_0^2(p_s^2+q_s^2)}{Y^2} + Y^2 - 2Y_0 p_s \frac{1+\mathscr{R}_\perp(\varphi_{0B})}{1-\mathscr{R}_\perp(\varphi_{0B})}\right] \mathrm{tg}^2\beta + 2\left(Y - \frac{Y_0^2}{Y}\right) q_s \,\mathrm{tg}\,\beta + Y_0^2 + p_s^2 + q_s^2 - 2Y_0 p_s \frac{1+\mathscr{R}_\perp(\varphi_{0B})}{1-\mathscr{R}_\perp(\varphi_{0B})} = 0.$$

It is not necessary to measure $\mathscr{R}_\perp$ for $\varphi_0 = \varphi_{0B}$. Any other angle of incidence, even $\varphi_0 = 0°$, can be used. It is even possible to use, besides $\mathscr{R}_{||}(\varphi_{0B})$, the measurement of $\mathscr{R}_{||}$ for an angle of incidence other than φ_{0B}. In that case, too, we are lead to the solution of an equation of the second degree in tg β.

2.2. POLARIMETRIC MEASUREMENTS

2.2.1. *Measurements of the reflected light*

These are relatively seldom used, probably because the elliptical analyzers are instruments less common than the spectrophotometers or the interferometers. The method has been described by VAŠIČEK [1947]. It is analogous to the classical method of Drude for the determination of the optical constants of metals. A plane wave, linearly polarized with its electric vector making an angle of 45° with the plane of incidence, is reflected by the thin film. We determine the orientation and the ellipticity of the reflected elliptical vibration.

Let us denote by Δ_R the phase difference between the parallel and perpendicularly polarized reflected components and by $\operatorname{tg}\psi_R$ the ratio $(\mathscr{R}_{||}/\mathscr{R}_{\perp})^{\frac{1}{2}}$, which means that we have $r_{||}/r_{\perp} = \operatorname{tg}\psi_R \exp(i\Delta_R)$. The expressions for these quantities are not simple. We find that

$$\operatorname{tg}^2\psi_R = \frac{(Y_0Y_s+Y^2)^2(Z_0Z_s-Z^2)^2\operatorname{tg}^4\beta+[Y^2(Y_0+Y_s)^2(Z_0Z_s-Z^2)^2+}{(Y_0Y_s-Y^2)^2(Z_0Z_s+Z^2)^2\operatorname{tg}^4\beta+[Y^2(Y_0-Y_s)^2(Z_0Z_s+Z^2)^2+}$$
$$\frac{+Z^2(Z_0-Z_s)^2(Y_0Y_s+Y^2)^2]\operatorname{tg}^2\beta+Y^2Z^2(Y_0+Y_s)^2(Z_0-Z_s)^2}{+Z^2(Z_0+Z_s)^2(Y_0Y_s-Y^2)^2]\operatorname{tg}^2\beta+Y^2Z^2(Y_0-Y_s)^2(Z_0+Z_s)^2} \quad (10)$$

and

$$\Delta_R = \Delta_N - \Delta_D \quad (11)$$

with

$$\operatorname{tg}\Delta_N = \frac{[Y(Y_0+Y_s)(Z_0Z_s-Z^2)+Z(Z_0-Z_s)(Y_0Y_s+Y^2)]\operatorname{tg}\beta}{YZ(Y_0+Y_s)(Z_0-Z_s)-(Y_0Y_s+Y^2)(Z_0Z_s-Z^2)\operatorname{tg}^2\beta},$$

$$\operatorname{tg}\Delta_D = \frac{[Y(Y_0-Y_s)(Z_0Z_s+Z^2)+Z(Z_0+Z_s)(Y_0Y_s-Y^2)]\operatorname{tg}\beta}{YZ(Y_0-Y_s)(Z_0+Z_s)-(Y_0Y_s-Y^2)(Z_0Z_s+Z^2)\operatorname{tg}^2\beta}.$$

The measurements furnish the values of Δ_R and ψ_R. It remains to solve a system of two equations with two unknowns in order to determine n and d. The solution of this system is not very simple. We will restrict ourselves to point out that we arrive at a system of two *algebraic* equations if we take as unknowns $x = n^2$ and $y = \operatorname{tg}\beta$.

There has been no systematic study concerning the solution of this system of equations. VAŠIČEK [1947] gives an example of the solution by graphical interpolation. It corresponds (Fig. 3) to: $n_0 = 1$, $n_s = 1.5687$, $\lambda = 5893$ Å, $\varphi_0 = 70°$. It had been found experimentally: $\psi_R = 29°04'$, $\Delta_R = 11°52'30''$. The interpolation consists of taking different values of n in the neighbourhood of the correct value and to calculate $\operatorname{tg}\beta$ according to the equation (10). Taking into account this value of $\operatorname{tg}\beta$, we calculate Δ_R by means of equation (11). The exact value of n is that which corresponds also to the measured value of Δ_R. Fig. 3 gives an indication of the sensitivity of this method.

2.2.2. *Use of the principal angle of incidence*

The calculations are considerably simplified if the measurements are taken for the principal angle of incidence. Then $\Delta_R = \frac{1}{2}\pi$ and equation (11) shows that

$$(Z_0^2Z_s^2 - Z^4)(Y_0^2Y_s^2 - Y^4)\operatorname{tg}^4\beta + [Y^2(Y_0^2 - Y_s^2)(Z_0^2Z_s^2 - Z^4)$$
$$+Z^2(Z_0^2 - Z_s^2)(Y_0^2Y_s^2 - Y^4) + 4Y_0Z_0YZ(Y^2 - Y_s^2)(Z^2 - Z_s^2)]\operatorname{tg}^2\beta$$
$$+Y^2Z^2(Y_0^2 - Y_s^2)(Z_0^2 - Z_s^2) = 0.$$

This time the equations (10) and (11) form a system of second degree equations for $\mathrm{tg}^2\beta$ whose solution is relatively easier. For the general case, equation (11) is of the fourth degree for $\mathrm{tg}\,\beta$. It would be desirable if this system of equations with n^2 and $\mathrm{tg}^2\beta$ as unknowns would be more closely examined.

2.2.3. *Measurements of the transmitted light*

In principle the foregoing considerations remain valid if we study a thin film by transmission. In practice, we are limited by the possible birefringence of the substrate. If it is possible to eliminate this, we

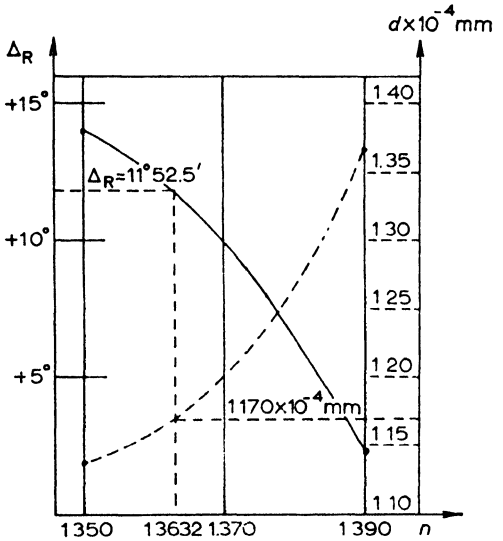

Fig. 3. Solution, by graphical interpolation, of the system of equations giving n and d from the measured values of Δ_R and ψ_R.

can measure the quantities ψ_T and Δ_T, which are analogue to ψ_R and Δ_R. We find that

$$\mathrm{tg}^2\psi_T = \frac{Y^2(Y_0+Y_s)^2 + (Y_0Y_s+Y^2)^2\,\mathrm{tg}^2\beta}{Z^2(Z_0+Z_s)^2 + (Z_0Z_s+Z^2)^2\,\mathrm{tg}^2\beta} \cdot \frac{Z_0Z_sZ^2}{Y_0Y_sY^2} \tag{12}$$

and $\Delta_T = \Delta_{TN} - \Delta_{TD}$, with:

$$\mathrm{tg}\,\Delta_{TN} = \frac{Y_0Y_s+Y^2}{Y(Y_0+Y_s)}\,\mathrm{tg}\,\beta, \qquad \mathrm{tg}\,\Delta_{TD} = \frac{Z_0Z_s+Z^2}{Z(Z_0+Z_s)}\,\mathrm{tg}\,\beta. \tag{13}$$

We arrive at a system of two second degree equations for $\mathrm{tg}\,\beta$. The elimination leads to an algebraic equation of a higher degree for n^2. Here also the mathematical study remains to be done. We do not know of any corresponding experimental work which could be quoted.

2.3. INTERFEROMETRIC MEASUREMENTS

2.3.1. *Normal incidence*

On a given thin film and for a given wavelength we could measure three phase shifts which we will call δ_r, $\delta_{r'}$ and δ_t (see Fig. 4). Actually, we measure in general

$$\varepsilon_r = \delta_r + \frac{4\pi n_0 d}{\lambda} + \pi, \qquad \varepsilon_r = \delta_{r'}, \qquad \varepsilon_t = \delta_t + \frac{2\pi n_0 d}{\lambda}.$$

If the thin film is non-absorbing, the three phase shifts δ_r, $\delta_{r'}$ and δ_t are not independent. In this case we find

$$\frac{rr'}{t^2} = \frac{n_0 - n_s + i(n_0 n_s/n - n)\operatorname{tg}\beta}{n_0 + n_s + i(n_0 n_s/n + n)\operatorname{tg}\beta} \cdot \frac{n_s - n_0 + i(n_0 n_s/n - n)\operatorname{tg}\beta}{n_s + n_0 + i(n_0 n_s/n + n)\operatorname{tg}\beta} \cdot \frac{[n_s + n_0 + i(n_0 n_s/n + n)\operatorname{tg}\beta]^2}{4n_0^2/\cos^2\beta}$$

$$\frac{rr'}{t^2} = \frac{-(n_0 n_s/n - n)^2 \sin^2\beta - (n_0 - n_s)^2\cos^2\beta}{4n_0^2} = \frac{n_s}{n_0}\sqrt{\frac{\mathscr{R}\mathscr{R}'}{\mathscr{T}^2}}\exp\left[i(\delta_r + \delta_{r'} - 2\delta_t)\right]$$

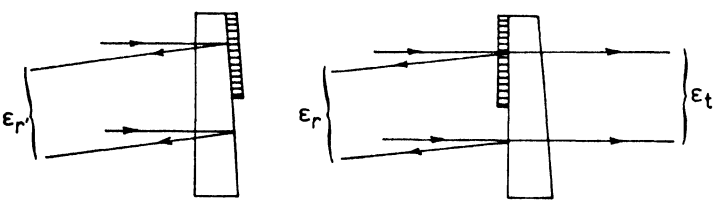

Fig. 4. Definition of the measurable phase shifts ε_r, $\varepsilon_{r'}$, and ε

which shows that:

$$\delta_r + \delta_{r'} - 2\delta_t = \pi + \text{integral multiple of } 2\pi.$$

According to the definition of the ε's, we find that:

$$\varepsilon_r + \varepsilon_{r'} - 2\varepsilon_t = \delta_r + \delta_{r'} - 2\delta_t + \pi,$$

which shows that, if we assume observable phase shifts, we have:

$$\varepsilon_r + \varepsilon_{r'} - 2\varepsilon_t = \text{integral multiple of } 2\pi. \qquad (14)$$

Two conclusions become evident:

(a) the measurement of phase shifts cannot supply more than two of the parameters which characterize the film (n and d);

(b) if the relation (14) does not hold, the film must be absorbing. As a matter of fact, we can show, in the same manner as we have done for a single film, that the relation (14) is satisfied in a general fashion if we are dealing with any system of non-absorbing thin films. This relation could therefore furnish a criterion for determining whether a thin film is absorbing or not absorbing.

We can easily show that:

$$\operatorname{tg} \varepsilon_{r'} = \operatorname{tg} \delta_{r'} = \frac{2nn_s(n_0^2 - n^2) \operatorname{tg} \beta}{(n_s^2 - n_0^2)n^2 + (n_0^2 n_s^2 - n^4) \operatorname{tg}^2 \beta}, \tag{15}$$

$$\operatorname{tg} \delta_t = -\frac{(n_0 n_s + n^2) \operatorname{tg} \beta}{n(n_0 + n_s)}. \tag{16}$$

The measurement of $\varepsilon_{r'}$ and ε_t results, for example, in a system of two equations for which the unknowns are n and d. These are two non-algebraic equations whose solution, in any case, is not excessively difficult.

The phase shift δ_r is obtained from (15) by interchanging n_0 and n_s.

2.3.2. *Oblique incidence*

The foregoing considerations remain valid if we utilize an incident vibration which is rectilinear and perpendicular or parallel to the plane of incidence. We must simply replace the actual refractive index by the effective indices (Y for the perpendicularly polarized and Z for the parallel polarized waves) in all formulae, except those for β and 2 (or 4) $\pi n_0 d/\lambda$, where we replace n by $n \cos \varphi$ and n_0 by $n_0 \cos \varphi_0$.

In this case we may generate a system of *algebraic* equations if we measure $\varepsilon_{r'} = \delta_{r'}$ for the same angle of incidence φ_0 and for the two polarizations (parallel and perpendicular). This question has not yet been studied thoroughly. We can simply indicate that (15) shows that we must solve a system of two equations of the second degree in $\operatorname{tg} \beta$, the coefficients of which are functions of n. The elimination of $\operatorname{tg} \beta$ by the classical method leads to an algebraic equation in n^2, but of a higher degree.

The utilization of the phase shifts alone is not very frequently made. In preference a mixed method, consisting of the measurement of a phase shift and the reflectance or transmission, is used.

2.4. MIXED METHODS

2.4.1. *Normal incidence*

(*a*) We measure $\mathscr{R}$ and $\varepsilon_{r'} = \delta_{r'}$. From the knowledge of these quantities we may then calculate n and β by means of the formulae

$$n^2 = \frac{n_0 n_s (n_0 a - n_s)}{n_0 (a^2 + b^2) - n_s a}, \qquad \operatorname{tg} \beta = \frac{n_0 a - n_s}{nb}, \tag{17}$$

with

$$a = \frac{1 - \mathscr{R}}{1 + \mathscr{R} - 2\sqrt{\mathscr{R}} \cos \varepsilon_{r'}}, \qquad b = \frac{2\sqrt{\mathscr{R}} \sin \varepsilon_{r'}}{1 + \mathscr{R} - 2\sqrt{\mathscr{R}} \cos \varepsilon_{r'}}.$$

The method provides sufficiently precise values for n and d, because in the plane, for which n and $\operatorname{tg} \beta$ are the axes, the curves which correspond to $\mathscr{R}$ = constant and $\varepsilon_{r'}$ = constant, are orthogonal.

(*b*) FLEISCHMANN and SCHOPPER [1951] make use of ε_t instead of $\varepsilon_{r'}$. We have seen that $\varepsilon_t = \delta_t + (2\pi n_0 d)/\lambda$ where δ_t is given by:

$$\operatorname{tg} \delta_t = -\frac{n_0 n_s + n^2}{n(n_0 + n_s)} \operatorname{tg} \beta. \tag{16}$$

In some cases, we may assume to a first approximation that the factor of $\operatorname{tg} \beta$ is equal to one, which simplifies the computations. Physically the approximation $\delta_t \simeq -\beta$ means, that multiple reflections in the film have been neglected, which is permissible only for films with a low index of refraction. Fleischmann and Schopper assume, furthermore, that n is approximately known.

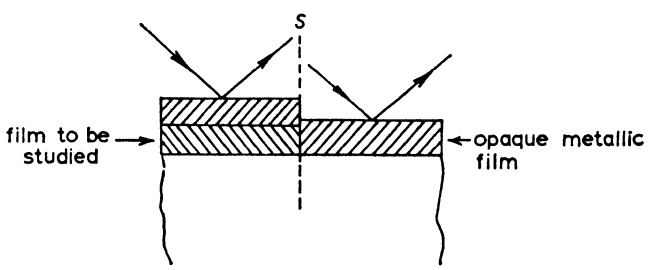

Fig. 5. Measurement of the thickness of a thin film. The film is coated with an opaque metallic layer and the step S is measured by an interferometer.

(*c*) We can also measure the mechanical thickness of the thin film. In order to do this, it is necessary that it presents a sharp edge. We coat the film with an opaque metallic film and measure, by means of an interferometer, the step which indicates the end of the thin film. (Fig. 5). The phase shift which is measured in this manner corresponds to $2d$. We may ask here, whether the thickness found by

this method is the true thickness. Detailed studies have, as a matter of fact, shown that this is well the case, provided there is no chemical or other deterioration of the surfaces (HEAVENS [1951], WEAVER and BENJAMIN [1956]).

The thickness of the thin film being known, we may determine n by measurement of $\mathscr{R}$. It must be noted, however, that in this case too, n is the solution of a non-algebraic equation, because it appears also in the expression for β.

2.4.2. *Oblique incidence*

We may also use the foregoing method for measurements with either a parallel or a perpendicularly polarized wave. The modifications which must be made to the expressions which are given above, are evident.

2.4.3. *Non-absorbing film on absorbing substrate*

(*a*) If the thin film is deposited on a metallic substrate, we could measure, for example, $\mathscr{R}_\perp$ and $\varepsilon_{r\perp}$ or $\mathscr{R}_{||}$ and $\varepsilon_{r||}$ for a given incidence. We must, however, now take into account that

$$\varepsilon_{r\perp,||} = \delta_{r\perp,||} + (4\pi n_0 d \cos\varphi_0)/\lambda - \theta_{0\perp,||},$$

where θ_0 represents the phase shift at the reflexion at the interface of the two media n_0 and $\tilde{n}_s$, which means that

$$\operatorname{tg}\theta_{0\perp} = \frac{2Y_0 q_s}{Y_0^2 - p_s^2 - q_s^2}, \qquad \operatorname{tg}\theta_{0||} = \frac{2Z_0 B_s}{Z_0^2 - A_s^2 - B_s^2}.$$

We may proceed by successive approximations in trying several values for d. To each of these values there corresponds a value of $\delta_r = \varepsilon_r + \theta_0 - (4\pi n_0 d \cos\varphi_0)/\lambda$.

We set

$$a_{||,\perp} = \frac{1 - \mathscr{R}_{||,\perp}}{1 + \mathscr{R}_{||,\perp} - 2\sqrt{\mathscr{R}_{||,\perp}}\cos\delta_{r||,\perp}},$$

$$b_{||,\perp} = \frac{2\sqrt{\mathscr{R}_{||,\perp}}\sin\delta_{r||,\perp}}{1 + \mathscr{R}_{||,\perp} - 2\sqrt{\mathscr{R}_{||,\perp}}\cos\delta_{r||,\perp}},$$

and find

$$Z^2 = Z_0 \frac{a_{||}(A_s^2 + B_s^2) - A_s Z_0}{A_s(a_{||}^2 + b_{||}^2) - Z_0 a_{||}}, \qquad Y^2 = Y_0 \frac{a_\perp(p_s^2 + q_s^2) - p_s Y_0}{p_s(a_\perp^2 + b_\perp^2) - Y_0 a_\perp}, \tag{18}$$

by applying the expression which corresponds to the polarization of the wave.

Knowing n, we obtain $\operatorname{tg}\beta$ by means of the relation

$$\operatorname{tg}\beta = \frac{A_s a_{||} + B_s b_{||} - Z_0}{B_s Z_0 + b_{||} Z^2} Z = \frac{p_s a_\perp + q_s b_\perp - Y_0}{q_s Y_0 + b_\perp Y^2} Y. \quad (19)$$

We then compare the value of d with the experimental value and repeat the calculation with the new value of d. The convergence will be fast enough if the initial value is not too far from the true value of d.

(*b*) If $\varphi_0 = \varphi_{0B}$, measuring $\varepsilon_{r||}$ gives immediately the thickness d of the thin film by means of the relation

$$\varepsilon_{r||} = \frac{4\pi d}{\lambda} \frac{n^2 - n_0^2}{\sqrt{n_0^2 + n^2}}.$$

This gives an idea of the precision we may have for d. Let us assume that the measurement of the phase shift is made at approximately λ/X. If we neglect, in the first approximation, the error which was made on n, we find that

$$\Delta d = \frac{\sqrt{n_0^2 + n^2}}{n^2 - n_0^2} \frac{\lambda}{2X}.$$

It becomes evident that the error increases with a decreasing difference between n and n_0.

The reason for this is the fact that $\varepsilon_{r||}$ is proportional to this difference $n - n_0$, if the precision, with which this quantity is measured, remains constant (and equal to λ/X). For instance, if $X = 1000$, $\lambda = 6000$ Å, $n = 2$, $n_0 = 1$, $\Delta d = 2$Å.

§ 3. Absorbing Thin Films

These films present more difficulties than the non-absorbing films, both from the theoretical and the experimental point of view. It is, therefore, appropriate to investigate non-absorbing thin films quite separately from absorbing ones.

3.1. PHOTOMETRIC MEASUREMENTS

We note at this point that we have two different reflection factors. They correspond respectively to waves which are incident in the media n_0 and n_s, and we denote them by $\mathscr{R}$ and $\mathscr{R}'$ respectively. The transmission is independent of the direction of propagation.

We give here the formulae for the two reflection factors and the transmission for the case of normal incidence:

$$\mathscr{R} = \frac{abe^{2k\eta} + cde^{-2k\eta} + 2r\cos 2n\eta + 2s\sin 2n\eta}{bde^{2k\eta} + ace^{-2k\eta} + 2t\cos 2n\eta + 2u\sin 2n\eta}, \tag{20}$$

$$\mathscr{R}' = \frac{cde^{2k\eta} + abe^{-2k\eta} + 2r\cos 2n\eta - 2s\sin 2n\eta}{bde^{2k\eta} + ace^{-2k\eta} + 2t\cos 2n\eta + 2u\sin 2n\eta}, \tag{21}$$

$$\mathscr{T} = \frac{16n_0n_s(n^2+k^2)}{bde^{2k\eta} + ace^{-2k\eta} + 2t\cos 2n\eta + 2u\sin 2n\eta}, \tag{22}$$

with

$$\begin{matrix} a \\ d \end{matrix} = (n \mp n_0)^2 + k^2, \qquad \begin{matrix} b \\ c \end{matrix} = (n \pm n_s)^2 + k^2,$$

$$\begin{matrix} r \\ t \end{matrix} = (n_0^2 + n_s^2)(n^2+k^2) - (n^2+k^2)^2 - n_0^2n_s^2 \mp 4n_0n_sk^2$$

$$\begin{matrix} s \\ u \end{matrix} = 2k(n_s \mp n_0)(n^2 + k^2 \pm n_0n_s).$$

3.1.1. *Normal incidence*

(*a*) Semitransparent films of unspecified thickness. We can determine $\tilde{n} = n - ik$ and d by measurement of $\mathscr{R}$, $\mathscr{R}'$ and $\mathscr{T}$. We are led in this way to a system of three nonalgebraic equations with three unknowns, which must be solved. For the solution of this system we may use a digital computer, because the computations are too lengthy to be done by means of a desk calculator. We may also use tables which give $\mathscr{R}$, $\mathscr{R}'$ and $\mathscr{T}$ for different values of n, k and $\eta = 2\pi d/\lambda$ with the assumption that n_s does not vary. The only problem is, therefore, the interpolation in a table which gives the variations of three functions of three variables (see on this matter MALÉ [1950]). In general, the values of the variables are not sufficiently closely spaced so that we could be satisfied with a linear interpolation, and it will be necessary to proceed by graphical interpolation. The precision is variable because it depends on $\tilde{n}$ and d. It is difficult to give much information on this subject. Let us simply state that it is in general possible to determine in this way the three parameters which are characteristic for a homogeneous and isotropic thin film to approximately several percent of their relative values.

We find in general two systems of values of $\tilde{n}$ and d which verify the basic equations. Theoretical considerations will then permit to select the correct solution.

(*b*) Very thin absorbing films. If the films are very thin, i.e. if $\eta = 2\pi d/\lambda \ll 1$, we can use limited expansions of the trigonometric and exponential functions which occur in the expressions for $\mathscr{R}$, $\mathscr{R}'$ and $\mathscr{T}$. As a matter of fact, it is necessary that $n\eta$ and $k\eta$ are very much smaller than 1. By limiting the expansions of the series to terms of η^2, WOLTER [1937] has shown that $\mathscr{R}$, $\mathscr{R}'$ and $\mathscr{T}$ are not independent, but that:

$$\frac{1-\mathscr{R}'-\mathscr{T}}{1-\mathscr{R}-\mathscr{T}} = \frac{\mathscr{A}'}{\mathscr{A}} = \frac{n_s}{n_0}, \tag{23}$$

where $\mathscr{A}$ and $\mathscr{A}'$ are the absorption factors of the thin film. By extending the series expansion to third order term in η, we find that Wolter's relation no longer holds, so that it should be possible in principle to deduce $\tilde{n}$ and d from the measurement of $\mathscr{R}$, $\mathscr{R}'$ and $\mathscr{T}$. In practice, such a method is too susceptible to experimental errors (ABELÈS [1953c]). For more details, we refer to the paper in question.

3.1.2. *Oblique incidence*

(*a*) Semitransparent thin films of unspecified thickness. The method is analogous to the one we have described for the case of normal incidence. It has not yet been employed, as far as we know. It would most probably be interesting to examine the possibilities of its use. One would use the formulae which are given above with the following substitutions:

$$\textit{Vibration } \perp\colon\ n_0 \to Y_0,\quad n - ik \to p - iq,\quad n_s \to Y_s.$$

$$\textit{Vibration } \parallel\colon\ n_0 \to Z_0,\quad n - ik \to A - iB,\quad n_s \to Z_s.$$

It should be noted that in the terms which contain exponential or trigonometric functions one must substitute, *for both vibrations*, $p - iq$ for $n - ik$.

(*b*) Very thin absorbing films. In this case, the expressions for the reflection and transmission factors for a vibration perpendicular to the plane of incidence may be written in the form

$$\frac{\mathscr{R}_\perp}{\mathscr{R}'_\perp} = \frac{A_0 \pm A_1\eta + A_2\eta^2}{B_0 + B_1\eta + B_2\eta^2}, \qquad \mathscr{T}_\perp = \frac{4Y_0Y_s}{B_0 + B_1\eta + B_2\eta^2}, \tag{24}$$

if the expansion is limited to second order terms in η. Here we have set:

$$\begin{matrix} A_0 \\ B_0 \end{matrix} = (Y_0 \mp Y_s)^2, \qquad \begin{matrix} A_1 \\ B_1 \end{matrix} = 2(Y_s \mp Y_0)\varepsilon_2 ,$$

$$A_2 = B_2 = \varepsilon_1^2 + \varepsilon_2^2 - (n_0^2 + n_s^2)\varepsilon_1 + n_0^2 n_s^2,$$

where $\varepsilon_1 - i\varepsilon_2 = (n - ik)^2$ (ABELÈS [1957]). Due to the fact that $A_2 = B_2$, Wolter's relation still holds, i.e., we have:

$$\frac{1 - \mathscr{R}'_\perp - \mathscr{T}_\perp}{1 - \mathscr{R}_\perp - \mathscr{T}_\perp} = \frac{\mathscr{A}'_\perp}{\mathscr{A}_\perp} = \frac{Y_s}{Y_0}.$$

It is, therefore, not sufficient to measure $\mathscr{R}_\perp$, $\mathscr{R}'_\perp$ and $\mathscr{T}_\perp$ for a given angle of incidence in order to deduce n, k and d. A fact, even more serious, is that the foregoing expressions show that the dependence with the angle of incidence of $\mathscr{R}_\perp$, $\mathscr{R}'_\perp$ and $\mathscr{T}_\perp$ for a given film are of the following form:

$$\begin{matrix} \mathscr{R}_\perp \\ \mathscr{R}'_\perp \end{matrix} = \frac{(Y_s - Y_0)^2 \pm a(Y_s - Y_0) + b}{(Y_s + Y_0)^2 + a(Y_s + Y_0) + b},$$

$$\mathscr{T}_\perp = \frac{4Y_0 Y_s}{(Y_s + Y_0)^2 + a(Y_s + Y_0) + b},$$

where a and b are constants, independent of φ_0. So, even the study of the variation of $\mathscr{R}_\perp$, $\mathscr{R}'_\perp$ and $\mathscr{T}_\perp$ with φ_0 is not sufficient to allow the determination of n, k and d.

The utilization of the vibration parallel to the plane of incidence permits the solution of the problem. The expressions for $\mathscr{R}_\parallel$, $\mathscr{R}'_\parallel$ and $\mathscr{T}_\parallel$ are still of the form (24), but with the following modifications (ABELÈS [1957]):

$$\begin{matrix} A_0 \\ B_0 \end{matrix} = (Z_0 \mp Z_s)^2, \qquad \begin{matrix} A_1 \\ B_1 \end{matrix} = 2(Z_s \mp Z_0)\left[1 \mp \frac{Z_0 Z_s n_0^2 \sin^2\varphi_0}{\varepsilon_1^2 + \varepsilon_2^2}\right]\varepsilon_2,$$

$$\begin{matrix} A_2 \\ B_2 \end{matrix} = (Z_0^2 + Z_s^2)(n_0^2 \sin^2\varphi_0 - \varepsilon_1) + Z_0^2 Z_s^2 \frac{(\varepsilon_1 - n_0^2 \sin^2\varphi_0)^2 + \varepsilon_2^2}{\varepsilon_1^2 + \varepsilon_2^2}$$

$$+ \varepsilon_1^2 + \varepsilon_2^2 \mp \frac{4Z_0 Z_s \varepsilon_2^2 n_0^2 \sin^2\varphi_0}{\varepsilon_1^2 + \varepsilon_2^2}.$$

Now we no longer have the equality $A_2 = B_2$, so that $Z_0\mathscr{A}'_\parallel \neq Z_s\mathscr{A}_\parallel$. It will, thus, in principle, be sufficient to measure $\mathscr{R}_\parallel$, $\mathscr{R}'_\parallel$ and $\mathscr{T}_\parallel$, for a given incidence in order to deduce n, k and d. In any case, it is necessary to recall that for incidence under the Brewster angle with respect to the substrate, $Z_0 = Z_s$ and $\mathscr{R}_\parallel = \mathscr{R}'_\parallel$. One should, there-

fore, perform the measurements for an incidence different from $\varphi_0 = \operatorname{tg}^{-1} n_s/n_0$ and, preferably, sufficiently large.

We find that $x = \varepsilon_2\eta$ is the solution of the following equation of the second degree:

$$2(Z_0 - Z_s)x^2 + \left[Z_0^2 - Z_s^2 + 2Z_0Z_s\frac{\mathscr{R}_{||} - \mathscr{R}'_{||}}{\mathscr{T}_{||}}\right]x + Z_0Z_s\frac{Z_s\mathscr{A}'_{||} - Z_0\mathscr{A}_{||}}{\mathscr{T}_{||}} = 0. \quad (25)$$

Now it is easily shown that

$$\frac{1}{\varepsilon_1^2 + \varepsilon_2^2} = \frac{\mathscr{R}_{||} - \mathscr{R}'_{||}}{(Z_0 - Z_s)\mathscr{T}_{||}xn_0^2\sin^2\varphi_0} + \frac{1}{Z_0Z_sn_0^2\sin^2\varphi_0}. \quad (26)$$

It is difficult to obtain the third unknown in a similarly simple manner. It will be possible to use the expression for $\mathscr{T}_{||}$ in order to have a third equation, but the problem has not yet been examined in detail.

3.2. POLARIMETRIC MEASUREMENTS

We find here measurements analogous to those we have already described in the case of non-absorbing films. Here the difficulty arises from the fact that the analysis of the elliptical vibration, which results from the reflection or transmission of a linearly polarized wave, does not furnish more than two parameters. We must, therefore, perform two measurements, which will permit to obtain four relations between the three parameters which characterize the films. One may thus see whether the hypotheses regarding the film under study are true (homogeneity and isotropy).

The polarimetric measurements have been used but little for the study of the optical characteristics of the films. In the general case, it will be recalled that $r_\perp$ is the quotient of two polynomials of the second degree in $p - iq$ and of the first degree in $\operatorname{tg}\tilde{\beta}$, whereas $r_{||}$ is a quotient of analogous polynomials in $A - iB$ and $\operatorname{tg}\tilde{\beta}$. It follows that the measurement of $\operatorname{tg}\psi_R \exp(i\Delta_r) = r_{||}/r_\perp$ and of

$$\operatorname{tg}\psi'_R \exp(i\Delta'_R) = r'_{||}/r'_\perp$$

will lead finally to the solution of a system of algebraic equations for $\tilde{n}^2$ and $\operatorname{tg}\tilde{\beta}$.

One might equally well use the measurements of transmission. At any rate, this may present a slight inconvenience in practice due to

the fact that metallic films which are a little thick have a low transmission.

The calculations are considerably simplified if the Brewster angle is chosen for the reflection air-substrate (this means that $\operatorname{tg} \varphi_0 = n_s/n_0$). The method has been described by FÖRSTERLING [1937]. Let us set $\operatorname{tg} \psi_T \exp(i\Delta_T) = t_{||}/t_\perp$. The angle of incidence has been chosen in such a way that $Z_0 = Z_s$; it follows that $r_{||} = r'_{||}$. We make use of the following two combinations:

$$\tilde{A} = \frac{1 - x}{1 + x}, \qquad x = \frac{\operatorname{tg} \psi'_R}{\operatorname{tg} \psi_R} \exp[i(\Delta'_R - \Delta_R)],$$

$$\tilde{B} = \frac{\operatorname{tg} \psi_R}{\operatorname{tg} \psi_T} \exp[i(\Delta_R - \Delta_T)].$$

It is easily shown that

$$\tilde{A} = \frac{Y_s - Y_0}{i(Y_0 Y_s/\tilde{Y} - \tilde{Y}) \operatorname{tg} \tilde{\beta}}, \qquad \tilde{B} = \frac{i(Z_0 Z_s/\tilde{Z} - \tilde{Z}) \operatorname{tg} \tilde{\beta}}{Y_0 - Y_s + i(Y_0 Y_s/\tilde{Y} - \tilde{Y}) \operatorname{tg} \tilde{\beta}} \frac{Y_0}{Z_0},$$

where $\tilde{Y} = p - iq$ and $\tilde{Z} = A - iB$.

The elimination of $\operatorname{tg} \tilde{\beta}$ from $\tilde{A}$ and $\tilde{B}$ leads to the relation

$$-(\tilde{A} - 1)\tilde{B} = n_0^2 \frac{(\tilde{n}^2 - n_0^2)(\tilde{n}^2 - n_s^2)}{\tilde{n}^2[(n_0^2 + n_s^2)\tilde{n}^2 - 2n_0^2 n_s^2]}, \tag{27}$$

which is a second degree equation for $\tilde{n}^2$.

According to Försterling, we may solve this equation in a simpler way by introducing the new variable:

$$y = \frac{4n_0^2 n_s^2}{n_0^2 + n_s^2} \left(\frac{2n_0^2 n_s^2}{n_0^2 + n_s^2} - \frac{1}{\tilde{n}^2} \right). \tag{28}$$

Then

$$y - \frac{1}{y} = \frac{n_s^2 - n_0^2}{4n_0 n_s} (\tilde{A} - 1)\tilde{B},$$

an equation of the form

$$y - \frac{1}{y} = Q, \tag{29}$$

where Q is a known quantity. If tables of the function $\sin z$ for complex argument are available, we may set $y = \exp(iz)$ and $Q = 2i \sin z$. Knowing $\tilde{n}$, it is possible to calculate $\tilde{\beta}$, starting from the relation

$$i \operatorname{tg} \tilde{\beta} = \frac{(Y_s - Y_0)\tilde{Y}}{\tilde{A}(Y_0 Y_s - \tilde{Y}^2)}. \tag{30}$$

Because $\tilde{\beta} = 2\pi\tilde{Y}d/\lambda$, we have two equations which give the thickness d of the film. The problem is simplified if $\tilde{\beta} \ll 1$. Then

$$\mathrm{i}\,\mathrm{tg}\,\tilde{\beta} \approx \mathrm{i}\,\tilde{\beta} = 2\pi\mathrm{i}\tilde{Y}d/\lambda$$

which permits us to write

$$\frac{d}{\lambda} = \frac{\sqrt{n_0^2 + n_s^2}}{2\pi\mathrm{i}\tilde{A}} \cdot \frac{n_s^2 - n_0^2}{2n_0^2 n_s^2 - (n_0^2 + n_s^2)\tilde{n}^2}. \tag{31}$$

This shows also that, because d/λ is a real number,

$$\mathrm{i}\,\tilde{A}[2n_0^2 n_s^2 - (n_0^2 + n_s^2)\tilde{n}^2]$$

must be real.

3.3. INTERFERENCE MEASUREMENTS

In principle it is sufficient to measure ε_r, $\varepsilon_{r'}$ and ε_t in order to be able to deduce $\tilde{n}$ and d. We give here the expressions for the phase shifts δ_r, $\delta_{r'}$ and δ_t, starting from which we will be able to obtain the values of the observed phase shifts:

$$\mathrm{tg}\,\delta_r = 2n_0 \frac{k\{[(n_s+n)^2+k^2]\mathrm{e}^{2k\eta} - [(n_s-n)^2+k^2]\mathrm{e}^{-2k\eta}\} + }{(n_0^2 - n^2 - k^2)\{[(n_s+n)^2+k^2]\mathrm{e}^{2k\eta} + [(n_s-n)^2+k^2]\mathrm{e}^{-2k\eta}\} + }$$

$$\frac{+ 2n\{-2n_s k\cos 2n\eta - (n^2+k^2-n_s^2)\sin 2n\eta\}}{+ 2(n_0^2+n^2+k^2)[(n^2+k^2-n_s^2)\cos 2n\eta - 2n_s k \sin 2n\eta]}, \tag{32}$$

$$\mathrm{tg}\,\delta_{r'} = 2n_s \frac{k\{[(n_0+n)^2+k^2]\mathrm{e}^{2k\eta} - [(n_0-n)^2+k^2]\mathrm{e}^{-2k\eta}\} + }{(n_s^2 - n^2 - k^2)\{[(n_0+n)^2+k^2]\mathrm{e}^{2k\eta} + [(n_0-n)^2+k^2]\mathrm{e}^{-2k\eta}\} + }$$

$$\frac{+ 2n\{-2n_0 k\cos 2n\eta - (n^2+k^2-n_0^2)\sin 2n\eta\}}{+ 2(n_s^2+n^2+k^2)[(n^2+k^2-n_0^2)\cos 2n\eta - 2n_0 k \sin 2n\eta]}, \tag{33}$$

$$\mathrm{tg}\,(\delta_t - \Theta) = -\frac{(x_1\mathrm{e}^{k\eta} - x_2\mathrm{e}^{-k\eta})\sin n\eta + x_3\mathrm{e}^{-k\eta}\cos n\eta}{x_3\mathrm{e}^{-k\eta}\sin n\eta + (x_1\mathrm{e}^{k\eta} + x_2\mathrm{e}^{-k\eta})\cos n\eta}, \tag{34}$$

with

$$\mathrm{tg}\,\Theta = \frac{k(n^2+k^2-n_0 n_s)}{n_0 n_s n + (n_0+n_s+n)(n^2+k^2)},$$

$$x_1 = [(n_0+n)^2+k^2][(n_s+n)^2+k^2],$$

$$x_2 = (n_0^2 - n^2 - k^2)(n^2+k^2-n_s^2) + 4n_0 n_s k^2,$$

$$x_3 = 2k(n_0+n_s)(n^2+k^2-n_0 n_s).$$

This method has never been used and we will not describe it here. The numerical calculations to which it leads should not be much longer than those which have been described in § 2.1. The reason

for the little interest which this method has received is probably due to the fact that the measurement of phase shifts in different spectral regions is more difficult and, perhaps, less precise than photometric measurements.

3.4. COMBINED METHODS

3.4.1. *Normal incidence*

(*a*) The calculations are relatively simple if one performs supernumerary measurements. SCHOPPER [1952a] proposes the simultaneous measurement of six quantities ($\mathscr{R}$, $\mathscr{R}'$, $\mathscr{T}$, ε_r, $\varepsilon_{r'}$ and ε_t) in order to obtain $\tilde{n}$ and d. It can be shown that

$$\tilde{n}^2 = n_0 n_s \frac{n_s\sqrt{\mathscr{R}}\exp(i\varepsilon_r)[1-\sqrt{\mathscr{R}'}\exp(i\varepsilon_{r'})]^2+\mathscr{T}\exp(i2\varepsilon_t)\{n_0-n_s[1-\sqrt{\mathscr{R}'}\exp(i\varepsilon_{r'})]\}}{n_0\sqrt{\mathscr{R}}\exp(i\varepsilon_r)[1+\sqrt{\mathscr{R}'}\exp(i\varepsilon_{r'})]^2-\mathscr{T}\exp(i2\varepsilon_t)\{n_s-n_0[1+\sqrt{\mathscr{R}'}\exp(i\varepsilon_{r'})]\}} \tag{35}$$

In order to obtain the thickness of the film we use the following two relations †:

$$\exp(i4\pi n_0 d/\lambda) = \sqrt{\mathscr{R}}\exp(i\varepsilon_r)\frac{n_s(\tilde{n}^2-n_0^2)}{\tilde{n}^2\{n_s-n_0[1+\sqrt{\mathscr{R}'}\exp(i\varepsilon_{r'})]\}+n_0 n_s\{n_0-n_s[1-\sqrt{\mathscr{R}'}\exp(i\varepsilon_{r'})]\}} = \rho_1\exp(i\Theta \tag{36}$$

$$\exp(i4\pi n_0 d/\lambda) = \frac{n_s}{n_0}\frac{\mathscr{T}(\tilde{n}^2-n_0^2)\exp(i2\varepsilon_t)}{\tilde{n}^2[1+\sqrt{\mathscr{R}'}\exp(i\varepsilon_{r'})]^2-n_s^2[1-\sqrt{\mathscr{R}'}\exp(i\varepsilon_{r'})]^2} = \rho_2\exp(i\Theta_2), \tag{37}$$

each of which is equivalent to two relations. We may verify that $\rho_1 = \rho_2 = 1$ and then that $\Theta_1 = \Theta_2$. This permits to insure that the initial hypotheses (homogeneous and isotropic films) are valid. Schopper has applied this method to the study of two films of Sb_2S_3 in the visible.

(*b*) We may also proceed according to a method analogous to the one described for the non-absorbing films (2.4.1c). We measure the physical thickness of the film and, in addition, the reflection and transmission. The method has been used often (HASS and WAYLONIS [1961], LESLOURDY [1961], DOREL [1962]) and it gives the results readily, especially if one has tables which give $\mathscr{R}$ and $\mathscr{T}$ as a function

† In the paper by Schopper one finds in the numerator $\tilde{n} - n_0$ instead of $\tilde{n}^2 - n_0^2$.

of n, k and η (for a given n_s) or if one can employ an electronic computer. In the first case, it is necessary to use a graphical representation because linear interpolation is not adequate (see 3.1.1(a)). We give an example of the application of the method (Fig. 6). Let us assume that $\mathscr{R} = 0.397$, $\mathscr{T} = 0.046$, $\eta = 2\pi d/\lambda = 0.875$, $n_s = 1.48$. To begin with, we trace $\mathscr{R}$ and $\mathscr{T}$ as a function of k for several values of n. One obtains in this way two curves, which give n as a function of k and where one of them corresponds to $\mathscr{R} = 0.397$ and the other one to $\mathscr{T} = 0.046$. The intersection of these two curves gives the desired n and k. The dashed curves in Fig. 6 indicate the limits of the experimental errors, which will allow to give an idea of the precision one may obtain in a rather unfavorable case.

MURMANN [1933, 1936], who was the first author to use this method, measured $\mathscr{R}$ and $\mathscr{R}'$ and traced the curves which give $\mathscr{R}$ and $\mathscr{R}'$ as a function of n for k constant (see also ROUARD [1937]).

By using one of the methods indicated in this section, two possible values of $\tilde{n}$ are generally found (see also 3.1.1(a)).

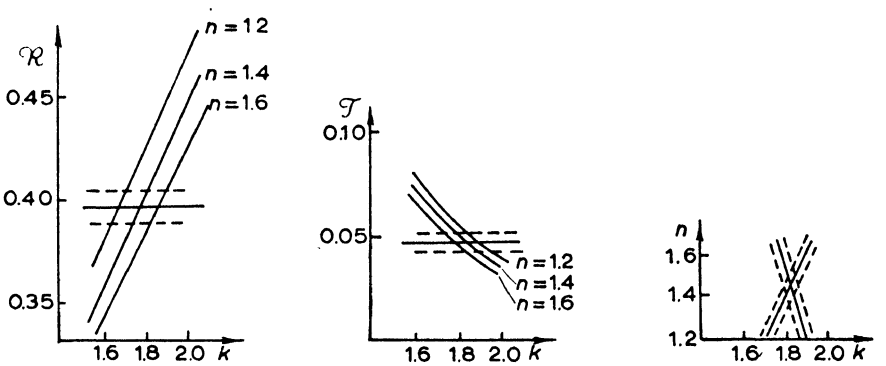

Fig. 6. Solution, by graphical interpolation, of the system of equations for n and k, for a thin metallic film of known thickness, using the measured values of $\mathscr{R}$ and $\mathscr{T}$.

(c) If $\tilde{n}$ does not change with the thickness of the film, we may use solely measurements of the transmission for different thicknesses. If the films are sufficiently thick, so that one may neglect multiple reflections, that means, if $\exp[-(4\pi kd)/\lambda] \ll 1$, one may write:

$$\mathscr{T} = \frac{16 n_0 n_s (n^2 + k^2)}{[(n_0 + n)^2 + k^2][(n_s + n)^2 + k^2]} \exp[-(4\pi kd)/\lambda]. \qquad (38)$$

We measure the thicknesses and the transmissions of at least two films and draw the representative straight line of $\ln \mathscr{T}$ as a function

of $4\pi d/\lambda$, the slope of which is $-k$, the ordinate at the origin being

$$\ln \frac{16 n_0 n_s (n^2 + k^2)}{[(n_0 + n)^2 + k^2][(n_s + n)^2 + k^2]}. \tag{39}$$

This allows to calculate n. To use this method it is also necessary to know how to measure weak transmissions ($\leqq 0.01$). This method has been used, for example, by SCHULZ [1954].

If the transmission is larger, and if the thicknesses of the films are smaller, the preceding approximation is no more valid. We may still apply this method, provided we use the complete expression for $\mathscr{T}$ (equation (22) of section 3.1).

Let us simply state that the precision with which we may hope to know $\tilde{n}$ must necessarily be smaller than in the preceding case (3.4.1(b)) because at least 4 measurements are utilized instead of the three which are strictly necessary.

In principle, we might proceed in the same way beginning with the measurements of $\mathscr{R}$ or of $\mathscr{R}'$. This has never been tried, probably, because even if the film is sufficiently thick, the expression for $\mathscr{R}$ is not as simple as that for $\mathscr{T}$.

3.4.2. *Oblique incidence*

Practically all the methods which have been described in the preceding section can be used for oblique incidence under the condition that the usual transpositions are made for the indices.

§ 4. Very Weakly Absorbing Thin Films

We will now examine the case of films which have $k \ll 1$.

4.1. NORMAL INCIDENCE

4.1.1. *Method of Hall and Ferguson*

HALL and FERGUSON [1955] have determined n, k and d for very weakly absorbing thin films by measuring the extrema of $\mathscr{R}$ and of $\mathscr{T}$. If k is sufficiently small, one may neglect, in the first approximation, the phase shifts at the reflection air-film and film-substrate (supposedly non-absorbing). Under these conditions, if nd is an uneven multiple of $\frac{1}{4}\lambda$ we will have a maximum of $\mathscr{R}$ and a minimum of $\mathscr{T}$; if, however, nd is an even multiple of $\frac{1}{4}\lambda$, we will have a minimum for $\mathscr{R}$ and a maximum for $\mathscr{T}$, if $n > n_s$. The opposite takes place if

$n < n_s$. HALL and FERGUSON [1955] suggest therefore, the measurement of the maxima and minima for $\mathscr{R}$ and $\mathscr{T}$.

If $\mathscr{R}_1$ is a maximum of $\mathscr{R}$ ($n > n_s$), we will have, according to equation (20)

$$n^2 = n_0 n_s \frac{1 + \sqrt{\mathscr{R}_1}}{1 - \sqrt{\mathscr{R}_1}} + nk\eta \left[n_0 \frac{1 + \sqrt{\mathscr{R}_1}}{1 - \sqrt{\mathscr{R}_1}} - n_s \right], \tag{40}$$

a relation which is valid whenever $k\eta < 0.05$, and which corrects the equation (10) of HALL and FERGUSON [1955].

If the optical thickness of the film is an integral multiple of $\frac{1}{2}\lambda$, i.e. if $2n\eta$ is an integral multiple of 2π, we will denote by $\mathscr{R}_2$ the value which is then taken by $\mathscr{R}$. It can be shown, starting with equation (20), that

$$k\eta = n \frac{n_0 - n_s + (n_0 + n_s)\sqrt{\mathscr{R}_2}}{n^2 - n_0 n_s - (n^2 + n_0 n_s)\sqrt{\mathscr{R}_2}}. \tag{41}$$

Let $\mathscr{T}_1$ be the value of $\mathscr{T}$ (see equation (22)), when $2n\eta = K\pi$, with K an odd integer. We have the relation

$$n + \frac{n_0 n_s}{n} = \left[\sqrt{\frac{\mathscr{T}_0}{\mathscr{T}_1}} - k\eta \right] (n_0 + n_s), \tag{42}$$

where $\mathscr{T}_0 = 4n_0 n_s/(n_0 + n_s)^2$ represents the transmission of the uncovered substrate.

If $2n\eta = K\pi$ with K an even integer, we have $\mathscr{T} = \mathscr{T}_2$ and we find, starting from equation (22),

$$k = \frac{n(n_0 + n_s)}{n^2 + n_0 n_s} \frac{\sqrt{\mathscr{T}_0/\mathscr{T}_2} - 1}{\eta}. \tag{43}$$

It is not necessary to know n with a high degree of precision in order to have an approximate value for k, because the fraction which contains n is a function which is only slowly varying with n.

4.1.2. *Method of Koppelmann and Krebs*

A convenient method for the determination of small values of k has been proposed by KOPPELMANN and KREBS [1959]. A slide as substrate, made of glass or quartz, Tr, is partially covered on one side with the film to be studied, S, and on the other side with a metallic film with the highest possible reflectivity, Sp. One measures the reflection of the part which is covered with S, ρ_s, and of the uncovered

part, ρ_0 (see Fig. 7). Let us denote by $\mathscr{R}_0$ the reflection of the uncovered substrate, by $\mathscr{R}_m$ the reflection of the highly reflecting mirror Sp, by $\mathscr{R}$ the reflection of the film to be studied and by τ the transmission of the substrate Tr. If $\mathscr{A}$ is the absorption of the film ($\mathscr{A} = 1 - \mathscr{R} - \mathscr{T}$), we can show that:

$$\mathscr{A} = \left[\rho_0 - \rho_s - \varepsilon^2\left(\frac{\mathscr{R}_0}{1-\mathscr{R}_0} - \frac{\mathscr{R}}{1-\mathscr{R}}\right)\right]\frac{1}{2[1-\varepsilon/(1-\mathscr{R})]}, \qquad (44)$$

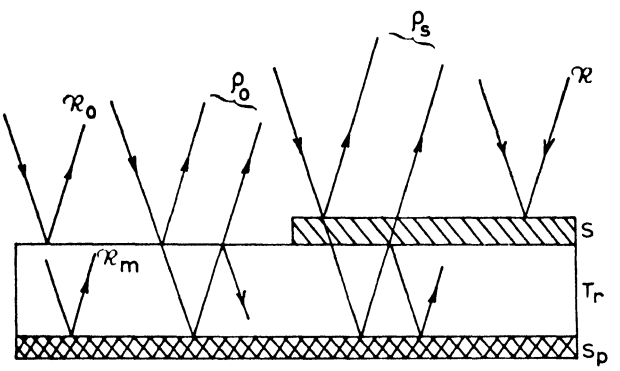

Fig. 7. Method of Koppelmann and Krebs for measuring small absorptions. In many instances, it is found that $2\mathscr{A} \approx \rho_0 - \rho_s$.

where $\varepsilon = 1 - \mathscr{R}_m\tau^2$. Equation (44) has been obtained by neglecting the powers of $\mathscr{A}$ and $\varepsilon\mathscr{A}$ higher than the first power and those of ε higher than the second power.

For the case of antireflecting films, where $\mathscr{R} < 0.04$, we may write, even more simply, by neglecting the term for ε^2:

$$\mathscr{A} \approx \frac{\rho_0 - \rho_s}{2(1-\varepsilon)}. \qquad (45)$$

On the other hand, it is possible to show that, if $k\eta$ is sufficiently small,

$$\frac{\mathscr{A}}{\mathscr{T}} = 2k\eta \qquad (46)$$

and also, because $\mathscr{T} \approx 1 - \mathscr{R}$,

$$k = \frac{\mathscr{A}}{1-\mathscr{R}}\frac{\lambda}{4\pi d}. \qquad (47)$$

The method is convenient, because we compare the reflectivities ρ_0 and ρ_s which are very close to each other. The index and the thickness of the film are determined by means of one of the methods which may

be used for the non-absorbing films. In this manner KOPPELMANN and KREBS [1959] were able to determine k for values between approximately 10^{-4} and 10^{-2}.

4.1.3. *Method of Giacomo*

In order to determine uniquely the values of k during the preparation (evaporation) of the film, GIACOMO [1956] observed the successive maxima and minima of $\mathscr{T}$ which occur whenever the optical thickness of the film is an integral multiple of $\frac{1}{4}\lambda$. The expression (3) shows that

$$\mathscr{T}_1 = \left[\frac{4\sqrt{n_0 n_s}\, n}{(n+n_0)(n+n_s)e^{k\eta} + (n-n_0)(n-n_s)e^{-k\eta}}\right]^2 \tag{48}$$

when $n\eta = \frac{1}{2}K_1\pi$, with K_1 an odd integer;

$$\mathscr{T}_2 = \left[\frac{4\sqrt{n_0 n_s}\, n}{(n+n_0)(n+n_s)e^{k\eta} - (n-n_0)(n-n_s)e^{-k\eta}}\right]^2 \tag{49}$$

when $n\eta = K_2\pi$, with K_2 an integer.

We can then deduce that

$$U = \ln\left(\mathscr{T}_1^{-\frac{1}{2}} - \mathscr{T}_2^{-\frac{1}{2}}\right) \simeq \ln\frac{(n-n_0)(n-n_s)}{2\sqrt{n_0 n_s}\, n} - k\eta$$

$$V = \ln\left(\mathscr{T}_1^{-\frac{1}{2}} + \mathscr{T}_2^{-\frac{1}{2}}\right) \simeq \ln\frac{(n+n_0)(n+n_s)}{2\sqrt{n_0 n_s}\, n} + k\eta\,.$$

In order to observe several successive maxima and minima, of $\mathscr{T}$, the evaporation must take a long enough time. Under these conditions, an absolute measurement of $\mathscr{T}$ becomes impossible, because the system, which is used for the measurement, shows always a slow drift. The measured magnitude is of the form $D\mathscr{T}$, where D is a slowly varying factor, which is eliminated if one takes the difference

$$W_T = V - U = \ln\frac{(n+n_0)(n+n_s)}{(n-n_0)(n-n_s)} + 2k\eta\,,$$

whose representative curve as a function of K must be a straight line with the slope $k\pi/n$.

In order to obtain precise measurements, it is necessary that the relative variations of $\mathscr{T}$ between $\mathscr{T}_1$ and $\mathscr{T}_2$ are important. This is the case only for films with a higher index of refraction. For the films with a low index, GIACOMO [1956] suggests the use of measurements of the reflectivity $\mathscr{R}$.

We can show that, if k is sufficiently small, $\mathscr{R}$ oscillates between the extreme values which are given by

$$\mathscr{R}_1 = \left[\frac{(n-n_0)(n+n_s)e^{k\eta} + (n+n_0)(n-n_s)e^{-k\eta}}{(n+n_0)(n+n_s)e^{k\eta} + (n-n_0)(n-n_s)e^{-k\eta}}\right]^2, \quad (50)$$

when $n\eta = K_1\pi/2$, with K_1 an odd integer;

$$\mathscr{R}_2 = \left[\frac{(n-n_0)(n+n_s)e^{k\eta} - (n+n_0)(n-n_s)e^{-k\eta}}{(n+n_0)(n+n_s)e^{k\eta} - (n-n_0)(n-n_s)e^{-k\eta}}\right]^2, \quad (51)$$

when $n\eta = K_2\pi$, with K_2 an integer.

By the same reasoning as used above in connection with $\mathscr{T}$, we are led to consider the quantity

$$W_R = \ln\frac{\sqrt{\mathscr{R}_1}+\sqrt{\mathscr{R}_2}}{\sqrt{\mathscr{R}_1}-\sqrt{\mathscr{R}_2}} \simeq \ln\frac{n^2-n_0^2}{16n_0n_sn^2(n^2-n_s^2)} + \frac{n^2+n_s^2}{nn_s}k\eta.$$

Here a W_R is also a linear function of K whose slope is

$$(n^2+n_s^2)k\pi/2n^2n_s.$$

For the cases of the measurements in reflection or transmission, we assume that the value of n is approximately known.

4.2. OBLIQUE INCIDENCE

4.2.1. *Transposition of the previous methods*

In principle, the methods which have been outlined in the preceding paragraph (4.1) may also be used in the case of oblique incidence, after making the customary modifications (utilization of the effective indices of refraction Y or Z). However, it seems that they have not so far been used in such cases.

4.2.2. *Method of Abelès and Bazin*

A method which has not been covered by the foregoing has been proposed by ABELÈS and BAZIN [1962] (see also BOUSQUET [1957]). The thin film to be studied is deposited on the base of a total reflection prism. If $k = 0$, the reflection will be 1, whatever may be the values of d and the polarization of the incident light. If $k \neq 0$, $\mathscr{R} < 1$. We can, therefore, very simply detect whether a film is absorbing or not by utilizing the arrangement which is shown in Fig. 8. The advantage of the method is that it is only necessary to compare two

luminous fluxes which are very close. This can be done with high precision. One may also obtain quantitative results by means of this method. For this purpose we give, to begin with, the exact expressions for $\mathscr{R}_\perp$ and $\mathscr{R}_{||}$. They are of the form (20) but with the following

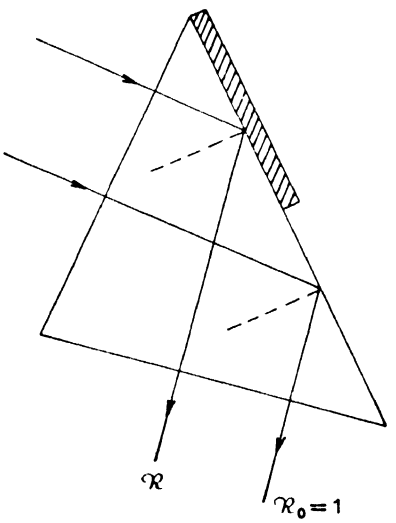

Fig. 8. Principle of the method of Abelès and Bazin for measuring small absorptions by comparing $\mathscr{R}$ and $\mathscr{R}_0 = 1$.

modifications for light polarized perpendicularly to the plane of incidence:

$$\begin{matrix} a \\ d \end{matrix} = (Y_0 \mp p)^2 + q^2, \qquad \begin{matrix} b \\ c \end{matrix} = p^2 + (q \pm \alpha)^2,$$

$$\begin{matrix} r \\ t \end{matrix} = (Y_0^2 - p^2 - q^2)(p^2 + q^2 - \alpha^2) \pm 4Y_0 pq\alpha,$$

$$\begin{matrix} s \\ u \end{matrix} = \mp 2Y_0 q(p^2 + q^2 - \alpha^2) + 2p\alpha(Y_0^2 - p^2 - q^2).$$

For the vibration which is parallel to the plane of incidence, we perform the substitutions which have been already indicated:

$$Y_0 \to Z_0, \qquad p - iq \to A - iB, \quad \text{and} \quad \alpha \to \alpha' = n_s^2/\alpha,$$

in all terms except those which contain exponential or trigonometric functions. We have put $\alpha^2 = n_0^2 \sin^2 \varphi_0 - n_s^2$; in this case, n_0 is the index of the prism, whereas n_s is the index of the last medium (in general, air).

In order to determine n, k and d we could, for example, measure $\mathscr{R}_\perp$ and $\mathscr{R}_{||}$ for the angle φ_0 which corresponds to the prism, and for

which we have total reflection for the passage film-air, as well as $\mathscr{R}$ for normal incidence at the side adjacent to air. If the thickness of the film is determined by an independent measurement, then the knowledge of $\mathscr{R}_\perp$ and $\mathscr{R}_{||}$ is sufficient for a determination of p and q, that means, n and k. Effectively, by limiting the expansion to terms of the first order in q, presumably very small, one must solve the following system (ABELÈS and BAZIN [1962]):

$$q = \frac{1-\mathscr{R}_\perp}{1+\mathscr{R}_\perp} \frac{(Y_0^2+p^2)(p^2+\alpha^2)+(Y_0^2-p^2)(p^2-\alpha^2)\cos 2p\eta+2p\alpha(Y_0^2-p^2)\sin 2p\eta}{4Y_0p(p^2+\alpha^2)\eta+4Y_0p\alpha(1-\cos 2p\eta)+2Y_0(p^2-\alpha^2)\sin 2p\eta}, \tag{52}$$

$$q = \frac{1-\mathscr{R}^{||}}{1+\mathscr{R}_{||}} \frac{(Z_0^2+A^2)(A^2+\alpha'^2)+(Z_0^2-A^2)(A^2-\alpha'^2)\cos 2p\eta+2A\alpha'(Z_0^2-A^2)\sin 2p\eta}{4Z_0A(A^2+\alpha'^2)+\left(1-\frac{n_0^2\sin^2\varphi_0}{p^2}\right)[4Z_0A\alpha'(1-\cos 2p\eta)+2Z_0(A^2-\alpha'^2)\sin 2p\eta]} \tag{53}$$

Let us give here a numerical example which indicates the precision which one may achieve in this way. We will assume that $n = 1.36$, $k = 0.001$, $\varphi_0 = 60°$, $n_0 = 1.5$, $\eta = 7$, which corresponds to an optical thickness nd of approximately $1.5\,\lambda$. It is found that $\mathscr{R}_\perp = 0.8309$, $\mathscr{R}_{||} = 0.8962$, by using the exact expressions for computing these quantities. The solution of the system of equations (52) and (53) gives the values $n = 1.3598$, $k = 0.001\,005$. Let us assume now that we had committed an error $\Delta\mathscr{R} = \pm 0.005$ for $\mathscr{R}_\perp$ and $\mathscr{R}_{||}$. The relative error $\Delta n/n \leqq 0.001$, so that $\Delta k/k$ is not larger than several hundredths. A relative error of 0.005 in the thickness ($\Delta d/d = 0.005$) causes $\Delta n/n \leqq 0.0003$ and $\Delta k/k \leqq 0.003$.

§ 5. Inhomogeneous Films

5.1. NON-ABSORBING, SLIGHTLY INHOMOGENEOUS FILMS

The problem has been examined by several authors (ABELÈS [1950], BOUSQUET [1957], HALL [1957], SCHROEDER [1941], KOPPELMANN and KREBS [1961] etc.). We will limit ourselves to several very brief indications of the appropriate methods. If the index of refraction of the film is a slowly varying function of z, such that

$$\left(\frac{\mathrm{d}n}{\mathrm{d}z}\cdot\frac{1}{n}\right)^2 \ll \left(\frac{2\pi n}{\lambda}\right)^2 \quad \text{and} \quad \frac{1}{n}\frac{\mathrm{d}^2n}{\mathrm{d}z^2} \ll \left(\frac{2\pi n}{\lambda}\right)^2,$$

one may express the reflectance of the film for normal incidence in the form

$$\mathscr{R} = \frac{(n_0\sqrt{n''/n'} - n_s\sqrt{n'/n''})^2 + (n_0 n_s/\sqrt{n'n''} - \sqrt{n'n''})^2 \operatorname{tg}^2\beta}{(n_0\sqrt{n''/n'} + n_s\sqrt{n'/n''})^2 + (n_0 n_s/\sqrt{n'n''} + \sqrt{n'n''})^2 \operatorname{tg}^2\beta}, \quad (54)$$

where n' and n'' are the values of the index of refraction of the film at the entrance ($z = 0$) and at the exit ($z = d$) of the film, and

$$\beta = \frac{2\pi}{\lambda}\int_0^d n\,\mathrm{d}z,$$

where d is, as usual, the physical thickness of the film.

The extrema of $\mathscr{R}$ occur whenever β is an integral multiple of $\frac{1}{2}\pi$, like in the case of homogeneous films. One finds that the values of $\mathscr{R}$ in these cases are

$$\mathscr{R}_1 = \left(\frac{n_0 n_s - n'n''}{n_0 n_s + n'n''}\right)^2$$

when $\beta = \frac{1}{2}K_1\pi$ with K_1 an odd integer,

$$\mathscr{R}_2 = \left(\frac{n_0 n'' - n_s n'}{n_0 n'' + n_s n'}\right)^2$$

when $\beta = K_2\pi$ with K_2 an integer.
One may, therefore, deduce n' and n'' at the same time from the maxima and minima of $\mathscr{R}(\lambda)$ if the dispersion of n may be neglected.

These results can be utilized for oblique incidence after making the usual changes. It must, however, be stated that the relation

$$n\cos\varphi = \sqrt{n^2 - n_0^2\sin^2\varphi_0}$$

must be used in order to perform the calculations.

In summing up, we may say that a non-absorbing, slightly inhomogeneous thin film is characterized by three parameters: the values of n at its extremities, which we have designated by n' and by n'', and the value of its optical thickness (which, in appropriate units, is represented by β).

5.2. INHOMOGENEOUS VERY THIN ABSORBING FILMS

Some information concerning such films can be found in a paper by ABELÈS [1957]. It is shown there that for an incident plane wave with the electric vector perpendicular to the plane of incidence, the

expressions given in section 3.1.2(*b*) are still valid, provided we replace ε_2 by $\bar{\varepsilon}_2$ in A_1 and B_1 and we set

$$A_2 = B_2 = \bar{\varepsilon}_1^2 + \bar{\varepsilon}_2^2 - 2n_0^2\bar{\varepsilon}_1 + 2(n_0^2 - n_s^2)\bar{\bar{\varepsilon}}_1 + n_0^2 n_s^2$$

where

$$\bar{\varepsilon}_1 - i\bar{\varepsilon}_2 = \frac{1}{d}\int_0^d \varepsilon dz\,,$$

$$\bar{\bar{\varepsilon}}_1 - i\bar{\bar{\varepsilon}}_2 = \frac{1}{d^2}\int_0^d dz \left\{\int_0^z \varepsilon dz\right\}, \qquad \varepsilon = \varepsilon_1 - i\varepsilon_2.$$

The equality $A_2 = B_2$ shows that we have again, and with the same accuracy, Wolter's relation. The variation with the angle of incidence φ_0 of $\mathscr{R}_\perp$, $\mathscr{R}'_\perp$ and $\mathscr{T}_\perp$ for a given film is the same as for a homogeneous one. Hence the study of their variation with φ_0 is not sufficient to make it possible to distinguish between a homogeneous and an inhomogeneous layer.

When the electric vector of the incident wave is in the plane of incidence, the situation is more complicated and we must introduce two new complex quantities. This case, as well as the case of inhomogeneous films of unspecified thickness has not been thoroughly studied.

§ 6. Birefringent Thin Films

The birefringent and absorbing thin films have been theoretically studied by SCHOPPER [1952b]. We cannot give all the details of his calculations, but it may be useful to indicate some of his results. We will assume that the z-axis is normal to the planes which limit the film, and the y-axis is located in the plane of incidence, and that the film can be described by three complex indices of refraction

$$\tilde{n}_x = n_x - ik_x, \qquad \tilde{n}_y = n_y - ik_y, \qquad \tilde{n}_z = n_z - ik_z.$$

(*a*) Determination of the optical constants in the plane of the film ($\tilde{n}_x$ and $\tilde{n}_y$). The formulae which are given above (3.4.1) are still valid if we utilize a vibration which is perpendicular to the plane of incidence. The following substitutions must then be made:

$$n_0 \to Y_0, \qquad n_s \to Y_s, \qquad \tilde{n} \to \tilde{a}_s = a - ib.$$

The number $\tilde{a}_s$ is related to $\tilde{n}_x$ by the relation $\tilde{a}_s^2 = \tilde{n}_x^2 - n_0^2 \sin^2\varphi_0$.

If we know $\tilde{a}_s$, $\tilde{n}_x$ can easily be found. To obtain $\tilde{n}_y$, we rotate the film by 90° around the z-axis and proceed as for $\tilde{n}_x$.

(*b*) In order to determine $\tilde{n}_z$, it is necessary that the incident vibration has a component in the z-direction which is not null. This is the case if we use a vibration in the plane of incidence. We will assume that $\tilde{n}_y$ is known. In general we will conserve our notation as much as possible, which leads us to a slight modification of the expressions given by SCHOPPER [1952b]. We obtain a certain effective index of refraction $\tilde{a}_p$, defined by the relation

$$\tilde{a}_p^2 = \tilde{n}_y^2 - \frac{\tilde{n}_y^2}{\tilde{n}_z^2} n_0^2 \sin^2 \varphi_0 . \tag{55}$$

Let us suppose that we have measured the three reflection factors $\mathscr{R}_p$, $\mathscr{R}'_p$ and $\mathscr{T}_p$ and the three phase shifts ε_{rp}, $\varepsilon_{r'p}$ and ε_{tp}.† We may then deduce

$$\tilde{a}_p^2 = \frac{\tilde{n}_y^4}{Z_0 Z_s} \frac{Z_0 \sqrt{\mathscr{R}_p} e^{i\varepsilon_{rp}} (1 - \sqrt{\mathscr{R}'_p} e^{i\varepsilon_{r'p}})^2 + \mathscr{T}_p e^{i2\varepsilon_{tp}} [Z_s - Z_0 (1 - \sqrt{\mathscr{R}'_p} e^{i\varepsilon_{r'p}})]}{Z_s \sqrt{\mathscr{R}_p} e^{i\varepsilon_{rp}} (1 + \sqrt{\mathscr{R}'_p} e^{i\varepsilon_{r'p}})^2 - \mathscr{T}_p e^{i2\varepsilon_{tp}} [Z_0 - Z_s (1 + \sqrt{\mathscr{R}'_p} e^{i\varepsilon_{r'p}})]} . \tag{56}$$

In the case where the film is sufficiently thick, so that $\mathscr{T}_p \simeq 0$, the preceding relation is simplified and we obtain:

$$\tilde{a}_p = \frac{\tilde{n}_y^2}{Z_s} \frac{1 - \sqrt{\mathscr{R}'_p} e^{i\varepsilon_{r'p}}}{1 + \sqrt{\mathscr{R}'_p} e^{i\varepsilon_{r'p}}} . \tag{57}$$

$\tilde{a}_p$, being known, we obtain $\tilde{n}_z$ by solving equation (55) with respect to this unknown.

For the determination of the thickness we have the following relations:

$$e^{i2Y_0\eta} = \sqrt{\mathscr{R}_p} e^{i\varepsilon_{rp}} \frac{Z_s (Z_0^2 \tilde{a}_p^2 - \tilde{n}_y^4)}{\tilde{n}_y^4 [Z_s - Z_0 (1 - \sqrt{\mathscr{R}'_p} e^{i\varepsilon_{r'p}})] + Z_0 Z_s \tilde{a}_p^2 [Z_0 - Z_s (1 + \sqrt{\mathscr{R}'_p} e^{i\varepsilon_{r'p}})]} \tag{58}$$

and

$$e^{i2Y_0\eta} = \mathscr{T}_p e^{i2\varepsilon_{tp}} \frac{Z_s}{Z_0} \frac{\tilde{n}_y^4 - Z_0^2 \tilde{a}_p^2}{\tilde{n}_y^4 [(1 - \sqrt{\mathscr{R}'_p} e^{i\varepsilon_{r'p}})^2 - Z_s^2 \tilde{a}_p^2 (1 + \sqrt{\mathscr{R}'_p} e^{i\varepsilon_{r'p}})^2]} . \tag{59}$$

We thus have four equations for the determination of the thickness of the film viz. eqs. (58) and (59). There are analogous equations for vibration which is perpendicular to the plane of incidence.

Some of Schopper's results must be modified or commented upon. He discusses the case, where the angle of incidence is $\varphi_0 = \mathrm{tg}^{-1} (n_s/n_0)$,

† We use here the index p as an indication that the incident vibration is parallel to the plane of incidence.

that means the Brewster angle with respect to the interface n_0/n_s. It is, however, impossible to measure ε_{rp} and $\varepsilon_{r'p}$ because the amplitude of the reflected vibration on the uncovered substrate is zero. Furthermore, it must be stated, that in this case, $\mathscr{R}_p = \mathscr{R}'_p$, because the external media have equal effective indices of refraction ($Z_0 = Z_s$).

In the paper already quoted, Schopper also discusses the utilization of polarimetric measurements and the use of Försterling's method (3.2). He shows that this method cannot easily be generalized in the case of anisotropic and absorbing thin films.

We did not discuss here non-absorbing anisotropic thin films, because such films have not yet been studied in a systematic manner. One can find some information in BOUSQUET [1957].

§ 7. Final Remarks

We did not discuss in the preceding paragraphs the following problem: how can one determine the number of parameters which are necessary in order to characterize a thin film for a given wavelength? We assumed that we already knew their number and their significance, but we did not show how it is possible to ascertain whether a thin film is absorbing or not, if it is birefringent, if it is homogeneous or not? In fact, some answers to these questions are given in the preceding pages. The detection of very weak absorptions ($k \ll 1$) has been discussed in the articles by KOPPELMANN and KREBS [1959] (4.1.2) and ABELÈS and BAZIN [1962] (4.2.2) already quoted. For the detection of small birefringences, the paper by BOUSQUET [1957] will give some information. Small inhomogeneities are discussed in the articles by KOPPELMANN and KREBS [1961] and BOUSQUET [1957]. There have been some attempts to prepare and to study inhomogeneous non-absorbing films, but the problem is still open. There has been an investigation of inhomogeneous non-absorbing films by RASSOW (1962c), who examined the state of polarization of light reflected by such films.

Another problem did not receive an answer yet: the measurement of the optical parameters of a pile of thin homogeneous layers. Generally, during the evaporation of a pile of thin films, witness specimens are used, on each of which a single layer is deposited. But that is not always a perfect solution and it may be found that the pile of thin layers has not the properties it should have if each of its constituents had the characteristics shown by the corresponding

witness specimen. Unfortunately, so far no solution has as yet been found to the problem of determining the optical parameters of a given pile of thin films.

These remarks are intended to show how many problems concerning the measurement of the optical parameters of thin films are still unsolved.

Acknowledgments

The author would like to thank Ingo Wilmanns, who helped with the English translation of the original French version and Miss C. Bazin who spent much time reading and commenting it.

References

ABELÈS, F., 1949, C.R. ***228***, 553.
ABELÈS, F., 1950, Ann. Physique ***5***, 596.
ABELÈS, F., 1953a, C.R. ***236***, 1412.
ABELÈS, F., 1953b, C.R. ***237***, 883.
ABELÈS, F., 1953c, Rev. Opt. ***32***, 257.
ABELÈS, F., 1957, J. Opt. Soc. Am. ***47***, 473.
ABELÈS, F., 1958, J. Phys. Rad. ***19***, 327.
ABELÈS, F. et C. BAZIN, 1962, C.R. ***254***, 2310.
BORN, M. and E. WOLF, 1959, *"Principle of Optics"* (London and New York, Pergamon Press).
BOUSQUET, P., 1955, C.R. ***240***, 2502.
BOUSQUET, P., 1957, Ann. Physique ***2***, 163.
DOREL, F., 1962, Thèse doctorat 3e cycle, spécialité optique (Paris).
FLEISCHMANN, R. and H. SCHOPPER, 1951, Z. Physik ***129***, 285.
FÖRSTERLING, K., 1937, Ann. Physik ***30***, 745.
GIACOMO, P. and P. JACQUINOT, 1952, J. Phys. (8), ***13***, 59A.
GIACOMO, P., 1956, Rev. Opt. ***35***, 442.
HALL, J. F., 1957, J. Opt. Soc. Am. ***47***, 662.
HALL, J. F. and W. F. C. FERGUSON, 1955, J. Opt. Soc. Am. ***45***, 714.
HASS, G., J. B. RAMSEY and R. THUN, 1959, J. Opt. Soc. Am. ***49***, 116.
HASS, G. and J. E. WAYLONIS, 1961, J. Opt. Soc. Am. ***51***, 719.
HEAVENS, O. S., 1951, Proc. Phys. Soc. B ***64***, 419.
HEAVENS, O. S. and S. D. SMITH, 1957, J. Opt. Soc. Am. ***47***, 469.
KINOSITA, K., T. MATSUMOTO, K. NATSUME and M. YOSHIDA, 1960, J. Appl. Phys. Jap. ***20***, 205.
KOPPELMANN, G. and K. KREBS, 1956, Z. Physik ***145***, 486.
KOPPELMANN, G. and K. KREBS, 1959, Z. Physik ***156***, 38.
KOPPELMANN, G. and K. KREBS, 1961, Z. Physik ***163***, 539.
LESLOURDY, C., 1961, Diplôme d'Etudes Supérieures (Paris).
MALÉ, D., 1950, C.R. ***230***, 1349.
MURMANN, H., 1933, Z. Physik ***80***, 161.

MURMANN, H., 1936, Z. Physik ***101***, 643.
POLSTER, D. and R. W. WOODRUFF, 1953, J. Opt. Soc. Am. ***43***, 346.
RASSOW, J., 1962a, Z. Physik, ***168***, 353.
RASSOW, J., 1962b, ibid., ***170***, 376.
RASSOW, J., 1962c, ibid., ***170***, 393.
ROUARD, P., 1937, Ann. Physique ***7***, 291.
SCHOPPER, H., 1952a, Z. Physik ***131***, 215.
SCHOPPER, H., 1952b, Z. Physik ***132***, 146.
SCHRÖDER, H., 1941, Ann. Physik ***39***, 55.
SCHULZ, L. G., 1954, J. Opt. Soc. Am. ***44***, 540.
TRAUB, A. C. and H. OSTERBERG, 1957, J. Opt. Soc. Am. ***47***, 62.
VAŠIČEK, A., 1947, J. Opt. Soc. Am. ***37***, 145.
WEAVER, C. and P. BENJAMIN, 1956, Nature, London ***177***, 1030.
WOLTER, H., 1937, Phys. Z. ***105***, 269.

AUTHOR INDEX

SUBJECT INDEX